Proteomic and functional analysis of chloroplast and thylacoids sub-compartments

Martino Tomizioli

UNIVERSITÉ DE GRENOBLE

THÈSE

Pour obtenir le grade de

DOCTEUR DE L'UNIVERSITÉ DE GRENOBLE

Spécialité : **Biologie Végétale**

Arrêté ministériel : 7 août 2006

Présentée par

Martino TOMIZIOLI

Thèse dirigée par **Giovanni FINAZZI**
codirigée par **Daphné SEIGNEURIN-BERNY, Norbert ROLLAND**

préparée au sein du **Laboratoire de Physiologie Cellulaire et Végétale**
dans **l'École Doctorale Chimie et Science du Vivant**

Identification de nouveaux acteurs de la régulation de la photosynthèse

Thèse soutenue publiquement le **20 octobre 2014**,
devant le jury composé de :

Mme Christelle BRETON
Professeur à l'Université Joseph Fourier, Grenoble (Présidente)
M Michael SCHRODA
Professeur à University of Kaiserslautern (Rapporteur)
M Christophe ROBAGLIA
Directeur de Recherche, CNRS-CEA-Univ.de la Méditerranée (Rapporteur)
M Wojciech MAJERAN
Maître de conférences, INSB-Univ.de Paris 7 (Examinateur)
M Giovanni FINAZZI
Directeur de Recherche, CNRS-iRTSV Grenoble (Directeur de thèse)
Mme Daphné SEIGNEURIN-BERNY
Chargée de Recherche, CNRS-iRTSV Grenoble (Codirectrice de thèse)

Université Joseph Fourier / Université Pierre Mendès France /
Université Stendhal / Université de Savoie / Grenoble INP

044. GRENOBLE — Téléférique sur l'Isère et le Moucherotte

Téléférique de la Bastille — Vue sur GRENOBLE

Cartes postales de Grenoble de Michel D. (1934)

Remerciements

Cette thèse a été financiée par l'agence nationale de la recherche ANR (ANR-2010 Chloro-Types ; ANR-10-LABEX-04) et preparée au sein du Laboratoire de Physiologie Cellulaire Végétale (LPCV) au CEA-Grenoble.

Je veux d'abord remercier le directeur du laboratoire Norbert Rolland pour m'avoir accueilli au sein de son laboratoire en septembre 2011. De plus, je remercie Norbert pour toute son aide pendant les travaux qui ont amené à la publication de l'article *Tomizioli et al., 2014*.

Je remercie M Schroda, M Robaglia, M Majeran et Mme Breton pour avoir accepté de juger ce travail de thèse.

Je remercie immensamente les deux personnes qui m'ont guidé pendant ce parcours : mon directeur de thèse, Giovanni Finazzi et ma co-directrice de thèse, Daphné Seigneurin-Berny. C'est grâce à eux si ce projet de thèse a pu être amené jusqu'à la fin. Leur présence quotidienne au cours de ces trois années m'a permis d'avoir un excellent encadrement. Giovanni et Daphné, chacun dans son domaine de compétence, ont toujours su me faire prendre les bonnes directions et cela témoigne de l'excellent niveau scientifique et pédagogique que l'on trouve au sein du laboratoire PCV. Tout ce qu' il y a de correct dans cette thèse c'est grâce à eux et les fautes... bah les fautes c'est à moi !

Un grand merci à Lucas Moyet, Daniel Salvi et Cécile Giustini pour tout ce qu'ils m'ont appris sur la vie du labo et l'aide technique qui a été inestimable.

Merci aux autres membres de l'équipe qui m'ont accompagné au quotidien dans le laboratoire : Gilles Curien, Marcel Kuntz, Michel Matringe, Leonardo Magneschi, Dimitris Petroutsos.

Merci aux autres étudiants du labo, avec lesquels j'ai pu échanger beaucoup et instaurer un rapport d'amitié qui continue aussi à l'extérieur du CEA : Emeline Sautron, Stephanie Chezeaud, James Connorton, Elisa Dell'aglio,

Rosi Pipitone, Laurence Boudier, Stephanie Bellego, Thomas Leonardo, Florie Schild, Marie Monieux, Fanny Moreau, Hicham Chahtane, Morgane Minnino, Elena Najar, Diane De Gouvion Saint Cyr, Guillaume Allorent, Diana Simionato, Stephen Kreida, Vanessa Checchetto, Sara De Bortoli, Lucilla Taddei.

Merci aux deux italiennes Valeria Villanova et Serena Flori pour avoir transformé, depuis leurs arrivées, le CEA et de faire de chaque jour un jour fantastique pour y travailler !

Merci à tous les membres du Laboratoire PCV, en particulier au personnel technique pour la précieuse aide dans les manips réalisées pendant ces trois ans. Emmanuel Thevenon, Thomas Vino-Poyo, Fabien Chevalier, Agnès Jourdain, Sassia Hadjadji, Marie Le Masson, Anne-Marie Boisson, Catherine Albrieux, Melissa Conte et Sylvie Figuet.

Merci à tout le personnel administratif du laboratoire, pour leur énorme travail du coté non-scientifique qui a contribué, de la même manière, à l'aboutissement de cette thèse : Sophie Mistri, Sylvianne Flammier, Nathalie Dupuy, Danielle Adelaide et Brigitte Palamini.

Un grand merci aussi aux autres étudiants, doctorant ou pas, qui ne sont pas du labo mais avec j'ai partagé ce merveilleux parcours à Grenoble : Carlos, Jorge, Matteo, Julie, Christian, Erik, Favio, Valeria, Benjamin, Livu, Luka, et tous les autres dont je ne me souviens pas en ce moment.

Merci à Donald Knuth, Leslie Lamport et aux membres de GuIT pour avoir rendu la redaction de ce manuscrit un peu plus facile et au meme temps passionnant.

... et plus que tout, merci à mes parents Gabriella et Marino-Adriano, à mon frère Giuseppe et à ma s½ur Elisabetta.

Merci, Martino

Grenoble, 20 Ottobre 2014

Contents

List of acronyms

α-DM	α dodecyl-maltosyde
ADP	adenosine di-phosphate
ATP	adenosine tri-phosphate
BBY	Berthold Babcock Yocum
Chl	chlorophyll
CURT1	curvature thylakoid 1
Cyt b_6f	cytochrome b_6f
DGDG	digalactosyl-diacyl- glycerol
ECS	electrochromic shift
FDR	false discovery rate
IEM	inner envelope membrane
ISP	iron-sulfur protein
K	Kelvin
LC	liquid chromatography
LHCI	light harvesting complex I
LHCII	light harvesting complex II
LTR	long-term reponse
MGDG	monogalactosyl-diacyl- glycerol
MS/MS	tandem mass-spectrometry
NAD(P)H	nicotinamide adenine dinucleotide phosphate
NDH	NADH de-hydrogenase
NPQ	non-photochemical quenching
OEM	outer-envelope membrane
PC	plastocyanin
PQ	plastoquinon
PQH2	plastoquinol
PSI	photosystem I
PSII	photosystem II
RCF	relative centrifugal force
RuBisCo	Ribulose-1,5-Bisphosphate Carboxylase/Oxygenase
SDS-PAGE	Sodium Dodecyl Sulphate - PolyAcrylamide Gel Electrophoresis
SEM	scanning electron microscopy
STs	state transitions
TEM	transmission electron microscopy
VDE	violaxanthin de-epoxidase
WT	wild type
ZE	zeaxanthin de-epoxidase

Abstract

This Ph.D thesis is focused on understanding how plants can cope (i.e. keep good photosynthetic performances) with varying environmental conditions. I chose to focus on two questions which constitute the main topics of this thesis : *(i)* how plants respond to varying quality of the absorbed light (state transitions or ST) and (ii) how plants protect themselves against high light intensities (non-photochemical dissipation of the excess absorbed energy or NPQ). *Tomizioli et al., 2014* (chapter 2) is a study that aimed at addressing the accurate proteomic based localization of the proteins in the two main sub-compartments of the thylakoid membrane (*i.e.* the photosynthetic membrane within each chloroplast). In fact, this membrane is structurally inhomogeneous and consists of two main sub-domains: (i) the grana, which are stacks of thylakoids and (ii) the stroma lamellae, which are unstacked membranes and connect the grana stacks. The study included the LC-MS/MS identification of 1295 chloroplast proteins ; among them 294 were found to be genuinely thylakoid proteins and were proved to be differentially distributed between stroma-lamellae and grana BBY in our plant model (wild-type *Arabidopsis thaliana*). Thanks to these localization results, it was possible to suggest new molecular actors for photosynthesis-linked activities. Findings in the paper corroborated previous observations obtained for photosynthetic proteins using non-proteomic approaches. The originality of this work relies in the identification of photosynthetic proteins whose differential distribution in the thylakoid sub-compartments might explain already observed biological phenomenon. In addition, about a hundred new minor thylakoid (or chloroplast) proteins were identified, some of them being potential regulators of the chloroplast physiology. Later, I used the information provided from this proteomic analysis to investigate differences in the protein segregation during state transitions. In fact, at varying light-quality, plants can respond by a structural reorganization of the proteins in the thylakoid membrane. State transitions include the reversible migration of the antenna pool between the two photosystems since these latter are localized in different thylakoid sub-compartments (PSI in stroma lamellae while PSII in granas) . This reversible migration is triggered by a phosphorylation mechanisms that induces state 2 (antenna associated to PSI in stroma-lamellae) and by a dephosphorylation mechanism that induced state 1 (antenna associated to PSII in granas). Proteins that catalyzes phosphorylation and dephosphorylation are already known (STN7 and PPH1) and their silencing produces mutants of *A.thaliana* unable to perform state transitions. Thanks to the proteomic analysis of the thylakoid subfractions from *A.thaliana stn7* and *pph1* mutants, we could confirm the exact antenna isoforms involved in

state transitions (lhcb 1 and lhcb 2), moreover we could identify about 80 new candidate proteins whose localization might also be regulated in a redox-controlled manner by light as in state-transitions. Unfortunatly, due to time limitation, this second aspect of the project was only partially developed and results were delivered in their preliminary form. Despite this, data is its ready-to-use form and will be easily exploited during forthcoming research activities of the laboratory. In the second part of this thesis, we investigated the high-energy quenching component (qE) of the NPQ (chapter 4). The main question that we posed concerned the mechanisms that can regulate ΔpH (and thus NPQ) in plants. To answer to the question we focused on a new and recently identified two-pore potassium channel, TPK3. Our findings indicated that TPK3 actively control photosynthesis in vivo by modulating the partitioning of the *pmf* between the ΔpH and $\Delta\Psi$ at physiological light intensities. Consistent with this finding, NPQ measures evidenced that *tpk3* mutants possessed reduced ability to dissipate excessive energy as heat and an altered chloroplast structure.

Résumé

Cette thèse de doctorat cherche à comprendre comment les plantes peuvent faire face à des conditions environnementales variables. J'ai choisi de me concentrer sur deux questions qui constituent les principaux sujets de cette thèse : (i) la réponse des plantes aux changements en qualité de lumière (transitions d'état) et (ii) comment les plantes se protègent contre les fortes intensités lumineuses (dissipation non-photochimique de l'excès d'énergie absorbée ou NPQ). *Tomizioli et al., 2014* (chapitre 2) est une étude qui vise à déterminer, avec une approche protéomique, la localisation des protéines dans les deux principaux sous-compartiments de la membrane des thylacoïds (*i.e.* la membrane photosynthétique au sein de chaque chloroplaste). En effet, cette membrane est structurellement inhomogène et se compose de deux sous-domaines : *(i)* les granas, qui sont des empilements de thylacoïdes et *(ii)* les lamelles stromales, qui sont des membranes non-empilées et relient les piles de granas.

Les résultats suggèrent que la localisation des complexes photosynthétiques est beaucoup plus dynamique que celle jusqu'alors proposée. De plus, la composition en sous-unités de ces complexes diffère selon leur localisation, dans les granas et dans les lamelles stromales, suggérant l'existence des processus de régulation de la photosynthèse jusqu'alors insoupçonnés. Cette approche a ensuite été appliquée sur des plantes mutantes d'*Arabidopsis* affectées dans les transitions d'état afin d'effectuer une analyse protéomique différentielle et identifier des protéines pouvant être impliquées dans ce processus d'adaptation. Les résultats préliminaires ont permit d'identifier environ 80 nouveaux candidats dont la localisation dans les sous-compartiments des thylacoïdes pourrait être régulée par la lumière (via un contrôle redox) lors des transitions d'état.

Dans la deuxième partie de cette thèse, j'ai étudié la réponse des plantes au stress lumineux (forte lumière). En particulier, je me suis intéressé au mécanisme de dissipation thermique de l'énergie lumineuse absorbée appelé *quenching non-photochimique* ou NPQ (non photochemical quenching). Sous des conditions de lumière importante, l'absorption d'énergie lumineuse peut être supérieure à celle que les réactions avales peuvent utiliser. Dans les cas où l'énergie lumineuse absorbée par les photosystèmes dépasse les capacités du métabolisme photosynthétique, l'accumulation des protons dans le lumen provoque une diminution du pH. Cette acidification entraine une augmentation de la dissipation thermique de l'énergie excédentaire au niveau du PSII (quenching non photochimique ou NPQ). L'objectif de l'étude a été de clarifier les aspects qui contrôlent la formation de cette différence de pH.

Préface

La photosynthèse est le processus bioénergétique qui permet aux plantes, aux algues et à certaines bactéries, de synthétiser de la matière organique en utilisant l'énergie lumineuse. Les plantes absorbent la lumière essentiellement grâce à des pigments appelés chlorophylles. Outre les chlorophylles, elles utilisent des carotènes et des xanthophylles. Ces pigments sont rassemblés chez les plantes et les algues dans des structures appelées antennes collectrices au sein desquelles les pigments sont organisés pour optimiser leur coopération. La photophosphorylation non cyclique consiste en un transfert d'électrons depuis une molécule d'eau vers une molécule de $NADP^+$ à travers une série de complexes protéiques membranaires et de protéines solubles avec génération d'un gradient de concentration en protons de part et d'autre de la membrane photosynthétique. Ce gradient de concentration de protons génère un gradient électrochimique utilisé par l'ATP synthase pour réaliser la phosphorylation de l'ADP en ATP, ce qu'on appelle un couplage chimiosmotique. Ainsi, au cours de la photophosphorylation non cyclique, l'eau est oxydée en oxygène (O_2) au niveau du photosystem II et le $NADP^+$ est réduit en NADPH. Plus précisément, l'absorption d'un photon par une molécule de chlorophylle P680 du photosystem II conduit à l'excitation d'un électron, qui acquiert suffisamment d'énergie pour être cédé à un accepteur d'électrons par un phénomène de séparation de charge photoinduite. L'accepteur d'électrons primaire est une molécule de chlorophylle dépourvue de l'atome de magnésium central appelée phéophytine. De là, l'électron excité passe sur une plastoquinone (PQ) puis à travers le complexe cytochrome b_6f avant d'être transporté sur une plastocyanine jusqu'au photosystem I. Celui-ci contient un dimère de chlorophylle P700 capable d'exciter un électron par absorption d'un photon, électron transmis par la suite à une ferrédoxine, qui le cède à une réductase pour réduire une molécule de $NADP^+$ en NADPH.

Chez les plantes et les algues, la photosynthèse se déroule dans des organites appelés chloroplastes. Une cellule typique de plante contient environ dix à cent chloroplastes. Ces derniers sont délimités par une enveloppe composée

d'une membrane interne et une membrane externe. L'intérieur du chloroplaste est constitué d'un espace aqueux appelé stroma. Dans le stroma se trouve un système membranaire interne, les thylacoïdes, siège de la phase lumineuse de la photosynthèse. Les thylacoïdes sont en forme de disques aplatis délimités par une membrane contenant un espace aqueux appelé lumen. Le thylacoïdes sont structurellement inhomogènes et sont constitués de deux sous-compartiments : des régions empilées (appelées les grana-BBY ou BBY) et des régions non-empilées (appelées les lamelles stromales).

Objectif de la thèse

Les complexes majeurs de la photosynthèse ne sont pas distribués de manière égale dans les thylacoïdes à cause de contraintes électrostatiques et stériques. Le photosystème I et l'ATP-synthase sont enrichis dans les régions non-empilées (lamelles stromales), le photosystème II est enrichi dans les régions empilées (BBY) alors que d'autres complexes, comme le cytochrome b_6f, ont une répartition équivalente dans les sous-compartiments des thylacoïdes. D'autre part, en plus de ces complexes photosynthétiques, d'autres protéines des thylacoïdes sont caractérisées par une répartition spécifique. Toutefois, jusqu'à aujourd'hui, aucune description exhaustive de la distribution des protéines dans les sous-compartiments des thylacoïdes n'a jamais été réalisée. L'objectif principal de cette thèse a été de determiner la sous-localisation spécifique (*i.e* BBY et lamelles stromales) des protéines des thylacoïdes en utilisant une approche d'analyse proteomique semi-quantitive. Pour intégrer cette étude, nous nous somme ensuite focalisés sur la réponse des plantes à la stimulation lumineuse. À une échelle de temps courte (environ 10 minutes), le phénomène de transition d'état permet de faire migrer une partie (15-20%) des antennes associées au PSII (enrichi dans les granas) vers le PSI (enrichi dans les stroma-lamellae) en permettant une redistribution de l'énergie d'excitation entre les deux types de photosystèmes. Avec la même approche décrite ci-dessus (protéomique différentielle), nous avons ainsi essayé d'identifier de nouveaux acteurs, autres que les antennes collectrices, impliqués dans les transitions d'état.

En parallèle, un autre projet développé au cours de ma thèse, a concerné l'étude de la réponse des plantes au stress lumineux (forte lumière). En particulier, nous nous sommes intéressés au mécanisme de dissipation thermique de l'énergie lumineuse absorbée appelé *quenching non-photochimique* ou NPQ (non photochemical quenching). Sous des conditions de lumière importante, l'absorption d'énergie lumineuse peut être supérieure à celle que les réactions

avales peuvent utiliser. Dans les cas où l'énergie lumineuse absorbée par les photosystèmes dépasse les capacités du métabolisme photosynthétique, l'accumulation des protons dans le lumen provoque une diminution du pH. Cette acidification entraine une augmentation de la dissipation thermique de l'énergie excédentaire au niveau du PSII (quenching non photochimique ou NPQ). Le NPQ est composé d'au moins trois composants, le *(i)* quenching de photoinhibition (appelé qI) qui correspond à une inactivation des protéines du PSII, le *(ii)* quenching de transition d'état (appelé qT) décrit ci-dessus et le *(iii)* quenching énergétique (appelé qE) qui est un mécanisme initié par la chute du pH du lumen. Toutefois, même si dans les plantes, la partie qE représente l'élément du NPQ le plus important, l'activation de ce mécanisme n'est pas constitutive et nécessite la formation d'un gradient de pH entre le stroma et le lumen des thylacoïdes (ΔpH). L'objectif de l'étude a été de clarifier les aspects qui contrôlent la formation de cette différence de pH.

Deciphering thylakoid sub-compartments using a mass spectrometry-based approach

L'article présenté au chapitre 2 (*Tomizioli et al., 2014*) représente le résultat le plus important de mon projet de doctorat. Il constitue la suite d'une étude précédente, réalisée dans notre laboratoire, qui a visé à la caractérisation proteomique de sous-compartiments (enveloppe, stroma et thylacoïdes) du chloroplaste chez *Arabidopsis thaliana*. Le travail présenté dans l'article est caractérisé par un très haut niveau de résolution puisqu'il a concerné deux nouveaux sous-compartiments de thylacoïdes : les grana-BBY et les lamelles stromales. Dans ce but j'ai donc développé des protocoles de purification des sous-compartiments des thylacoïdes (granas et lamelles stromales) à partir de chloroplastes de plantes sauvages d'*Arabidopsis thaliana*. Ensuite, grâce à une approche d'analyse protéomique semi-quantitative, nous avons pu déterminer la localisation d'environ 300 protéines des thylacoïdes. Les résultats suggèrent que la localisation des complexes photosynthétiques est beaucoup plus dynamique que celle jusqu'alors proposée. En effet, même s'ils sont préférentiellement identifiés dans un sous-compartiment, certains complexes photosynthétiques présentent une double localisation qui était inattendue. De plus, la composition en sous-unités de ces complexes diffère selon leur localisation, dans les granas et dans les lamelles stromales, suggérant l'existence de processus de régulation de la photosynthèse jusqu'alors insoupçonnés. Cette approche a ensuite été appliquée sur des plantes mutantes

d'*Arabidopsis* affectées dans les transitions d'état afin d'effectuer une analyse protéomique différentielle et identifier des protéines pouvant être impliquées dans ce processus d'adaptation. Les résultats préliminaires ont permit d'identifier environ 80 nouveaux candidats dont la localisation dans les sous-compartiments des thylacoïdes pourrait être régulée par la lumière (via un contrôle redox) lors des transitions d'état.

A Thylakoid-Located Two-Pore K^+ Channel Controls Photosynthetic Light Utilization in Plants

L'article présenté au chapitre 4 (*Carraretto et al., 2013*) fait partie d'une collaboration entre notre laboratoire et celui dirigée par Mme Ildiko Szabo à l'Université de Padoue (Italie). Le projet de recherche a concerné la caractérisation d' un canal putatif pour le potassium (appelé TPK3). TPK3 appartient à la famille des canaux TPK (Two-pore K^+) et est homologue à la protéine SYNK, un canal sélectif pour le K^+ identifié chez les cyanobactéries. Ce dernier serait impliqué dans la regulation de la photosynthèse chez les cyanobactéries car les mutants *synk* présentent un phénotype de photosensibilité Compte tenu du rôle de SYNK chez les cyanobactéries, il a été proposé que TPK3 pourrait jouer un rôle similaire chez les plantes supérieures. Jusqu'à présent, rien n'était connu sur les caractéristiques de TPK3, son rôle physiologique, ni sur son éventuelle implication dans la photosynthèse chez les plantes. Après avoir effectué des études de localisation subcellulaire (réalisées avec des techniques de biochimie et de microscopie confocale), le canal TPK3 a été exprimé dans *E. coli* pour le caractériser biochimiquement (techniques d ?électrophysiogie). De plus, des plantes qui n'expriment plus la protéine TPK3 ont été obtenues grâce à des techniques d'interférence par l'ARN (ou RNAi) et utilisées dans des conditions de croissance différentes pour déterminer le rôle de TPK3 *in vivo*. Grâce à des approches biophysiques et biochimiques, nous avons ainsi démontré que TPK3 est impliqué, chez *Arabidopsis*, dans la modulation des deux composantes de la force proton motrice (pmf), le gradient de pH (ΔpH) et la différence de potentiel ($\Delta\Psi$). En contrôlant la répartition de la force proton motrice, TPK3 contrôle aussi la formation du NPQ et permet ainsi une utilisation correcte de la lumière en dissipant l'excès d'énergie et en évitant ainsi que la chaîne photosynthétique ne soit endommagée.

Chapter 1

Introduction

1.1 The plant cell

Green plants (*Viridiplantae* in Latin), are multicellular eukaryotes of the kingdom *Plantae*. When compared to animal cells, plant cells are characterised by some distinctive features (figure 1.1)

— The cell wall, which surrounds the cell. It is composed of cellulose and hemicellulose, pectin and in many cases lignin.
— The vacuole, which is filled with water (and other organic/inorganic molecules) and it is used by the cell to maintains its turgor.
— The plastids, which are specialized organelles and site of biosynthesis and storage of important chemical compounds used by the cell.

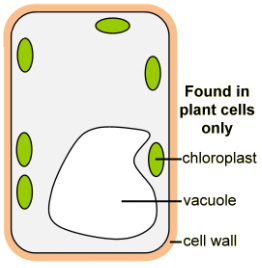

Figure 1.1 – Schematic representation of a plant-cell with its key features. Adapted from `http://www.bbc.co.uk/schools/gcsebitesize/science/`

In plants, plastids may differentiate into several forms such as chloroplasts (to host photosynthesis in green tissues), chromoplasts (for pigment synthesis and storage) or amyloplasts (for starch storage). Among plastids, the chloroplast is the most notable, and represents the subject for this thesis work.

1.2 The Chloroplast

Chloroplast is a major component of plant cells. It likely originated from a cyanobacterial symbiont about 1.5 billion years ago [1][2] and became fully integrated into the life cycle of the photosynthetic eukaryote host. In seed plants, chloroplasts develop from proplastids, these latter being non-photosynthetic. Proplastids are transmitted between generations through the ovule and are maintained in meristematic stem cells. More than 95% of the ancestral cyanobacterial genes were transferred to the host cell nucleus [3][4][5][6], where precursor proteins are encoded. They are synthesised in the cytosol thanks to the 80S ribosomes, and subsequently imported into the chloroplast [7][8]. Not all the chloroplast proteins are encoded in the host nuclear genome since some few key genes (around 100) are still present in the plastid genome and are translated using the 70S prokaryotic type ribosomes [9]. Thanks to structural studies (mainly based on electron microscopy) and biochemical analysis, three main sub-compartments of the chloroplast have been identified: *(i)* the envelope, *(ii)* the stroma and *(iii)* the thylakoids (figure 1.2).

1.2.1 Envelope

The envelope is the membrane network that surrounds the chloroplast. In *viridiplantae*, the chloroplast is surrounded by a two-membrane system: the outer envelope membrane (OEM) and the inner envelope membrane (IEM) membranes. The inner envelope membrane provides a selective barrier between the chloroplast stroma and the cell cytosol and represents, together with the outer envelope membrane, the minor chloroplast component in terms of protein content (containing only $\sim 1\%$ of the total chloroplast proteins). Envelope membranes are a very lipid-rich structure compared to mitochondrial membranes and this confers to the envelope membranes a low density [11]. Hence, envelope possesses several polar neutral lipids containing galactose and called galactolipids [12]. The outer envelope membrane is enriched

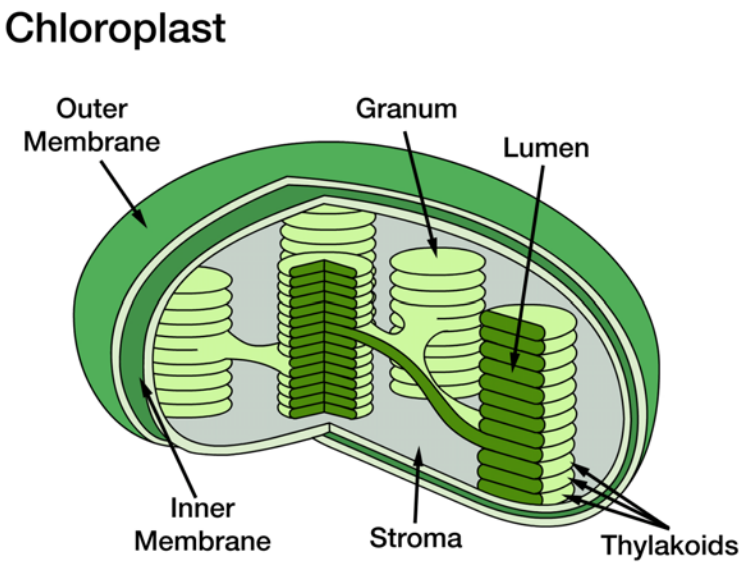

Figure 1.2 – Schematic representation of chloroplast structure and of its membrane composition.

in DGDG (digalactosyl-diacyl-glycerol), whereas the main glycerolipid constituent of the inner envelope membrane is MGDG (monogalactosyl-diacyl-glycerol). The envelope is the site of specific biosynthetic functions like the *(i)* synthesis of plastid membrane components (glycerolipids, pigments and prenylquinones), *(ii)* synthesis of lipid-derived signaling molecules (fatty acid hydroperoxydes, growth regulators, or chlorophyll precursors)(for a review, see [13]) and *(iii)* chlorophyll breakdown. Moreover, the envelope regulates fluxes of ions, proteins and metabolites between the cytosol and the stroma. Import of nuclear encoded proteins into the organelle is mediated by hetero-oligomeric protein complexes in the outer and inner envelope membranes that surround each plastid. These complexes are called TOC and TIC (for *T*ranslocon at the *O*uter/*I*nner envelope membrane of the *C*hloroplast) [10][14][15][16]. Except for the proteins localised to the outer envelope membrane, interaction of protein passenger to the translocation machinery is generally mediated by a signal called the transit peptide. Once a preprotein has been translocated into the stroma, the transit peptide is proteolytically cleaved by the stromal processing peptidase (SPP), allowing the mature protein to get its functional conformation or to engage further targeting to the thylakoid membranes. However, in the last few years, several studies have re-

vealed the existence of alternative targeting signals and import pathways [17]. Examples for this are TIC32 [18] or a protein homologous to the quinone oxidoreductases of bacteria, yeasts, and animals designated chloroplast-envelope quinone-oxidoreductase homolog, ceQORH [19][20].(for reviews see [7][8]).

1.2.2 Stroma

Stroma, somewhat analogous to the mitochondrial matrix, is the compartments devoted not only to the synthesis of different biomolecules (*e.g.* amino acids or fatty acids) but also to carbon fixation in a cycle of reactions known as the Calvin cycle. CO_2 diffuses into the stroma of chloroplast and combines with ribulose 1,5-biphosphate (a five-carbon sugar) [21]. The enzyme that catalyses this reaction is referred to as Ribulose-1,5-Bisphosphate Carboxylase/Oxygenase (commonly known by the abbreviation RuBisCO), a large complex that may be the most abundant protein on the Earth [22]. This reaction produces a 6-carbon intermediate which decays almost immediately to form two molecules of the 3-carbon compound 3-phosphoglyceric acid. The fact that this 3-carbon molecule is the first stable product of photosynthesis leads to the practice of calling this cycle the C_3 cycle. In *Arabidopsis thaliana* (from now on, referred to as *Arabidopsis*) as in others C_3 plants, photosynthesis, carbon fixation and Calvin cycle all occur in a single chloroplast.

1.2.3 Thylakoids and their biogenesis

The term thylakoids indicates the chloroplast internal membrane network which hosts the light-phase of photosynthesis (see section 1.3 at page 24 and fig.1.3). Thylakoid membranes form a physically continuous three-dimensional network that encloses a single aqueous space, the thylakoid lumen [23].

Thylakoid biogenesis requires the coordinated assembly of lipids, proteins, and chlorophylls, which together account for >98% of the mass of the thylakoid membrane [24]. Within the proplastid, the thylakoid membrane system is much simpler than that found in a mature chloroplast. In the absence of light, the proplastid matures into an etioplast, whose inner membrane forms a semi-crystalline network of interconnected tubules called prolamellar body [25]. During exposure to light, prolamellar body loses its semi-crystalline structure and the extruded lamellae align in parallel throughout the stroma. The transformation of the semicrystalline prolamellar body into planar thylakoids can take from 1 hour to over a day (the

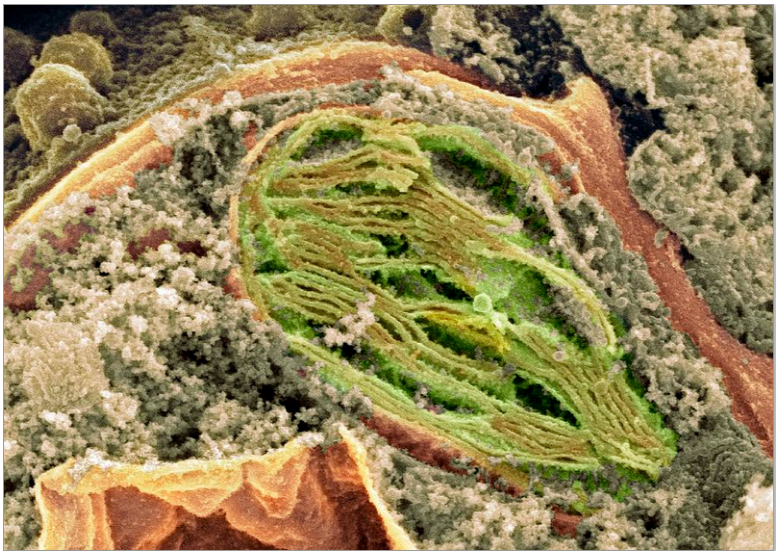

Figure 1.3 – Coloured scanning electron micrograph (SEM) of a section through a plant cell, showing a fractured chloroplast. Photographed by Dr. David Furness, Keele University.

whole process is reviewed in [26]). Thylakoids contain five major lipids : monogalactosyl-diacyl-glycerol MGDG, digalactosyl-diacyl-glycerol DGDG, sulpho-quinovosyl-diacyl-glycerol SQDG and phosphatidyl-glycerol PG (in a ratio of around 17:9:5:1) [27][28]. Thylakoid biogenesis is also influenced by the insertion of protein complexes into the lipid bilayer. In fact, the vast majority of the thylakoid surface is occupied by protein complexes, which account for 70% of the total membrane area [27].

1.3 Oxygenic photosynthesis

Photosynthesis is the process used by some organisms (*i.e.* plants, algae and some bacteria) to convert light energy into reducing power and energy to fix carbon dioxide (CO_2). Onset of photosynthesis was a milestone in the process of evolution and still supports life on earth. The entire process can be represented schematically by equation 1.1:

$$6\,CO_2 + 6\,H_2O \xrightarrow{\text{Light}} C_6H_{12}O_6 + 6\,O_2 \tag{1.1}$$

Photosynthesis comprises two different phases; they are usually referred to as the light-dependent and the light-independent phases (even though, in this latter, light is needed to activate RuBisCo through RuBisCo activase). In the light dependent phase, solar energy is used to generate an excited state in a chlorophyll molecule. This is used to transfer electrons along a chain of redox reactions and to generate reducing power (in the form of NADPH). At the same time, a proton gradient is built across the photosynthetic membranes, which is used for the synthesis of ATP. Light-dependent reactions are performed by a set of multi-protein complexes localised in the photosynthetic membrane: photosystems I and II (with their light harvesting complexes), cytochrome b_6f and ATP synthase. The products of the light-dependent reaction are subsequently used to sustain cellular metabolism during the light-independent phase (*i.e* the Calvin-cycle, see section 1.2.2 at page 22).

1.3.1 The Z-scheme

The Z-scheme describes how electrons generated by light are shuttled from water to $NADP^+$ in a linear electron transport chain within the photosynthetic membrane. According to this scheme, electrons are transferred from a donor (reductant) to an acceptor (oxidant). The direction of that transfer is established by the difference in redox potential between a given donor and acceptor (figure 1.4), going spontaneously from the more negative to the positive values. A more positive potential implies stronger oxidative power (*i.e.* capacity to accept electrons). A more negative potential implies stronger reducing power (*i.e.* capacity to donate electrons).

In the early phase of photosynthesis, photons are captured by specific proteins (the light-harvesting complexes LHCI and LHCII) of the PSII and PSI and transferred to their reaction centers (P680/P700 respectively), where charge separation occurs. This is a very fast reaction occurring in a few picoseconds (10^{-12}s) and is the only step where light energy is converted to chemical energy since the rest of the steps are downhill energy-wise. As it

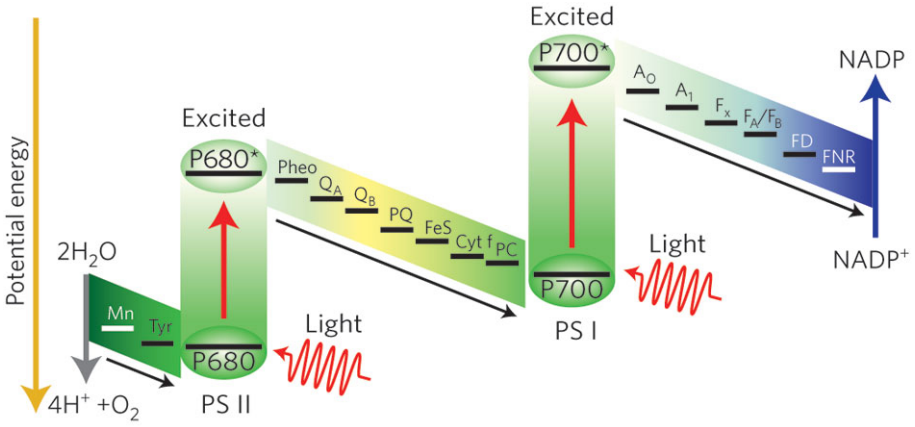

Figure 1.4 – The Z-scheme of photosynthetic electron transfer chain and of various redox processes. The name comes from the fact that it was first drawn in the form of the letter *Z* in the older literature. Currently, it is being drawn to emphasize the energy levels of the components and it has been turned 90 degrees counterclockwise. Image from Tachibana et al., Nature Photonics 2012.

will be detailed later (sections 1.4.1, 1.4.2, 1.4.3 and 1.4.4), excited P680* transfers an electron to the primary electron-acceptor molecule, pheophytin (Pheo), which is a modified chlorophyll molecule lacking the Mg coordinating atom. This electron is then transferred through a chain of membrane transporters constituted of plastoquinones molecules to finally reduce plastocyanin (a mobile copper-containing protein) via the cytochrome b_6f complex. $P680^+$ recover to P680 in a few millisecond time scale by receiving an electron from a water molecule. In parallel, excited P700* transfers an electron to A_0 (a chlorophyll *a* monomer) and oxidises plastocyanin. The electron is subsequently transferred to $NADP^+$ via several other intermediates (*i.e.* phylloquinone, ferredoxin, ferredoxin-$NADP^+$ reductase FNR). Electron transfer is associated to the transfer of protons across the photosynthetic membrane promoting the instauration of a gradient of pH (ΔpH). This ΔpH contributes to the formation of an electrochemical proton motive force (*pmf*) which is used by the ATP-synthase enzyme to synthesize ATP using ADP and inorganic phosphate (P_i). In the next section, the function of the major maxi-complexes involved in the Z-scheme is discussed together with their subunits composition.

1.4 Major photosynthetic complexes

1.4.1 Photosystem I

Photosystem I (PSI) catalyses the electron transfer from plastocyanin (PC) on the lumenal side of the thylakoid membrane to ferredoxin (Fd) on the stromal side. Electrons are then mainly used for the reduction of the $NADP^+$ via the ferredoxin-$NADP^+$ reductase (FNR). In higher plants, PSI consists of a large number of protein subunits. Among these, fifteen proteins are found to form the core-complex of the photosystem (PsaA to PsaL and PsaN to PsaP) and at least four proteins form the light-harvesting apparatus. The antenna complex of plant photosystem I consists of the closely related Lhca proteins (Lhca1-4) which bind to the reaction center with varying stoichiometries depending on light conditions and other environmental factors [30]. Each of these Lhca proteins possesses approximately 15 chlorophyll (*a* and *b*) molecules. X-ray crystallography studies of PSI-LHCI supercomplexes showed how the four Lhca antenna proteins are assembled with the PSI core complex as two heterodimers; Lhca1-Lhca4 and Lhca2-Lhca3 (fig.1.5B) [29][31]. These two dimers associate in series to form a half-moon shaped belt at the PsaF side of the reaction center. Chlorophyll molecules positioned at the contact regions between the Lhca monomers ensure rapid energy transfer along the antenna belt itself.

Subunits PsaA, B and C constitute the core complex of the PSI and they are highly conserved in all the organisms (figure 1.5). PsaA, B and C directly bind the following electron transport cofactors: P700, A_0, A_1, F_X, F_A and F_B. P700 is the primary electron donor, it consists of a Chl a/a homodimer which is oxidised by the light-induced charge separation. P700 donates an electron to the primary electron acceptor A_0 which is a chlorophyll *a* monomer. Electrons are then transferred to the phylloquinone A_1 and then to ferredoxin via the three 4Fe4S clusters F_X, F_A and F_B (figure 1.5). F_X is bound to PsaA/PsaB heterodimer while F_B and F_A are bound to the extrinsic subunits PsaC. PsaC is highly conserved within the organisms and lack of PsaC in *Chlamydomonas reinhardtii* results in complete destabilization of the PSI complex, which does not accumulate [32].

PsaD and PsaE are hydrophilic subunits, which are exposed to the stroma and are bound to the PsaC subunits. PsaC, PsaD and PsaE constitute the so-called *stromal ridge* of PSI and these proteins do not contain any transmembrane parts. PsaE and PsaD probably provide the docking site for soluble ferredoxin on the stromal side of the thylakoid membrane [35]. Mutants which do not express PsaE are found pale green, high fluorescing

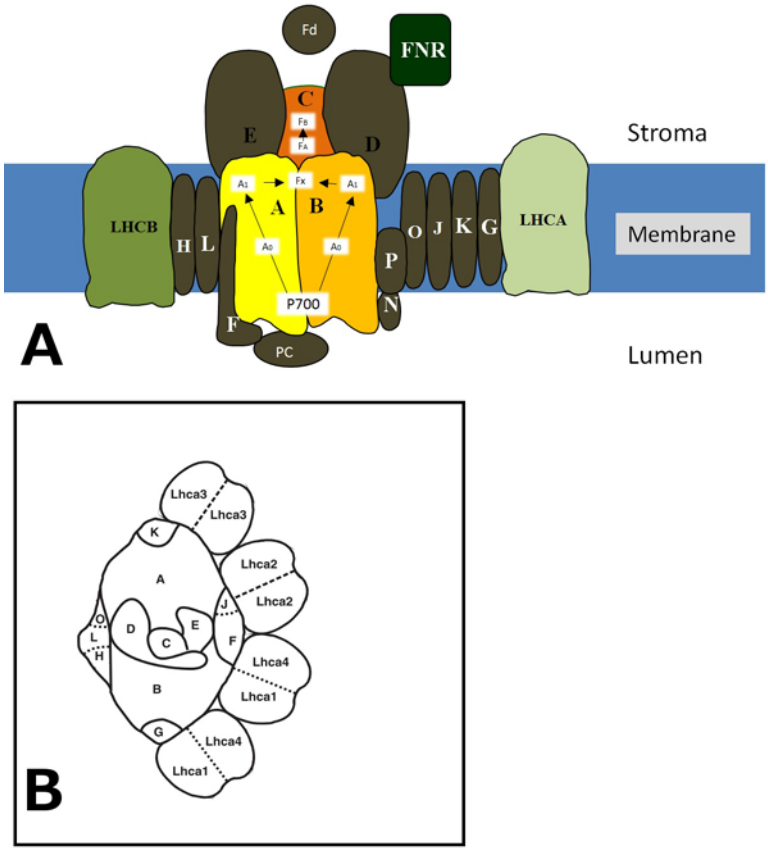

Figure 1.5 – (A) Illustration of the structure and subunit composition of PSI of higher plants. The peripheral and soluble proteins of PSI shuttle electrons to $NADP^+$, thereby reducing it to NADPH. The proton required for this reaction comes from the stroma compartment. (Arrows) Electron transfer pathway from plastocyanin (PC) to ferredoxin (Fd) reduction (see text). Subunit H act in the docking of LHCII to PSI during state transitions. Image was adapted from *Choquet et Vallon* [33] (B) Schematic figure of plant photosystem I viewed from the stromal side. PsaN is located on the lumenal side and is not visible in this schematic figure. Image from *Jensen et al., 2007*

and susceptible to photoinhibition (see section 1.6.1.3 at page 42) with a growth rate reduced of 50% [36].

PsaG and PsaK are two small intrinsic membrane proteins of approximately 10-11 kDa with two transmembrane α-helices connected by a stromal-exposed loop [37][38]. PsaG is unique to higher plants and algae while PsaK

is also present in cyanobacteria. Within the PSI complex, PsaK is bound to PsaA while PsaG is bound to PsaB at a roughly symmetry-related position [39]. Removal of PsaK in plants using either antisense or gene knock-out technology demonstrated that this subunit is involved in binding of Lhca2 and Lhca3 [40][41][42]. In contrast to this, plants devoid of PsaG have a 20-40% reduction of PSI content but an unaffected functional antenna size of the remaining PSI [41][42], suggesting that PsaG affects stability of the PSI complex but is not strictly needed for binding of Lhca1 and Lhca4.

PsaF is a membrane protein of about 18 kDa and plays a role in the docking of plastocyanin [43]. Plants lacking PsaF are severely affected in the energy transfer from LHCI to PSI. Thus, although Lhca1 and Lhca4 remain in the PSI complex, they cannot transfer energy to the reaction center in the absence of PsaF. This suggests that PsaF in LHCI-containing plants and green algae should have regions optimized for interaction with LHCI. Phenotype of *Arabidopsis* lacking of this subunit results in tiny plants which grow very slowly [44].

PsaH is a 10 kDa PSI subunit which was only found in green plant and algae. PsaH was demonstrated to be involved in state transitions (see section 1.6.1.2 at page 41 of this PhD thesis for a description of this phenomenon) since plant devoid of this subunit are insensitive to change in the spectrum composition of light [45][46]. It was proposed that PsaH form the binding site for the interaction between phosphorylated LHCII (P-LHCII) and PSII. In normal growing condition, plants which lack PsaH subunit display no clear phenotype and the deficiency in PsaH is compensated by a larger accumulation of PSI. This compensation is sufficient to enable proper growth in mutants.

PsaL, which was not reported in green algae, is an integral membrane protein found in plants and cyanobacteria of about 18 kDa. Results from plant-mutants in which this subunit was downregulated indicated a parallel decrease also in the PsaH subunit. Therefore, it was proposed that, in plant, PsaL may play a role in the interaction with PsaH. Moreover, the presence of both PsaH and PsaL is mandatory for the binding of the 10 kDa extrinsic subunit PsaO [47].

PsaJ is a hydrophobic subunit of 6 kDa that is located close to PsaF [39]. PsaJ is characterised by a stroma-located N-terminus and a lumen-located C-terminus [35]. Tobacco plants with an inactivated *psaJ* gene are slightly smaller and paler than wild-type plants due to an approximate 20% reduction in PSI [48] content. The specific PSI activity measured as $NADP^+$ photoreduction *in vitro* revealed a 55% reduction in electron transport through PSI in the absence of PsaJ. Immunoblotting analysis revealed a secondary loss of the lumenal PsaN subunit in PSI particles devoid of PsaJ. Presumably,

PsaJ affects the conformation of PsaF which in turn modulates the binding of PsaN. Thus, PsaJ is an important subunit that together with PsaF and PsaN is required for formation of the plastocyanin binding domain of PSI. PsaJ is furthermore important for the stability and/or assembly of the PSI complex.

1.4.2 Photosystem II

PSII is a thylakoid multisubunit complex which is found within all types of plants, algae and cyanobacteria. It functions as a light energy-driven water-plastoquinone oxidoreductase. At the moment, 20 subunits have been identified, and are referred to as intrinsic and extrinsic subunits (fig.1.6).

PSII reaction center (RC) consists of two homologous intrinsic proteins, D1 and D2, and two intrinsic chlorophyll-containing proteins (CP43 and CP47). Moreover, several extrinsic proteins are associated to the lumenal side of the RC in order to protect it from the catalytic site of water splitting. This catalytic site consists of four mixed valence manganese ions, a calcium ion, and five oxo ligands (the Mn_4CaO_5 cluster). Optimised light absorption is guaranteed by an outer light-harvesting system (LHCII) which is composed, in the case of higher plants, of intrinsic Lhcb proteins. Photons are captured by chlorophylls and β-carotene and transferred to the special form of chlorophyll *a* (P680) contained in the RC. Chlorophyll excitation produces the high reducing species $P680^-$ which, in turn, donates an electron to a pheophytin *a* molecule (as mentioned above pheophytin is a chlorophyll molecule lacking of the Mg^{2+} ion). At this point, the radical pair $P680^+Pheo^-$ is formed. The cationic state $P680^+$ of Chl *a* in the RC of PSII extracts an electron from water via an intervening amino acid residue *tyrZ*(within D1) and the manganese cluster. In parallel $Pheo^-$ reduces a firmly bound plastoquinone molecule (Q_A) which in turn reduces a second plastoquinone (Q_B) to form Q_B^-. A second photochemical turnover reduces Q_B^- to Q_B^{2-} which is protonated to generate plastoquinol (PQH_2). The latter diffuses into the lipid bilayer in order to reduce the cytochrome b_6f complex.

PSII intrinsic subunits CP47, CP43, D1, D2 and cytochrome b_{559} are required for proper oxygen evolution [51][52][53]. However, it was observed that maximal oxygen evolution rate was reached only when the three additional extrinsic subunits are also present: PsbO, PsbP and PsbQ. PsbO is a protein particularly conserved across the higher plants, algae and cyanobacteria. Numerous investigations were carried out in order to elucidate its role and data have shown that this subunit is essential for efficient and stable oxygen evolution [54][55]. In *Arabidopsis*, two genes encode for the PsbO-1 and

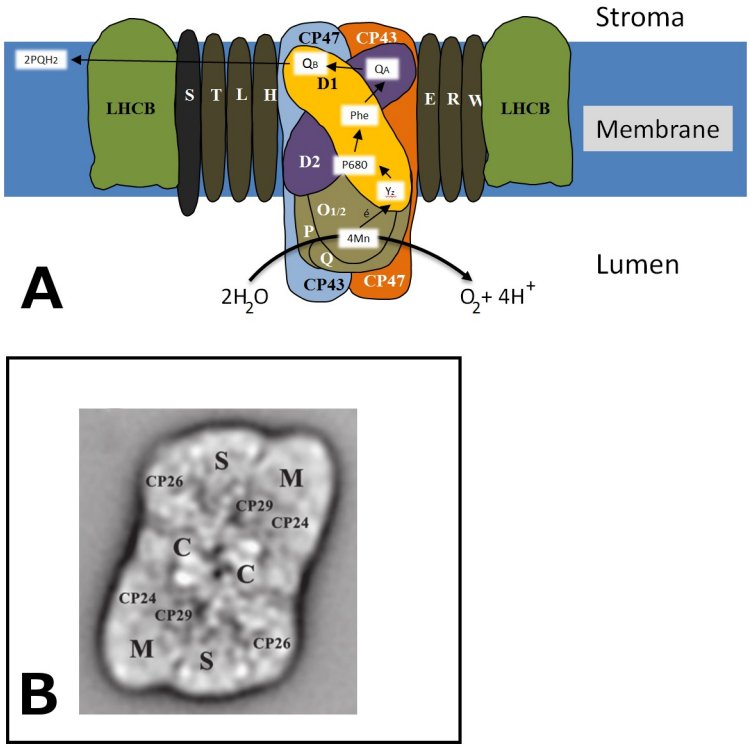

Figure 1.6 – (A) Illustration of the structure and subunit composition of PSII of higher plants. The enzymatic heart of the complex comprises two polypeptides known as the D1 and D2 proteins. The special pair, P680, is found between these proteins. The pheophytin and Q_A are found on the D2 protein, and the redox-active tyrosine, Y_Z, and the Q_B plastoquinone are found on the D1 protein. (Arrows) Electron transfer pathway from water oxidation to plastoquinone reduction (see text). Image was adapted from *Choquet et Vallon* [33] (B) Top view projection maps of the PSII-LHCII C2S2M2 supercomplexes from *Arabidopsis*. Images from E. J. Boekema [50].

PsbO-2 isoforms which differ for 11 amino acids [56]. It was proposed that these two isoforms could perform separated functions. The primary function of the PsbO-1 protein would be to support the normal oxygen evolution and the PsbO-2 protein principally would act to regulate the phosphorylation state and turnover of the D1 protein [57]. PsbP and PsbQ are two extrinsic proteins which are found in PSII of higher plants (their counterpart in cyanobacteria are PsbU and PsbV). They are known to modulate the calcium and chloride requirement for oxygen evolution [58]. Recently it was

suggested that the lack of PsbP might affect the supramolecular organization of PSII. In fact, when RNA interference was used in order to silence *PSBP* gene expression, a severe decrease in the amount of PSII-LHCII supercomplex and a significant increase of the free LHCII trimers were observed [59]. Genomic and proteomic studies using model plant species pointed out several homologs for both PsbP and PsbQ and this indicates that massive gene duplication has occurred in parallel with the acquisition of PsbP and PsbQ in PSII [60]. There are two PsbP-like proteins (PPL1/2), seven PsbP-domain proteins (PPD1/7), and three PsbQ-like proteins in *Arabidopsis* and in *Oryza sativa* (rice) [61]. Moreover, these PsbP/Q-like proteins are not associated to the LHCII-PSII but rather to the lumenal side of the chloroplast NAD(P)H dehydrogenase (NDH), a complex involved in cyclic electron transport around PSI (see section 1.4.5 at page 34). The antenna complex of the photosystem II is mostly trimeric and consists of different combination of the Lhcb1-3 proteins. Based on sequence similarity, all members of the Lhc family are thought to have a similar structural arrangement [62] and Lhcb1 and Lhcb2 are the predominantly expressed isoforms (90%) [63]. Each LHCII trimer binds 42 chlorophyll molecules and 12 carotenoids; these latter play a mostly photoprotective role [64]. A frequently isolated PSII-LHCII assembly is the so-called C_2S_2 supercomplex; it is composed of a dimeric PSII core (C_2) and two strongly bound LHCII trimers S_2. In addition, the complex contains two copies of each minor antenna proteins CP26 and CP29, which mediate the association of the two LHCII trimers to the complex. In *Arabidopsis*, the C_2S_2 supercomplex is usually supplemented by two CP24 proteins, which promote the docking of two additional moderately bound LHCII trimers (M-trimers) (figure 1.6B) [39].

1.4.3 Cytochrome b_6f

Cytochrome b_6f provides the electronic connection between the two photosystems and contributes to the generation of the transmembrane proton electrochemical potential that drives ATP synthesis. It can be described as a symmetric dimer complex made of 8 different subunits and 7 prosthetic groups. Its molecular weight is 220 kDa (as dimer) and it is the plastidial (and cyanobacterial) counterpart of the bacterial cytochrome bc_1. There are four core subunits: *(i)* cytochrome b_6 (PetB), *(ii)* cytochrome f (PetA), *(iii)* subunit IV (PetD) and *(iv)* the Rieske-type iron sulfur protein (ISP or PetC) (figure 1.7). Crystal structures of cytochrome b_6f complexes are available for the green algae *Chlamydomonas reinhardtii* [65] and the thermophilic cyanobacterium *Mastigocladus laminosus* [66]. Cytochrome b_6f catalyses the

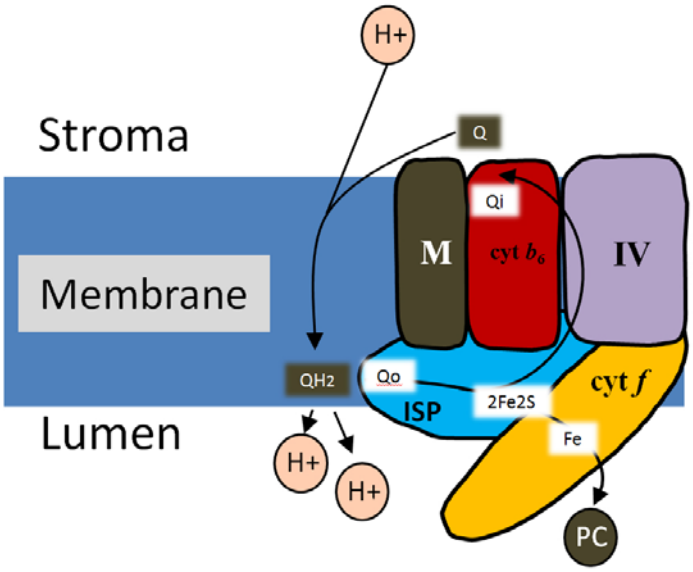

Figure 1.7 – Illustration of the structure and subunit composition of cyt b_6f. Quinol oxidation occurs in a bifurcated reaction, in which one electron is transferred to a high potential chain and the other to a low potential chain. Image was adapted from *Choquet et Vallon* [33]

transfer of electrons from plastoquinol to plastocyanin, while pumping two protons from the stroma into the thylakoid lumen. This reaction is described by the Q-cycle in which plastoquinol (PQH_2), that interact with cytochrome b_6f at the Q_o site (lumenal), is oxidised in two steps. A first electron is transferred to the so called *high potential electron transfer chain* that contains the [2Fe-2S] cluster and cytochrome *f*. Two protons are translocated in the lumen phase of the thylakoids at this stage (figure 1.7). The second plastoquinol electron is forced to flow through the second low-potential electron transfer chain (called *low potential* one). After two consecutive cycles, a molecule of plastoquinone is reduced on the stromal side of the membrane at the Q_i (stromal) site of the complex. Therefore, for each molecule of PQH_2 oxidised, one electron is recycled back to the plastoquinone pool. Finally, cytochrome b_6f couples the transport of two protons into the thylakoid lumen per electron transferred.

Cytochrome b_6f is also involved in signaling within state transitions (see section 1.6.1.2 at page 41) as it acts as the primary sensor triggering activation of a specific kinase that phosphorylates the light-harvesting proteins

LHCII a in redox-regulated manner. Indeed, characterisation of mutants lacking the cytochrome b_6f complex have shown that the cytochrome b_6f is required for kinase activation [67][68]. The model for kinase activation implicates plastoquinol binding to the Q_o site and the movement of the Rieske ISP (PetC) [69]. This generates an activating signal, which is transduced from the luminal side of the membrane, where the Q_o site is located, to the stromal side, where LHCII phosphorylation takes place (see section 1.6.1.2 at page 41).

1.4.4 ATP synthase

ATP synthase (also referred to as ATPase) complex is ubiquitous in all living organisms where it is used to synthesise ATP thanks to the dissipation of a chemiosmotic gradient generated across the biological membrane. The ubiquitous distribution of ATP synthase has prompted the suggestion that this complex was present in the last common ancestor of *Archaea* and *Bacteria* [70]. In thylakoid membrane, photosynthetic electron flow is coupled to synthesis of ATP (fig. 1.8) by the following processes:

- Oxidation of water, which gives electrons to P680 and releases proton into the lumen.
- Reduction of plastoquinone to plastoquinol ($PQ \longrightarrow PQH_2$) since two protons are picked up from the stroma at the same time. These two protons are subsequently released into the lumen when reduced Q_B (PQH_2) is oxidised by the cyt b_6f complex.
- Q-cycle of the cytochrome b_6f level since every two turnovers, two electrons are recycled back to the plastoquinone pool which takes protons from the stroma and reduces again cytochrome b_6f.
- Reduction of the $NADP^+$ which involves the uptaking of protons from the stroma with further increase of the gradient across the membrane.

In chloroplasts, the ATP synthase comprises nine different subunits arranged in two subcomplexes. The first one, named CF_0 is embedded in the thylakoid membranes and is responsible for proton translocation across the thylakoid membrane into the stroma. The second, CF_1 is the extrinsic catalytic part and it is exposed to the stroma (figure 1.8). ATP production (or hydrolysis) occurs at the level of this latter. CF_1 consists of five subunits namely α, β, γ, δ and ϵ which are assembled in a 3:3:1:1:1 stoichiometry. Since electrochemical potential is converted into mechanical work by the CF_0 subcomplex, CF_1 cannot catalyze ATP synthesis when it is detached from CF_0. CF_0 is composed of four subunits designated I, II, III, and IV. Whereas subunits I, II, and IV are present in single copies, subunit III is an oligomer

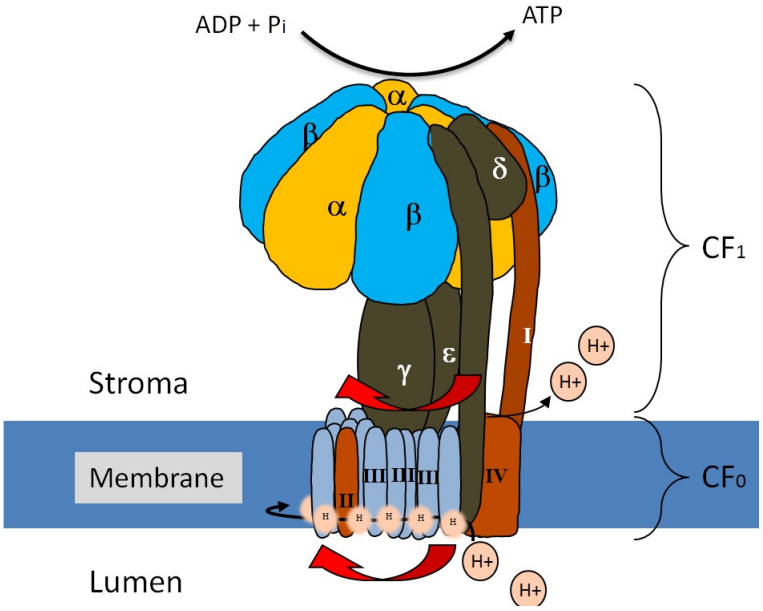

Figure 1.8 – Illustration of the structure and subunit composition of ATP-synthase of higher plants. According to the current model, the passage of protons across the membrane (via the F_0 region) drives the synthesis of ATP (Arrows). Image was adapted from *Choquet et Vallon* [33]

arranged in a ring-like structure. Stoichiometry can vary between 10 to 15 monomeric units according to the species with spinach CF_0 containing 14 monomers [71].

1.4.5 NAD(P)H-dehydrogenase

Chloroplast NAD(P)H-dehydrogenase (NDH) is proposed to play a key role in one of the two main pathways involved in the cyclic electron flow (CET) around PSI. In cyclic electron flow, electrons generated by PSI at its stromal side are reinjected into the plastoquinone pool to ultimately reduce cyt b_6f and $P700^+$. Cyclic electron flow provides ATP synthesis without a net production of NADPH, and it is therefore likely required to meet proper ATP demand (for a review see [72]). NDH-dependent pathway is essential in plant during stress conditions since it seems to participate in protection against oxidative stress by preventing over reduction of the stroma [73]. Historically,

the discovery of the NDH complex was performed thanks to the identification of plastid genes that were homologs of genes encoding for the subunits of mitochondrial complex I [74]. At the moment, the only available crystal structure of the complex is the one arising from bacterial NDH-1 [75]. Nevertheless, electron microscopy (EM) studies are available on cyano-bacteria and plant NDH. They show that this complex has an L-shaped structure similar to the bacterial NDH-1 [76]. NDH was demonstrated to interact with PSI and detailed studies were carried out showing that two copies of PSI can be associated to NDH via two minor light-harvesting antenna proteins, Lhca5 and Lhca6 [77] (figure 1.9).

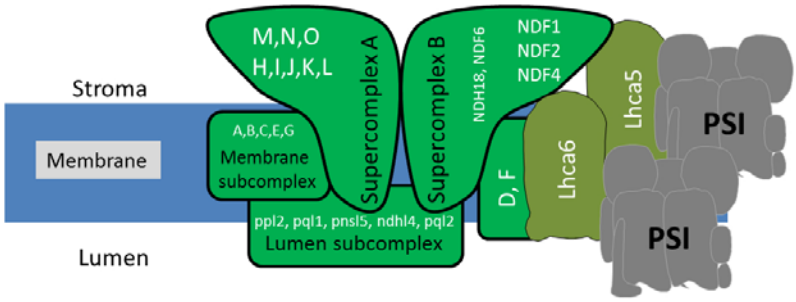

Figure 1.9 – Illustration of the hypothetical structure and subunit composition of NDH complex of higher plants. Image was adapted from *Choquet et Vallon* [33].

On the basis of the analogy with *E.coli* NDH-1, chloroplast NDH complex is considered to be divided into four subcomplexes: the *(i)* membrane subcomplex (subunits NdhA/F) which is well conserved in the various types of NDHs, *(ii)* subcomplex A (NdhH-O), *(iii)* subcomplex B (subunits NDF1-2-4-6(NDFH6) and NDH18(PNSB5)) and the *(iv)* lumen subcomplex (figure 1.9). This latter subcomplex is mainly constitute of PsbP-Q-like proteins. These proteins are homologous to PsP and PsbQ subunits of the oxygen-evolving complex (see section 1.4.2). PPL1 (PsbP-like-1 protein) was proposed to be involved in the efficient repair of PSII, while PPL2 (PsbP-like-2 protein) is probably required for the activity of the NDH complex [78]. Moreover three PQLs (PsbQ-like proteins) are also found to colocalise with NDH by mass analysis of the NDH-PSI supercomplex [77][79] and demonstrated to be necessary for the accumulation of the NDH complex [78][79][80].

1.5 Lateral heterogeneity of the photosynthetic complexes

As mentioned above, thylakoid membranes within a chloroplast form a continuous three dimensional network characterised by an extensive folding. As consequence, the thylakoid membranes of plants and some green algae are structurally inhomogeneous. They consist of two main sub-domains: *(i)* the grana, which are stacks of thylakoids and *(ii)* the stroma lamellae, which are unstacked membranes and connect the grana stacks. Moreover, within grana discs, we can furtherly identified the BBY [1] region (which corresponds to the inner part of the disc) and the grana margins (see section 1.5.1 at page 38). The various photosynthetic complexes largely differ in their distribution in these sub-compartments of the thylakoid membrane and this characteristic is known as *lateral heterogeneity* [30][50][81][82][83]. While grana stacks are more enriched in PSII and LHCII, stroma-lamellae contain mostly photosystem I, LHCI and ATPase complexes. The location of the cytochrome b_6f is not well defined and this latter is generally assumed to be almost equally distributed among the stacked and unstacked regions of the thylakoid membrane [50].

The physicochemical forces that control the lateral segregation are not completely understood. For the major trimeric LHCII, models were proposed pinpointing electrostatic attraction between mutual positive and negative charges localised at stromal protein surfaces of adjacent LHCII complexes [84] as the major determinant for stacking between adjacent thylakoids. Taking in account the narrow intermembrane distance being only 3.5 nm [85], it has also been proposed that while the relative flat stromal surface of LHCII and PSII would allow them to stay in tightly stacked thylakoids, PSI and particularly ATP synthase would be excluded from stacked grana by steric hindrance because of their bulky protrusions on their stromal side [86][87]. Grana, which have the shape of a cylinder, are made of stacks of thylakoid membranes with a diameter of 300-600 nm and are, on average, 4 nm thick [88]. The primary reason for the thylakoid membrane to form such stacked structure is unclear. Most likely, the main reason for making grana stacks is to increase the light harvesting capacity of the chloroplast, by concentrating a huge amount of structurally ordered antenna proteins within a rather small volume. Other reasons may include prevention of spillover of excitation energy between the two photosystems through physical separation of

1. the name BBY arises from the initials of the authors Berthold, Babcock and Yocum [146]

photosystems, fine-tuning of photosynthesis and switching between linear and cyclic electron flow [30][50][85][89][90][91][92][93].

The exact three-dimensional architecture of the grana is still debated and two main models are considered: the helical model and the fork or bifurcate model (for review [81][85]). In the helical model [94], thylakoids comprise a fretwork of stroma lamellae, which winds around grana stacks as a right-handed helix connecting individual grana discs via narrow membrane protrusions (figure 1.10). In the last revision of the model [95], it was suggested that the granum body constitutes a bipartite structure made of discs piled on top of each other, around which the stroma lamellae are wound as right-handed helices. By contrast, in the bifurcate model, the grana themselves are formed by a bifurcation of stroma-lamellae. In this conception, the granum, is composed of piles of repeated units, each one containing three grana discs. These latter are formed by symmetrical invaginations of a thylakoid pair caused by bifurcation of the thylakoid membrane [96] (figure 1.10). According to recent tomographic data, the helical description of the thylakoid structure seems to be the most correct one [97].

1.5.1 Grana margins

Thylakoid architectural organization is known to be largely affected by variation in the spectral composition and intensity of light. In fact, the thylakoid membrane turns out to be a highly flexible system which can quickly respond to changes in ambient light condition and vary its architectural organization. Low light conditions are well known for increasing the number of layers within the grana stacks [98], while high light intensities lead to significant reduction in the diameter, and to partial transversal unstacking of grana discs [99][100][101]. While some of these structural rearrangements could facilitate molecular photoprotective mechanisms such as the turnover of photodamaged D1 [101][102], other structural changes seem to occur as a consequence of the redistribution of protein components within the thylakoid membrane driven by adaptation mechanisms, including state transitions. Thylakoid morphology, and in particular stacks formation, include the presence of zones of curvature in the membrane. Described as the part of the membrane that connect two grana membranes at their luminal side, grana-margins, are sometime ascribed as the third sub-compartment of the thylakoid membrane (figure 1.11).

Early studies suggested that this compartment is protein-free [24]. This observation was deduced by the fact that protein complex usually located in a flat membrane (stroma-lamellae or grana) would find it difficult to lo-

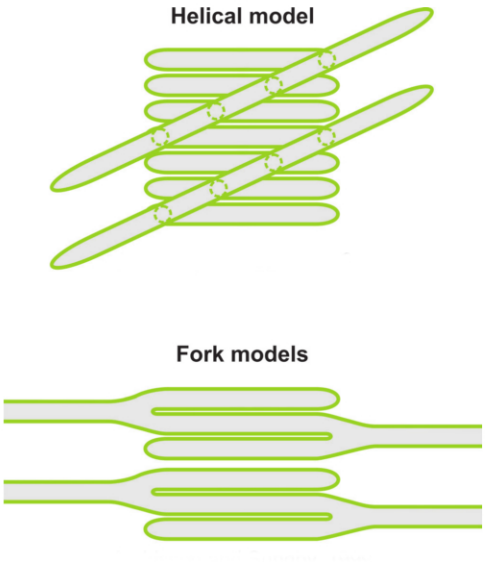

Figure 1.10 – Models of thylakoid architecture. In the helical model, a fretwork of stroma lamellae connects to individual grana discs via narrow membrane protrusions. In fork models, stroma lamellae bifurcate to generate grana discs. Image from *Pribil et al., 2014* [103]

cate also in an extremely curved membrane. However, by immunodetection, it was recently shown that the low-molecular weight protein family CURT1 (CURvature Thylakoid 1 A,B and C) is localised to the grana-margins in *Arabidopsis* [104]. This family of proteins is demonstrated to be directly involved in the grana formation. In particular, it is proposed that the level of CURT1 proteins controls the dimension of the grana stacks. Indeed, plants devoid of CURT1 proteins display grana with a significantly increased diameter and fewer layers of membranes which form pseudo-grana without margins [104]. Moreover, by comparison with the CURT1 overexpressor, it was demonstrated that the number of grana stacks correlates with the amount of CURT1 proteins [104]. To conclude, margin specific CURT1 family proteins appear to control the level and dimension of grana stacking. This finding might indicate a role for grana margins in regulating the extent of thylakoid membranes in the appressed regions present in grana [104].

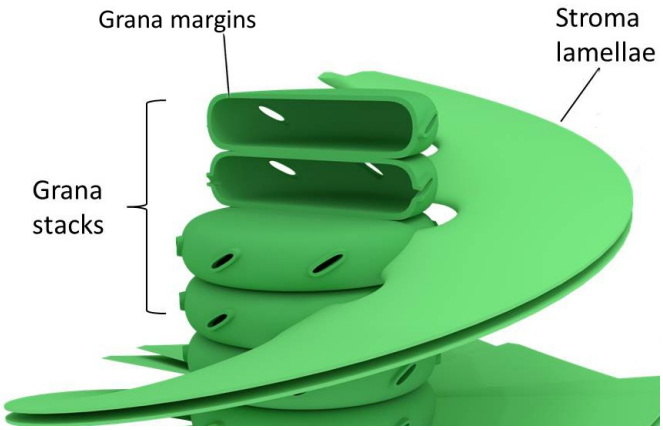

Figure 1.11 – The grana-margins are evidenced in this 3D model of the thylakoid membrane. Image by J.Roose and Kelvinsong (Own work) `http://creativecommons.org/licenses/by-sa/3.0`

1.6 Photoprotection

The photosynthetic chain, together with the described photosynthetic complexes, are susceptible to photo oxidative damage under a large variety of natural environmental conditions. This phenomenon, mostly concerns photosystem II which is indeed characterised by a fast turnover rate [105]. In fact, inhibition of PSII activity becomes evident only when the rate of damage exceeds the rate of repair. In contrast to PSII, PSI seems to be more efficiently protected against photodamage although, as it will be detailed later, in rare cases of damage, the subsequent recovery of PSI is slow [106]. To avoid photodamage, plants have developed means to modulate the light absorption/utilization capacity of their photosystems which are collectively called *non-photochemical quenching* (NPQ).

1.6.1 Non-photochemical quenching

Non-photochemical quenching of the chlorophyll fluorescence (NPQ) is a set of processes by which excessive light energy absorbed by chlorophyll is dissipate mainly as heat [107]. NPQ can be divided into at least three different components according to their relaxation kinetics in dark, following a period of illumination [108]. The major and most rapid component in most algae and plants is the pH or energy-dependent component, *qE*. A

second component, qT, relaxes within minutes and it is attributed to the phenomenon of state transitions (see section 1.6.1.2 at page 41). qI, the third component of NPQ, shows the slowest relaxation and is related to the photoinhibition of the photosystems.

1.6.1.1 High energy state quenching, *qE*

As discussed above, photosynthetic electron transport generates a transmembrane ΔpH. This pH difference between the thylakoid lumen and chloroplast stroma may become important when the absorption of light exceeds the actual capacity of the plant to fix carbon-dioxide. Acidification of the lumen (below 6) is the immediate signal (within seconds) which triggers the feedback regulation of light harvesting by qE. This component of the NPQ is the most effective in counterbalancing the negative effects of high light in plants. The working-model states that, the decreased lumenal pH leads to the protonation of PSII-proteins and the interconversion of specific xanthophyll pigments (oxygenated carotenoids) that are mostly bound to LHC proteins. This interconversion occurs on a timescale of minutes as part of the xanthophyll cycle. In plants, the violaxanthin cycle consists of the pH-dependent conversion from violaxanthin, a xanthophyll with two epoxide groups, first to antheraxanthin (one epoxide group) and then to zeaxanthin (no epoxide group)(figure 1.12).

The conversion of violaxanthin to zeaxanthin is supposed to promote a specific conformational change of LHCII, switching the PSII into a quenched state characterised by a low fluorescence yield [110]. Characterisation of mutants defective in qE (but with a normal xanthophyll level) has also allowed to point out the role of the subunit PsbS as essential component of qE [111][112]. PsbS is part of the LHC protein superfamily and is characterised by four transmembrane helices [113] but does not bind pigments [114]. Instead, it functions as a sensor of lumen pH that turns on NPQ [115]. The exact biochemical mechanism is, at the moment, poorly characterised. However, it seems that the protonation of PsbS promotes again the rearrangement of the LHCII-PSII supercomplex [116][117].

1.6.1.2 State transitions, *qT*

State transitions are a less importance NPQ component in plants [118] but they are supposed to play a role in balancing excitation between the two photosystems at a low light. In particular, PSII and PSI have a different composition in their antenna apparatus and hence a different light absorp-

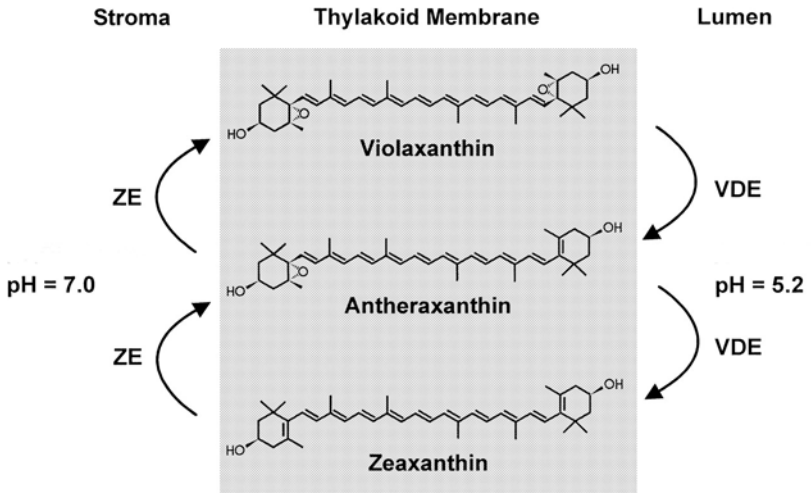

Figure 1.12 – The xanthophyll cycle in higher plants. Reactions are catalysed by the enzymes VDE (violaxanthin de-epoxidase) and ZE (zeaxanthin expoxidase). From *Yamamoto et al*[109]

tion spectrum. Under light conditions in which PSII is preferentially excited, the plastoquinone pool is reduced to plastoquinol (PQH_2). This activates the protein kinase STN7 via the cytochrome b_6f (figure 1.13). This event triggers the phosphorylation of some LHCIIs, the release of the phosphorylated LHCIIs from PSII which migrate towards PSI, thereby balancing the light excitation energy between the two photosystems.

State transitions is a reversible process, since a preferential excitation of PSI by the far-red component of the environmental light induces the dephosphorylation of LHCII and its return to PSII (figure 1.13). The two conditions are called state-2 and state-1, since they are induced by a light preferentially absorbed by PSII and PSI respectively. The phosphatase PPH1 has been identified as the phosphatase responsible for LHCII dephosphorylation and the transition from state-2 to state-1 [119]. Beside this generally accepted view, other mechanisms have been proposed to account for state transitions and regulation of excitation energy distribution between PSII and PSI. Results obtained from mechanical subfractionation of thylakoids membranes from *Arabidopsis* [120] suggest that, during LHCII-phosphorylation in grana stacks, there are protein migrations in two directions: *(i)* movement of PSI-LHCI towards the grana by attractive electrostatic forces and/or by *van der Waals* forces and the *(ii)* P-LHCII-PSII movement towards the stroma lamellae due to charge repulsion between adjacent P-LHCII proteins. The meeting

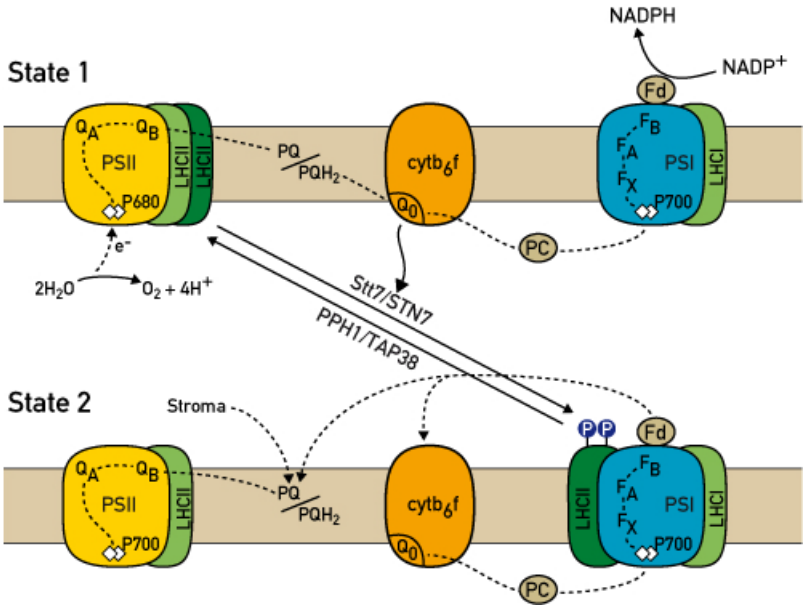

Figure 1.13 – Reduced plastoquinone pool induces state transitions. Phosphorylated LHCII (P-LHCII) dissociates from PSII and binds to PSI. Upon preferential excitation of PSI, the kinase is inactivated and the PPH1 phosphatase dephosphorylates LHCII, which moves back to PSII. From *Rochaix* [230]

point of these complexes during their movement in the opposite directions is the margin fraction of the thylakoid membrane (see section 1.5.1 at page 38). These movements lead to a decrease in the lateral heterogeneity of the thylakoid membrane allowing the excitation energy to flow from PSII-LHCII to PSI. In this view, the dynamic nature of grana margins allows the capture of excitation energy by PSI from PSII-LHCII. It is estimated that, in plant, only 15% of the total LHCII pool is phosphorylated during state transitions and this explains the little importance of qT in NPQ.

1.6.1.3 Photoinhibition, *qI*

PSII centers become susceptible to damage at all light intensities which overcome the capacity of photosynthesis to use light energy photochemically. This process concerns mostly the core subunits of the photosystem (*e.g.* PsbA, also referred to as D1). Several PSII core proteins such as D1, D2, CP43, and PsbH as well as specific antenna of the LHCII, are phosphoproteins reversibly phosphorylated [121][99]. Phosphorylation

of the PSII-core subunits is an essential component of the PSII repair cycle [99][121][122][123]. Kinases specific to LHCII and PSII core proteins have been identified as STN7 and STN8, respectively [124][125]. Recent experiments on *stn7*, *stn8* mutant and *stn7stn8* double mutants have revealed that PSII core proteins phosphorylation plays an essential role in PSII repair cycle during photoinhibition by facilitating an efficient migration and degradation of damaged PSII reaction center proteins from appressed membranes (grana) to the non-appressed membranes (stroma-lamellae) (see section 1.5 at page 36) [121][125]. Furthermore, phosphorylation of PSII core proteins by *stn8* (which specifically phosphorylates the PSII core protein D1) modulates macroscopic folding and rearrangement of the entire thylakoid membrane [124]. This facilitates the lateral mobility of thylakoid membrane proteins [121][126]. Two protein phosphatases (PPH1 and PBCB) were recently identified to efficiently counteract the activities of the STN7 and STN8 kinases respectively [119][126][127]. As a part of the PSII repair cycle, damaged D1 proteins are rapidly degraded by two different families of chloroplast proteases [128][129][130][131]: the ATP-dependent zinc metalloproteases FTSH (filament temperature sensitive H) family [132] and the ATP-independent serine endoproteases DEG/HTR family [133]. It is important to note that, even if D1 degradation could mainly be associated to photodamage, its high turnover rate is not only induced by photoinhibitory conditions but is also observed in normal growth conditions [134][135].

As mentioned above, PSI seems less sensitive to photodamage than does PSII. Nevertheless, when this process occurs to PSI, the associated repair cycle is much less performant. Furthermore, most of the photoinhibited PSI reaction centers are not repaired but degraded after photoinhibition together with their bound chlorophylls [136]. The present working model states that electrons supplied to PSI from PSII can react with molecular oxygen and form hydrogen peroxide (H_2O_2) which ultimately destroys the iron-sulfur centers [137]. Moreover it was evidenced that addition of DCMU (an inhibitor of PSII) completely suppresses the PSI photoinhibition in intact leaves or in isolated thylakoid membranes [106]. Thus, the electron flow from PSII, is essential for the photoinhibition of PSI *in vivo* [138]. Only a couple of plant species were reported to show the selective photoinhibition of PSI *in vivo* with smaller effect on PSII. In fact, once the photoinhibition of PSI is induced, electron transfer is blocked at PSI, resulting in the over-reduction of the PQ pool. Consequently, such acceptor limitation leads to photoinhibition of PSII.

Aim of the thesis

When light absorbed by the antenna complex of the photosystems exceeds the actual capacity of the plant to use it, the photosynthetic chain is susceptible to photo oxidative damage. As seen in section 1.6 at page 39, plants have developed several means to modulate the light absorption/utilization capacity of their photosystems.

This thesis aimed at investigate and clarify some aspects of the responses of *Arabidopsis* to light *stimuli*, delivering new insights into their mechanisms and physiological consequences.

During this study, I mainly focused on:

- state transitions qT (LHCII proteins phosphorylation to regulate excitation energy distribution between PSII and PSI)
- qE (high energy state quenching and main component of NPQ in plants).

As previously seen, state transitions involve the reversible migration of the LHCII among the thylakoid sub-compartments (stroma-lamellae and grana). Beside LHCII, little is known about the possible involvement of other thylakoid proteins in state transitions. The main objective was to investigate the effects of state transitions on the overall protein segregation within the photosynthetic membrane. In order to accomplish the study, I needed to move some steps backward. I firstly performed the complete survey of the protein composition of stroma-lamellae and grana-BBY in *Arabidopsis* WT thanks to a semi-quantitative proteomic approach. Results are presented in section 2.5.

Later (chapter 3), I used the information provided from the first study (*e.g.* purification techniques, protein localisation) in order to assess changes in the protein distribution (other than LHCII) in stroma-lamellae and grana-BBY during state transitions.

In chapter 4.3, I focused on the research work on qE (a main component

of the non-photochemical quenching in plant). As seen in section 1.6.1, the instauration of a difference of pH across the thylakoid membrane (ΔpH) is an essential feature to trigger LHCII in its quenched state. The objective was to shed some light on the mechanisms that control ΔpH (and thus regulate NPQ) in plants. In order to accomplish the study, we focused on a new and recently identified two-pore potassium channel, TPK3 and we performed a deep biochemical and biophysical analysis on *Arabidopsis* plants devoid of TPK3.

Chapter 2

Deciphering thylakoid sub-compartments using a mass spectrometry-based approach

2.1 Preface

The article presented in this chapter (*Tomizioli et al., 2014* [139]) represents the most important result of my Ph.D project. It constitutes also the continuation of a previous study, performed in our laboratory, that was targeted to the characterisation of the chloroplast sub-compartments proteomes in *Arabidopsis* and led to the establishment of the AT_CHLORO database [140]. The AT_CHLORO database (`http://www.grenoble.prabi.fr/at_chloro`) constitutes a repository of 1323 chloroplast proteins and comes with detailed proteomic information such as peptide sequences, molecular weight, chromatographic retention times, and MS/MS identification statistics. Moreover, it addresses the accurate proteomic-based localisation of chloroplast proteins in the three major chloroplast compartments: envelope, stroma and thylakoids.

In *Tomizioli et al., 2014* [139], I performed a new in-depth proteomic investigation of the thylakoid membrane. The work is characterised by an enhanced level of resolution since it concerned two new thylakoid sub-compartments: the grana-BBY and the stroma-lamellae (see section 1.5 at

page 36 for major details about the thylakoid sub-compartments). To this purpose, *(i)* I developed a new protocol to obtain highly purified thylakoid subfractions from *Arabidopsis* WT leaves, *(ii)* I evaluated the purity of the fractions (both biochemically and spectroscopically), *(iii)* we performed a MS/MS and statistical analysis in collaboration with the team *Étude de la Dynamique des Protèomes* (EDyP) at the *Laboratoire Biologie à Grand Échelle* iRTSV (CEA) and, after protein annotation accomplished by Norbert Rolland, *(iv)* I performed a complete survey of the protein composition of stroma-lamellae and BBY.

The present chapter is organised in two sections. In the first section (section 2.2), I present the experimental steps that I followed in order to develop the purification protocols of the thylakoid subfractions from *Arabidopsis*. It will be the occasion to deliver additional technical details which were not included in the published paper *Tomizioli et al., 2014* [139]. In the second section (section 2.3), I present an introduction to proteomics for those who might not be familiar with it. In particular, after a brief overview, I focus on the general steps that need to be followed during a proteomic study paying particular attention to the case of plant material. I conclude with a short summary of previous proteomic studies which focused on the chloroplast and chloroplast sub-compartments (envelope, stroma and thylakoids). In the third section (section 2.5), the article *Tomizioli et al., 2014* [139] is presented; supplemental tables are available online at `http://www.mcponline.org/content/early/2014/05/28/mcp.M114.040923/suppl/DC1`

2.2 Thylakoid sub-compartments purification

In order to accomplish the purpose of the thesis, it was first necessary to develop a robust protocol that, starting from Percoll purified and intact chloroplasts, allowed to obtain highly purified fractions of the thylakoid membrane: BBY, stroma lamellae and grana margins.

2.2.1 Intact chloroplasts purification

Intact chloroplasts from 5 weeks old *Arabidopsis* plants were obtained according to a protocol that was previously developed in our laboratory [141]. This protocol relies on the use of a 50% Percoll gradient. Percoll gradient allows to select dense and intact chloroplasts, but it is usually associated to a loss in the final chlorophyll yield greater than 95% [141]. This purification step is essential for the following proteomic analysis, as it allows to get rid of the possible contamination arising from mitochondria or nucleus (for major discussions see section 2.3.1 at page 59). Furthermore, mitochondria and other cell components are known to affect activity of the preparations or induce accelerated rate of ageing of the purified chloroplasts [142]. Within a Percoll gradient, nucleus, cell debris, t-DNA, starch and intact cells are found in the pellet while mitochondria co-purify with broken chloroplasts (figure 2.1).

After chloroplast collection from the 50% percoll gradient (figure 2.1 red-starred layer), we then verified intactness and activity of our chloroplasts using a Clark-type electrode system. In the following section the principle of the technique is explained.

2.2.1.1 Measure of the oxygen evolution rate

The clark-type oxygraph (figure 2.2) consists of a semi-hermetic chamber and two electrodes (positive and negative). At the cathode, molecular O_2 is consumed along with the electrons. The movement of electrons from the anode to the cathode creates a current which can be measured. For each molecule of oxygen that comes into contact with the cathode, a proportional current travels through the circuit. Constant stirring is essential since oxygen is constantly being consumed at the cathode. With constant stirring, a change in current indicates a change in O_2 partial pressure in the solution.

Chloroplasts contain soluble proteins in the stroma compartment which are released into the medium when the envelope membrane is ruptured [143]. Ferredoxin, the essential intermediate of photosynthetic electron transport to

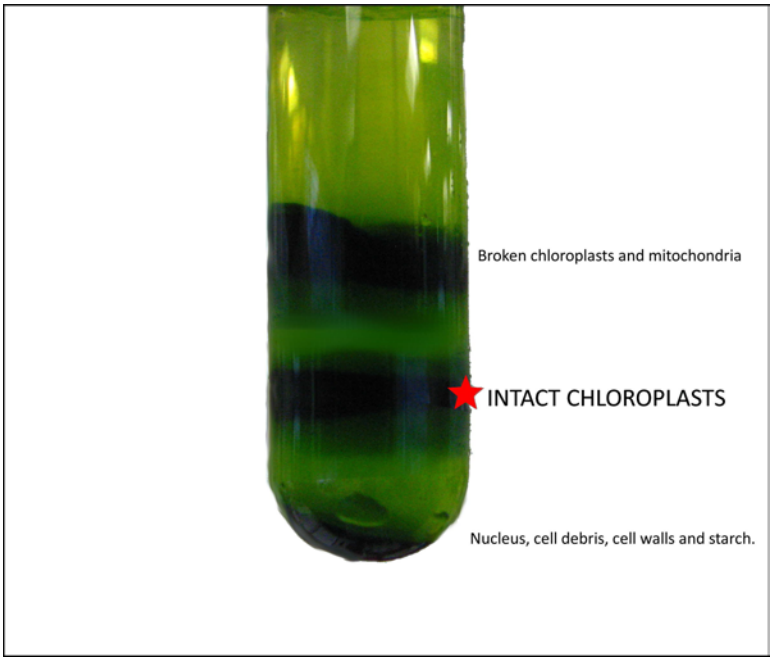

Figure 2.1 – 50% percoll gradient for purification of intact chloroplasts (red-starred layer). Broken chloroplast and mitochondria purify in the upper layer. Nucleus are found in the pellet together with cell debris, t-DNA, cell walls and starch.

NADP, is also present as a soluble protein in the stroma. Loss of part of the stromal proteins in broken chloroplasts would therefore be expected to result in a decrease in O_2 evolution activity. On the other hand, broken chloroplasts are normally capable of O_2 evolution and photophosphorylation in the presence of appropriate oxidants and cofactors [144]. Potassium ferrocyanide ($K_4[Fe(CN)_6]$) is an artificial electron acceptor used to sustain the transport of electrons and cannot enter into intact chloroplasts. The basic idea of this approach is to measure the oxygen evolution rate of the preparation before and after an osmotic shock always in presence of $K_4[Fe(CN)_6]$. Percentage of photosynthetically active chloroplasts can be estimated by the difference between the two oxygen evolution rates. Half an hour after the purification, around 70% of the chloroplasts were detected to have retained their photosynthetic activity. The finding that the percoll-purified intact chloroplasts contained also 30% of inactive chloroplasts may be explained essentially by their high fragility. It is likely that degradation of the preparation might have occurred after the collection and before the measure.

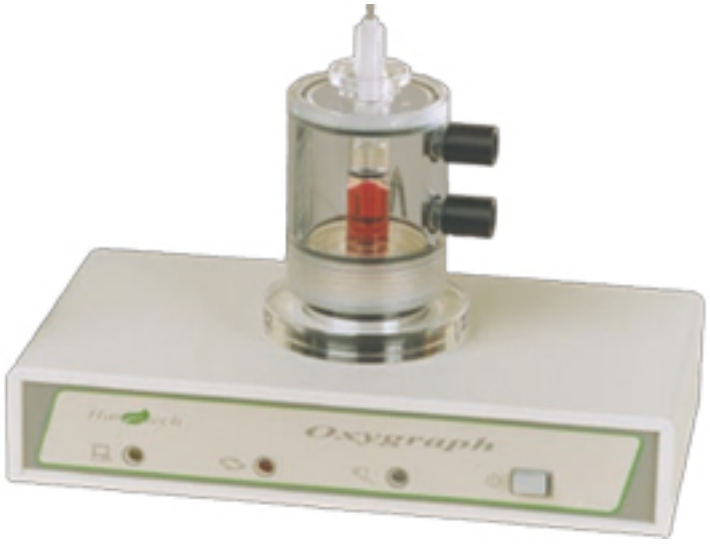

Figure 2.2 – Photo of the clark-type oxygraph set-up

2.2.2 Thylakoid subfractions purification

Intact chloroplasts were broken with an osmotic shock to obtain thylakoids. In order to purify the three sub-compartments of the thylakoids (stroma-lamellae, grana and grana-margins), we tested different protocols and optimized them for our model organism *Arabidopsis*. Stroma lamellae were purified following both the protocol used in *Bassi et al., 1988* [145] and in *Timperio et al., 1981* [146]. These two protocols are based on a mechanical fractionation (which allows to purify stromatic lamellae) and on a detergent fractionation (which allows to purify both stromatic lamellae and grana margins) respectively.

In *Bassi et al., 1988*, thylakoid membranes (0.8 mg Chl ml^{-1}) are transferred to a Yeda Press and kept at a pressure of 130 atm for 10 minutes at 4°. Stroma-lamellae are then isolated by a passage of the thylakoid membranes from the high pressure inside the yeda-press chamber to the normal atmosphere pressure (around 1 atm). The lighter fraction of the thylakoid membrane is collected from the pellet after a centrifugation at 110.000 RCF for 30 minutes. In *Timperio et al., 1981*, thylakoid membranes (0.5 mg $Chl.ml^{-1}$) are incubated with 0.5% digitonin (a large and bulky detergent), for 30 minutes at 4°. After a first centrifugation at 70.000 RCF, the grana margins are collected from the pellet while the supernatant is re-centrifuged at a higher speed (140.000 RCF). Stroma-lamellae fraction of the thylakoid

is enriched in the pellet fraction.

In order to purify grana-discs, we tried two different protocols: one described in *Berthold et al., 1981* [146] and one described in *Morosinotto et al., 2010* [147]. These two protocols rely on a strong detergent (to purify the inner part of the disc, referred to as BBY) and to a milder one (to purify large grana discs) respectively. In *Berthold et al., 1981* thylakoid membrane (1 mg Chl.ml^{-1}) are incubated with 10 mg TRITON X-100/mg Chl for 30 minutes at 4°. The heavier fraction of the thylakoid membrane is purified after two sequential centrifugations. The first one at 3500 RCF for 5 minutes (where the pellet is discharged) and a second at 40.000 RCF for 30 minutes. In *Morosinotto et al., 2010*, thylakoid membranes (1 mg Chl.ml^{-1}) were incubated with a different concentrations of n-Dodecyl-α-D-Maltopyranoside α-DM (a mild detergent, smaller than digitonin, with a long aliphatic chain). We tested four conditions, which differed both in detergent concentration and time of centrifugation of the suspension:

— incubation for 30 minutes with 0.8 % α-DM followed by centrifugation for 30 minutes
— incubation for 30 minutes with 0.8 % α-DM followed by centrifugation for 60 minutes
— incubation for 30 minutes with 1 % α-DM followed by centrifugation for 30 minutes.

The average final yields for the different preparations in term of chlorophyll content are summarised in table 2.1.

Conditions	fraction purified	chlorophyll yield
0.8% α-DM 30 min	grana discs	9%
0.8% α-DM 60 min	grana discs	10%
1% α-DM 30 min	grana discs	14%
10 mg Triton/ mg Chl 30 min	grana BBY	5%
0.5% digitonin 30 min	stroma-lamellae	2%
130 atm yeda-p. 10 min	stroma-lamellae	n.a.

Table 2.1 – Final yields for the different preparations of thylakoid sub-compartments in term of chlorophyll content. Chlorophyll yields are calculated as difference between the initial intact-chloroplast chlorophyll content and that measured in the purified fractions. Final chlorophyll yield is not available for stroma-lamellae issued from yeda-press (n.a.).

2.2.3 Spectroscopic evaluation of the purity of the samples

In order to assess the most effective protocol, we performed a quick spectroscopic analysis on the samples after each preparation. The principle of the technique relies on a physical process which takes place when a molecule of chlorophyll is excited: the fluorescence. In the next section, the principle of the process is explained.

Chlorophyll Fluorescence

Chlorophyll molecule can absorb light energy and re-emit it as radiation energy. When a photon is absorbed, chlorophyll molecule is excited from the ground state (S_0) to the first electronic excited singlet state (S_1)(figure 2.3). This process takes about 10^{-15} seconds. It is important to note that this molecule can be excited to a higher energy levels (S_2, S_n) and can relax to S_1 via vibrational relaxation in a time comprised between 10^{-12} seconds. Finally, the molecule will relax to the ground state through the emission of a photon. This process is called fluorescence emission and the energy of the emitted photon is equal to the changes in the energy level.

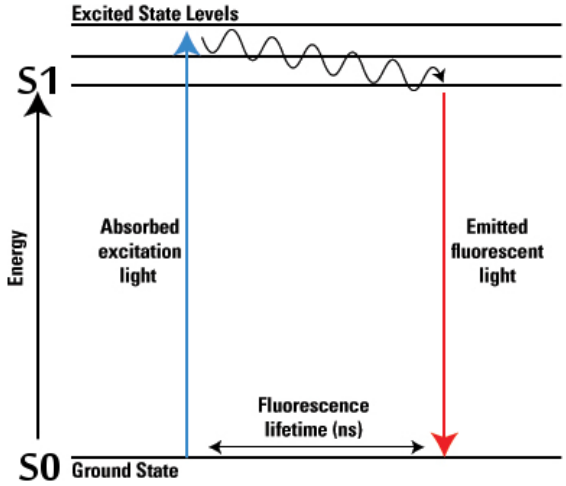

Figure 2.3 – Energy diagram of fluorescence.

77°K fluorescence emission

Measure of the fluorescence emission from thylakoid fractions has to be carried out at a liquid-nitrogen temperature (77°K). In fact, at room-temperature PSI does not emit fluorescence. This is because PSI (and not PSII) is characterised by a great efficiency (∼1) and almost all of the light collected is used to perform photochemistry [148]. Moreover, some chlorophyll species are present in the proximity of the PSI-RC characterised by a energy level slightly lower than that of P700 [149]. Room temperature is sufficient to allow free-transfer of photons from these chlorophyll species to the RC and perform photochemistry. At cryogenic temperatures, this energy transfer is blocked. High fluorescence emission from PSI finally appears because these special fluorescing Chl species, absorbing at 710-720 nm, compete with P700 in trapping the energy [149]. 77K spectroscopy relies on the fact that when a mixture of thylakoid is excited with blue light, the relative fluorescence emission spectra collected in the near infrared region is characterised by three main peaks (fig.2.4A). The two peaks between approximately 680 and 695 nm correspond to fluorescence emitted from chlorophyll molecules in PSII, while the peak at 735 nm corresponds to the fluorescence from the chlorophyll molecules in PSI (fig 2.4A). When signals are normalised with respect to a chosen peak (*e.g.* PSII) amplitudes are proportional to the size of the antenna associated to a given photosystem [150].

We performed the same experiment on our purified sub-thylakoid fractions and resulting spectra are reported in figures 2.4 B, C and D. Stroma-lamellae obtained from the purification protocol with the yeda-press display an almost identical amplitude for both peaks of PSI and PSII (fig 2.4B). Moreover, the fact that the PSI-fluorescence peak is detected at a wavelength lower than 735 nm clearly indicates a damage of the antenna apparatus probably due to the method of purification. By contrast, when stroma lamellae are purified with digitonin, the peak associated to PSII is dramatically diminished and, by consequence, that of PSI gains largely in amplitude (fig 2.4B). Different levels of enrichment PSI/PSII were also found in the case of the purification of grana and grana inner discs (BBY). When α-DM was used as detergent, little difference is seen in the amplitude between the peaks PSI/PSII (fig 2.4B). Furthermore, neither the detergent concentration nor the time of centrifugation seem to have a beneficial effect on the quality of the purification (fig 2.4C). Spectrum performed with the grana-BBY issued of the TRITON X-100 treatment display the most important difference between the amplitudes of the peaks PSI/PSII. In fact, even if not totally abolished, the peak relative to PSI is largely diminished when compared to that of PSII (fig 2.4D). It is important to note that the peak associated to PSI

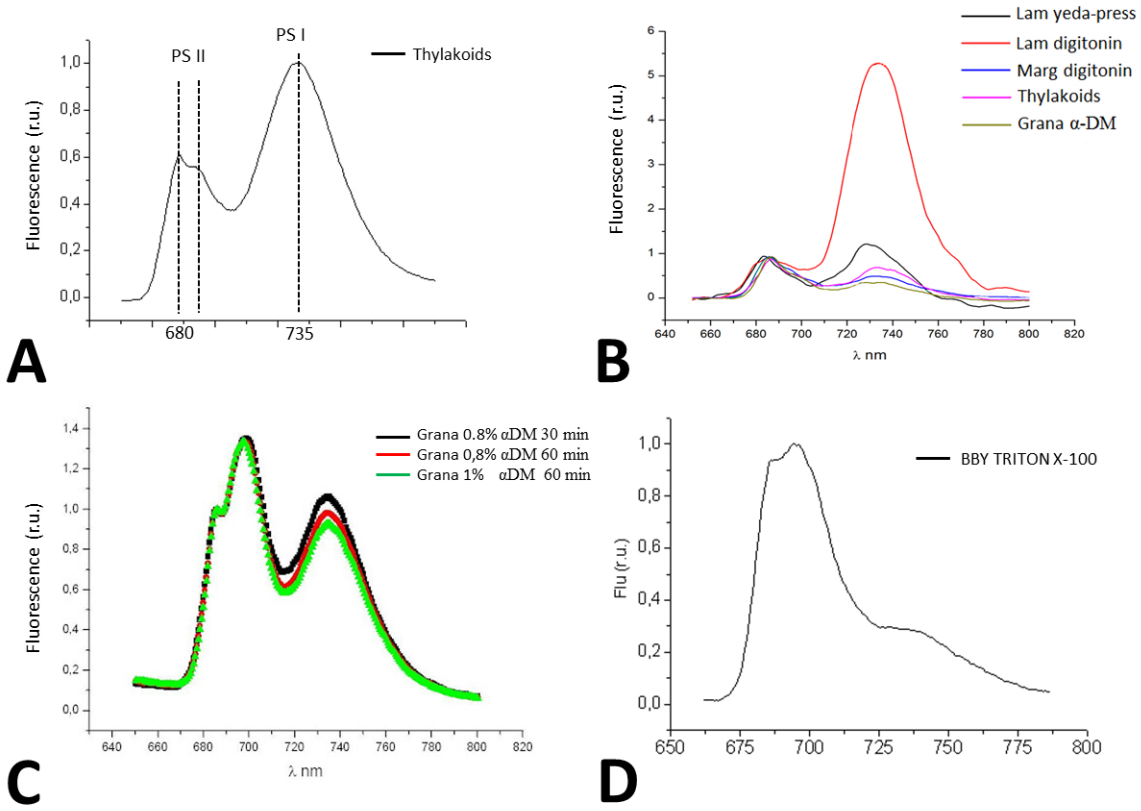

Figure 2.4 – 77K chlorophyll fluorescence emission spectra of thylakoid membrane subfractions isolated from *Arabidopsis* with different methods. Thylakoid proteins (or thylakoid subfractions) samples were loaded on to a metal cuvette, which was directly bathed into a liquid nitrogen solution. Fluorescence spectra were recorded upon excitation at 470 nm. Peaks were normalized for comparison purposes. A, isolated thylakoids. B, Lamellae, margins, grana and thylakoids purified by different protocols. C, grana purified with varying concentration of detergent and time of centrifugation. D, grana inner-discs (BBY) purified with TRITON X-100 10 mg.mgChl^{-1}.

may be in someway over-estimated, since part of the emission of the PSII is re-absorbed by PSI and re-emitted at a longer wavelength. Margins fraction purified with digitonin (fig 2.4B) displays a relative PSI/PSII peak amplitude mostly comparable indicating that both photosystems are probably present.

In conclusion, in order to obtain the purest sample to be analysed by mass-spectrometry, we chose to limit our purification protocols to the use of 5% digitonin in the case of stroma-lamellae and grana margins, and to 10 mg TRITON X-100/ mg Chl for the purification of the inner discs of the grana (grana-BBY).

2.2.3.1 Measure of the oxygen evolution rate, Chl *a/b* and P/C ratio

Stroma-lamellae and grana-BBY fractions issued of the selected protocols were furtherly challenged by direct measurement of the chlorophyll *a/b* ratio and oxygen evolution. In plant, chlorophyll molecule is present in two different forms which essentially differ in the composition of a single side chain (figure 2.5). Chlorophyll *a* is a large molecule that has a porphyrin ring with a magnesium atom at its center. Attached to the porphyrin is a long, insoluble carbon-hydrogen chain which interacts with the proteins of the thylakoids and serves to anchor the molecule in the internal membrane of the chloroplast. Chlorophyll *b* differs from chlorophyll *a* only in one of the functional groups bonded to the porphyrin (a -CHO group in place of a $-CH_3$ group). It is an accessory pigment and acts indirectly in photosynthesis by transferring the light to chlorophyll *a* [152]. In particular chlorophyll *b* is mainly associated to the sole PSII-LHCII complex thus more enriched in the grana-BBY fraction. The ratio of chlorophyll *a* to chlorophyll *b* in the chloroplast (and thylakoid) is around 1:3 but varies significantly within the thylakoid subfractions [153].

Data summarised in table 2.2 (lane *Chl a/b ratio*) confirm the successful separation of the two fractions. In fact, stroma-lamellae fraction displays the higher chlorophyll *a/b* ratio indicating a low content in PSII antenna. By contrast, thylakoid and grana-BBY fraction which contain a higher concentration of LHCII (this is especially true for grana-BBY) have a lower chlorophyll *a/b* ratio. Later, we wanted to determine if the water-splitting activity of the PSII was retained after purification. At this purpose, we performed a test in which the oxygen evolution rate was measured by a clark-type oxygraph. Thylakoid and thylakoid subfractions were placed in the oxygraph chamber and artificial electron acceptors were added in order to sustain the primary photosynthetic reaction (ferricyanide and 2,5-dichloro-p-benzoquinone). Oxygen evolution rates were measured in dark conditions and during illumination at 750 μE. Data reported in table 2.2 (column *activity*) indicate that our grana-BBY fraction was able to retain up to 80% of the activity of the intact thylakoids (57 and 70 nmol O_2 h^{-1}. μgChl $^{-1}$ respec-

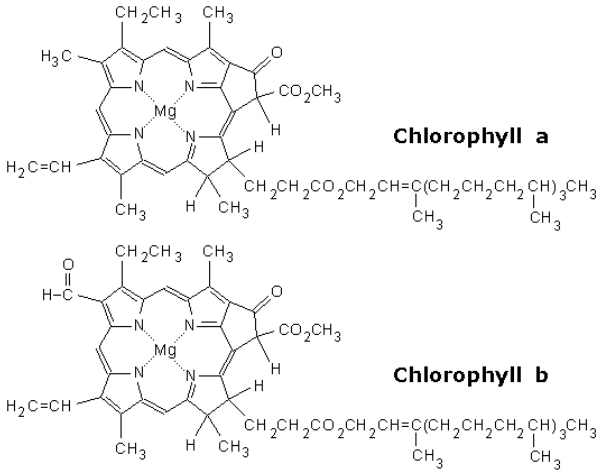

Figure 2.5 – Chlorophyll *a* and *b* structure

fraction	Chl *a*/*b* ratio	Prot/Chl ratio	activity (nmol $O_2.h^{-1}.\mu g$ chl)
thylakoids	2.90 ± 0.01	4.44 ± 0.04	70.0 ± 10.5
grana-BBY	1.73 ± 0.08	2.25 ± 0.18	56.9 ± 6.6
stroma-lamellae	4.28 ± 0.01	6.45 ± 0.17	non detectable

Table 2.2 – Measure of the oxygen evolving activity of thylakoids, grana-BBY and stroma-lamellae. Fraction were essayed with ferricyanide (3.5 mM) plus 2,5-dichloro-*p*-benzoquinone (250 μM).

tively). As expected, stroma-lamellae were not able to evolve any detectable amount of oxygen. This is explained by the fact that only photosystem II can successfully accomplished light-induced water-splitting. Moreover, this finding furtherly demonstrates the good level of purity in our stroma-lamellae preparations since they are particularly deprived of PSII.

2.3 Proteomic Analysis: Introduction

Proteomics is the study of global protein composition within an organism, tissue, cell or organelle. It has delivered important enhancements and unique insights into the characterisation of the biological systems since its introduction in the last decades [154]. The characterisation of the proteome is

of prime importance for a complete understanding of plant functions, biosynthetic and signaling pathways.

Chloroplast is not only an important center of metabolic reactions but also it is an important signaling hubs that determines the expression of numerous nuclear encoded genes in retrograde signaling cascades [155]. Consequently, the characterisation and study of its proteome is of crucial importance and constitutes an important economic issue in plant biotechnology. Chloroplast proteome composition and relative expression levels of proteins vary in function of developmental stage, as well as environmental conditions. Understanding these modifications is essential to improve knowledge of the organelle functions and regulation. Proteomics focused on the chloroplast does not only aim at identifying or determining level of protein expression but gives access to a whole wide range of information such as protein-protein interactions (see [156]) or protein sub-localisation within the organelle (see for example [140]). Indeed, *Arabidopsis* has been the organism of choice for the proteomic analysis of the chloroplasts and is currently the only plant for which a truly comprehensive set of established chloroplast proteins is available. Moreover, *Arabidopsis* has a wide range of comprehensive resources already available such as the entire genome sequenced and a large collection of mutants. Several fundamental information platforms and databases exist such as The *Arabidopsis* Information Resource TAIR (`http://www.arabidopsis.org/`).

Today, a significant percentage of the chloroplast proteome is characterised and much of this progress is certainly due to the improvements of the mass-spectrometry technologies [157]. When compared to those of 10 years ago, latest proteomic instruments are characterised by: *(i)* much improved sensitivity (routinely at 1-50 fmol) [158][159], *(ii)* accelerated duty cycle (now tandem mass spectrometry [MS/MS] scans within a few hundred ms), *(iii)* improved mass accuracy (down to a few ppm for peptides), and *(iv)* increased resolution of the latest generation mass spectrometers. Nevertheless, even if such important technological improvements have been delivered, some weak-points still remain. In particular identification of highly hydrophobic proteins, proteins that are expressed only under particular conditions (*e.g.* adverse growth conditions, developmental stage, etc.), and proteins with very low expression levels (*e.g.* more than 10,000-fold lower than RuBisCo) still remain challenging [157]. The following section will give an overview of the scheme that is supposed to be followed during a subcellular-focused proteomic investigation (and of course during chloroplast proteome investigation).

2.3.1 Organelle purification

In order to perform an high-quality proteomic study, purification of the desired organelle is mandatory. The main steps for a classical cell fractionation are: *(i)* disruption of the cell wall and *(ii)* purification of the organelle of interest from the homogenate. During cell disruption, pH, ionic strength, buffering capacity and osmoticum of the disruption buffer have to be carefully controlled to avoid any damage to the sub-cellular compartments. In particular, sucrose or mannitol are used to maintain organelle structure by limiting breakage of the membrane, while a neutral or alkaline pH buffer, (between 7.2 and 7.8) quenches the acidity from the rupture of the vacuoles. A reductant, such as dithiothreitol (DTT) minimizes damage from oxidants. Cell fractionation is generally carried out by a first filtration of the homogenate through a nylon mesh (>50 μm) to remove large debris. Later, a series of differential centrifugations are commonly used to enrich the fraction with the target organelle and concomitantly eliminate other compartments and contaminants. The choice of speed and time of centrifugation is based on the size and density of the organelle to be purified. Larger and denser organelles are pelleted at lower speed of centrifugation. The enriched fraction can eventually be the object of a deeper purification with a centrifugation in a density gradient. Concerning chloroplasts, Percoll gradients were shown to allow the recovery of highly purified chloroplasts (see section 2.2.1 at page 49). Indeed, Percoll-purified chloroplasts preparations are devoid of contaminations by extraplastidial marker enzymes and non-chloroplastic membrane lipids (for review see [160]).

2.3.2 Assessment of the quality of the purified subfractions

Subcellular proteomic studies are essential to get access to protein location in relation with their function. It is also a way to detect minor proteins (indeed organelle subfraction is less complex than a whole extract). An informative subcellular proteomic approach requires highly purified organelle subfractions; thus the purity of the subfractions have to be validated before mass spectrometry and protein identifications. A large variety of methods are currently employed to assess the level of purification of the preparation prior to downstream applications. They mostly rely on microscopic observations (both optical and electronic) and biochemical evaluation.

Direct microscopic observation allows to determine not only the purity but also the integrity and morphology of the purified organelle. Moreover,

many organelles of proteomic interest have a characteristic appearance under electron microscopy (EM), particularly when suitable staining methods are applied. Two types of EM are used: transmission EM (TEM) and scanning EM (SEM). Among them, TEM achieves the highest resolution and can discriminate between related classes of organelle and structures. The main drawbacks of electron microscopy observation are essentially related to the cost of the facilities, to the time necessary for the preparation of the sample prior to the analyse (fixation) and to the need of specific trainings and experienced personnel to perform the observations.

Biochemical evaluation of the purity of the subfractions mostly relies on a western blot approach using protein markers specific to various subcellular localisations. When compared to EM, biochemical evaluation is less expensive and the assessment can be carried out relatively quickly. Proteins of the purified subfractions are separated by denaturing gel electrophoresis (SDS) and subsequently transferred to a specific membrane for detection with antibodies raised against specific markers (*i.e.* proteins with known subcellular localisation). For example, in this thesis, antibodies raised against the RuBisCo or against the phosphate transporter PHT4;4 were used to highlight contamination of our purified fractions by the stroma or by the envelope.

2.3.3 Mass spectrometry analysis

Shotgun proteomics, together with the availability of genomic sequences, has rapidly become the reference point for many researches (for review see [161]). Shotgun strategies allows the high-throughput analysis of a large sets of samples as it aims at identifying as many proteins as possible. Proteins contained in the purified fraction are separated on SDS-PAGE and subsequently enzymatically cleaved by trypsin to generate tryptic peptides. Depending on the sample complexity, these latter can be separated by liquid chromatography (LC) prior to mass-spectrometry analysis (either in single (MS) or tandem (MS/MS) modes). LC-separation is mainly focused at enlarging the dynamic range since, when sample complexity is reduced, low abundance proteins are less likely to be obscured by more abundant ones. Moreover, as analytical sensitivity increases, the difficulty to distinguish between contamination and low-abundance (but genuine) proteins increases as well, and filtering the first is essential. The most practical solution is to repeat the analysis of independent organelle preparations in a common experimental work flow; this is because proteins that are observed at high frequency across the preparations are more likely to be genuine organelle proteins. The proper MS analysis is carried out either in single or tandem mode (MS/MS). Peptide

ions, which are called precursor ions, undergo a characteristic fragmentation in the mass spectrometer and the fragment mass patterns can be used to establish the sequence information. Protein identification is usually performed through database searching starting from the sequence information [162]. In the next paragraph more details are given.

2.3.3.1 Protein identification

There are different approaches to identify proteins following a MS/MS analysis. The first one is referred to as the database-driven method and relies on online tools such as Mascot (`http://www.matrixscience.com`), Sequest, X! Tandem (`(http://www.thegpm.org/TANDEM`) or Phenyx (`http://www.phenyx-ms.com/`). Despite the chosen tool, they generally compare the collected MS/MS spectra to theoretical MS/MS spectra generated from a virtual tryptic digestion of a protein sequence database (which is called *in silico* digestion). Candidate proteins are given a score with respect to the level and number of matching spectra. Database-driven protein identification is fast and particularly suitable for the processing of a large amount of data sets. By contrast, in the case of close-homolog proteins (for species lacking a full-annotated genome) results can be unsatisfactory since minor changes in the amino acid sequence translate in important changes in spectra [157]. A second approach is referred to as the *de novo* sequencing and the amino acid sequence is extracted directly from the MS/MS spectrum in a fully database independent way [163]. Several *de novo* sequencing tools were developed and some of them achieve good quality sequencing results when applied to high quality spectra [164][165]. These tools however, are compromised by MS/MS inaccurate measurements, missing peaks (gaps) and chemical or instrument noise. Reliable *de novo* sequences are then searched against a protein database from a close relative of the organism under investigations, using MS-BLAST (`http://genetics.bwh.harvard.edu/msblast/`(an error tolerant search tool which allows identifying peptides on the basis of close homology to peptides in the database) [163][166][167][168][169][170]. Compared to the database-driven method, *de novo* sequencing can cope with homologous proteins since it can easily handle mutations between the actual peptide and the proteins reported in the database.

2.3.3.2 Validation of the results

Despite the method used to identify proteins within the sample, results need to be evaluate for their reliability. Furthermore it is important to con-

sider that actual manual verification could not be feasible on the hundreds of proteins which can be assigned following a single LC-MS/MS run. For this purpose, dedicated informatic tools are of a great help in distinguish between correct and incorrect peptide assignments. As mentioned above, all database-driven search engines provide a score which represents the quality of the matching; moreover two further approaches were developed in order to increase the overall reliability. The first one is statistic-based; each spectrum-to-peptide assignment is evaluated with respect to all other assignments (including also the incorrect ones). The method applies *machine-learning* techniques and employs different parameters, such as scores and peptide properties and it calculates a probability of correct matching for each spectrum-to-peptide assignment [171]. The second approach is based on database searches using a fictitious database. This strategy is based on the assumption that the false discovery rate (FDR) can be estimated with respect to assignments to a false database. This last is obtained with inversion of the protein sequences of the original database. Furthermore, it is assumed that incorrect assignment of the spectra to the target or reversed sequences are equally likely. The total number of false positives is calculated as in equation 2.1 where n_{fwd} is the number of peptides identified in the correct database while n_{rev} in the reversed one.

$$FDR = 2\frac{n_{rev}}{n_{rev} + n_{fwd}} \tag{2.1}$$

2.3.4 Mass spectrometry-based protein quantification

During a comprehensive proteomic investigation, the possibility to quantify proteins can be extremely interesting. Applications are comprised in a wide range of fields. For example, comparative quantitative proteomics can deliver extraordinary insights in how cells and organelles change during development or respond to environment stimuli, stress, pathogen attack, etc. In our study we exploited relative quantification to highlight different accumulation of the photosynthetic complexes within the thylakoid sub-compartments. The need for quantitative information in proteomics has motivated the development of MS-based analytical methods that determine protein abundance both relative or absolute [157].

2.3.4.1 Relative quantification

Label-free approaches

One of the main difficulty during protein quantification is due to the fact that observed ion intensity in a MS spectrum is not directly correlated to the real abundance of the given peptide. This is because different peptides show different ionization properties. Nevertheless, for the same peptide under the same MS conditions, differences of ion intensities can reflect actual differences in the abundance [157]. When these considerations are taken in mind, two are the main approaches adopted for protein relative quantification: label-free and label-based. Label-free approaches are characterised by the fact that samples to be compared are not labeled before the mass-spectrometry analysis, and they are analysed separately. Resulting MS (or MS/MS) analyses are compared using appropriate computer tools. One of the most common approach used to perform label-free relative quantification (used in this thesis project) is referred to as the *spectral counting*[172]. The basic idea is to quantify a protein by the number of MS/MS spectra that led to its identification. The rationale for this approach is based on the MS/MS acquisition mode; in fact the mass spectrometer runs in the LC-MS mode and regularly triggers an MS/MS analysis based on the MS ion-intensity. The higher is the area under the LC-MS curve, the more often the MS/MS analysis mode will be triggered for this peptide and the more spectra associated to this polypeptide will be accumulated. Relative protein abundance is then inferred by the number of spectra. In literature, several examples of application of spectral counting to semiquantitative studies of *Arabidopsis* are reported. For example, it was used in *Ferro et al*[140] to perform a large-scale proteomic analyses of the three chloroplast compartments in *Arabidopsis*.

Label-free approaches, are particularly suitable for semi-quantitative studies as no additional sample preparation step is needed [157]. However, quality control must be sufficiently tight on each purification/analytical step in order to get a reliable comparison. Moreover, differential protein degradation can occur during sample collection and ionization efficiency for peptides is observed to depend on the sample concentration. Therefore, in order to reduce the variability (generated both before and during MS/MS analysis) sample derived from different biological and technical replicates are subject of a deep statistical analysis [173].

Label-based quantification

Labeling of (at least) one of the samples is performed in order to reduce variability. Samples are then mixed and analyzed together in one run by LC-MS or LC-MS/MS analysis. Pairs of peptides are chemically identical but with a constant mass increment in labeled samples over non-labeled and they can be distinguished by a mass-spectrometer. The ratio between the signals for a given peptide in the different samples provides a strong indication of its relative abundance. Several labeling techniques (*i.e.* enzymatic, chemical) can be employed for relative quantification. The more commonly used are *(i)* iTRAQ [174], *(ii)* stable isotope labeling with amino acid SILAC [175] and *(iii)* $H_2{}^{18}O$ labeling [176]. These different labeling strategies require specific sample preparation. In literature, several examples of applications to *Arabidopsis* (or *Chlamydomonas*[284]) are reported. As in *Jones et al.*[182], where the iTRAQ method was used to profile phosphoproteome changes during the defense response of *Arabidopsis* to pathogens; or as in [285] where ^{15}N-metabolic labeling was applied to study leaf senescence.

2.3.4.2 Absolute quantification

MS analysis can also deliver absolute quantification when appropriate internal standards are provided. Absolute quantification provides information about the exact concentration of a given polypeptide and it mostly relies on stable-isotope mass spectrometric approach. Selected reaction monitoring (SRM) or multiple reaction monitoring (MRM) is a method of absolute quantitation (also terms AQUA) in targeted proteomics analyses [178]. In this approach, specific and known quantity of isotope-labeled reference peptides, which act as internal standards, are spiked into the samples after tryptic digestion but before MS analysis. It is important to note that, because the standards are not introduced at the beginning of sample preparation, severe quantification error may occur because of differential and/or cumulative loss of material during the preparation of the sample [157]. Recently, a techniques to avoid this problem was developed where the labeled standard can be introduced at the earliest steps of sample preparation. This technique is called PSAQ (protein standard absolute quantification) and the quantification is is based on the use of labeled proteins as standards [218]. Despite the technique adopted, absolute quantification is achieved by direct comparison of the MS signal intensities of a given peptide (derived from the proteolytic cleavage of the mother-protein) with those arising from the isotope-labeled reference peptides.

2.3.5 The whole chloroplast experimental proteome

In the last decades, several analyses have been performed using specific bioinformatic tools to predict the plastid proteome. The current consensus, based on the protein sequences predicted from available nuclear genome sequences, estimates that around 3000 proteins compose the chloroplast proteome. In the past 10 years, prediction approaches have also been integrated by large scale-proteomic analysis and many plant proteomes have been published. Moreover some of them were made available on-line as public repositories and are summarised in table 2.3.

Name	Specificity	species	url
Aramemnon	membrane	*A.thaliana, O.sativa*	`http://goo.gl/DEieub`
PPDB	plastid	*A.thaliana, Z.mays*	`ppdb.tc.cornell.edu`
SwissProt	plastid	*A.thaliana, N.tabacum*	`http://goo.gl/CCWwSc`
TAIR	generic	*A.thaliana*	`www.arabidopsis.org`
AT_Chloro	chloroplast	*A.thaliana*	`www.grenoble.prabi.fr/at_chloro`
SUBA	generic	*A.thaliana*	`http://goo.gl/GKsXC2`
MASCGator	generic	*A.thaliana*	`http://gator.masc-proteomics.org/`

Table 2.3 – Non-exhaustive list of major public repositories

In 2004, Baginsky and co-workers [17], delivered a proteomics-based study targeted to the *Arabidopsis* chloroplast proteome. This study identified 700 proteins with near-complete protein coverage for key chloroplast pathways (*i.e.* carbon fixation, photosynthesis). Later Zybailov and co-workers (2008) [179] performed a large-scale analysis of purified chloroplasts from *Arabidopsis* leaves and identified a total of 1325 proteins. Further annotation allowed the identification of more than 900 polypeptides which could be assigned unambiguously to the chloroplast; these included some previously unknown plastid components. Data was reposited in `http://ppdb.tc.cornell.edu` (PPDB). Ferro and co-workers (2010)[140] focused, in the same set of experiment, on the localisation of proteins in the stroma, thylakoids and envelope membranes. LC-MS/MS-based analyses allowed to create the AT_CHLORO database, a comprehensive repertoire of more than 1300 chloroplast proteins. Spectral counting was used to assess the partitioning of each protein in the three chloroplast compartments. These data, together with an in depth investigation of the literature were compiled to provide accurate sub

plastidial localisation of previously known and newly identified chloroplast proteins. Moreover the same strategy was further used to revisit the sub plastidial compartmentation of the chloroplast metabolisms and functions by *Joyard et al., 2009* [180]. In the next section it will be given a detailed description of previous proteomic investigation targeted to the chloroplast sub-compartments.

2.4 Previous proteomic investigations of chloroplasts sub-compartments

Each different compartment of the chloroplast (envelope, stroma and thylakoids) plays different and specific functions within the organelle metabolism and therefore is characterised by a specific subset of proteins, or sub proteomes. In addition, proteins can be present at different sub-chloroplast locations, (*e.g.* thylakoid and envelope membranes, stroma and envelope or thylakoid membranes). These different purified chloroplast sub proteomes have been investigated using a variety of approaches and plant species (in particular *A. thaliana, P. sativum* and *S. oleracea*). Chloroplast proteomics has clearly benefited from all the different purification and fractionation techniques, as will also be evident from the following paragraphs.

2.4.1 Proteomics of the chloroplast envelope

Envelope fraction has an intrinsic low abundance and contains only 1-2% of the total chloroplast proteins. Moreover some envelope membrane proteins (in particular membrane transporters) are hydrophobic being characterised by 1 or more transmembrane domains. These latter proteins need a specific enrichment with organic solvents in order to be properly characterised during a MS analysis. In *Seigneurin-Berny et al., 1999* [181] organic solvent treatment combined with 1-D SDS-PAGE successfully identified hydrophobic proteins and a small number of genuine envelope proteins from spinach chloroplasts, some of which were never detected before. Later *Ferro et al., 2002* [183] identified 54 envelope proteins thanks to the optimisation of treatments used to remove highly abundant soluble contaminants derived from the stroma (like RuBisCo) in spinach chloroplasts. Other proteomic studies were then performed in *Arabidopsis*, whose genome was fully sequenced, in order to establish a more complete list of chloroplast envelope proteins. *Ferro et*

al., 2003 and *Froehlich et al., 2003* [184][185] identified 100 and 350 proteins respectively thanks to the development of two independent approaches. In the first work, targeted to the hydrophobic core, different treatments (alkaline, salt, solvent treatments) were employed in the purification steps before MS analysis. By consequence most of the identified polypeptide were genuine hydrophobic envelope proteins. In the second work, no pre-enrichment step of the purified proteins was performed and therefore a higher number of proteins was detected. However, among them a significant proportion was composed of either known stroma protein or proteins derived from thylakoid or other subcellular compartments [186]. More recently *Ferro et al., 2010*[140] performed large-scale analyses of the three chloroplast compartments of *Arabidopsis* chloroplasts using a semiquantitative proteomics approach (spectral counting) and an in-depth investigation of the literature. In this study, more than 700 proteins were detected in the purified envelope fraction and, among them, around 460 were demonstrated to be more abundant in purified envelope fractions when compared to other plastid sub-compartments.

2.4.2 Proteomics of the chloroplast stroma

Few studies were performed on the stroma in order to characterise the stromal proteome (for reviews see [186] and [187]). A major advance was delivered by *van Wijk et al., 2004* [186] where, given the protome complexity, only a small number of protein complexes were characterised. *Peltier et al., 2006*[188] performed a proteomic analysis of chloroplast from *Arabidopsis* leaves and successfully identified 241 proteins from the stroma. These proteins covered not only already known chloroplast functions (including protein biogenesis and protein association to primary or secondary metabolism) but also identified a number of new components. Later, the same group revisited the *Arabidopsis* chloroplast stroma proteome and identified 550 proteins which are now included in the PPDB database (`http://ppdb.tc.cornell.edu/`)[179]. Nearly at the same time, focusing on the cold-stress response of *Arabidopsis*, *Goulas et al., 2006*[189] evidenced changes in the chloroplast soluble proteome. In particular it was found that both short- and long-term acclimation to cold promoted important changes in protein abundance within the stroma. In particular, 43 proteins were found to be differentially expressed during stress conditions. In *Ferro et al., 2010*[140] around 490 proteins were shown to actually reside at the stroma fraction and among them 337 were demonstrated to be only or mostly detected in purified stroma when compared to other plastid sub-compartments.

2.4.3 Proteomics of the thylakoids and thylakoid lumen

Protocols for lumen purification were first developed in spinach leaves in 1998 [190]. Two years later, the soluble luminal fraction of *Arabidopsis* chloroplast was published. It included 300 protein spots resolved on a 2-DGE (two dimensional gel electrophoresis) and, among them, it identified two proteins (plastocyanin and a putative ascorbate peroxidase [191]). Thanks to the availability of the full-sequenced *Arabidopsis* genome, *Peltier et al., 2002* used MS/MS analysis and identified a total of 81 proteins. Moreover they developed an approach to predict the thylakoid lumen proteome *in silico* by using characteristic protein parameters derived from the sequenced proteins. *Arabidopsis* lumen proteome was further integrated by the study of *Schubert et al., 2002*[192] where 36 new proteins were discovered. When combined, the above-cited proteomic studies provided more than 100 proteins; moreover semiquantitative approaches indicated that lot of them are present at concentrations at least 10K-fold lower than proteins involved in the photosynthetic electron transport chain [193]. An exhaustive description about previous proteomic investigations of the thylakoid membrane is reported in *Tomizioli et al., 2014* (section 2.5.1[139]). This section will main focus on studies carried out on the aqueous intermembrane space, the lumen.

2.5 Deciphering thylakoid sub-compartments using a mass spectrometry-based approach [1]

Martino Tomizioli[1,2,3,4], Cosmin Lazar[1,5,6], Sabine Brugière[1,5,6], Thomas Burger[1,5,6,7], Daniel Salvi[1,2,3,4], Laurent Gatto[8], Lucas Moyet[1,2,3,4], Lisa M. Breckels[8], Anne-Marie Hesse[1,5,6], Kathryn S. Lilley[8], Daphné Seigneurin-Berny[1,2,3,4], Giovanni Finazzi[1,2,3,4], Norbert Rolland[1,2,3,4]‡, Myriam Ferro[1,5,6]‡.

1-Univ. Grenoble Alpes, F-38000 Grenoble, France.
2-CNRS, UMR5168, F-38054 Grenoble, France. 3-CEA, iRTSV, Laboratoire Physiologie Cellulaire et Végétale, F-38054 Grenoble, France.
4-INRA, USC 1359, F-38054 Grenoble, France.
5-CEA, iRTSV, Laboratoire Biologie à Grande Echelle, F-38054 Grenoble, France.
6-INSERM, U1038, F-38054 Grenoble, France.
7-CNRS, FR3425, F-38054 Grenoble, France.
8-Cambridge center for Proteomics, Department of Biochemistry, University of Cambridge, CB2 1QR, United Kingdom.
‡ To whom correspondence should be addressed: Univ. Grenoble Alpes, 17 rue des Martyrs, F-38000 Grenoble, 38054 France. Tel.: 33-04-04-38-78-25-49; E-mail: `myriam.ferro@cea.fr`; `norbert.rolland@cea.fr`

Abstract

Photosynthesis ranks amongst the greatest inventions of nature. After it arose $\sim$ 3.5 billion years ago in anoxygenic bacteria, it has shaped atmospheric and ocean chemistries and probably changed the climate as well, as oxygen is released from water as part of the photosynthetic process. In photosynthetic eukaryotes, this process occurs in the chloroplast, an organelle containing the light harvesting chlorophyll a/b-protein complex, LHCII, and also the most abundant biological membrane, the thylakoids. The thylakoid membranes form a physically continuous three-dimensional network that encloses the lumen. The thylakoids of plants and some green algae are structurally inhomogeneous, consisting of two main domains: the grana, which are piles of membranes gathered by stacking forces, and the stroma-lamellae, which are unstacked thylakoids connecting the grana. The major photosynthetic complexes are unevenly distributed, within these compartments, due to steric and electrostatic constraints, as indicated by biochemical and spectroscopic

1. Supplementary tables available at `http://goo.gl/D8Q8qi`

analysis. Although proteomic analysis of thylakoids has been instrumental to define its protein components, their post-translational modifications or their localisation in the membrane and lumen compartments, no extensive proteomic study of sub-thylakoid localisation of proteins in the BBY (grana) and the stroma-lamellae fractions has been achieved so far. To fill this gap, we performed a complete survey of the protein composition of these thylakoid sub-compartments using thylakoid membrane fractionations. We employed semi-quantitative proteomics coupled with a data analysis pipeline and manual annotation to differentiate genuine BBY and stroma-lamellae proteins from possible contaminants. Using this approach, we were able to improve the dynamic range detection of minor thylakoid proteins. About 300 thylakoid (or potentially thylakoid) proteins were shown to be enriched in either the BBY or the stroma-lamellae fractions. Overall present findings corroborate previous observations obtained for photosynthetic proteins that used non-proteomic approaches. The originality of the present proteomic relies in the identification, at the molecular level, of photosynthetic proteins whose differential distribution in the thylakoid sub-compartments might explain already observed phenomenon such as LHCII docking. Besides, from the present localisation results we can suggest new molecular actors for photosynthesis-linked activities. For instance, most PsbP-like subunits being differently localised in stroma-lamellae, these proteins could be linked to the PSI-NDH complex in the context of cyclic electron flow around PSI. In addition we could identify about a hundred new likely minor thylakoid (or chloroplast) proteins, some of them being potential regulators of the chloroplast physiology.

2.5.1 Introduction

As primary producers, plants are at the basis of the food chain for most ecosystems and control the planet atmosphere via photosynthesis. In eukaryotes, this process, responsible for carbon fixation and for the release of gaseous oxygen into the atmosphere, takes place in a specialized compartment, the chloroplast. This semi-autonomous organelle plays a number of essential functions, including photosynthesis, nitrogen assimilation, sulfur reduction and assimilation, synthesis of amino acids, fatty acids and many secondary metabolites [13][180][194][195][196][197]. The chloroplast is not the only type of plastid. Plastids are indeed found in every plant tissue (with a very few exceptions such as angiosperm pollen grains) and in apicomplexan parasites [198][199]. Plastids play diverse and developmentally regulated functions including carotenoids accumulation in flowers and fruits (chromoplasts) and starch accumulation (amyloplasts). Chloroplasts are the most studied plastid type. They are distributed throughout the cytoplasm of leaf cells and contain several key sub-compartments including: *(i)* the chloroplast envelope, which is a double membrane system surrounding the organelle and modulating the communication of the chloroplast with the plant cell; *(ii)* the stroma, mainly composed of soluble proteins, which is the site where CO_2 assimilation takes place thanks to the consumption of reducing equivalents and ATP produced by light-driven electron flow *(iii)* the thylakoid membrane, which is a highly organized internal membrane network formed of flat compressed vesicles and which is the center of oxygenic photosynthesis. The thylakoid vesicles delimit another discrete compartment, the lumen. Being the place of the light phase of photosynthesis, the thylakoid compartment has been deeply investigated from a functional, structural and biochemical point of view. Several complexes are located in the thylakoid membranes to catalyze this activity: the two photosystems, PSI and PSII, the cytochrome b_6f and the ATP synthase CF_0-F_1. They mostly act in series and their function must be tightly regulated to avoid excess (or unbalanced) light absorption or saturation of the electron flow chain, which leads otherwise to photodamage [200]. To do so, the rather simple photosynthetic membrane present in cyanobacteria has progressively evolved into a more sophisticated structure in some algae and plants. There, the thylakoid membranes form a physically continuous three-dimensional network consisting of two main domains: the grana, which are stacks of thylakoids, and the stroma-lamellae, which are unstacked thylakoids connecting the grana stacks. The grana stacks are surrounded by unstacked membranes, called grana ends and margins [50].

High throughput analysis techniques, combined with genome sequencing data, have largely modified the experimental approaches to study protein

localisation within a cell and changed our perception of the functional consequence of this localisation [201][202][203]. This is also true for the chloroplast, where several proteome catalogues have been produced so far [140][179][204]. They include descriptions of whole chloroplast proteomes, as well as of its sub-compartments. In particular thylakoids have been subjected to numerous proteomic investigations, mostly focusing on two biochemically different thylakoid protein populations: soluble proteins located in the lumen and more hydrophobic proteins present in the thylakoid membranes. Initial studies targeting the composition of the spinach and *Arabidopsis* thylakoid lumen were performed using 2-DGE analysis [190][191]. More than 60 soluble and peripheral membrane proteins were subsequently identified from purified pea thylakoid and detailed analysis of their targeting signals was performed [205]. Thanks to the availability of the *Arabidopsis* genome annotation, a proteomic study targeting luminal and peripheral proteins [193] allowed identification of a total of 81 proteins using MS/MS and a new approach to predict the thylakoid lumen proteome in silico. This work was completed by several independent approaches [189][192], leading to a consensus of more than 100 thylakoid lumenal proteins [186][189]. Interestingly, these studies have shown that the chloroplast lumen proteins are not restricted to the generation of the pH gradient that fuels ATP synthesis, but also play important roles for the regulation of photosynthesis, supporting protein turnover and protecting against oxidative stress.

The proteome of the thylakoid membranes has also been extensively studied. Initial MS-based studies of the thylakoid membrane proteins were essentially performed, in spinach and pea, on antennae or reaction-center subunits to identify the composition of the photosynthetic complexes and to detect post-translational modifications associated with these abundant proteins. Whitelegge and co-workers used ESI-MS to catalog intrinsic membrane proteins of the D1 and D2 reaction-center subunits from spinach thylakoids, to identify protein complexes components and to provide insights into native protein/protein interactions and their post-translational modifications [206]. Furthermore, MS analysis of tryptic peptides released from the surface of *Arabidopsis* thylakoid membranes was used to characterise the reversible phosphorylation of chloroplast thylakoid proteins [207]. These studies confirmed earliest data demonstrating that various subunits of the PSII and light-harvesting polypeptides (LHCII) are phosphorylated. Some of these phosphorylation events were also found to be reversible in response to light/dark transitions. Zolla and co-workers also studied the light-harvesting proteins (LHCI or LHCII) from various monocot and dicot species and determined their intact molecular weights [208]. Whitelegge and co-workers also coupled ESI-MS with reverse-phase chromatography to catalog all detectable proteins

in samples of PSII-enriched thylakoid membrane sub-domains (grana) from pea and spinach [209][210]. Only 30 proteins were identified, with important information on the phosphorylation of several PSII subunits. Later, the same group reported a set of 58 nuclear-encoded thylakoid membrane proteins from four plant species [208][211] and assigned experimentally the N-termini of all these proteins. This allowed testing the reliability of the different existing tools to predict chloroplast localisation and/or cleavage sites starting from experimentally identified transit peptides. The first in-depth analysis of the thylakoid membrane was published by van Wijk and co-workers [211], resulting in the identification of 154 proteins. The same group later identified more than 240 thylakoid membrane proteins, of which 86 were unknown [212]. A recent study of thylakoid membrane dynamics, especially on environmentally modulated phosphoproteome induced by environmental changes was targeted to the photosynthetic membranes of Chlamydomonas reinhardtii [213]. This study revealed that major changes in phosphorylation are clustered at the interface between the PSII core and its LHCII antennae. These data also suggest that the controlling mechanisms for photosynthetic state transitions and LHCII uncoupling from PSII under high light stress allow thermal energy dissipation. In a subsequent study also relying on intact mass measurements of membrane proteins, Zolla and co-workers analysed all PSI and LHC proteins in ten different plant species, and identified PSI proteins present within stroma-lamellae of the thylakoid membrane [214]. More recently, we performed large-scale analyses that aimed at identifying the whole chloroplast proteome. In this context, we focused, in the same set of experiments, on the localisation of proteins in the stroma, thylakoids and envelope membranes [140]. The partitioning of each protein in these three chloroplast compartments was assessed using a semi-quantitative proteomics approach (spectral counting). These data, together with an in depth investigation of the literature, were compiled to provide accurate sub-chloroplastic localisation of previously known and newly identified chloroplast proteins. Amongst the 500 proteins that were identified in the thylakoid fraction, 220 could be assigned to the thylakoid compartment (see AT_Chloro database at `http://www.grenoble.prabi.fr/at_chloro/`).

Although proteomic analysis of thylakoids has allowed defining their protein composition, post-translational modifications and localisation in the membrane and lumen compartments, a complete survey of the protein composition of the thylakoid sub-compartments is still lacking. The objective of the present work was to complete previous studies and gain further information about the protein segregation in the grana and stroma-lamellae domains. To this aim, we have performed a complete survey of the protein composition of these thylakoid sub-compartments using a semi-quantitative

proteomic approach to validate the differential distribution of thylakoid proteins between stroma-lamellae and grana. In this study we not only confirm previous information about the localisation of photosynthetic proteins, but also observe unexpected protein composition in photosynthetic complexes localised in both the BBY and the stroma-lamellae. This allows us to generate hypotheses about the assembly/function of thylakoid proteins.

2.5.2 Results

Optimized thylakoid fractionation to generate sub-thylakoid proteomes: overview of the strategy

Purification of thylakoid subfractions (fig.2.6) started from Percoll-purified intact chloroplasts from *Arabidopsis* leaves [141]. The rationale for this approach was to minimize contamination by mitochondria, which are largely removed from the sample during the isolation of intact chloroplasts. After chloroplast lysis in a hypotonic medium, thylakoids were solubilized with digitonin (10 mg $mgChl^{-1}$).

After centrifugation at 15,000 g, the pellet was used for the purification of the inner grana fraction (BBY), following the protocol established by *Berthold et al*[146]. The supernatant was washed, and centrifuged at 140,000 g to recover stroma-lamellae (fig.2.6). Starting from 100 - 200 g of *Arabidopsis* leaves, we obtained 40 μg of chlorophyll for the stroma-lamellae and 80 μg of chlorophyll for the BBY (corresponding to 250 μg and 200 μg of proteins respectively).

To obtain statistically reliable results, three biological replicates were prepared and two technical replicates were generated for each chloroplast biological replicate. Therefore, six samples were produced for each of BBY, stroma-lamellae (LAM), margin (MAR) and thylakoid (THY) fractions during the purification process (fig.2.6). All the protein samples were concentrated on a SDS-PAGE between the stacking and the separating gels according to [184] prior to LC-MS/MS analyses that were performed using a LTQ-Orbitrap VelosPro coupled to a nano-LC system (fig.2.6). As previously described in the context of the sub-chloroplastic localisation of proteins [140], spectral counting was used for relative quantification in order to determine the sub-thylakoid localisation of identified proteins. Different spectral counting measures can be obtained for a given identified protein group: total number of MS/MS spectra corresponding to the identified peptides, the number of MS/MS spectra corresponding to proteotypic peptides, or weighted spectral counts. In order to accurately deal with peptides shared between different protein groups, weighted spectral counts were used. Indeed, it was shown that distributing spectral counts of shared peptides, based on the presence of unique peptides in a given protein group, generated the best results [215]. Consequently we chose to calculate weighted spectral counts as suggested in Abacus [216] and used these metrics for subsequent statistical analysis. Then, both statistical and clustering analyses were performed in order to identify proteins that were significantly differentially distributed be-

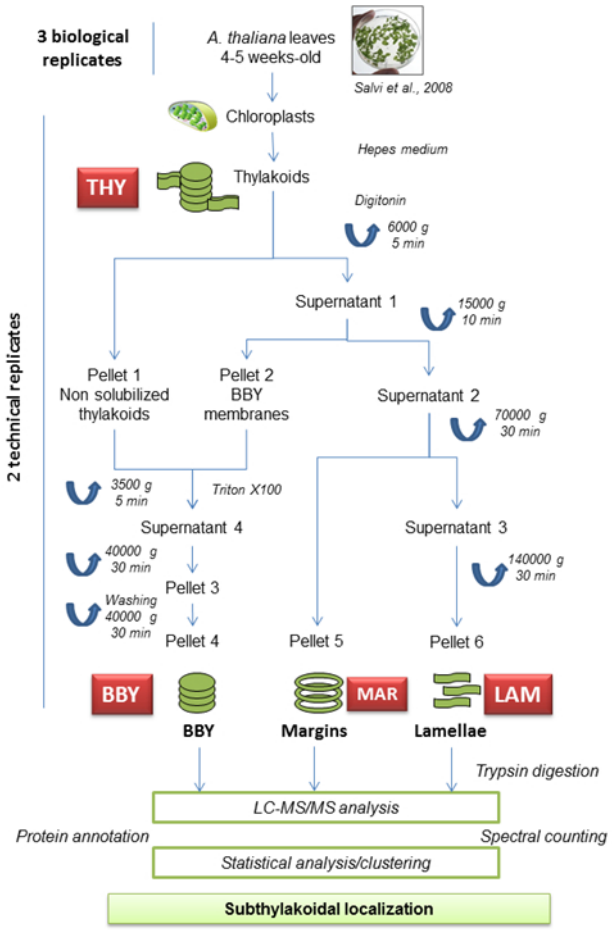

Figure 2.6 – **Purification of chloroplast subfractions: overview of the complete strategy.** Chloroplasts from *Arabidopsis* leaves were purified on Percoll density gradients. The stroma-lamellae, margins and BBY fractions were purified using different detergents and sequential centrifugations

tween the different sub-thylakoid fractions. In addition, all identified proteins were thoroughly annotated with respect to their known or expected subcellular and sub-chloroplastic localisations and function for further data mining purposes. Eventually, 1295 proteins were identified from all the analyses performed (Supplemental_Table 1).

Evaluation of cross contaminations at the sub-cellular, sub-chloroplastic and sub-thylakoid levels

Cross-contaminations at the sub-cellular level was evaluated using analysis of the 1295 proteins identified from all the analyses performed and manual annotation or prediction of their sub-cellular localisation (Supplemental_Table 1). In good agreement with proteomic analyses previously performed on compartments derived from Percoll-purified chloroplasts [140], spectral counting analysis of our data indicate that cross-contamination with other sub-cellular compartments is very low (*i.e.* less than 5%; fig.2.7).

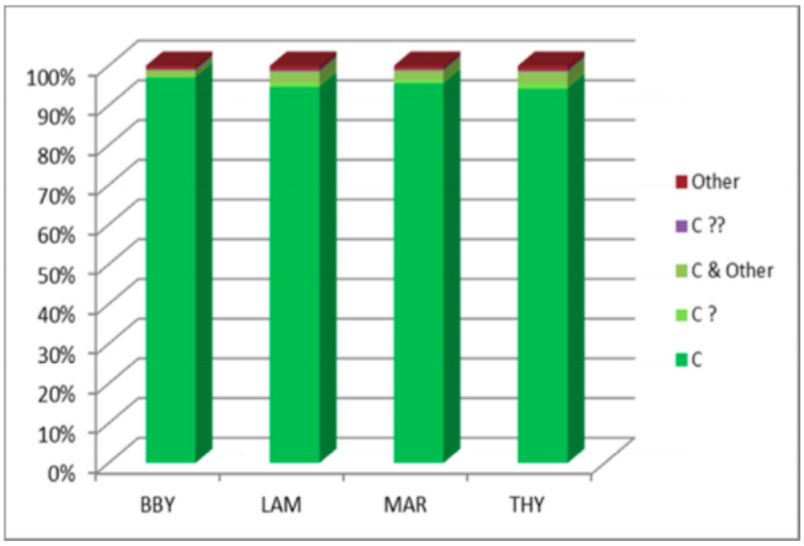

Figure 2.7 – **Estimation of subcellular cross-contamination using spectral count data.** All 1295 identified proteins were considered. BBY: inner grana; LAM: stroma-lamellae; MAR: margin; THY: thylakoids. The following classification refers to the "Main subcellular localization? column of Supplemental_Table 1. C: chloroplast localization; C ?: likely localization in the chloroplast; C and other: localization in the chloroplast and in other subcompartments; C ??: unknown sub-cellular localization; Other: localization in sub-cellular compartments other than the chloroplast. For each fraction, percentages are calculated from Supplemental_Table 1 using the normalized weighted spectral count sum (columns XXX_Sum_norm).

We also quantified the cross-contamination of the sub-thylakoid fractions

(stroma-lamellae and BBY) using marker proteins associated to the stroma and envelope sub compartments, the two other main sub-chloroplastic compartments. This was done using specific antibodies raised against marker proteins from the different sub-chloroplastic fractions (the large subunit of RuBisCO, a known marker from the stroma and PHT4;4, a phosphate transporter associated to the inner membrane of the chloroplast envelope). For each analysis, three different biological replicates were tested. The level of cross-contamination was qualitatively evaluated by direct comparison of the intensities of the signals (Western-blots) arising from the fractions to be tested and those arising from a range of dilutions between 3 and 100% of purified fractions derived from other chloroplast compartments. Data reported in fig.2.8 indicate an average level of cross-contamination between 3 and 20% for all the purified fractions analysed. Overall, stroma and envelope contaminations appeared to be lower than 3% in the BBY fraction, whereas a larger contamination by envelope proteins (between 10-15%) was detected in the stroma-lamellae fraction. Contamination of the stroma-lamellae fraction with the marker from the stroma was found to be lower than 10%.

We next assessed the specific protein composition of sub-chloroplastic fractions (fig.2.9) using SDS-PAGE and Western-blot analyses targeting known markers of the various purified subfractions.

As shown in fig.2.9A, a Coomassie blue staining of the proteins present in the different fractions and separated on a SDS-PAGE identifies different polypeptide profiles, when compared to that of intact chloroplasts or isolated thylakoids. Indeed, as expected, LHCII (fig.2.9A, LHCII), the major antenna complex of the PSII, was observed to be highly enriched in the BBY fraction (fig.2.9A, lane B) while it was less enriched in the stroma-lamellae fraction (fig.2.9A, lane L). Subunits of the ATP synthase complex (Fig2.9A, α/β ATPase), which are known to be present in the non-appressed regions of the thylakoids, could not be detected in corresponding lane of the SDS-PAGE (fig.2.9A, lane B) consistent with the absence of this complex in the grana stacks. Both in BBY and stroma-lamellae fractions, we barely detected known abundant markers associated to other chloroplast sub-compartments, such as the RuBisCO (fig.2.9A, RBCL) for the stroma (fig.2.9A, lane S) or the phosphate/triose-phosphate transporter (TPT) for the envelope (fig.2.9A, lane E).

The enrichment of specific complexes in purified stroma-lamellae and BBY fractions was further confirmed by Western-blot analyses, using specific antibodies. fig.2.9B shows that CP43, a chlorophyll protein associated with PSII, was largely enriched in the BBY fraction (fig.2.9B, lane B) when compared to the thylakoids (fig.2.9B, lane T) or the intact chloroplasts (fig.2.9B, lane C) fractions. By contrast, no CP43 could be detected in the

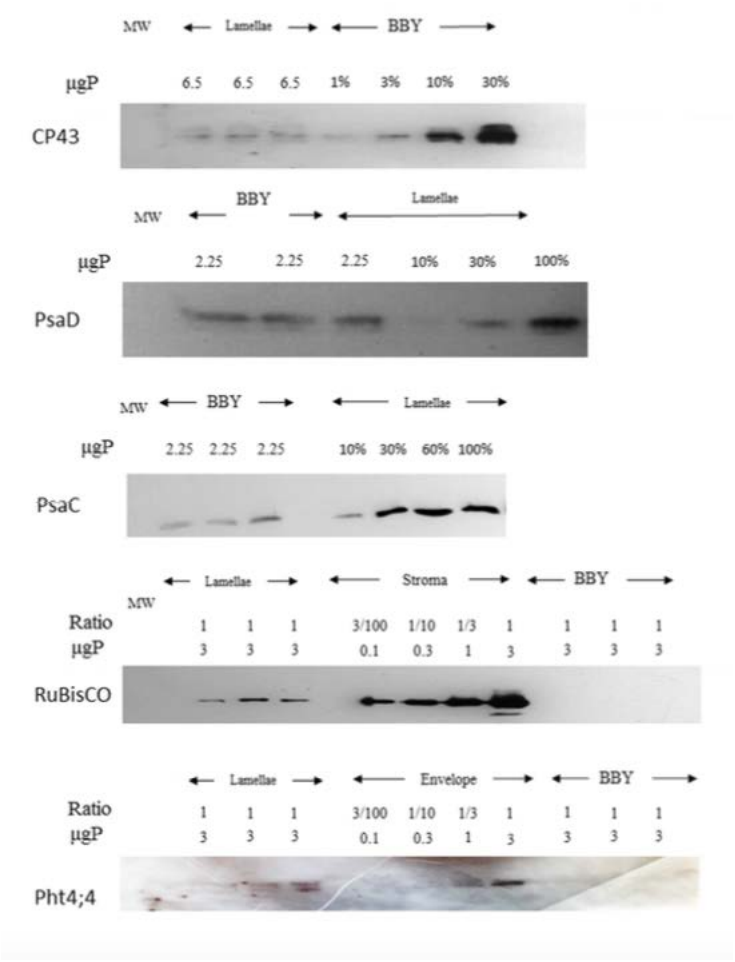

Figure 2.8 – **Estimation of sub-compartment cross-contamination in stroma-lamellae and BBY preparations from *Arabidopsis* chloroplasts.** Three different biological replicates of BBY and stroma-lamellae were tested to estimate the level of contamination by stroma and envelope proteins. Cross-contamination BBY/stroma-lamellae was also evaluated. Western-blots were performed with using polyclonal antibodies raised against RbcL (AtCg00490, stroma marker), Pht4;4 (At4g00370, envelope marker), CP43 (AtCg00280, BBY marker), PsaD (At4g02770, stroma-lamellae marker) and PsaC (AtCg01060, stroma-lamellae marker).

stroma-lamellae fraction (fig.2.9B, lane S). AtpB and PsaD, components of the ATP synthase CF_0-F_1 and of PSI respectively (two complexes known to

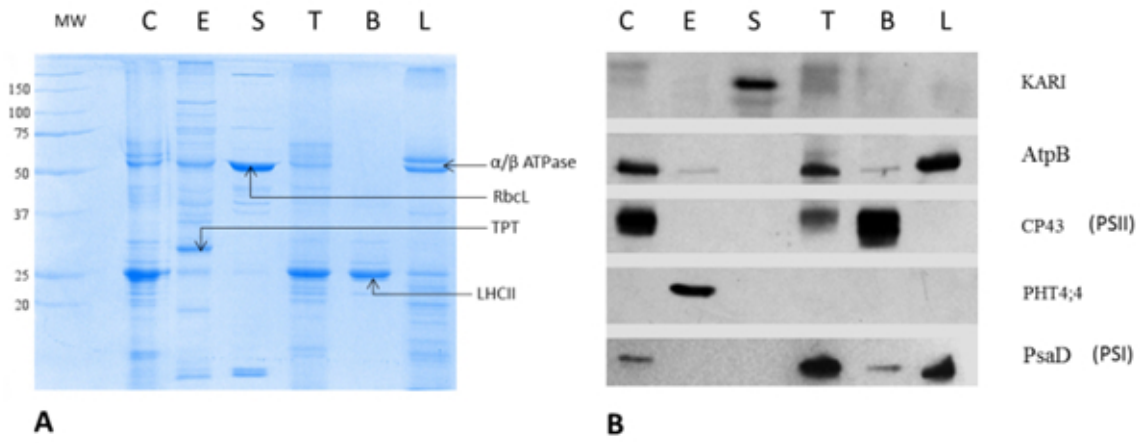

Figure 2.9 – **characterisation of Percoll-purified *Arabidopsis* chloroplast and sub-plastidial fractions.** C, crude chloroplast proteins; E, envelope membrane proteins; S, stroma proteins; T, thylakoid proteins; B, BBY proteins; L, stroma-lamellae proteins. Each fraction contained 6 μg proteins. (A) Fractions were analysed on a 12% SDS-PAGE. α/β ATPase: alpha and beta subunit of the ATPase (stroma-lamellae marker), RBCL: Large subunit of RuBisCO (stroma marker), TPT: Phosphate-triose-phosphate translocator (envelope marker), LHCII: Light harvesting complex proteins (BBY marker). (B) Western-blots were performed with using polyclonal antibodies raised against KARI (At3g58610, stroma marker), AtpB (ATCG00480) and PsaD (At4g02770) (stroma-lamellae markers), CP43 (AtCg00280, BBY marker), PHT4;4 (At4g00370, envelope marker).

be predominant in the stroma-lamellae), were found both in the thylakoids (fig.2.9B, lane T) and in the chloroplasts (fig.2.9B, lane C). AtpB and PsaD were enriched in the stroma-lamellae (fig.2.9B, lane S), while being largely diminished in the BBY fraction (fig.2.9B, lane B).

As our objective was to obtain accurate data about sub-thylakoid localisation, we then assessed the presence of stroma-lamellae-enriched complexes in the BBY, and vice versa, using the same Western-blotting approach (fig.2.8). We found that $> 10\%$ of the PsaD subunit was localised in the BBY. However, numbers became smaller in the case of another PSI subunit (fig.2.8; lanes PsaD and PsaC), suggesting a possible heterogeneity at the level of this complex (see below). On the other hand, less than 3% of the PSII complexes (fig.2.8, lane CP43) were located in the stroma-lamellae. This

indicates that, as expected from previous studies (for a review, see [148]), none of the major photosynthetic complexes were exclusively localised in a single compartment (with the possible exception of the ATPase). However, a clear enrichment of the major complexes in one compartment is seen. This was further confirmed by measuring the fluorescence spectra of the different fractions at cryogenic temperatures (fig.2.10).

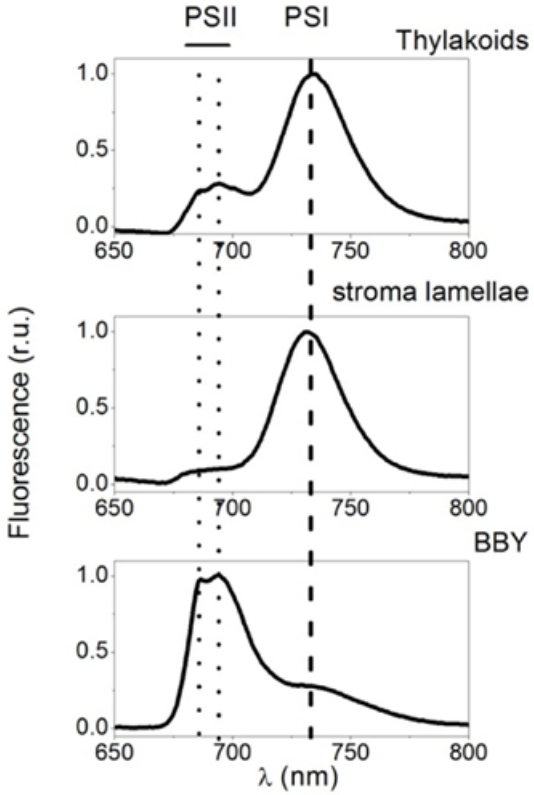

Figure 2.10 – 77K chlorophyll fluorescence emission spectra of thylakoid membrane subfractions isolated from *Arabidopsis*. Thylakoid proteins (or thylakoid subfractions) samples were loaded on to a metal cuvette, which was directly bathed into a liquid nitrogen solution. Fluorescence spectra were recorded upon excitation at 470 nm. Peaks were normalized for comparison purposes. Top spectrum: isolated thylakoids. Medium spectrum: stroma lamellae. Bottom spectrum: BBY fraction.

At variance with room temperature, PSI fluorescence becomes visible at 77K. Therefore, three main fluorescence emission peaks were detected in the

red region of the visible spectrum, upon excitation of purified thylakoids with blue light. The first two peaks (685 and 695 nm) represent fluorescence emission from PSII, while the large fluorescence peak seen at 730 nm stems from PSI. The two PSII peaks were barely detectable in the purified stroma-lamellae fraction and the PSI fluorescence peak alone turned out to be extremely reduced in the purified BBY fractions when compared to the thylakoids (fig.2.10). In no case, was emission from energetically uncoupled chlorophyll observed, indicating that no damage to the two photosystems was induced by our purification protocol. Measurements of the chlorophyll *a/b* ratio and oxygen evolution capacity of the different fractions (Supplemental_Table 2) also confirmed the successful separation of the two fractions. The chlorophyll *a/b* ratio of BBY fraction turned out to be much lower (1.7) than that of thylakoids and stroma-lamellae (2.9 and 4.2 respectively) consistent with the well-established notion that chlorophyll *b* is accumulated in the PSII antenna [148] because it is mainly contained in the LHCII complexes. Measurements of oxygen evolution in presence of exogenous electron acceptors (ferricyanide and 2,5-dichloro-p-benzoquinone) showed that our BBY preparation retained most of the O_2 evolution capacity of the starting material (thylakoids) while no oxygen evolution was detectable in the stroma-lamellae fraction. This confirmed the large enrichment of PSII in the BBY preparations when compared to the stroma-lamellae.

In conclusion, Western-blot, cryogenic temperature fluorescence, oxygen evolution and assessment of the chlorophyll *a/b* ratios analyses indicate that cross-contaminations between stroma-lamellae and BBY fractions, or their contamination by other chloroplast compartments were low enough to justify a MS-based analysis of the sub-thylakoid localisation of the proteins embedded in the photosynthetic membranes.

An updated repertoire of chloroplast and thylakoid proteins

The present study allowed the identification of 1295 proteins (Supplemental_Table 1). We first evaluated the coverage of the chloroplast thylakoid proteome by combining present data with earlier large-scale analyses targeted to the chloroplast. To this aim, we compared proteins identified during this work with those previously reported by Ferro *et al.* [140] (AT_CHLORO database) and Zybailov *et al.* [179], that is, two extensive studies, performed at the whole chloroplast level, where similar numbers of proteins were identified (fig.2.11). These previous chloroplast data and present results were collated to obtain a total of 2103 non-redundant proteins. The overlap of the present study with the other data shows that the AT_CHLORO database

contained more than 300 proteins that were not identified during the study of Zybailov *et al.* [179]. This could be easily explained by the specific enrichment (a factor of ~ 50) resulting from the purification of the envelope fraction that was specific to the study of Ferro *et al.* [140] and allowed detection of minor chloroplast envelope proteins.

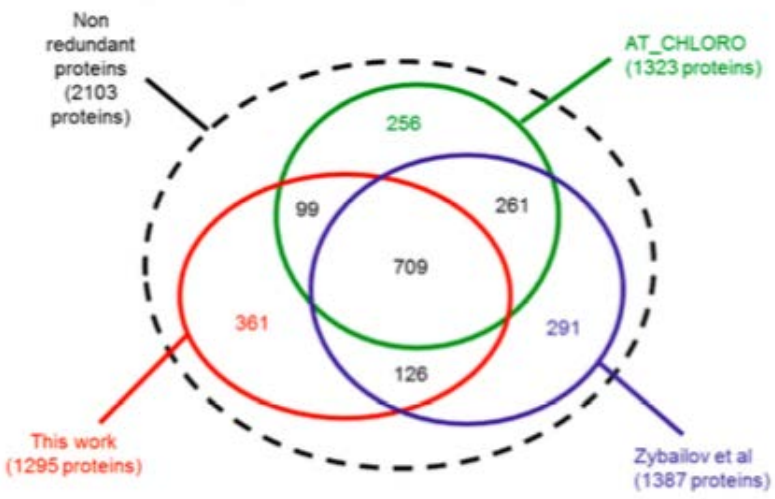

Figure 2.11 – **Venn diagram indicating the overlap of proteins identified during this work with previous data obtained by Ferro *et al.* or Zybailov *et al.*** This work: proteins identified in the present work; AT_CHLORO: proteins from AT_CHLORO; Zybailov *et al.*: protein identified by Zybailov *et al.* Note that 361 proteins (47%) were identified only in the present work (Supplemental_Table 3).

When compared to previous large scales proteomic analyses targeting the chloroplast, of the 1295 proteins identified in the thylakoid fractions, 361 (28%) novel proteins were identified in the present study (Supplemental_Table 3). Most of them were identified with some of the lowest spectral count measures (Supplemental_Table 3, columns R, S, T and U), and often detected in only one of the fraction (Supplemental_Table 3, columns D, E, F and G). In order to estimate the proportion of the proteins that are genuine chloroplast proteins we analysed their subcellular and sub-chloroplastic localisation using data from the literature and targeting prediction tools (Supplemental_Table 3, columns L, M, N and O). About 70 proteins, which are known to be major components of other cell compartments (plasma mem-

brane, cytosol, nucleus, golgi, vacuole, mitochondria, peroxysome), were classified as cross-contaminants (Supplemental_Table 3, columns H and I, *Others*). However, more than one third of these 361 proteins are either known or predicted (using ChloroP and or TargetP tools) to be targeted to the chloroplast, and few more proteins, while lacking a predicted targeting peptide, are genuine chloroplast proteins (Supplemental_Table 3, columns H and I, *C?*). Finally, many other proteins ($\sim$ 150), while also lacking a predicted targeting peptide, were never detected in another cell compartment using previous proteomic approaches targeting the other cell compartments cited above. Thus, some of these proteins (Supplemental_Table 3, columns H and I, *C??*) may clearly be genuine chloroplast components that could be detected here thanks to the combination of i) thylakoid membrane fractionation (enrichment of minor components) and ii) the improved sensitivity of state-of-the-art mass spectrometers. Amongst those 361 proteins only 14 (At3g27690, At3g21055, At1g51400, At2g26500, At1g18730, At4g14870, At3g56010, At5g02160, At4g38100, At3g17930, At3g26580, At2g45180, At5g46390 and At3g63540) were previously identified in studies aimed at the characterisation of thylakoid proteomes (Supplemental_Table 4).

We next compiled the main thylakoid proteome studies which correspond to four types of investigations targeting different thylakoid fractions: thylakoid membranes [211][212], thylakoid lumen [192][193], whole thylakoid [140] and BBY/stroma-lamellae (present work). A set of 1400 proteins was collated (Supplemental_Table 4). In order to determine what is the minimal thylakoid proteome, as defined from proteomics experiments, successive different levels of curation were applied. Based on present curated annotations, we removed contaminant proteins (Supplemental_Table 4, protein labeled as *na* in the *Main subplastidial localisation* column). Referring to MapMan classes [217], we also removed proteins that belong to classes for which proteins are acknowledged to be localised either in other chloroplast compartments, that is, stroma and envelope, or in other subcellular compartments. These MapMan classes are the following ones: Calvin Cycle, DNA, envelope transporters, glycolysis, mitochondria electron transport, mitochondria transporters, protein aa (amino acid) activation, protein synthesis (ribosomal proteins), RNA processing, RNA transcription, RNA.RNA binding, starch metabolism and TCA (tricarboxylic acid cycle proteins). Proteins that belong to the class *PS/light reaction* were labeled as thylakoid proteins. We also labeled as thylakoid proteins those that were identified in the thylakoid with a percentage $\geq$ 50% of occurrence in our AT_CHLORO database [140]. In addition, proteins that were annotated in Supplemental_Table 1 to be Ch/Th were labeled as being thylakoid proteins. Proteins being annotated to be located in either in the stroma or the envelope were referred to as

non-thylakoid proteins. Remaining proteins were labeled *unknown*. Thus, from the present annotation of thylakoid proteomes, one can consider that $\sim$ 300 proteins are true thylakoid proteins. Besides, 400 proteins are potentially thylakoid proteins but for those proteins less biological evidences are available (Supplemental_Table 4). Therefore about half of the 1400 proteins collected can be considered to be contaminants either from other sub-cellular compartments or from other sub-chloroplastic fractions. Although this number seems important, it has to be relativized with respect to the actual amount of each protein identified in a given fraction. Moreover, when considering those proteomic analyses of thylakoid fractions, it is obvious that some contaminants from the stroma are difficult to avoid (*e.g.* highly abundant Calvin cycle and ribosomal proteins). Analysis of the compilation of major thylakoid proteomes indicate that 812 proteins were not identified in previous thylakoid proteomics investigations (fig.2.12). Amongst those 812 identified proteins, 25 were known to be located or partly located in thylakoids (*e.g.* several NADH DH proteins) and 281 proteins were annotated for not having determined sub-chloroplastic localisation. The latter class of proteins is particularly interesting as it potentially gathers new thylakoid proteins. Indeed, cross-contamination analysis suggests that these proteins are very likely to be new chloroplast proteins as contamination from other subcellular compartments is very low (less than 5%) and results from abundant and well-known proteins (*e.g.* cytosolic ribosomal proteins, mitochondrial ATP synthase, vacuolar ATPases). However, the actual localisation of those chloroplast proteins at the sub-chloroplastic level needs additional information to be collected.

Thus, from the comparison with chloroplast and thylakoid proteome previous studies we decided to extract potential new thylakoid proteins. From the proteins specifically identified in the present study, compared to chloroplast and thylakoid proteomes (see above), we filtered out the most likely contaminants from other cell and chloroplast compartments. An eventual set of 218 proteins was retrieved (fig.2.13). We chose to perform a detailed analysis of those 218 potentially new thylakoid proteins that were identified during this work. Most of these proteins were never detected using recent large-scale proteomic analyses and are thus expected to be low abundant proteins in the chloroplast or in other cell compartments contaminating the purified thylakoid fractions. To classify these proteins, we first used targeting prediction tools (ChloroP and TargetP) and database annotations (SUBA, PPDB) for the analysis of their subcellular and sub-plastidial localisation. We also screened the literature and other databases (TAIR, MapManBin, UniProtKB), to extract information about the available protein descriptions and functions (Supplemental_Table 5, rank 1-63). Out of these 218 proteins,

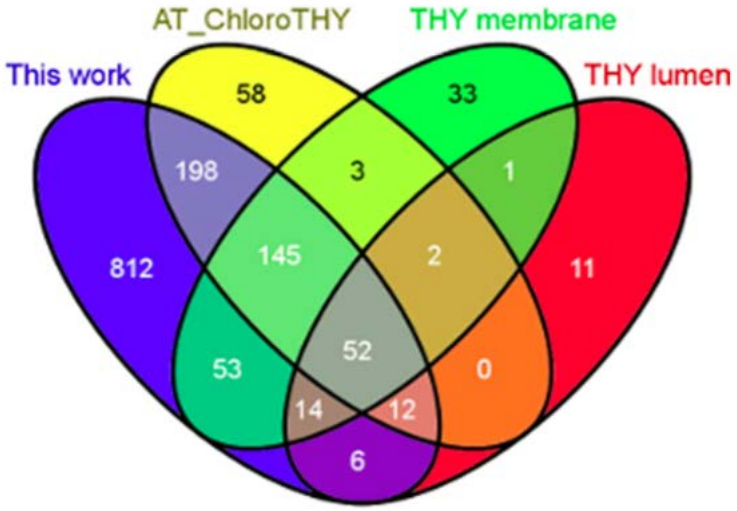

Figure 2.12 – **Venn diagram of proteins identified in major thylakoid proteomic investigations.**This work: proteins identified in the present work; AT_CHLORO THY: proteins from AT_CHLORO identified in thylakoid fractions (1); THY membranes: proteins identified in thylakoid membrane proteomic studies (3, 4); THY lumen: proteins identified in thylakoid lumen proteomic studies (5, 6). Lists of proteins can be found in Supplemental_Table 3

63 were predicted to be targeted to plastids using both ChloroP and TargetP targeting prediction tools, most of them (50 proteins) being thus also annotated as putative plastid proteins in the SUBA database. We thus considered that these 63 proteins were indeed good candidates for new chloroplast and thylakoid components.

We then carefully analysed the remaining 155 proteins and selected an additional set of 40 proteins that could also be associated to the list of these new chloroplast components, these proteins being predicted to contain a chloroplast transit peptide using either ChloroP or TargetP, or already classified as plastid protein in SUBA or, for very few proteins, experimentally associated to the chloroplast in more targeted studies (Supplemental_Table 5, rank 64-103). A detailed analysis (description, function, protein sequence, literature mining) of these proteins allowed supporting this classification. For instance, the YCF3 (ATCG00360) is chloroplast encoded and thus does not contain

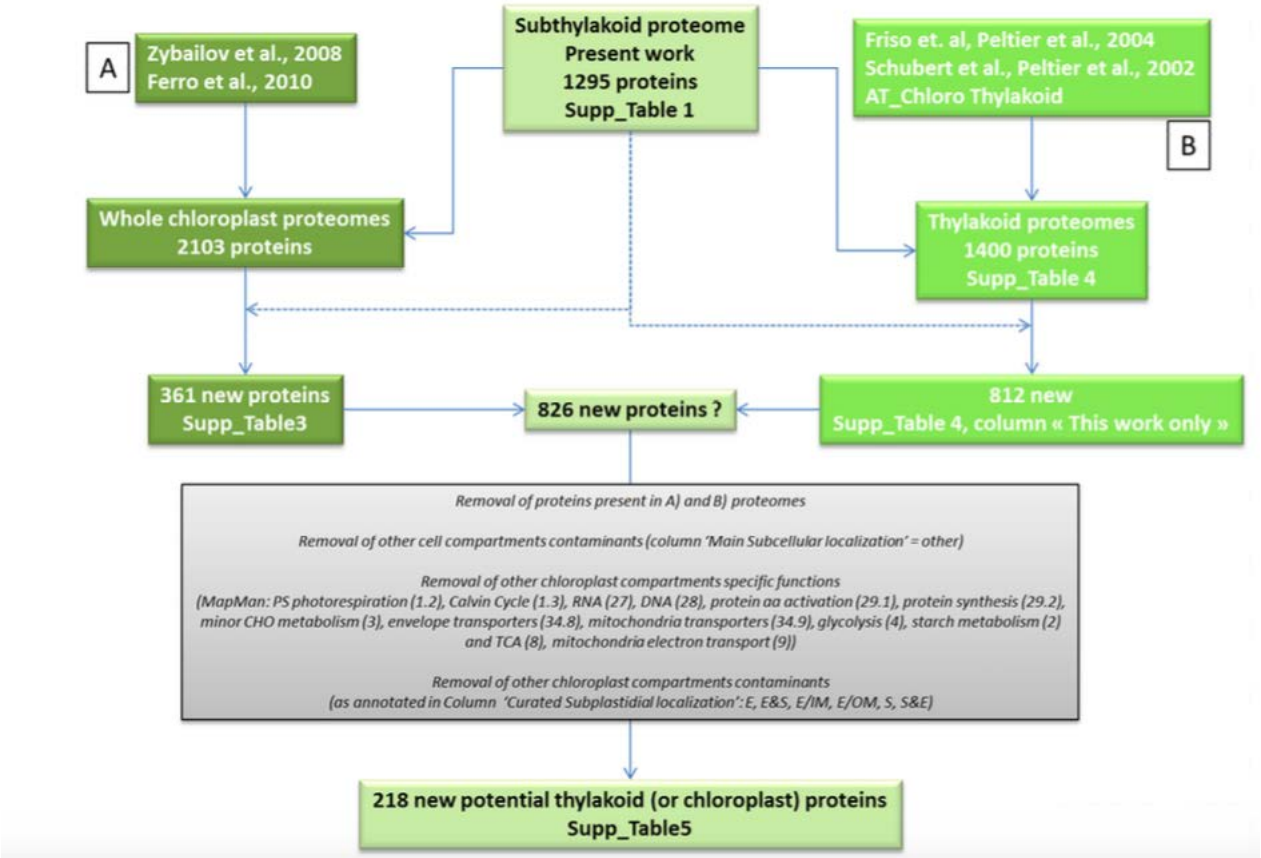

Figure 2.13 – **Potential new thylakoid proteins**

a predictable chloroplast transit peptide. The dynamin-like protein ARC5 (AT3G19720), an outer chloroplast envelope protein, is, according to the predictions, also devoid of a chloroplast transit peptide like most outer envelope proteins [219]. *Arabidopsis* ARC6 coordinates the division machineries of the inner and outer chloroplast membranes through interaction with PDV2 in the intermembrane space. As another example, a CAAX-like protease (AT1G14270) did not appear in our list of ChloroP positive proteins. However, checking the other putative gene models in TAIR revealed that one of the CAAX-like gene models (AT1G14270.1) is predicted to contain a chloroplast transit peptide using this ChloroP tool.

Consequently, out of the 218 new proteins identified here, at least 103 of them (63 + 40) might be genuine thylakoid (or at least chloroplast) proteins. Very few of the remaining 115 proteins could be further considered

for a tentative chloroplast localisation since most of them are either totally unknown proteins or only contain domains that allow to suspect or predict a putative function such as proteases, phosphatases, kinases, transporters, TPR or PPR proteins (Supplemental_Table 5, rank 104-218).

In conclusion, bioanalysis of the present results together with previous chloroplast and thylakoid proteomic analyses, indicates that a core of ∼300 well-characterised thylakoid proteins have been identified in chloroplast or thylakoid proteomic studies so far. In addition, from this data collection we showed that we identified about 200 potential new thylakoid proteins as discussed below.

Statistical analysis of differential abundances for protein localisation and proteins clustering

The present work is the first study aimed to specifically address the accurate proteomic-based localisation of thylakoid proteins, in the two major thylakoid sub-structures: BBY and stroma-lamellae (LAM). The main goal of the present study was to provide reliable data for a better understanding of the respective role of these compartments, especially with respect to PS protein complexes.

The discovery of proteins which are more enriched in grana compared to stroma-lamellae (or *vice-versa*) raises the question of how it is possible to differentiate genuine grana and stroma-lamellae proteins from possible contaminants. The issue of protein differential abundance is similar to the discovery of differentially expressed genes, as revealed by microarray gene expression analyses [220]. From the plethora of hypothesis testing algorithms proposed, we decided to perform the differentially abundance analysis using LIMMA [221][222] (with the moderated t-test and with an adjusted p-value threshold [222] of q = 0.05) (see the Materials and Methods section for details). This results in a number of 515 proteins which are differentially distributed between grana and stroma-lamellae. Among them, the proteins with LogFC > 0 are more abundant in stroma-lamellae, while those with LogFC < 0 are more abundant in grana (fig.2.14).

Based on these results we could identify 65 proteins more abundant in BBY compared to stroma-lamellae (p-value < 0.05 and LogFC < 0) and 450 proteins more abundant in stroma-lamellae than in BBY (p-value < 0.05 and LogFC > 0) (Supplemental_Table 6).

The same approach was used to test an additional fraction that was purified in our samples, *i.e.* the grana margins and end membranes (MAR fraction; fig.2.6). This fraction is defined as the portion of the appressed

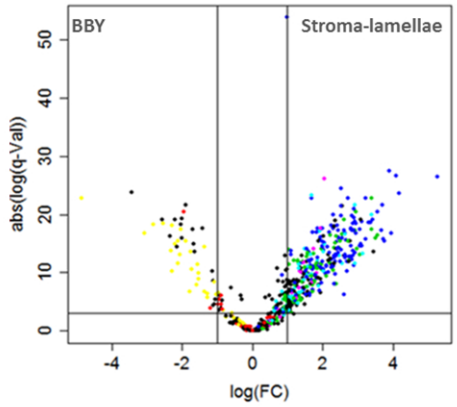

Figure 2.14 – **Volcano plot of quantified proteins for the BBY vs stroma-lamellae samples.** One dot corresponds to one protein; the color code corresponds to the labels from the proteins cluster analysis

thylakoids in contact with the stroma and, according to previous studies, represents an essential compartment for photosynthetic activity [223]. When performing differentially abundance analysis between margin fraction samples and BBY samples we identified a number of 296 differentially abundant proteins (p-value < 0.05), among which 238 are more abundant in margins (LogFC > 0). However, most of them, 229 proteins ($\sim$ 96%), were also enriched in stroma-lamellae when compared to BBY. The remaining 59 differentially abundant proteins were more enriched in BBY samples (LogFC < 0), and amongst those 59 proteins, 51 ($\sim$ 87%) of them are also found as being more abundant in grana when compared to stroma-lamellae samples. Overall, only 20 proteins are found as being more abundant in margins compared to stroma-lamellae samples (LogFC < 0), from which only five (At3g23700, AtCg00580, At5g01920, At5g67050, At1g77090) appear not to be significantly distributed in BBY or stroma-lamellae when BBY and stroma-lamellae were compared (Supplemental_Table 7). From these results we can conclude that the vast majority of proteins have similar representation in the stroma-lamellae and in the margins samples. Indeed the lists of differentially abundant proteins found as being more abundant in stroma-lamellae and margins respectively, when compared to BBY-enriched proteins, contain $\sim$ 96% common proteins. In addition there are few proteins which are more abundant in margins than in stroma-lamellae. Two explanations can be proposed for this finding. First, the purification pure margin fraction is an extremely difficult task, due to their physico-chemical properties, which

are very similar to those of the stroma-lamellae [83]. Second, margins are likely to have a protein composition that strongly reminds that of the stroma-lamellae. Being non-appressed regions of the grana, the margins are likely to host proteins that cannot be retrieved in the stacks because of their bulky stromal exposed parts. Therefore, we concluded that the present study does not allow determining accurately the margin proteome.

We further explored the proteins distribution among BBY and stroma-lamellae in order to reveal groups of proteins with similar abundance in BBY and stroma-lamellae. Thus, cluster analysis was performed on the BBY and stroma-lamellae relative mean abundances, calculated as the mean value across the 6 samples in each group, divided by the mean abundances across the thylakoid samples. The decision upon the number of clusters was taken by analysing both the goodness of fit as well as the stability of a wide range of clustering solutions. By doing so, we ensured that the chosen solution would both find the data structures which best fit the actual data in terms of intergroup separability and cohesion, and would reveal the most stable data structures. Finally we partitioned the proteins into 7 clusters, which are discussed in the following section. In addition, the clustering algorithm, its tuning and validation are thoroughly described in the Materials and Methods section.

In conclusion, an adapted statistical analysis showed that numerous proteins differentially distributed in either BBY or stroma-lamellae fractions could be identified while the margin fraction was characterised by a very low number of significantly distributed proteins.

Identification of thylakoid proteins that are differentially abundant between the BBY and the stroma-lamellae domains

As described above, differential analysis between BBY and stroma-lamellae samples allowed to point out 515 proteins, which were enriched either in BBY or stroma-lamellae fractions. However, a significant fraction represents contaminating proteins that were differentially found in the BBY and stroma-lamellae, due to differential contaminations of these two fractions by stroma or chloroplast envelope proteins. As discussed above, this leads to a mixed list of proteins that are genuinely enriched either in the BBY or in the stroma-lamellae fractions, along with stroma or chloroplast envelope proteins that are differentially contaminating the purified thylakoid fractions.

In addition, exploring the data by cluster analysis provides a complementary view on the way that the proteins group based on their relative abundance in BBY and stroma-lamellae. Cluster analysis has been performed for

exploratory reasons and has been conducted in parallel with differentially abundance analysis in order to observe whether we could identify, at first glance, additional groups of proteins known to have the same chloroplastic localisation. The main gain added by cluster analysis is to validate the results obtained by differentially abundance analysis, in the sense that, many proteins identified as being differentially abundant in one compartment were also found as grouping together in a natural way by cluster analysis. The partition of proteins based on cluster analysis is available in Supplemental_Table 1 and Supplemental_Table 6, column PAM cluster/THY proteins. In addition the composition of clusters can be visualized in fig.2.15.

Thus, cluster 1 (203 proteins) contains proteins with a high relative abundance both in stroma-lamellae and BBY fractions, meaning that it contains the major BBY and stroma-lamellae proteins. As shown in fig.2.14 (black dots), the proteins within this cluster are spread both on the left and the right-hand side of the volcano-plot. Proteins of this cluster, that are members of the PSI and PSII photosystems, the cytochrome b_6f and the ATP synthase complexes will be particularly discussed (see below). On the contrary, the proteins grouped within cluster 2 (369 proteins) exhibit low relative abundance both in BBY and stroma-lamellae. Therefore, most of them could be considered minor proteins within these compartments. The proteins within clusters 3 (125 proteins), 4 (198 proteins), 5 (66 proteins) and 6 (31 proteins) appear to be stroma-lamellae specific proteins which present low relative abundance in BBY; the four clusters are separated according to their relative abundance in stroma-lamellae, the proteins in cluster 6 exhibiting the highest relative abundance, while the proteins in cluster 3, the lowest. Clusters 4 and 5 contain stroma-lamellae specific proteins with medium relative abundance. Note that in fig.2.14, the dots associated to the colors of these clusters are located on the right-hand side, which corresponds to proteins enriched in the stroma-lamellae fraction, as identified by the significance analysis of differentially abundance for BBY vs stroma-lamellae case. An interesting cluster is cluster 7 (48 proteins), which concentrates BBY-enriched proteins which were not, or hardly, detected in stroma-lamellae. Indeed in fig.2.14 (yellow dots), these proteins are located in the left-hand side, which corresponds to BBY proteins. Functional analysis of cluster 7 proteins shows that most of them are proteins related to chloroplast transcription (nucleoid-related proteins, DNA/RNA binding proteins, chloroplast transcriptionally active proteins or chloroplast-encoded RNA polymerase proteins subunits). All these proteins are annotated in the literature to be mainly located in the stroma. However the identification of nucleoid proteins in BBY fractions is consistent with the fact that nucleoids are known to be located at the center of the chloroplast, in close vicinity to the thylakoids in mature chloroplasts

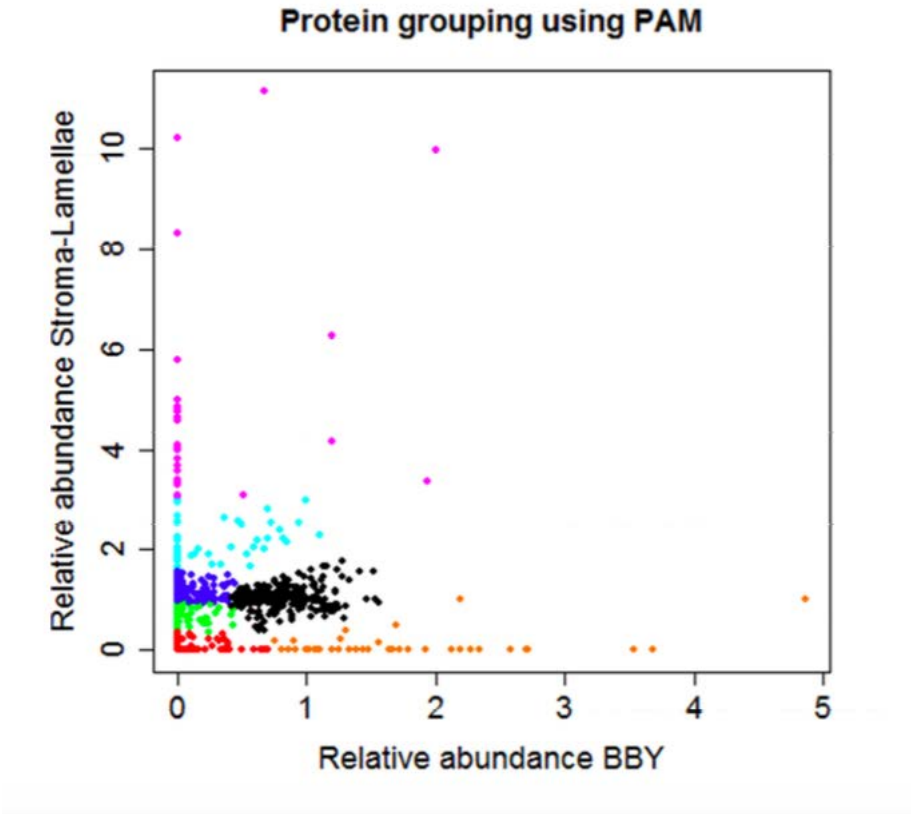

Figure 2.15 – **Clusters** Clustering results (7 classes) of proteins according to their relative abundance in thylakoids. The clustering solution has been chosen as described in section Materials and Methods. Color code: black cluster (cluster 1) corresponds to highly abundant proteins, red cluster (cluster 2) corresponds to low abundant proteins; green (cluster 3), blue (cluster 4), cyan (cluster 5) and magenta (cluster 6) clusters ? the proteins within these clusters appear to be stroma-lamellae specific proteins which present low relative abundance in grana; yellow (cluster 7) - these proteins appear to be grana specific proteins. Note that in the corresponding volcano-plot, they are located in the left-hand side, which corresponds to grana proteins

[224][225]. In addition, *Liu and Rose* showed that nucleoids co-fractionate with the thylakoids and that a region of the chloroplast DNA is bound to the thylakoids [226]. The present study shows that nucleoids are specifically and exclusively bound to BBY domains.

In order to be able to remove cross-contaminants deriving from stroma and envelope compartments, we performed a curated annotation of the 515 proteins that show a differential localisation in the BBY or the stroma-lamellae fractions, to provide a detailed analysis of their sub-chloroplastic localisation (Supplemental_Table 6). The protein names, their function or presence in a specific protein complex were carefully determined (see Materials and Methods section) as well as their subcellular and sub-chloroplastic localisations that were deduced from the screening of the literature, using previously known published information (*e.g.* from the AT_CHLORO and the PPDB databases) or from predictions using bioinformatics tools (*e.g.* ChloroP). After removing 12 proteins that are well-known major components of the plasma membrane, the tonoplast, the peroxisome or the mitochondria (Supplemental_Table 6, ranks 504-515), proteins that were previously associated to the stroma or the envelope compartments (Supplemental_Table 6, ranks 307-475), proteins from cluster 7 (except At2g34420; Supplemental_Table 6, ranks 475-503) and additional stromal ribosomal proteins (Supplemental_Table 6, ranks 295-306) 294 proteins were identified as being differentially distributed in BBY and stroma-lamellae fractions.

Thus, 27 and 267 thylakoid proteins were found to be more abundant in BBY and in stroma-lamellae fractions, respectively (Supplemental_Table 6 and fig.2.16). These results both confirm current knowledge about localisation of some classes of proteins and bring new insight over the protein content of BBY and stroma-lamellae, as discussed in the following sections.

An unexpected heterogeneity in the subunit distribution of the photosynthetic complexes

In order to get a better understanding on the differential subunits composition and distribution of the photosynthetic complexes in the fractions, we analysed further the results obtained from differential analysis. Data obtained allowed us to corroborate the biochemical data concerning the differential localisation of these complexes and to test possible differences in every complex between thylakoid fractions analysed here. In particular, the LogFC value could be associated to the enrichment of a given protein in either BBY or stroma-lamellae fractions. We exploited this information to determine the relative subunit composition and abundance for four different photosynthetic maxi-complexes. fig.2.17 presents the results obtained in the case of the major components of the photosynthetic chain. Two different color gradations were used there to indicate enrichment in the BBY (brown) or in the stroma-lamellae (green) fractions respectively for the four major pho-

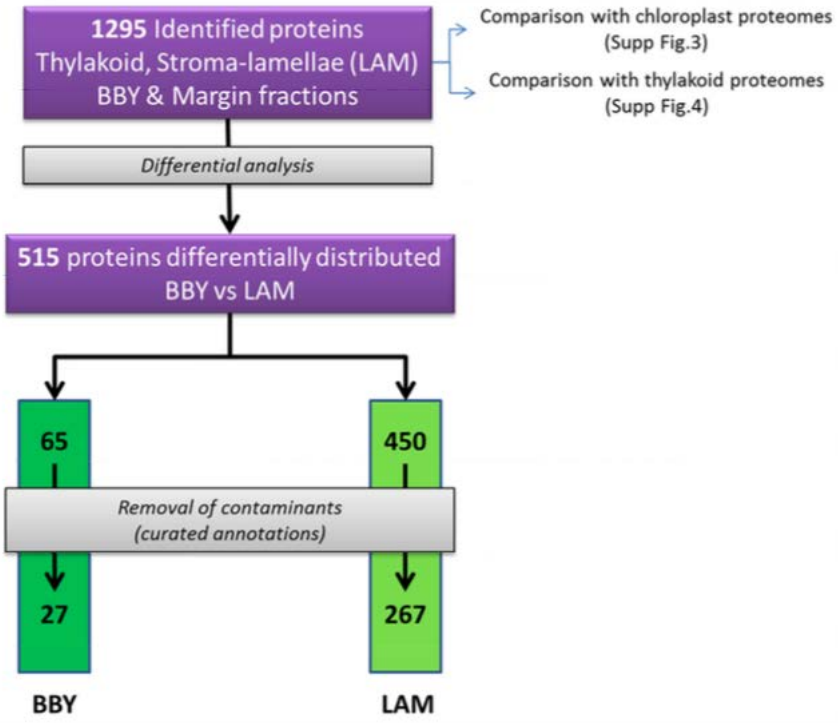

Figure 2.16 – Retrieval of differentially distributed proteins

tosynthetic complexes (Supplemental_Table 6): ATP synthase, cytochrome b_6f, PSII and PSI-NDH super complex. Subunits of the photosynthetic complexes that did not show differential localisation (p value > 0.05) are marked in black.

The overall picture emerging from the present proteomic study is consistent with previous description of the localisation of the main photosynthetic complexes in the thylakoid membranes (reviewed in [50][83]): PSI and the ATP synthase complexes are accumulated in the unstacked stroma-lamellae (together with the chlororespiratory complex NDH), while PSII is mostly found in the BBY stacks (fig.2.17). The cytochrome b_6f complex is more ubiquitous, although slightly more concentrated in the stroma-lamellae. However, a closer look at these data reveals an unexpected heterogeneity in the subunit composition of the different complexes. In particular within a given complex, the localisation of different subunits between the BBY/stroma-lamellae turned out to be variable, as clearly evidenced by the case of PSI. As expected, this complex accumulates preferentially in the

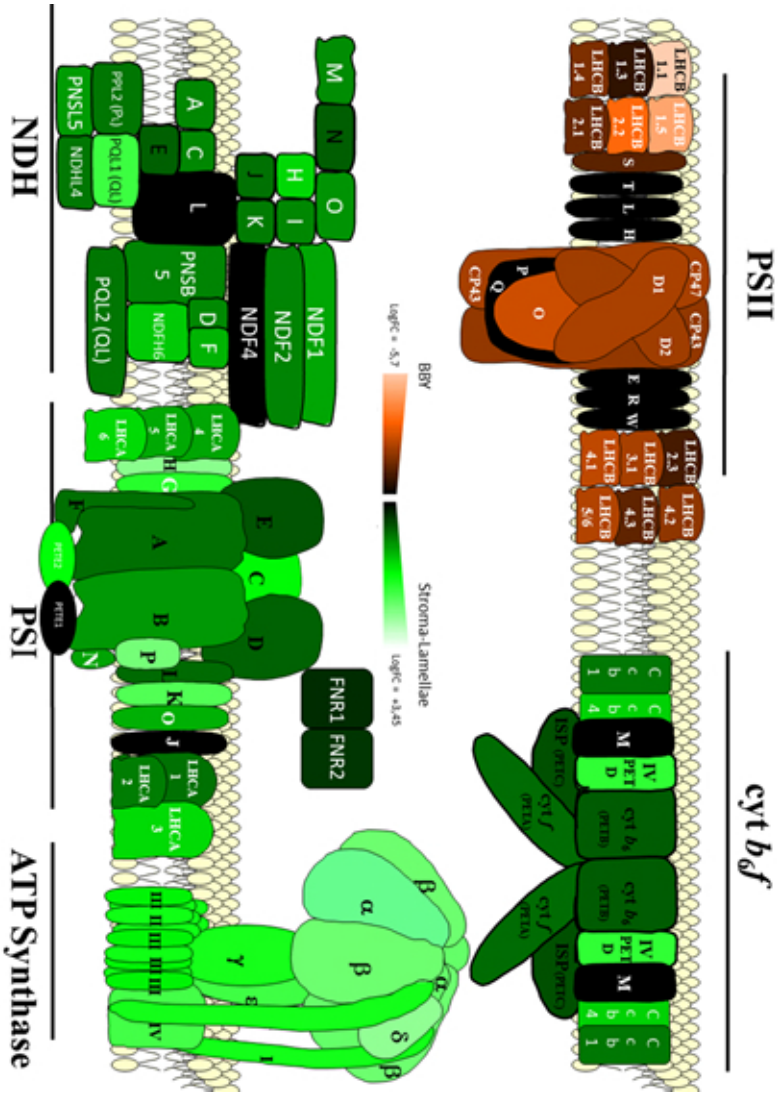

Figure 2.17 – **Photosynthetic complexes distribution in the major thylakoid subfractions as determined by proteomic analysis. PSII, cytochrome b6f, PSI, NDH and ATP synthase CF0-Fi complexes are represented** Schematic representations of the different photosynthetic complexes were redrawn according to Choquet and Vallon (110). Each subunit is indicated by its common name, or by the letter of the gene (psb, pet, psa) that encodes it. Two sets of color gradations codes were employed to designate the specific localisation of every subunit in the grana/stroma-lamella regions. Light brown indicates high preferential localisation in the BBY, while light green indicates high preferential localisation in the stroma-lamellae. Figures were taken from Supplementary_Table 6. The common name for proteins with a preferential_localisation can be found in Supplemental_Table 6. ATPx, PSAx, NDHx, PTEx, PSBx Subunits with no preferential localisation were identified from the initial 1295 protein list (black color). Common names employed correspond to the following proteins: AtCg00630 (PSAJ), At1g70760 (NDHL), At3g16250 (NDF4 = CEF1), At2g26500 (PETM), At3g21055 (PSBT), AtCg00560 (PSBL), AtCg00710 (PSBH), AtCg00580 (PSBE), At1g79040 (PSBR), At4g28660 (PSBW), At1g06680 (PSBP), At4g21280 and At4g05180 (PSBQ).

stroma-lamellae fraction. However, not all its subunits show the same ratio between the stroma-lamellae and the BBY fractions. For example the PsaC subunit had a higher score for stroma-lamellae than other nearby core subunits (*e.g.* PsaD). This finding was confirmed by Western blot analysis using specific antibodies (fig.2.8), showing that the amount of PsaC found in the BBY samples is lower than in the case of PsaD. In principle, this finding could reflect a purification artifact. Some peripheral PSI subunits (*e.g.* PsaK, PsaG, PsaH), which also share with PsaC the property of being enriched in stroma lamellae, could have been differentially extracted by the two types of detergents used to isolate the BBY and the stroma-lamellae, leading to an apparent enrichment in a specific fraction. To test this hypothesis, we performed experiments to analyse the sensitivity of these proteins towards extraction by detergents. Thylakoids were incubated with increasing concentration of digitonin or Triton and the amount of proteins present in the supernatant and the pellet was compared. We focused on three PSI subunits: an intrinsic one (PsaB) and two more peripheral ones (PsaC, PsaD) and found that they were all similarly extracted by both types of detergents (fig.2.18). Thus it appears that the differential enrichment of some PSI subunits in the BBY and stroma lamellae fractions is not caused by a different sensitivity to detergent, suggesting instead that the PSI subunit composition may vary depending on its location in the thylakoids.

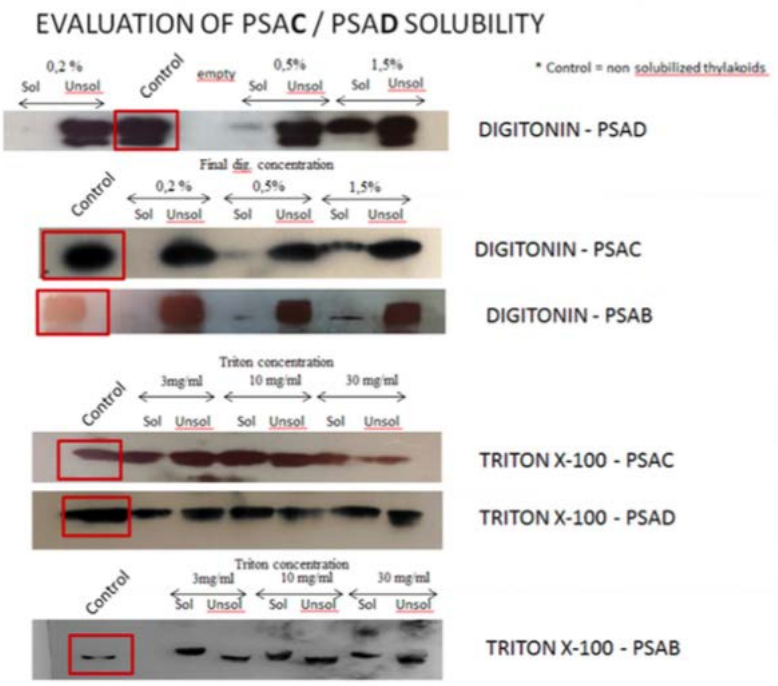

Figure 2.18 – **Evaluation of the sensibility to detergent solubilisation for B,C,D subunits of the photosystem I** Thylakoid samples were incubated with digitonin or triton at three different concentrations (x0.5, x1 x3 times the amount of detergent used during the fraction preparation). Solubilized and insolubilized fractions were collected and analyzed in Western blot with antibodies raised against PsaB, PsaC and PsaD proteins.

2.5.3 Discussions

Distribution of the photosynthetic complexes

This article addresses the protein composition in the main sub-compartments of the thylakoid membranes: the grana (here represented by the innermost part, the BBY) and the stroma-lamellae. As discussed above, our differential analysis allows discriminating these two fractions, while does not allow determining accurately the proteome of the third thylakoid compartment: the margins. This differential analysis is extremely informative to reveal possible differences in the composition of super-complexes associated either to stroma-lamellae or BBY membranes. Furthermore, it may unravel functional differences between complexes localised in the two fractions. In most cases, a differential and specific repartition between stroma-lamellae and BBY was found. The ATP synthase CF_0-F_1 is the most homogeneous complex according to our analysis. All its subunits are equally (and almost exclusively) found in the stroma-lamellae with a strong level of enrichment (LogFC > 2) (fig.2.17). PSI is also enriched in this fraction although to a lesser extent. If we refer to the LogFC value, the finding that PSI is more present in the BBY fraction (relatively to occurrence in the stroma-lamellae fraction) than the ATP synthase CF_0-F_1 is not surprising, as it corroborates previous ideas on the necessity for this complex to accumulate in the PSII rich regions to ensure proper electron flow [83]. As discussed above, this complex shows a larger heterogeneity at the level of its subunits, which according to our data, does not reflect a purification artifact but rather a genuine difference in the subunit composition between complexes present in the stroma-lamellae and the BBY particles. The finding that PsaC (AtCg01060) is more represented than other subunits in the stroma-lamellae fractions is surprising, as this subunit has been previously shown to represent the docking site for the interaction of the PsaD and PsaE ones during complex assembly in thylakoids [227]. Indeed previous analysis in *Chlamydomonas* has revealed that mutants lacking this subunit cannot assemble the PSI complex [228]. Moreover, this subunit bears two of the three terminal FeS centers, suggesting that PSI complexes devoid of this subunit should not be functional. However, previous data obtained from cyanobacteria, suggests that PSI can accumulate in a functional state even in the absence of this PsaC subunit [229]. This opens the possibility that the PSI complexes found in the BBY fraction could represent a genuine form of this complex, still bearing some electron flow capacity. Other peripheral PSI subunits, PsaG (At1g55670) PsaH (At3g16140, At1g52230), PsaK (At1g30380) also show a preferential location in the stroma-lamellae. Among them, PsaG and K are involved in the docking of the PSI anten-

nas (LHCI) binding to the core complex [148]. It is interesting to note that Lhca3 (At1g61520), which is directly bound to PsaK in the 3D structure of this complex [148], is also preferentially localised in the stroma-lamellae. It is tempting therefore to propose that this PsaK-Lhca3 sub-complex could be partially released from the PSI complex present in the grana. Another subunit, PsaH, is required for the docking of LHCII to PSI during state transitions [46], *i.e.* the redox induced reversible phosphorylation of PSII antenna, which lead to their displacement from PSII and binding to PSI [230]. Thus, the finding that this subunit in enriched in the stroma-lamellae PSI complex is consistent with the occurrence of LHCII docking to PSI in the stromal fraction during state transitions. The hypothesis of a different subunit composition in the BBY and stroma-lamellae PSI fractions is also plausible based on the finding that the two minor LHCI species (Lhca5, At1g45474 and Lhca6, At1g19150) were also highly enriched in the stroma-lamellae. These subunits provide a molecular platform for the interaction between PSI and the NDH complex, leading to the formation of a PSI-NDH super-complex, which is found in the stroma-lamellae [77]. In our proteomic survey, most of the subunits previously attributed to this super-complex co-accumulate in the stroma-lamellae, suggesting a rather homogeneous structure of this super-complex. Moreover, we noticed that, besides PPL2 (At2g39470) and the two PsbQ-like proteins (At1g14150 and At3g01440) previously found in this complex, several other pseudo-PSII subunits specifically localised in the stroma-lamellae. It is tempting to propose that these PsbP-like subunits, that show a totally different localisation when compared to PSII, could also be linked to the NDH complex. The finding of a PSI-NDH super-complex in the stroma-lamellae is corroborating the notion that this chlororespiratory complex is required for cyclic electron flow around PSI [231]. Consistent with this, we found that the Pgr5 (At2g05620) and Pgrl1 isoforms (At4g11960, At4g22890), which are also required for cyclic electron flow in plants [231] were also highly enriched in the stroma-lamellae fractions. Based on these results, it is therefore tempting to speculate that the heterogeneous composition of PSI complexes seen in the two compartments may reflect a different functional role of PSI in the two compartments: PSI in the grana has been proposed to participate in linear electron flow working in series with PSII, while stromal PSIs would mainly perform cyclic electron flow.

Among the major photosynthetic complexes, the cytochrome b_6f is the one showing the most homogeneously localisation in the thylakoids, being only moderately concentrated in the stroma-lamellae. Overall, the fraction of the cytochrome b_6f that is localised in the BBY appears to be higher in this analysis than in previous reports based on immunolocalisation [232][233]. However, our findings are consistent with previous investigations on thy-

lakoid fractions isolated upon mechanical fractionation of these membranes, followed by biochemical analysis (*e.g.* [235] and references therein). Indeed, most of its core subunits (cytochrome b_6 (AtCg00720), and f (AtCg00540), and the Rieske iron-sulfur protein PetC (At4g03280)) showed similar relative enrichment. This is not the case for subunit IV (AtCg00730), which is a central subunit of this complex and is most exclusively located in the stroma-lamellae. This is again unexpected, as cytochromes b_6f complexes should not be able to accumulate in the absence of subunit IV [236]. At present no explanation can be proposed for this finding. Besides subunit IV, the CCB proteins (CCB1 (At3g26710), and CCB4 (At1g59840)), *i.e.* the chaperones required for the assembly of the high spin heme c$'$ to the stromal side of the complex [237], are also largely enriched in the stroma-lamellae fractions. These subunits however are not required for complex activity but only for complex assembly. Thus their peculiar localisation can be rationalized based on earlier suggestions that the unstacked membranes are the site where photosynthetic complexes are assembled or repaired, as previously demonstrated in the case of the insertion of the subunit D1 (PsbA, AtCg00020) into PSII during the repair cycle which follows photoinhibition [238]. If the same scenario is translated to the cytochrome b_6f complex, it is reasonable to envisage that insertion of the c$'$ heme, which requires rather complex molecular machinery, would also preferentially take place in membranes that are easily accessible from the stroma, *i.e.* the stroma-lamellae. The conclusion that assembly/repair of the photosynthetic complexes is located in the stroma-lamellae is expected [238] and also supported by the finding that all the thylakoid-bound proteases (Deg, FtsH and ClP), which are required for disassembly of these complexes, are enriched in the stroma-lamellae (see next section).

As expected, the only photosynthetic complex that is preferentially located in the BBY fraction is PSII. Again, a significant heterogeneity is seen at the level of its different subunits. While all the core complex subunits including D1 (PsbA), D2 (PsbD, AtCg00270), CP43 (PsbC, AtCg00280), CP47 (PsbB, AtCg00680) and PsbO (At5g66570, At3g50820) are almost exclusively found in the BBY, other subunits of the water-oxidising complex (PsbP and PsbQ) have a less defined localisation. This difference could, in principle, reflects a problem in distinguishing between the true PSII subunits (PsbP1 (At1g06680), PsbQ1 (At4g21280) and PsbQ2 (At4g05180)) and the so called PsbP-like and PsbQ-like proteins, which are not bound to PSII but rather located in the stroma-lamellae, being possibly bound to the NDH complex (see above; PQL1 (At1g14150), and PQL2 (At3g01440), proteins). Note that PsbP-like were all found in cluster 3, which reflects similar relative abundance and behavior. PsbS (At1g44575), the small PSII subunit

involved in photoprotection via the induction of enhanced thermal dissipation in the PSII antenna [111] also showed a less pronounced accumulation in the grana stack than the core complex subunits. This finding is consistent with earlier investigation [239] suggesting that this protein provides a flexible link between the PSII core and its antenna complexes. Therefore, this protein could be easily detached form the core complex during sample purification. However, a possible localisation of some PsbS in the non appressed regions cannot be totally excluded based on recent data in *Chlamydomonas*, where a displacement of LHCSR3 (the functional homologue of PsbS in microalgae) between PSII and PSI was observed depending on the physiological conditions [240]. Finally, the distribution of the minor (Lhcb 4 At5g01530, At3g08940, At2g40100, Lhcb 5 At4g10340 and Lhcb 6 At1g15820) and trimeric (Lhcb 1 At1g29920, At1g29930, At2g34430, At2g34420, Lhcb 2 At2g05100, At2g05070, At3g27690 and Lhcb 3 At5g54270) light harvesting complexes between the stroma-lamellae and BBY fractions is much more heterogeneous than that of the core PSII subunits. In principle, this could reflect the existence of antenna complexes with a different mobility in the membranes (*e.g.* the L, M and S LHCII complexes, [241]) which could differentially move to the stroma-lamellae during the state-1 to state-2 transition [230]. However, our data concerning the differential location of PSII antenna in the two fractions are not consistent with the recent detailed analysis of the mobility of the different LHCII subunits during state transitions [242]. This suggests that other structural causes are probably responsible for the observed heterogeneity. As an alternative hypothesis, we propose therefore that the peculiar distribution of LHCII could reflect their migration to the stroma-lamellae during the PSII reparation cycle that follows photoinhibition [238].

Eventually, the finding that a non-negligible fraction of the two FNR (ferredoxin-NADP reductase, At5g66190 and At1g20020) isoforms is located in the BBY is unexpected based on previous results, which indicates that FNR should be completely absent from this compartment [50]. In principle this could be explained by the finding that cyt b_6f complexes is rather abundant in our BBY fractions, at variance with previous reports [50]. Since FNR is bound to this complex [243] its presence could simply reflect the cyt b_6f enrichment in BBY.

Thylakoid FTSH and DEG proteases

FtsH proteins are membrane-bound ATP-dependent metalloproteases. FtsH proteases localised in the chloroplast have been shown to play a ma-

jor role in assembly and maintenance of the plastid membrane system (for review, see [132]). In *Arabidopsis*, only FtsH1 (At1g50250), 2 (At2g30950), 5 (At5g42270) and 8 (At1g06430) have been shown to reside in the thylakoid membranes. In this study, those four proteases were identified in both thylakoid sub-compartments, with a strong enrichment in the stroma-lamellae. This is in good agreement with recent data showing that FtsH proteins were present in both thylakoid sub-compartments, as monomers and homo/heteromeric dimers in stromal region and as hexameric complexes in the grana regions [100]. The thylakoid located FtsH complex in *Arabidopsis* is responsible for degradation of photodamaged D1 protein (PsbA) in concert with lumenal Deg proteases (see for reviews [244][245]). All FtsH proteins that were found differentially located in the stroma-lamellae fractions belong to cluster 1, indicating that they are abundant.

Deg proteins are serine proteases and, unlike FtsH, are not ATP-dependent. It is assumed that in plants FtsH digests D1 after the first proteolytic cleavage has been performed by a Deg protease [245]. The Deg1 (At3g27925), Deg5 (At4g18370) and Deg8 (At5g39830) were previously reported to be present in the thylakoid lumen. In the present study, only Deg1 was identified as being significantly enriched in the stroma-lamellae. This protease has been shown to be involved in D1 protein degradation but also in PSII assembly [245]. Thus one could expect that Deg1 could be present in the stroma lamellae, there being involved in the PSII repair cycle [238]. Four other Deg proteases were identified in our 1295 list of proteins (Deg2 At2g47940, Deg3 At1g65630, Deg5 and Deg8). Except Deg1, most of these Deg proteins were found in cluster 2, which gathers low abundant proteins. In addition Deg2, 3, 5 and 8 were not significantly found to be enriched in either the BBY fraction or the stroma-lamellae fractions. However Deg5 was identified in BBY fractions but not in stroma-lamellae, which indicates that Deg5 might be enriched in grana. This observation is consistent with a role for Deg5 in the repair of damaged PSII, possibly by performing an initial cleavage of the D1 protein within lumen-directed loops [129]. Also, Deg2 and Deg3 were detected in stroma-lamellae but not in BBY fractions. Thus Deg2 is likely to be more enriched in stroma-lamellae, which is consistent with the fact that Deg2 was found to be peripherally attached to the stromal side of the thylakoid membrane. This protease could be part of a large network of enzymes that ensure protein quality control in PSII, and could be also involved in the degradation of Lhcb6, the minor light-harvesting protein of PSII [246].

Transporters of the thylakoid sub-compartments

Few thylakoid transporters have been identified in the present study, probably because samples were analysed without specific enrichment of hydrophobic proteins before mass spectrometry analysis. Indeed, transporters are often minor and highly hydrophobic proteins, and their identification needs dedicated treatments like solubilization in organic solvent or in detergent [247], prior to separation on SDS-PAGE and trypsin digestion. About ten transporters were shown to be differentially distributed between the stroma-lamellae and the BBY sub-structures. The only transporter known to be located in the thylakoids and identified as being differentially distributed is AtHMA8 (At5g21930), a copper transporter belonging to the P_{IB}-type ATPases family. This transporter allows the import of copper into the lumen of thylakoids to supply the plastocyanin which uses copper as cofactor. From characterisation of *Arabidopsis hma8* mutant and investigation of the localisation of AtHMA8 by several approaches (transient expression of GFP fusion and *in vitro* import experiments on a truncated precursor), it was suggested that this transporter was localised in the thylakoids [248]. In the present work, AtHMA8 was identified in stroma-lamellae but not in BBY fractions. This is consistent with the localisation of the two isoforms of plastocyanin (Pete2, At1g20340, and Pete1, At1g76100) that were found both in BBY and stroma-lamellae fractions for the Pete1 isoform or highly enriched in the stroma-lamellae for the Pete2 isoform. Four putative thylakoid transporters NTF2 (At1g71480), KEA3 (At4g04850), NHD1 (At3g19490) and ABCD2 (At1g54350) were also found to be differentially distributed and were previously identified in chloroplasts [179] or plasma membrane for NHD1 [249]. In this study, NTF2, KEA3, NDH1 and ABCD2 were all detected in the stroma-lamellae but none were identified in BBY fractions, suggesting that they should be involved in transport of ions or metabolic specifically required in stroma-lamellae. Six additional transporters were identified, like the phosphate-triose phosphate (TPT, At5g46110) and the oxoglutarate/malate translocator (DiT1, At5g12860, and DiT2-1, At5g64290), that were already known to be associated with the chloroplast envelope. In the AT_CHLORO database, they have been associated mainly with the envelope but also with the thylakoid membranes. The phosphate/triose phosphate and oxoglutarate/malate translocators with the protein OEP16-1 (At2g28900) were all found in BBY and stroma-lamellae fractions with enrichment in the latter sub-fraction. This specific enrichment is consistent with a contamination by envelope membranes which is higher in stroma-lamellae than in BBY fraction, the envelope membrane having similar density compared to the stroma-lamellae one. The last three transporters, IEP18 (At5g62720),

BASS2 (At2g26900) and NHD1 (At3g19490) were not identified in the BBY fraction. Since, the function of IEP18 is still unknown, we cannot conclude about the relevance of its localisation both in chloroplast envelope and in the stroma-lamellae. Characterisation of an *Arabidopsis bass2* mutant suggested that this protein is a sodium-dependent pyruvate transporter of the chloroplast envelope [250]. In this study, the authors also suggested that sodium influx could be balanced by the sodium:proton antiporter NHD1. This transporter, previously identified both in chloroplast and plasma membrane proteomes ([249][179]), was recently characterised as a sodium exporter of the chloroplast envelope [251]. In the AT_CHLORO database, BASS2 was found associated with both envelope and thylakoid membranes, although NDH1 was not detected. Thus, beside their characterised function as transporters of the chloroplast envelope, we cannot exclude a dual localisation in sub-chloroplast compartment with a physiological function that remains to be determined in the thylakoids.

One question that we wanted to address through identification of the stroma-lamellae proteome concerns the controversy about envelope localisation of some transporters. Indeed, both the ATP/ADP carrier TaaC (At5g01500) and Na^+-dependent phosphate transporter PHT4;1 (ANTR1, At2g29650) were found exclusively associated to the envelope in the AT_CHLORO database [140] although they were described as thylakoids transporters [252][253]). Moreover, none of these two proteins were identified in proteomic investigations dedicated to the study of membrane or lumen thylakoid (Supplemental_Table 4). In the present study, both proteins were found to be enriched in the stroma-lamellae fraction. Thus, considering previous proteomic studies and present enrichment in stroma-lamellae fractions, TAAC and PHT4;1 were considered as being likely contaminants from the envelope. The envelope localisation was confirmed by Western-blot analyses in which the phosphate transporter PHT4;1 was only detected in envelope fraction and no signal appears in the stroma-lamellae (fig.2.19). Furthermore, a recent study showed that the TAAC transporter is indeed a 3′-phosphoadenosine 5′-phosphosulfate/5′-phosphoadenosine 3′-phosphate transporter of the chloroplast envelope [254], in good agreement with a chloroplast envelope localisation and thus our proteomic data ([140] and this work).

Potential new thylakoid proteins

From the present study we could identify 218 proteins that were not previously identified in proteomics studies dedicated to the chloroplast or the thylakoids (Supplemental_Table 5). At least 103 of them might be

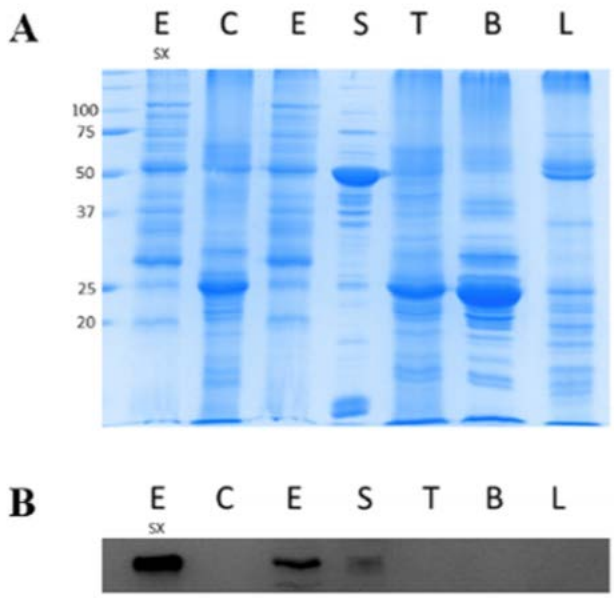

Figure 2.19 – **Localization of the Na^+-dependent phosphate transporter PHT4;1 (ANTR19)** Esx, envelope fraction purified from over-expressing Pht4;1 *Arabidopsis* plants, C, crude chloroplast proteins; E, envelope membrane proteins; S, stroma proteins; T, thylakoid proteins; B, BBY proteins; L, stroma-lamellae proteins. Each gel lane was loaded with 6 μg proteins. (A) Fractions were analyzed on a Coomassie blue-stained SDS-PAGE. (B) Western-blot was performed with a polyclonal antibody raised against Pht4;1 (At2g29650). Note that, except for the envelope fraction purified from over-expressing Pht4;1 *Arabidopsis* plants (Esx).

genuine thylakoid (or at least chloroplast) proteins. Very few of the remaining 115 proteins could be further considered for tentative chloroplast localisation because most of them are either totally unknown proteins or only contain domains that allow to suspect or predict a putative function (supplemental Table S5, rank 104?218). However, quite surprisingly, components of the ubiquitin-proteasome system were detected amongst those 115 proteins. A recent study has demonstrated that plastid biogenesis is directly regulated by the ubiquitin-proteasome system [255]. Using forward genetics, a new outer chloroplast envelope protein was identified, SP1

(AT1G63900) which encodes a RING-type ubiquitin E3 ligase that mediates ubiquitination of the TOC translocon. Interestingly, while SP1 was not detected during the present study (as expected since purified envelope fractions were not analysed during this work), several proteins could be identified that share some functional similarities with SP1. Indeed, one protein of the F-box/kelch-repeat superfamily (AT4G39590) and a protein of the RING/U-box superfamily (At5g40140) are present in the list of 103 proteins that are predicted to be targeted to the chloroplast using ChloroP and TargetP. Furthermore, nine other components of the ubiquitin-proteasome system (At1g22500, At3g59250, At5g03100, At1g06900, At5g64760, At5g60250, At2g24540, At5g03100, At1g78100, At5g05560) were detected in the analysed chloroplast fractions and are listed in the list of 115 proteins that are not predicted to be targeted to the chloroplast. While we have no other explanation than cross-contamination events for the detection of these last nine components of the ubiquitin-proteasome system in the various thylakoid subcompartments that were analysed during this study (BBY, stroma-lamellae or margins), identification of these proteins at least suggests that present-days proteomic studies reveal very minor components that were not accessible during previous analyses.

In the list of 103 potentially new thylakoid proteins, we performed an exhaustive analysis of the known or predicted functions of these previously undetected chloroplast or thylakoid components. As expected, almost one third of these proteins have no known function or even predicted functional domain (Supplemental_Table 5 see column *Curated function (this work)*). Around 10% of these newly identified proteins might be involved in lipid metabolism or transport (lipases, desaturases, acyl-transferases etc.). Seven proteins are known or predicted to be involved in the metabolism of vitamins or pigments and four putative ion or metabolite transporters could also be detected. Although 15 different LHCII isoforms were previously detected in large-scale proteomic analyses, including an LhcII2.3 protein (see Supplemental_Table1), an LhcII2.3-like protein (At1g76570) is listed in the short list of four proteins that are directly linked to photosynthesis. More interestingly, this list of 103 proteins also contains numerous regulatory proteins like the two proteins that are involved in cyclic electron flow around the Photosystem I, *i.e.* CEF1 (At3g16250) and NDHL (At1g70760) [256], or the cytochrome b_6f biogenesis protein CCDA (At5g54290) [257] that could not be detected in previous proteomic studies targeted to the chloroplast or the thylakoid membranes. Beside proteins that might be additional actors of the regulation of the chloroplast physiology, eleven detected proteins are suspected to be chaperones or proteases, four proteins are predicted kinases, one is a putative kinase regulator, one is a phosphatase, and seven are putative RNA

binding proteins (mostly TPR or PPR proteins).

2.5.4 Conclusions

The investigation presented here targets the thylakoid membrane of the chloroplast that harbors the light-dependent reactions of photosynthesis by which green plants synthesize organic compounds from water and carbon dioxide. This work, performed on the model organism *Arabidopsis*, provides a strong basis to carry out targeted approaches in physiologically and economically important organisms such as crops or green algae. The present work is the first study designed to address the precise localization of thylakoid proteins with respect to two major subcompartments: the grana and the stroma-lamellae, using a proteomics-based approach. The present work provides a more exhaustive repertoire of minor chloroplast proteins, thus representing a new resource for thylakoid proteins with respect to both functional and localization issues. Thus, this study complements our previous large-scale approach aiming to provide detailed information about the subchloroplastic localization of proteins [140].

Overall, the data from the proteomic study presented here corroborates previous conclusions on the distribution of photosynthetic complexes in the thylakoids. However, thanks to an in depth proteomic analyses coupled to a dedicated data analysis pipeline, new information with respect to several aspects of the thylakoid proteome has been achieved. Indeed, the present data unravels a structural heterogeneity between the photosynthetic complexes located in the different compartments, which is particularly evident in the case of the two photosystems. Differential protein segregation of PSII or PSI proteins in the thylakoid compartments may reflect the different content of antenna complexes that was previously seen between stroma and grana PSII complexes [200]. This segregation also strongly suggests that PSI needs to recruit new subunits to allow the formation of the PSI-NDH supercomplex in the stroma-lamellae. Now that we have achieved a robust map of proteomes within thylakoid membranes, then next step will be to carry out analysis of the functional consequences of the structural heterogeneity of photosynthetic complexes by employing targeted experiments to screen the impact of knock-out mutations or of different environmental conditions on the regulatory processes that control these protein segregations.

2.5.5 Materials and methods

Plant growth conditions

Arabidopsis thaliana (ecotype Columbia, Col-0) were grown in culture chambers at 22°C with a light intensity of 100 μmol $m^{-2}.s^{-1}$ (10-h light cycle) for 4-5 weeks before harvesting.

Purification of intact chloroplasts and thylakoid sub-compartments

All operations were carried out at 0-5°C. Percoll-purified chloroplasts were obtained from 100-200 g of *A. thaliana* leaves as previously described [141]. Purified intact chloroplasts were lysed to retrieve thylakoids membrane in hypotonic medium in the presence of protease inhibitors (20 mM 4-(2-hydroxyethyl)-1-piperazineethanesulfonic acid (HEPES), pH 7.8, 0.2 mM benzamidine, 1 mM acid ϵ-amino caproic, 0.2 mM phenylmethylsulfonyl fluoride (PMSF) and 10 mM $MgCl_2$. Thylakoids membrane were centrifuged at 9,700 g for 10 min and resuspended in the same buffer. Chlorophyll was extracted in 80% (v/v) acetone, and its concentration determined according to Porra *et al.* [258]. **Margins and stroma-lamellae purification** Thylakoids at 0.5 mg chlorophyll/ml were incubated with 0.5% (w/v) digitonin (SIGMA) for 30 min at 4°C under agitation in order to solubilize the lighter fraction of the membranes. The mixture was diluted 10 times in the same hypotonic medium and subsequently centrifuged at 6,000 g for 5 min. The pellet, consisting of non- solubilized thylakoids, was collected and stored at 4°C for further BBY purification while the supernatant was centrifuged at 15,000 g. Again, the pellet was collected for the subsequent BBY purification whereas the supernatant was centrifuged again at 70,000 g. The pellet, enriched in grana-margins was stored and resuspended in 10 mM HEPES, 5 mM $MgCl_2$, 0.4 M sorbitol (in the presence of protease inhibitors) and stored in liquid nitrogen. The remaining supernatant was centrifuged at 140,000 g to pellet the stroma-lamellae fraction of the thylakoids which was stored in the same buffer. **BBY purification**. Membranes, consisting of Pellet 1 (non-solubilized thylakoids) plus Pellet 2 (grana obtained after solubilization with digitonin) were washed in resuspension buffer and diluted at 1 mg chlorophyll/ml concentration. The sample was incubated with Triton X-100 at 10 mg/mg chlorophyll for 30 min, in the dark, at 4°C, under agitation. The mixture was centrifuged for 5 min at 3,500 g at 4°C. The supernatant was collected and centrifuged at 40,000 g for 30 min, at 4°C. The pellet, consisting of BBY (i. e. the inner part of the grana stacks) was washed in resuspension buffer and centrifuged at 40,000 g for 30 min, at 4°C. Mem-

branes were stored in liquid nitrogen in 10 mM HEPES, 5 mM $MgCl_2$, 0.4 M sorbitol (in the presence of protease inhibitors).

Oxygen evolution measurements

Oxygen evolution was measured with a Clark-type electrode (Hansatech, UK). The reaction medium contained in a total volume of 1,5 ml 0.4 M sorbitol, 10 mM Hepes-KOH pH 7, 5 mM $MgCl_2$, 0.2 mM PMSF, 0.2 mM benzamidine and 1 mM ϵ-amino capronic acid. Exogenous electron acceptors (3.5 mM ferricyanide and 250 μM 2,5-dichloro-p-benzoquinone) were added before measuring activity as evolution of molecular oxygen [259]. Thylakoids or purified fractions (BBY and stroma-lamellae) were added at a final concentration of 12 μg chl^{-1}.

Solubilization test for thylakoid membrane proteins

To test selective solubilization of membrane proteins, freshly isolated thylakoid membranes were incubated for 30 min with the same detergents (digitonin or TRITON X-100) employed to isolate the stroma-lamellae and BBY fractions. Three different concentrations corresponding to (i) one half, (ii) the same and (iii) the double concentration used in the purification protocol (see above) were tested in a volume of 100 μL containing 20 mM 4-(2-hydroxyethyl)-1-piperazineethanesulfonic acid (HEPES), pH 7.8, 0.2 mM benzamidine, 1 mM acid ϵ-amino caproic, 0.2 mM phenylmethylsulfonyl fluoride (PMSF) and 10 mM $MgCl_2$. At the end of the incubation (30 min at 4°C), samples were centrifuged, and the pellet and supernatant fractions were collected. Proteins in the pellets were recovered in the same volume as the supernatants and stored in 10 mM HEPES, 5 mM $MgCl_2$, 0.4 M sorbitol (in the presence of protease inhibitors). The two fractions were then analysed by SDS-PAGE and Western blots.

SDS-PAGE and Western blot analysis

Proteins were separated by SDS-PAGE as described by Chua [260]. For Western-blot analyses, proteins were transferred to a nitrocellulose membrane (BA85, Schleicher and Schuell, Whatman) which was blocked with 5% (w/v) dried-milk in Tris-buffered saline (TBS) containing 0.5% (v/v) Triton X-100. To assess the purity of the samples, antibodies raised against proteins associated to specific chloroplast sub-compartments were used: AtpB

(stroma-lamellae marker, Agrisera) at a 1:10,000 dilution, PsaD (stroma-lamellae marker, Agrisera) at a 1:3000 dilution, PsaC (stroma-lamellae marker, agrisera) at a 1:10000 dilution, PsaB (stroma-lamellae marker, agrisera) at 1:5000 diluition, CP43 (BBY marker) at a 1:10,000 dilution (kindly provided by Dr. Luca dallOsto, University of Verona), HMA1 (chloroplast envelope marker) at a 1:1,000 dilution (40), PHT4;4 (chloroplast envelope marker) at a 1:1,000 dilution (41), KARI (stroma marker) at a 1:5,000 dilution (kindly provided by Dr. Renaud Dumas, University of Grenoble). Proteins were detected by ECL.

77K fluorescence emission

To measure fluorescence emission spectra at cryogenic temperatures, a small (10 μL) aliquot of the purified fraction was taken and loaded in the cuvette of a CCD spectrophotometer (JbeamBio, France) to measure fluorescence emission at 77 K. Fluorescence was excited with a blue LED peaking at 470 nm, and emission was recorded between 650 and 800 nm using a diode array. Spectra were normalized to the maximum peak (PSII for the BBY and PSI for the thylakoids and stroma-lamellae, respectively).

Protein digestion

For MS analysis, 4 μl of sample were loaded on a 12% SDS-PAGE Protein extracts were concentrated on a band, between the stacking and the separating gels [184]. (7-cm gels, Bio-Rad, 4.5% stacking gel). Protein content varied between 2.6 and 9.3 μg for the stroma-lamellae, 1.7 and 2.8 μg for the thylakoids and between 2.5 and 8.2 μg for the BBY. The gel bands were manually excised and cut in pieces before being washed by 6 successive incubations of 15 min in 25 mM NH_4HCO_3 and in 25 mM NH_4HCO_3 containing 50% (v/v) acetonitrile using a Freedom EVO150 robotic platform (TECAN). Gel pieces were then dehydrated with 100% acetonitrile and incubated for 45 min at 53°C with 10 mM DTT in 25 mM NH_4HCO_3 and for 35 min in the dark with 55 mM iodoacetamide in 25 mM NH_4HCO_3. Alkylation was stopped by adding 10 mM DTT in 25 mM NH_4HCO_3 and mixing for 10 min. Gel pieces were then washed again by incubation in 25 mM NH_4HCO_3 before dehydration with 100% acetonitrile. 0.15 μg of modified trypsin (Promega, sequencing grade) in 25 mM NH_4HCO_3 was added to the dehydrated gel pieces for an overnight incubation at 37°C. Peptides were then extracted from gel pieces in three 15 min sequential extraction steps in 30 μL of 50% (v/v) acetonitrile, 30 μL of 5% (v/v) formic acid and finally 30 μL of 100%

acetonitrile. The pooled supernatants were then dried under vacuum.

Nano-LC-MS/MS analyses

All the thylakoid fractions were run as biological triplicates and technical duplicates. The dried extracted peptides were resuspended in 5% (v/v) acetonitrile and 0.1% (v/v) trifluoroacetic acid and analysed by online nanoLC-MS/MS (Ultimate 3000, Dionex and LTQ-Orbitrap Velos Pro, Thermo Fischer Scientific). Peptides were sampled on a 300 μm x 5 mm PepMap C18 precolumn and separated on a 75 μm x 250 mm C18 column (PepMap, Dionex). The nanoLC method consisted in a 120-minutes gradient at a flow rate of 300 nL/min, ranging from 5% (v/v) to 37% (v/v) acetronitrile in 0.1% (v/v) formic acid during 114 min before reaching 72% (v/v) for the last 6 minutes. MS and MS/MS data were acquired using Xcalibur V2.1.0 SP1 (Thermo Fischer Scientific). Spray voltage and heated capillary were respectively set at 1.4 kV and 200°C. Survey full-scan MS spectra (m/z = 400-1600) were acquired in the Orbitrap with a resolution of 60,000 after accumulation of 106 ions (maximum filling time: 500 ms). The twenty most intense ions from the preview survey scan delivered by the Orbitrap were fragmented by collision induced dissociation (collision energy 35%) in the LTQ after accumulation of 104 ions (maximum filling time: 100 ms).

Database searching

Peak lists were generated with the Mascot Distiller version 2.4.3.3 software (Matrix Science) from the LC-MS/MS raw data. Using the Mascot 2.4.0 search engine (Mascot Daemon, Matrix Science), MS/MS spectra were searched against a compilation of the *Arabidopsis* protein database provided by TAIR (nuclear, mitochondrial, and chloroplast genomes; TAIR version 10; 35,386 entries; `http://www.arabidopsis.org/`) and a home-made list of contaminants frequently observed in proteomics analyses (260 sequences, [140]). Both databases were concatenated with the corresponding decoy database in order to calculate false discovery rate. One missed trypsin cleavage was allowed, and trypsin/P was used as the enzyme (cleavage at the C terminus of Lys/Arg). The mass tolerances were 10 ppm for precursor ions and 1.0 Da for fragment ions. The variable modifications allowed were N-acetylation (protein N termini), methionine oxidation and dioxidation. A fixed modification was set: carbomidomethyl cystein. Mascot search results were automatically filtered using the home-developed IRMa 1.31.1 software [261]. The following parameters were applied: i) the number of report hits

was fixed automatically to retrieve proteins with a p value, as defined by Mascot, such as $p < 0.05$; ii) only peptides ranked first and with an homology threshold such as the p value, as defined by Mascot, corresponding to $p < 0.05$, were kept. Every duplicated peptide sequence was conserved to calculate spectral counts. Consistent protein grouping for all the analyses (same master protein reported) was ensured using the IRMa software. In order to avoid redundancy, only the master proteins (*i.e.* the protein representing a protein group) were given in the provided results. For each database search, protein groups were identified with a 1% false discovery rate [140]. Database searching results and raw files were exported in the PRIDE format and deposited to the ProteomeXchange server with identifier PXD000546 and DOI 10.6019/PXD000546 and PRIDE accession 31943 (`www.proteomexchange.org`). Lists of proteins and peptides can also be found in the Supplemental_Data file.

Data processing

Total spectral counts and spectral counts for proteotypic peptides were retrieved from the IRMa filtered results for each of the MS/MS analyses. Weighted spectral counts were calculated as described in Abacus [216] and were imported in R (version 3.0.1) [262], which is an open source statistical analysis environment. The raw quantitative data were converted into a *MsnSet* class object from the R package MSnbase [262][263]. The MsnSet class is derived from the *eSet* class and mimics the *ExpressionSet* class used for microarray data. An *MSnSet* object contains quantified expression data for MS proteomic data as well as the experimental meta-data, and allows the analysis of quantitative MS-based data using advanced statistical tools implemented in R, and particularly that of the pRoloc R package [264] (`http://www.bioconductor.org\discretionary{-}{}{}/packages/2.12/bioc/\discretionary{-}{}{}html/pRoloc.html`), which takes as input objects of the MSbase classes. Raw quantitative data were subjected to some pre-processing steps (fig.2.20), including missing value imputation, log-transformation and sample normalization in order to render it compliant with the basic standards of good quality data (completeness, consistency and accuracy). Note that within the whole pipe-line dedicated to the quantitative data analysis, all type of replicates (biological or technical) for a given group (*e.g.* the BBY group) have been treated equally.

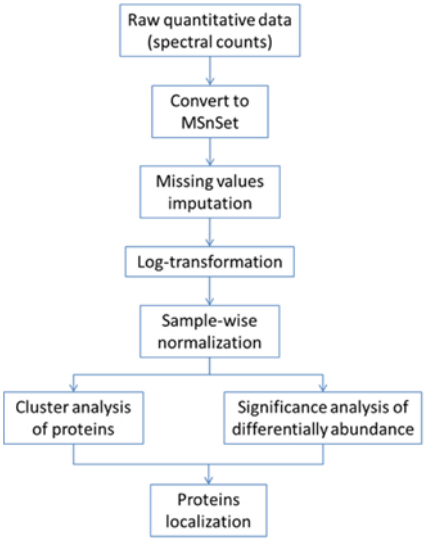

Figure 2.20 – **Pipeline for data analysis**

Missing value imputation

Quantitative proteomics data are well known for high rates of missing values. This fact requires deeper consideration when trying imputing them. In the present study, 1295 proteins were identified in four groups of samples (thylakoids, stroma-lamellae, margins and BBY). However, not all proteins were identified in each individual group. For such proteins, the quantitation algorithm associated a NA (non attributed) value to all samples where that protein was not identified. The actual missing values (MVs) were recorded for proteins which had been identified in at least one sample in a particular group, and they were also assigned with NAs. The proteins concerned are unlikely to be absent in a particular biological compartment as they have already been identified in at least one sample. According to [266], in quantitative proteomics, MVs can be explained by several potential mechanisms: 1) the protein/peptide is present at abundance the instrument should detect it, but it is not detected or incorrectly identified; 2) the protein/peptide is present at an abundance that the instrument cannot detect them; and 3) the protein/peptide is not present at all. MVs recorded as a result of 2) and 3) are called censored missing values, and it has been shown that their simple imputation based on observed values is not appropriate, leading to an overestimate of peptides abundance and to biased results [267]. Conversely, if the MVs are recorded according to 1) (the so-called Missing Completely at Ran-

dom - MCAR), one can use the observed values for their imputation. Thus, depending on the nature of the MVs, different strategies should be employed for their imputations. For MCAR data one can use simple MVs imputation methods which rely on the observed values [267], while for the censored data one strategy is replace the MV with the minimum value observed [266]. Our strategy for MV imputation was based on the above considerations. Although different probabilistic models are proposed to separate between MCAR data and censored data [268][269], our approach is based on a statistical investigation of the data in order to verify whether the missing values are abundance dependent or not. To do so, in each group of samples and for each protein we estimated the mean value of the non-missing values, and we visualized the distribution for all proteins. This provided useful information that helped infer whether the missing values are abundance dependent or not and provided guidance in declaring the missing values as being censored or MCAR. The MVs imputation strategy consisted of replacing the censored MVs by the minimum value observed, while the MCAR MVs they were imputed using a nearest neighbor strategy [270], which was implemented as a routine preprocessing in MSnset [263] (Supplemental_Material).

Data normalization

For the 24 samples corresponding to the 4 biological groups (thylakoids, BBY, margins and stroma-lamellae), the distributions of the log-transformed abundances were examined in order to investigate about the presence of technical bias. For each of the 4 groups of samples, quantiles normalization [271] was performed after the imputation of missing values implemented in the MSnSet R package (Supplemental_Material).

Statistical analysis of differential abundance

We employed the R package LIMMA [221] which implements a robust method for differentially abundance assignment widely used for microarray data, based on linear protein-wise models as well as an empirical Bayesian model for robust estimates of protein-wise standard errors. As the MSnSet class mimics the *ExpressionSet* class used for microarray data, and as this latter is used as input object for LIMMA, it appears that any proteomics dataset converted into the MSnSet format is compliant with a LIMMA use. The method in LIMMA is based on a modified version of Student t-test (called moderated t-test), where the standard errors are reduced towards a common value using a simple Bayesian model. This means that, when esti-

mating the variable-wise standard error, the model borrows the information from the other genes (or in this case, proteins), which leads to more robust estimates. As a consequence, the model is well-suited to assess differentially abundance for datasets with few samples. In a recent comparison study on the significance testing for small microarray experiments [272], LIMMA has been found as being the method that balances the best the number of true positives and false positives. Within this comparison study, the authors used experiments with small sample size ranging from 2 to 5 samples per group. The approach consists in first fitting a linear model to each protein and second, estimating the corresponding moderated t-statistic using the empirical Bayes procedure. p-values were calculated using the moderated t-statistic. Multiple testing corrections were then performed by adjusting the p-values for multiple testing using Benjamini and Hochberg's method to control the false discovery rate [222]. We set the adjusted p-value (referred to as q-value) threshold for declaring a protein differentially expressed to 0.05, meaning that the expected proportion of false discoveries in the selected group of proteins is controlled to be less than 5%.

Proteins cluster analysis

For each group of samples (BBY, margins and stroma-lamellae) we derived a representative sample as being the mean over the 6 available replicates divided by the mean abundance values across the 6 thylakoid samples, in order to take into account for the difference in abundance of thylakoid proteins. Working with such relative abundance values will homogenize low and high abundant proteins, providing that proteins more abundant in BBY with respect to stroma-lamellae will not be sensitive to the actual protein abundance. As a consequence, a number of 255 proteins which were not identified in the thylakoids samples were not considered. Cluster analysis was performed using PAM (Partition Around Menoids) [273], a particular implementation of the k-medoids algorithm. k-medoid is one of the numerous variations of the extremely well-known k-means algorithm. This latter is implemented in the R package pRoloc [179] (`http://www.bioconductor.org/packages/2.12/bioc/html/pRoloc.html`), as well as numerous more sophisticated algorithms, such as kernel k-means, spectral clustering [274](by mapping to the corresponding R package [275]), or hyperspherical clustering [276] (by direct implementation). As methods to automatically assess the right number of clusters are still under development for the next version of pRoloc, this point was tackled as described in Supplemental_Material.

Curated annotation of proteins

Information about identified proteins were retrieved and compiled from the literature (http://www.ncbi.nlm.nih.gov/pubmed) using AGI numbers or protein names and screening for recently published data, from UniProtKB (http://www.uniprot.org/), TAIR (http://www.arabidopsis.org/), PPDB [277] (http://ppdb.tc.cornell.edu/), AT_Chloro [140] (http://www.grenoble.prabi.fr/at_chloro/), SUBA3 [278] (http://suba.plantenergy.uwa.edu.au/) and the ontological tool MapMan [217] (http://mapman.gabipd.org) which was specifically designed to cover plant-specific pathways and processes [279].

Deciphering thylakoid sub-compartments using a mass spectrometry-based approach

Supplementary table 1

Supplementary tables 2-7 are available at the following address `http://goo.gl/D8Q8qi`

Accession	Protein name (this work)	Curated function (this work)	LogFC	Adj.pvalue
AT1G29920.1	LHCB1.1 (LHCII-1.1, CAB2)	PS LHCII	-5.76961939753	2.58139896219
AT1G29930.1	LHCB1.3 (LHCII-1.3)	PS LHCII	-0.31133967277	0.00450640625
AT2G34430.1	LHCB1.4 (LHCII-1.4)	PS LHCII	-1.40854222942	2.45016642292
AT2G34420.1	LHCB1.5 (LHCII-1.5, LHB1B2)	PS LHCII	-4.86268998777	1.34276486971
AT2G05100.1	LHCB2.1 (LHCII-2.1)	PS LHCII	-1.13445935347	3.64627767501
AT2G05070.1	LHCB2.2 (LHCII-2.2)	PS LHCII	-3.43278131412	4.34697049147
AT3G27690.1	LHCB2.3 (LHCII-2.3)	PS LHCII	-0.59928865037	0.00062812634
AT1G76570.1	LHCB2.3-like (LHCII-2.3)	PS LHCII	0.166666666666	0.48959455631
AT5G54270.1	LHCB3.1 (LHCII-3)	PS LHCII	-2.01262634284	1.18040029247
AT5G01530.1	LHCB4.1 (LHCII-4.1, CP29.1)	PS LHCII	-2.33755001769	8.09556458001
AT3G08940.2	LHCB4.2 (LHCII-4.2, CP29.2)	PS LHCII	-1.66427318838	3.50998645447
AT2G40100.1	LHCB4.3 (LHCII-4.3, CP29.3)	PS LHCII	-0.97532631345	0.00140447697
AT4G10340.1	LHCB5 (LHCII-5, CP26)	PS LHCII	-2.21468093953	5.36195035181
AT1G15820.1	LHCB6 (LHCII-6, CP24)	PS LHCII	-2.13737014243	5.45974293484
ATCG00020.1	PSBA (D1)	PS PSII	-2.04593801351	1.18444846801
ATCG00680.1	PSBB (CP47)	PS PSII	-1.99617854538	4.34277216378
ATCG00280.1	PSBC (CP43)	PS PSII	-1.69379824904	2.79345139642
ATCG00270.1	PSBD (D2)	PS PSII	-1.89658501687	4.32356657897
ATCG00580.1	PSBE	PS PSII	0.654108340896	0.14976594947
ATCG00710.1	PSBH	PS PSII	0.076901649166	1,00
ATCG00560.1	PSBL	PS PSII	0.056799478900	1,00
AT5G66570.1	PSBO1 (OEE1-1, OEC33)	PS PSII OEE	-2.56584659714	5.30998874328
AT3G50820.1	PSBO2 (OEE1-2, OEC33)	PS PSII OEE	-1.63458053092	1.18289613501
AT1G06680.2	PSBP1 (OEE2, OEC23, OE23)	PS PSII OEE	0.018829111756	1,00
AT3G56650.1	PSBP-like (PPD6)	PS PSII OEE ?	1.310850510791	1.04528859188
AT1G76450.1	PSBP-like 2 (OEC23-like-2)	PS PSII OEE ?	1.749074974189	1.69767965429
AT4G15510.3	PSBP-like 3 (PPD1, OEC23-like-3)	PS PSII	1.664503512382	1.80525526940
AT3G55330.1	PSBP-like 4 (PPL1, OEC23-like-4)	PS PSII OEE ?	1.525261516160	3.23766860797
AT2G28605.1	PSBP-like 4-2 (OEC23-like-4)	PS PSII	0,00	1,00
AT1G77090.1	PSBP-like 5 (OEC23-like-5, PPD4)	PS PSII OEE ?	0,00	1,00
AT5G11450.1	PSBP-like 6 (OEC23-like-6)	PS PSII OEE ?	1.68546079328	8.52790092326
AT4G21280.1	PSBQ1 (OEE3-1, OEC16)	PS PSII OEE	-0.03831542003	1,00
AT4G05180.1	PSBQ2 (OEE3-2)	PS PSII OEE	0.368870918278	0.25424152112
AT1G79040.1	PSBR	PS PSII	0.471588577365	0.29049206693
AT1G44575.1	PSBS (NPQ4, CP22)	PS PSII NPQ	-0.91904689798	0.00224535128
AT3G21055.1	PSBT (PsbTn)	PS PSII	0	1
AT1G51400.1	PSBT-like (PsbTn)	PS PSII	0	1
AT4G28660.2	PSBW (PSB28)	PS PSII	0.166666666666	0.48959455631
AT1G03600.1	PSBZ-like (PSB27-like)	PS PSII	-0.12915351307	0.76690774136
AT3G54890.4	LHCA1 (LHCI-1-1)	PS LHCI	0.990896303438	0.00014921596
AT3G61470.1	LHCA2 (LHCI-2.1)	PS LHCI	1.088904608746	0.00035319091
AT1G61520.3	LHCA3 (LHCI-3, CAB4)	PS LHCI	1.896449949044	1.74075681034
AT3G47470.1	LHCA4 (LHCI-4)	PS LHCI	1.444160114856	0.00021685261
AT1G45474.1	LHCA5 (LHCI-5)	PS LHCI	1.474364287548	6.06275543373

Accession	Protein name (this work)	Curated function (this work)	LogFC	Adj.pvalue
AT1G19150.1	LHCA6 (LHCI-6 or LHCA2.1)	PS LHCI	1.891268481171	0.00047675941
ATCG00350.1	PSAA	PS PSI	0.969391358579	3.16011651452
ATCG00340.1	PSAB	PS PSI	1.313039655470	0.00018834996
ATCG01060.1	PSAC	PS PSI	2.160311661574	2.19972201178
AT4G02770.1	PSAD-1	PS PSI	0.861350150311	0.00024075644
AT4G28750.1	PSAE-1	PS PSI	0.729362598250	0.00017842363
AT2G20260.1	PSAE-2	PS PSI	1.093821117491	0.00021370775
AT1G31330.1	PSAF	PS PSI	0.973570999311	2.42804565620
AT1G55670.1	PSAG	PS PSI	2.554474165881	8.69612219617
AT3G16140.1	PSAH-1	PS PSI	2.649285103190	5.96946530346
AT1G52230.1	PSAH-2	PS PSI	3.401550466994	2.00111362553
ATCG00630.1	PSAJ	PS PSI	0	1
AT1G30380.1	PSAK	PS PSI	2.908446485843	1.01351130489
AT4G12800.1	PSAL	PS PSI	0.931598773709	0.00283283338
AT5G64040.1	PSAN	PS PSI	1.418590570449	4.18824880907
AT1G08380.1	PSAO	PS PSI	1.534992711314	7.49742683892
AT2G46820.2	PSAP (TMP14, pTAC8)	PS PSI	3.220238311724	1.38199041841
AT1G52220.1	PSAP-like	PS PSI ?	2.311726906093	2.11606719678
ATCG00540.1	PETA (CYF)	PS b6-f	0.940015506454	2.25251294857
ATCG00720.1	PETB (CYB6)	PS b6-f	0.802487113765	0.00215464650
AT4G03280.2	PETC (UCRIA)	PS b6-f	0.701971703849	2.29761837227
ATCG00730.1	PETD	PS b6-f	2.614554274081	0.00190917844
AT2G26500.3	PETM	PS b6-f	0.388888888888	0.25116670134
AT5G23060.1	CaS	PS State transition ?	0.033682282286	1,00
AT1G68830.1	STN7	PS State transition ?	0.039221461053	1,00
AT5G01920.1	STN8	PS State transition ?	-0.61692164715	0.08378791920
AT4G27800.1	TAP38 (PPH1)	PS State transition ?	1.052590445496	0.00498075243
AT3G47070.1	TSP9	PS State transition ?	0.696125605269	0.19735350918
ATCG00120.1	ATPA (CF1a)	PS ATPase	3.082647220950	4.66238767138
ATCG00480.1	ATPB (CF1b)	PS ATPase	2.557041677634	4.73950366348
AT4G04640.1	ATPC1 (ATPG1, CF1y)	PS ATPase	2.397960834418	8.24021243951
AT4G09650.1	ATPD (CF1d, PDE332)	PS ATPase	3.452659270333	1.18289613501
ATCG00470.1	ATPE (CF1e)	PS ATPase	2.750093571902	6.15183587969
ATCG00130.1	ATPF (CF0-I)	PS ATPase	2.370779371403	5.47956397817
AT4G32260.1	ATPG (CF0-II, PDE334)	PS ATPase	2.332379983715	9.92883260453
ATCG00140.1	ATPH (CFO-III)	PS ATPase	2.118222837829	1.64246457999
ATCG00150.1	ATPI (CFO-IV)	PS ATPase	2.788331364544	3.06977828694
AT2G05620.1	PGR5	PS cyclic electron flows	1.746408600447	7.25770303984
AT4G22890.3	PGRL1A (PGR5-LIKE A)	PS cyclic electron flows	1.391745787033	2.24801815267
AT4G11960.1	PGRL1B (PGR5-LIKE B)	PS cyclic electron flows	2.879342727608	3.31660723982
AT3G15840.4	PIFI	PS CEF cyclic electron flow ?	0.077863452083	1,00
AT1G76100.1	PETE1	PS b6/f PSI electron transfer	0.333333333333	0.24291854354
AT1G20340.1	PETE2 (PLAS2, PC-1, DRT112)	PS b6/f PSI electron transfer	2.224277431732	7.18090730984
AT1G60950.1	FD2 (FER2, PETF, PETF1)	PS redox	0.5	0.08977044469

Accession	Protein name (this work)	Curated function (this work)	LogFC	Adj.pvalue
AT1G32550.2	FDC2 (FDX-like)	PS redox	0.166666666666	0.48959455631
AT3G16250.1	CEF1 (PnsB3)	NDH or PS PSI cyclic	0.166666666666	0.39324311087
AT1G15980.1	NDF1 (NDH48, PnsB1)	NDH	1.447512254107	0.00146008353
AT1G64770.1	NDF2 (NDH45, PnsB2)	NDH	1.153593528929	0.00940352334
ATCG01100.1	NDHA (NDH1)	NDH	1.190567783036	5.35098188013
ATCG00440.1	NDHC (NDH3)	NDH	1.186732484551	5.26515636899
ATCG01050.1	NDHD (NDH-4)	NDH	1.202522235115	0.00038804551
ATCG01070.1	NDHE (NU4LC)	NDH	0.833333333333	7.04432569891
ATCG01010.1	NDHF (NDH5)	NDH	1.560071900754	0.00127483930
AT1G18730.3	NDHF6 (PnsB4, NDF6)	NDH	1.754789637066	7.49742683892
ATCG01110.1	NDHH (NDH7)	NDH	1.871783163180	0.00011454656
ATCG01090.1	NDHI	NDH	1.174904433383	0.00094080751
ATCG00420.1	NDHJ	NDH	0.996641164531	0.00035885053
AT1G70760.1	NDHL	NDH	0.333333333333	0.34526636549
AT4G37925.1	NDHM	NDH	1.210621510194	0.00066149055
AT5G58260.1	NDHN	NDH	0.823085537423	0.00914381023
AT1G74880.1	NDHO	NDH	1.286757365725	0.00890324255
AT4G23890.1	NDHS (CRR31)	NDH	1.296055494571	0.00051927185
AT4G09350.1	NDHT	NDH chaperonne	0,00	1,00
AT5G21430.1	NDHU (CRR31, CCRI)	NDH or chaperone and protease ?	1.587144750640	0.00051580441
AT5G43750.1	PNSB5 (NDH18)	NDH	1.154440056210	0.00379450412
AT2G39470.2	PPL2 (PnsL1)	PS PSII or NDH ?	1.028188471304	0.00026412376
AT1G14150.1	PQL1 (PnsL2, PQL2)	PS PSII OEE or NDH ?	2.729378715104	6.36183252128
AT3G01440.1	PQL2 (PnsL3, OEE3-like)	PS PSII OEE or NDH ?	1.034360734688	0.00124933606
ATCG00430.1	PSBG (NDHK)	PS PSII	1.072824138043	0.00774867495
AT5G66190.1	FNR1 (FENR)	redox	0.382748079619	0.00354452031
AT1G20020.1	FNR2	redox	0.476581137163	0.00242831896
AT5G47110.1	LIL3:1	Stress light	2.527887725465	2.25206565198
AT4G17600.1	LIL3:2	Stress light	2.550649046933	1.27659503697
AT5G02120.1	OHP1	stress light	1.931433554631	2.21437662642
AT1G34000.1	OHP2	PS PSII stress oxidative	2.289269322853	1.45325194139
AT5G36790.1	PGLP1B	unknown	0,00	1,00
AT3G14415.3	GOX1	stress oxidative	0,00	1,00
AT3G14420.2	GOX2	stress oxidative	0,00	1,00
AT2G13360.2	SGAT (AGT1)	unknown	0,00	1,00
AT4G32520.1	SHMT3	unknown	0,00	1,00
AT1G68010.1	HPR	metabolism carbon	0,00	1,00
AT1G80380.4	GLYK	metabolism carbon	-0.37527152789	0.22806218787
ATCG00490.1	RBL (RBCL)	metabolism carbon Calvin cycle	2.605990630867	2.55532197956
AT3G04790.1	PRI (EMB3119)	metabolism carbon Calvin cycle	1.830934382318	2.17955322107
AT5G61410.1	RPE	metabolism carbon Calvin cycle	0,00	1,00
AT1G32060.1	PRK2 (KPPR, PRKASE)	metabolism carbon Calvin cycle	1.732078918383	1.80647294468
AT1G14030.1	LSMT-L	metabolism carbon Calvin cycle	0,00	1,00
AT2G39730.1	RCA	metabolism carbon Calvin cycle chaperone and	1.411950018690	2.56253651624

Accession	Protein name (this work)	Curated function (this work)	LogFC	Adj.pvalue
AT1G73110.1	RCA-like (RCA2)	metabolism carbon Calvin cycle chaperone and	0.333333333333	0.24291854354
AT1G67090.1	RBS1A (RBCS-4)	metabolism carbon Calvin cycle	1.393369788085	0.00494599766
AT5G38430.1	RBS1B (RBCS-1B)	metabolism carbon Calvin cycle	2.317637897258	6.01073999947
AT5G38420.1	RBS2B (RBCS-2B)	metabolism carbon Calvin cycle	2.811798882309	2.53822389701
AT3G12780.1	PGK1 (PGKH)	metabolism carbon Calvin cycle	3.495719418942	1.17695925176
AT1G56190.1	PGK2 (PGKH)	metabolism carbon Calvin cycle	1.309992959629	0.00209813341
AT3G26650.1	GAPA-1 (G3PA)	metabolism carbon Calvin cycle	1.461304610118	5.86196088217
AT1G12900.1	GAPA-2	metabolism carbon Calvin cycle	1.765360143707	1.62124248249
AT1G12900.2	GAPA-2	metabolism carbon Calvin cycle	0,00	1,00
AT1G42970.1	GAPB (G3PB)	metabolism carbon Calvin cycle	2.172591855219	6.08804151407
AT2G21170.1	TPIC (TIM, TPI-1)	metabolism carbon	0,00	1,00
AT2G21330.1	FBA1 (SFBA-1, ALFC)	metabolism carbon Calvin cycle	2.858358479053	2.63006930729
AT4G38970.1	FBA2 (SFBA-2, ALFC)	metabolism carbon Calvin cycle	2.496138489006	2.08994333969
AT2G01140.1	SFBA-3 (ALFC3)	metabolism carbon Calvin cycle	0.436040933439	0.10352169369
AT3G54050.1	FBP (FBPA, F16P1, FBPase)	metabolism carbon Calvin cycle	0.818317544962	0.03776134068
AT3G60750.2	TKL-1 (TKTC)	metabolism carbon Calvin cycle	0.833333333333	0.00127483930
AT3G55800.1	S17P (SBPase)	metabolism carbon Calvin cycle	1.843695330588	2.28599158740
AT5G18070.1	AGM1 (PAGM, DRT101)	DNA Binding	0.166666666666	0.39324311087
AT4G16790.1	nd	nd	0.166666666666	0.39324311087
AT1G70710.1	CEL1	unknown	0,00	1,00
AT4G38990.1	nd	unknown	-0.19916458337	0.39324311087
AT1G02640.1	nd	nd	0.166666666666	0.39324311087
AT3G14310.1	nd	nd	-0.05555555555	0.39324311087
AT3G11980.1	FACR2 (FAR2 MS2)	metabolism lipid ?	0.166666666666	0.39324311087
AT3G16950.2	LPD1 (PTLPD1)	metabolism lipid	0.075196341286	0.84540998010
AT3G63170.1	nd	metabolism flavonoids ?	0,00	1,00
AT2G38040.1	ACCDa (HP88b, CAC3)	metabolism lipid	1.473538577861	0.00066149055
ATCG00500.1	ACCDb	metabolism lipid	3.100535603214	4.89536289474
AT5G35360.1	CAC2	metabolism lipid	0,00	1,00
AT5G16230.1	STAD3	metabolism lipid ?	0.166666666666	0.39324311087
AT3G02620.1	STAD4 (S-ACP-DES4)	metabolism lipid ?	0.111111111111	0.76690774136
AT3G02630.1	STAD5 (S-ACP-DES5)	metabolism lipid	0,00	1,00
AT2G43710.1	STAD7 (FAB2)	metabolism lipid	0,00	1,00
AT1G62640.2	FABH (KASIII)	metabolism lipid	0.166666666666	0.48959455631
AT1G74960.2	KAS2 (FAB1)	metabolism lipid	0,00	1,00
AT5G46290.3	KASC1	metabolism lipid	0,00	1,00
AT5G52920.1	nd	nd	0.166666666666	0.39324311087
AT3G22960.1	PKP1 (PK1, PKP)	metabolism lipid	0.5	0.08977044469
AT3G25860.1	LTA2 (E2)	metabolism lipid	-0.40840085839	0.12439838274
AT1G34430.1	LTA2-like (E2, EMB3003)	metabolism lipid	-0.08344282491	1,00
AT1G01090.1	PDH-E1 ALPHA	metabolism lipid	-0.06759701924	1,00
AT2G34590.1	PDH-E1 BETA	metabolism lipid	-0.27483323631	0.24291854354
AT4G16155.1	PTLPD2 (E3)	metabolism lipid	-0.22311696203	0.48959455631
AT1G24360.1	FABG	metabolism lipid	-1.93877552126	1.28242869708

Accession	Protein name (this work)	Curated function (this work)	LogFC	Adj.pvalue
AT2G22230.1	FabZ	metabolism lipid	-0.94652257433	0.00475530950
AT5G10160.1	FabZ	metabolism lipid	-1.56015505054	1.05926672598
AT2G05990.1	Enr-A	metabolism lipid	0,00	1,00
AT4G14070.1	AAE15 (HP81)	metabolism lipid	3.952768958281	4.84369191606
AT1G77590.1	LACS9 (HP76)	metabolism lipid	2.507862067149	6.18944511321
AT1G54570.1	PES1	stress abiotic	1.056048770526	0.03130635433
AT3G26840.1	PES2	metabolism lipid ?	0.789836188490	0.03203137445
AT2G39290.1	PGPS1 (HP32c, PGP1)	metabolism lipid	1.187680988967	5.86359413437
AT3G06510.1	SFR2	stress freezing	0.262611731033	0.38089755469
AT4G31780.2	MGD1 (MGDA)	metabolism lipid	-0.08847657650	1,00
AT5G01220.1	SQD2	metabolism lipid	1.389205303532	4.40209430928
AT1G19800.1	TDG1	transporter lipids	0.854347655633	0.02792654564
AT3G20320.1	TGD2 (HP41b, ABCI15)	transporter ABC lipids	2.941212364684	5.33375366030
AT1G65410.1	TGD3 (NAP11, ABCI13)	transporter ABC lipids	1.225663885323	0.00415729375
AT3G06960.1	TGD4-like (HP50-like, PDE320-like	unknown	0.755905401098	0.14210339028
AT3G11170.1	FAD7 (FAD3C, FADD, FAD8)	metabolism lipid	0.476519256907	0.27720447892
AT4G30950.1	FAD6C (FADC, FAD6)	metabolism lipid	1.820075228696	5.17310384768
AT2G46090.1	LCBK2	metabolism lipid	1.335258114389	2.17641018744
AT3G60620.1	CDS5	metabolism lipid	0.166666666666	0.39324311087
AT3G55030.1	PGPS2 (HP25b, PGP)	metabolism lipid	0.833333333333	0.00127483930
AT5G57690.1	DGK4	metabolism lipid	0,00	1,00
AT4G15130.1	nd	nd	0,00	1,00
AT2G40690.1	GLY1 (GPDH)	metabolism lipid ?	0.597493750120	0.10635533374
AT3G47860.1	AtCHL	Stress light	1.047841663541	0.03130635433
AT2G38540.1	LTP1	metabolism lipid ?	0,00	1,00
AT3G10840.1	HP50b	metabolism lipid ?	0.422572067764	0.39324311087
AT5G67050.1	Lipase-like	metabolism lipid	-0.75744971898	0.09750061288
AT4G13550.1	Lip-like	metabolism lipid ?	0.666666666666	0.01996908054
AT3G20520.1	SVL3 (SHV3-like 3, SEUSS-like 3)	metabolism lipid ?	0.5	0.08977044469
AT2G15620.1	NIR (NIR1)	redox	0,00	1,00
AT5G04140.1	GLTB1	metabolism carbon	0,00	1,00
AT3G17820.1	GLN13 (GS1, GLN1-3, MEB5.4)	metabolism aa glutamine	0.166666666666	0.39324311087
AT1G48470.1	GLN15 (GLN1;5)	metabolism aa glutamine	0.456502855157	0.39324311087
AT5G35630.2	GSLI (GLNA2, GS2)	metabolism carbon	0.275998874234	0.67812797904
AT5G04740.1	ACR12	unknown	0.430827083453	0.39324311087
AT4G31990.1	AAT5	metabolism aa Asp	0,00	1,00
AT2G19940.1	nd	unknown	0,00	1,00
AT3G57560.1	NAGK	unknown	0,00	1,00
AT1G75330.1	OTC	unknown	0,00	1,00
AT4G24830.1	ASSY	metabolism amino acids	0.166666666666	0.48959455631
AT4G29840.1	TS1	metabolism amino acids Arginine	0,00	1,00
AT2G44040.1	DAPB1	metabolism amino acids lysine	0.166666666666	0.48959455631
AT4G33680.1	DAP (AGD2)	metabolism aa Asp	0,00	1,00
AT3G53580.1	DAPF	metabolism aa Asp	0,00	1,00

Accession	Protein name (this work)	Curated function (this work)	LogFC	Adj.pvalue
AT5G13280.1	AK1 (AK, AK-LYS1)	metabolism aa Asp	0,00	1,00
AT5G14060.1	AK2 (AK-LYS2, CARAB-AK-LYS)	metabolism aa Asp	0,00	1,00
AT1G14810.1	nd	metabolism aa Asp	0,00	1,00
AT2G17265.1	HSK (KHSE)	metabolism aa Asp	0,00	1,00
AT2G31810.3	ALS2 (AHAS, ILVH2)	metabolism amino acids branched chain	-0.16548140449	0.89767134793
AT3G58610.1	nd	metabolism amino acids branched chain	0,00	1,00
AT4G13430.1	IIL1	metabolism amino acids branched chain	0,00	1,00
AT1G74040.1	IPMS2 (LEU12)	metabolism amino acids branched chain	0,00	1,00
AT1G18500.1	LEU11 (IPMS1, MAML-4)	metabolism amino acids branched chain	0.166666666666	0.48959455631
AT1G31180.1	IMDH1 (LEU31) 3-isopropylmalate	metabolism amino acids branched chain	0,00	1,00
AT4G34200.1	3-PGDH (EDA9)	metabolism aa Ser	1.775346708612	0.00018625300
AT1G17745.2	3-PGDH (SERA)	metabolism aa serine	0.333333333333	0.24291854354
AT3G19480.1	nd	metabolism aa Ser	0,00	1,00
AT4G35630.1	PSAT	metabolism aa serine	0,00	1,00
AT1G18640.2	PSP	metabolism aa serine	0,00	1,00
AT3G03630.1	CYSK4 (OAS-TL)	metabolism aa cystein	-0.46240557635	0.27270704469
AT3G59760.1	CYSKM (OASTL C, OASC)	metabolism aa cysteine	0.166666666666	0.48959455631
AT2G43750.2	CYSKP (OASTL-B, OASB)	metabolism aa Cys	-0.87527152789	0.00252858111
AT4G39980.1	AROF (DAHPS-like)	metabolism aminoacids aromatic	0,00	1,00
AT1G22410.1	DAHPS-like	metabolism aminoacids aromatic	0.082378729346	1,00
AT4G33510.1	DHS2 (AROG)	metabolism aa	1.602922139535	6.12679956839
AT3G06350.1	DHQSD	metabolism aminoacids aromatic	0,00	1,00
AT3G26900.1	SKL1	metabolism aminoacids aromatic	0,00	1,00
AT5G05730.1	ASA1 (TRPE)	metabolism aa tryptophan	0,00	1,00
AT5G17990.1	PAT1 (TRPD)	metabolism amino acids Tryptophan	1.285174739087	5.61354813912
AT2G04400.1	IGPS (TRPC)	metabolism amino acids Tryptophan	0,00	1,00
AT5G48220.2	nd	metabolism amino acids Tryptophan	0,00	1,00
AT1G09795.1	ATP-PRTase 2	metabolism amino acids Histidine	0,00	1,00
AT5G63890.2	HISN8	metabolism amino acids Histidine	0,00	1,00
AT1G67280.1	nd	unknown	0,00	1,00
AT1G11860.2	GDCST	unknown	0,00	1,00
AT3G10670.1	ABC6I	transporter ABC	0,00	1,00
AT4G26500.1	SUFE	unknown	0,00	1,00
AT3G22890.1	APS1	sulfate assimilation	0.166666666666	0.48959455631
AT5G43780.1	APS4	sulfate assimilation	0,00	1,00
AT2G14750.1	APK1 (AKN1)	metabolism sulfur	0,00	1,00
AT5G04590.1	SiR	metabolism aa Cys	0,00	1,00
AT5G01600.1	FER1 (FRI1)	Iron binding	0.166666666666	0.48959455631
AT5G14910.1	HMA-like	transporter metals ?	0.408672062172	0.34991639843
AT3G32030.1	TPS30	metabolism isoprenoids	-0.16666666666	0.39324311087
AT1G74470.1	GGDR	metabolism vitamin and pigment	3.361321995159	8.85955256903
AT4G36810.1	GGPP1	metabolism isoprenoids non-mevalonate pathv	0,00	1,00
AT4G38460.1	GGR	metabolism isoprenoids non-mevalonate pathv	0,00	1,00
AT2G18640.1	GGPP4	metabolism isoprenoids non-mevalonate pathv	0	1

Accession	Protein name (this work)	Curated function (this work)	LogFC	Adj.pvalue
AT5G62790.2	DXR	metabolism isoprenoids	0,00	1,00
AT2G26930.1	ISPE (CMK, PDE227)	metabolism isoprenoids	-0.19916458337	0.48959455631
AT5G60600.2	ISPG	metabolism isoprenoids	0,00	1,00
AT4G34350.1	ISPH	metabolism isoprenoids	0,00	1,00
AT3G63410.1	VTE3 (APG1, IEP37)	metabolism vitamin and pigment	2.617537191563	3.23177894678
AT4G32770.1	VTE1 (TOCC, SXD1)	metabolism vitamin and pigment	0.264160416786	0.48959455631
AT1G64970.1	VTE4 (GTOMC, G-TMT)	metabolism vitamin and pigment	0.333333333333	0.24291854354
AT5G67030.1	ABA1 (LOS6, ZEP)	metabolism vitamin and pigment	3.237043195765	1.20928546762
AT4G19170.1	CCD4 (NCED4)	metabolism vitamin and pigment	2.191066645851	7.70734244322
AT1G57770.1	CrtH	metabolism vitamin and pigment ?	0,00	1,00
AT1G06820.1	CRTSO (CrtISO, CCR2)	metabolism vitamin and pigment	1.435877112967	7.27400053401
AT3G09580.1	HP52b (PDS-like)	metabolism vitamin and pigment ?	1.962901282436	1.14483845375
AT3G53130.1	LUT1 (P450 CYP91C1)	metabolism vitamin and pigment	0.5	0.08977044469
AT5G17790.1	VAR3	chloroplast biogenesis	-0.05555555555	0.39324311087
AT1G10830.1	Z-ISO (ZCIS)	metabolism vitamin and pigment	1.318157022064	1.14483845375
AT5G17230.3	PSY1 (PSY)	metabolism vitamin and pigment carotenoids	0.764160416786	0.02792654564
AT4G14210.1	PDS3 (CRTI)	metabolism vitamin and pigment	3.553022339408	1.28242869708
AT1G08550.2	NPQ1 (VDE)	metabolism vitamin and pigment carotenoids	1.425445353236	6.38518254691
AT2G21860.1	VDE-like	metabolism vitamin and pigment ?	0.998880298184	0.00634788153
AT3G04870.2	ZDS1 (ZCD)	metabolism vitamin and pigment	0.333333333333	0.24291854354
AT5G57030.1	LUT2	metabolism vitamin and pigment ?	1.826049787621	0.00010711570
AT2G46570.1	Lac6	metabolism phenols ?	0.166666666666	0.39324311087
AT5G25980.2	TGG2 (BGLU37)	signaling abscisic	-1.06060495675	0.03800403729
AT5G23010.1	MAM1	unknown	0,00	1,00
AT1G64920.1	nd	nd	0.166666666666	0.39324311087
AT1G53520.1	FAP3	metabolism flavonoids	0,00	1,00
AT2G42820.1	HVA22-like	metabolism hormone absicic acid ?	0,00	1,00
AT5G56650.1	ILL1 (ILR1-like 1)	metabolism hormone auxin	-0.38056776994	0.30816218192
AT5G16010.1	Steroid_dh-like	metabolism hormone brassinosteroid	1.551530184485	7.19410386822
AT5G35750.1	AHK2	kinase signaling	-0.47694236115	0.34311785110
AT5G25900.1	KO (CYP701A3, GA3, KO1)	metabolism hormone gibberellins	0.5	0.08977044469
AT1G75750.2	GASA1	unknown	0,00	1,00
AT3G45140.1	LOX2 (LOXC)	metabolism lipid	3.770610139836	1.86529395860
AT3G25760.1	AOC1 (ERD12-1)	metabolism hormone jasmonate	2.001205568126	6.15183587969
AT5G42650.1	AOS (P450 CYP74A)	metabolism hormone jasmonate	5.262468893947	3.04803088541
AT3G25770.1	AOC2 (ERD12-2)	metabolism hormone jasmonate	2.678856989659	1.77196578387
AT5G54770.1	THI4	unknown	0,00	1,00
AT1G51560.1	PNP oxidase-like	metabolism vitamin and pigment vitamin b6 ?	-0.59749375012	0.33305884105
AT3G21140.1	PNP oxidase-like	metabolism vitamin and pigment vitamin b6 ?	-0.27777777777	0.25886504320
AT1G21640.1	NADK2	metabolism NAD	-0.22222222222	0.39324311087
AT2G44050.1	nd	unknown	0,00	1,00
AT4G35760.1	LTO1	metabolism vitamin and pigment	1.275971969656	0.00530075201
AT1G60600.1	UbiA-like	metabolism vitamin and pigment folate & vitar	0.166666666666	0.39324311087
AT3G21200.1	PGR7	PS PSI cyclic electron flow	0.166666666666	0.48959455631

Accession	Protein name (this work)	Curated function (this work)	LogFC	Adj.pvalue
AT5G64050.1	GluRS	unknown	0,00	1,00
AT1G08520.1	CHLD (ALBINA1, PDE166)	metabolism vitamin and pigment	-0.43763576394	0.30274071979
AT5G13630.1	CHLH (GUN5, ABAR)	metabolism vitamin and pigment & hormone	0.166666666666	0.48959455631
AT4G18480.1	CHLI1	metabolism vitamin and pigment	0,00	1,00
AT5G45930.1	CHLI2	metabolism vitamin and pigment	0,00	1,00
AT4G25080.1	CHLM	metabolism vitamin and pigment	2.928755619269	3.23177894678
AT3G56940.1	CHL27 (CRD1, AT103)	metabolism vitamin and pigment	2.703192250795	7.21117019053
AT5G18660.1	DVR (PCB2)	metabolism vitamin and pigment chlorophyll	2.887212545645	3.23177894678
AT4G27440.1	PORB	metabolism vitamin and pigment	2.323887006073	1.60075275450
AT1G03630.2	PORC	metabolism vitamin and pigment	2.437326755435	6.00210218963
AT3G51820.1	CHLG (G4)	metabolism vitamin and pigment	1.548509436649	0.00010331529
AT1G44446.3	CAO (CHL, CH1)	metabolism vitamin and pigment chlorophyll	0.666666666666	0.01996908054
AT1G58290.1	HEMA1 (GluTR, HEMA,HEM11)	metabolism vitamin and pigment	0.908683292864	0.05559886297
AT2G30390.1	FC2	metabolism vitamin and pigment	2.857108121318	1.07581541429
AT5G63570.1	GSA1	metabolism vitamin and pigment	0,00	1,00
AT3G48730.1	GSA2	metabolism vitamin and pigment	0,00	1,00
AT1G69740.2	HEM2 (ALAD-1, ALADH)	metabolism vitamin and pigment	0.166666666666	0.48959455631
AT3G14110.3	FLU (TPR-like)	metabolism vitamin and pigment	0.887527468101	0.00158910128
AT3G59400.1	GUN4	metabolism vitamin and pigment chlorophyl a	0.166666666666	0.48959455631
AT5G08280.1	HEM3	metabolism vitamin and pigment	0,00	1,00
AT1G04620.1	HCAR	metabolism vitamin and pigment	0.5	0.08977044469
AT5G04900.1	NOL-like (NYC1-like, SDR-like)	metabolism vitamin and pigment	0.360160674573	0.52784394172
AT3G44880.1	PAO (ACD1)	metabolism vitamin and pigment	2.368700936405	6.15183587969
AT2G26540.1	UROS	metabolism vitamin and pigment	0,00	1,00
AT2G40490.1	DCUP	metabolism vitamin and pigment	0,00	1,00
AT1G03475.1	HEM6	metabolism vitamin and pigment	0,00	1,00
AT5G14220.1	PPO2 (PPOX, HEMG2/MEE61)	metabolism vitamin and pigment	2.844769444279	2.49188191698
AT4G01690.1	PPOC (PPOX)	metabolism vitamin and pigment	3.895827574004	1.19372518867
AT5G19220.1	ADG2 (APL1)	metabolism carbon Starch biosynthesis	0,00	1,00
AT5G48300.1	APS1 (ADG1, GLGS)	metabolism carbon	0.166666666666	0.48959455631
AT1G32900.1	GBSS-I	metabolism starch	0,00	1,00
AT4G18240.1	SS4 (SSY4)	starch biosynthesis	-0.11111111111	0.48959455631
AT5G24300.2	SSY1 (SS1	starch biosynthesis	-0.56499583341	0.10006772306
AT1G11720.2	SSY3	starch biosynthesis	0,00	1,00
AT4G29130.1	HXK1	metabolism carbon	0.333333333333	0.39324311087
AT1G69830.1	AMY3	starch degradation	0.166666666666	0.48959455631
AT4G00490.1	BAM2	metabolism carbon	0,00	1,00
AT2G32290.1	BAM6	metabolism carbon	0,00	1,00
AT3G52180.1	DSP4 (PTPKIS1, SEX4)	starch degradation	-0.03249791670	1,00
AT3G01510.1	LSF1	metabolism starch	0,00	1,00
AT3G29320.1	PHO1	metabolism carbon	0,00	1,00
AT1G10760.1	GWD1	metabolism carbon	0,00	1,00
AT5G26570.1	PWD	metabolism starch	0,00	1,00
AT5G47260.1	DRL38	stress biotic	-0.19916458337	0.48959455631

Accession	Protein name (this work)	Curated function (this work)	LogFC	Adj.pvalue
AT3G50480.1	HR4	stress biotic	0.666666666666	0.01996908054
AT4G16890.1	nd	nd	0,00	1,00
AT2G34930.1	LRR-like	stress ?	0.166666666666	0.39324311087
AT1G63360.1	nd	nd	-0.11111111111	0.39324311087
AT1G58410.1	nd	nd	0,00	1,00
AT3G25010.1	RLP41	unknown	0.5	0.33305884105
AT3G09440.2	HSP70-3	chaperone and protease	0,00	1,00
AT2G29970.1	nd	nd	0,00	1,00
AT1G29395.1	CRIM1 (COR413IM1, COR413TM1	stress cold	0.512759306612	0.24291854354
AT4G15430.2	ERD-like	stress drought ?	0.166666666666	0.39324311087
AT3G01100.1	HYP1	unknown	0.166666666666	0.39324311087
AT1G76180.2	ERD14	stress dehydration	0,00	1,00
AT5G20630.1	GER3 (GLP2)	unknown	0,00	1,00
AT4G18810.1	Ycf39-like (Tic62-like) UOS1-like	protein targeting tic ? Stress ?	0.166666666666	0.48959455631
AT5G08740.1	NDC1 (DhnA-like)	redox ? metabolism nucleotide ?	2.747212771260	6.09008492085
AT5G65840.1	PRX-like2	redox	0.666666666666	0.01996908054
AT4G03520.1	AtTrxm2	redox	0.930827083453	0.00271659414
AT1G76080.1	CDSP32	redox	0,00	1,00
AT3G06730.1	CITRX (TRXP)	redox	-1.35494346910	5.57861504486
AT2G41680.1	NTR3	redox	0,00	1,00
AT2G32920.1	PDIL2-3	redox	0,00	1,00
AT5G51010.1	Rub-like	redox	0.066181095582	1
AT4G29670.1	TRL22 (ACHT2)	redox	0,00	1,00
AT1G52990.1	TRX-like	redox	0.333333333333	0.39324311087
AT1G03680.1	TRXM1 (ATHM1)	redox	0.634168749959	0.01950362271
AT3G15360.1	TRXM4 (ATHM4)	redox	1.041938194564	1.02722991694
AT4G35000.1	APX3	stress oxidative or redox ?	1.670615278934	2.19972201178
AT5G16710.1	DHAR-2 (DHAR3)	redox	0.166666666666	0.48959455631
AT1G63940.1	MDAR	redox	0,00	1,00
AT1G77490.1	TAPX	stress oxidative	1.187880458136	0.00016188147
AT2G25080.1	GPX2 (GPX1, PHGPx)	stress oxidative	0.398329166746	0.43751657406
AT4G23100.1	GSH1	unknown	0,00	1,00
AT5G20140.1	HP43	unknown	2.414551424012	7.55379674954
AT3G10130.1	nd	unknown	0,00	1,00
AT4G28730.1	GRXC5	redox ?	0,00	1,00
AT5G03880.1	TRX-like	redox ?	3.687814810470	4.32356657897
AT4G10000.1	TRX-like	redox ?	3.052717698814	4.76723188232
AT5G06290.1	BAS1B (PrxB, 2CPB)	redox	1.047733301505	9.35556529925
AT3G54900.1	GRS14 (CAXIP1)	redox	0.166666666666	0.48959455631
AT3G11630.1	PrxB (BAS1, PrxA)	redox	2.378377984298	8.20398994913
AT3G52960.1	PrxII E	redox	1.090369077103	0.04360575583
AT3G26060.1	PRXQ	redox	0.645015449371	0.05010555420
AT1G20620.5	CATA3 (CAT3, SEN2)	stress oxidative	-1.18296650197	0.02073934814
AT2G28190.1	CSD2 (SODCP, Cu,Zn-SOD)	stress oxidative	0.887329938610	0.03066878005

Accession	Protein name (this work)	Curated function (this work)	LogFC	Adj.pvalue
AT5G51100.1	FSD2 (APG8)	stress oxidative	-0.94707604180	0.00422114289
AT5G23310.1	FSD3	stress oxidative	-0.45388472230	0.15702372625
AT3G20330.1	PYRB	metabolism nucleotide	0,00	1,00
AT4G34740.1	ASE2	metabolism nucleotide	0,00	1,00
AT3G57610.1	PURA	metabolism nucleotide	0,00	1,00
AT4G18440.1	nd	metabolism nucleotide	0,00	1,00
AT2G35040.2	nd	metabolism nucleotide	0,00	1,00
AT1G32380.1	PRS2 (KPRS2)	metabolism nucleotide	-0.38888888888	0.14447729974
AT2G44530.2	PRS5 (KPRS5)	metabolism nucleotide	-1.09068506962	0.00023257488
AT5G63420.1	EMB2746	metabolism nucleotide	-2.28690410465	3.34697210197
AT3G17810.1	nd	metabolism nucleotide	0,00	1,00
AT1G27450.1	APT1	metabolism nucleotide	0,00	1,00
AT5G35170.1	AK	metabolism nucleotide	1.926497886910	0.00012602742
AT5G47840.1	KAD2	metabolism nucleotide	0,00	1,00
AT5G63310.1	NDPK2	metabolism nucleotide	0,00	1,00
AT1G15690.2	AVP1 (AVP-3)	transporter ATPase	0.333333333333	0.24291854354
AT5G09650.1	PPA	metabolism Pi	0,00	1,00
AT4G20960.1	RIBD	unknown	0,00	1,00
AT3G46940.1	DUT1	metabolism nucleotide UMP	0.333333333333	0.34526636549
AT4G37930.1	GLYM1	unknown	0,00	1,00
AT5G10610.1	CYP81K1	redox	0.5	0.33305884105
AT3G32047.1	nd	nd	0.166666666666	0.39324311087
AT3G26300.1	nd	nd	0,00	1,00
AT5G38450.1	nd	nd	-0.05555555555	0.39324311087
AT1G31800.1	P450 CYP97A3 (LUT5)	cytochrome P450	1.673787145998	4.93073068874
AT4G15110.1	P450 CYP97B3	cytochrome P450	1.866727175067	1.65314204122
AT4G32320.1	APX6	stress oxidative or redox	0.333333333333	0.24291854354
AT5G44020.1	HAD-like	phosphatase	-0.82823682639	0.03088567114
AT3G16390.1	NSP3	stress biotic nitrile formation	0.333333333333	0.24291854354
AT3G61760.1	DRP1B (ADL1B)	trafficking	-0.22222222222	0.33640002988
AT1G10290.1	DRP2A (ADL6)	trafficking	0,00	1,00
AT1G03160.1	FZL (FZO-like)	unknown	3.677104863382	3.23177894678
AT1G48010.1	nd	nd	0,00	1,00
AT4G33330.2	GUX2 (PGSIP3)	cell wall biogenesis	-0.05555555555	0.48959455631
AT2G31990.1	HP55	unknown	0.333333333333	0.24291854354
AT3G02100.1	UGT83A1 (U83A1)	unknown	0.5	0.08977044469
AT2G10940.1	LTP-like	unknown	-0.16666666666	0.48959455631
AT2G45180.1	nd	unknown	0,00	1,00
AT4G23420.1	nd	nd	0.166666666666	0.39324311087
AT5G10050.1	nd	nd	0.166666666666	0.39324311087
AT3G08920.1	HP25d-like	unknown	2.948223847329	9.67446860712
AT5G19370.1	STR12	unknown	0,00	1,00
AT4G27700.1	Str14 (HP25d)	unknown	2.388584407063	0.00028909346
AT4G01050.1	STR4 (TROL)	chaperone and protease ?	0.549621497817	0.04417010423

Accession	Protein name (this work)	Curated function (this work)	LogFC	Adj.pvalue
AT3G25480.1	STR4A	unknown	1.849765870581	2.26397598316
AT2G42220.1	STR9 (AtStr9)	chaperone and protease ?	2.057710616742	2.89994524658
AT1G24040.2	nd	unknown	0,00	1,00
AT3G14210.1	ESM1	metabolism lipid	-0.29573890968	0.48959455631
AT1G29670.1	nd	unknown	0,00	1,00
AT1G28610.2	nd	unknown	0.166666666666	0.39324311087
AT5G23240.1	DjC86 (DNAJ-like)	chaperone and protease	1.573369291854	0.00051013054
AT2G42750.1	DNAJ-like	chaperone and protease	1.123169521824	0.00010505108
AT2G26890.1	GRV2 (GFS2, KAM2)	chaperone and protease	-0.05555555555	0.39324311087
AT1G08640.1	CJD1	chaperone and protease	1.698108766662	0.00028783864
AT4G39960.1	DjA5 (HSP40/DNAJ-like)	chaperone and protease	-0.94910603654	0.03130635433
AT2G22360.1	DjA6 (DNAJ-like)	chaperone and protease	-0.35638167785	0.24368166033
AT1G80030.3	DNAJ	chaperone and protease	0.105104831673	1,00
AT5G06130.1	DNAJ-like	chaperone and protease ?	1.605475982923	5.86359413437
AT2G34860.1	EDA3	chaperone and protease	1,00	4.06321633668
AT3G45050.4	HP16c	unknown	0.930827083453	0.00271659414
AT1G75690.1	LQY1	PS PSII ? Or stress light	0.930827083453	0.00271659414
AT5G61670.1	Or-like	chaperone and protease	0.571215168295	0.10091627153
AT4G13670.1	PTAC5	unknown	1.025076409647	0.00239828388
AT1G71500.1	PSBS-like	redox ? PSII ? NPQ ?	2.014952073021	8.43049824879
AT1G51110.1	FIB10 (FBN10, PAP)	PAP_fibrillin	3.407946169552	4.61686496723
AT4G00030.1	FIB11 (PAP11)	PAP_fibrillin	0.333333333333	0.24291854354
AT4G04020.1	FIB1a (FBN1a, PAP)	PAP_fibrillin	2.963577986229	7.02707329141
AT4G22240.1	FIB1b (FBN1b, PAP2)	PAP_fibrillin	2.104757869535	8.33878832444
AT2G35490.1	FIB2 (FBN2, PAP3)	PAP_fibrillin	2.555222781336	6.44803452721
AT3G26070.1	FIB3a (FBN3a, PAP)	PAP_fibrillin	1.590745144595	0.00015218947
AT3G26080.1	FIB3b (FBN3b, PAP)	PAP_fibrillin	0.915769449194	0.01669689018
AT3G23400.1	FIB4 (FBN4, PAP)	PAP_fibrillin	3.397583398730	2.86554282400
AT5G19940.1	FIB6 (PAP, HP26d)	PAP_fibrillin	2.922628046168	1.46036786833
AT3G58010.1	FIB7a (FBN7a, PAP)	PAP_fibrillin	1.763310453631	0.00020764606
AT2G42130.3	FIB7b (FBN7b)	PAP_fibrillin	2.296057218077	3.07330511235
AT2G42130.4	FIB7b (FBN7b)	PAP_fibrillin	1.480825246355	0.02935288468
AT2G46910.1	FIB8 (FBN8 or PAP10)	PAP_fibrillin	1.823698228935	9.90380556515
AT1G78915.2	TPR-like	RNA Binding ?	0.5	0.08977044469
AT3G57090.1	FIS1A (BGY1, TPR-like)	RNA binding ?	0.166666666666	0.48959455631
AT3G18420.1	HP35c (TPR-like)	RNA binding ?	0.833333333333	0.00127483930
AT3G17970.1	Toc64-III (HP64b)	protein targeting Toc	0.345805158439	0.41200273091
AT5G48390.1	ZIP4-like (TPR-like)	RNA Binding ?	0	1
AT4G31390.1	ABC1K1	kinase	3.734380684737	1.48970605035
AT1G79600.1	ABC1K3	kinase	4.165168202853	5.33616249048
AT1G71810.1	ABC1K5	kinase	2.312568471357	1.05926672598
AT3G24190.1	ABC1K6	kinase	2.456207615003	2.33395215485
AT5G05200.1	ABC1K9	kinase	2.091068385001	5.17310384768
AT4G24810.3	ABC1-like	kinase	0.166666666666	0.48959455631

Accession	Protein name (this work)	Curated function (this work)	LogFC	Adj.pvalue
AT5G64940.1	ATH13 (ABC1K8, OSA1)	transporter ABC ?	1.081093445211	0.03086277347
AT3G07700.3	MLP3.15	kinase	0.854347655633	0.02792654564
AT4G13010.1	ceQORH (IE41)	redox ?	1.179971711869	0.00367674517
AT2G35660.1	CTF2A	unknown	1.529700626712	3.33624949774
AT1G15140.1	FAD_FR-like	redox	0.666666666666	0.01996908054
AT5G37980.1	nd	nd	-0.11111111111	0.39324311087
AT5G05320.1	nd	unknown	0,00	1,00
AT1G23740.1	QORL	redox ?	0,00	1,00
AT2G34810.1	BBE-like	redox ?	0.5	0.08977044469
AT5G44000.1	GST-like	stress oxidative	0.333333333333	0.24291854354
AT1G09340.1	CRB (RAP38, CSP41B)	RNA Binding	-0.52486737476	0.20243491013
AT3G17040.2	HCF107 (TPR-like)	PS PSII and b6f biogenesis RNA Binding	0.333333333333	0.34526636549
AT3G20390.1	nd	RNA metabolism?	0,00	1,00
AT2G04270.3	nd	nd	-0.19916458337	0.39324311087
AT5G53770.1	NTP_transf-like	RNA Binding ?	0,00	1,00
AT3G09650.1	TPR-like	RNA Binding ?	-0.11111111111	0.39324311087
AT3G18390.1	CRS1/YhbY-like (EMB1865)	RNA Binding ?	-0.19916458337	0.39324311087
AT1G11520.1	HP22c	unknown	0.111111111111	0.62418415731
AT3G03710.1	PNP1	unknown	0,00	1,00
AT4G37510.1	RNaseIII-like	RNA Binding	-0.25472013892	0.39324311087
AT1G11430.1	MORF9	RNA editing	-0.31027569448	0.27341583319
AT3G15000.1	nd	nd	-0.11111111111	0.39324311087
AT4G24770.1	CP31	RNA Binding	0,00	1,00
AT2G02980.1	PPR-like	nd	-0.16666666666	0.39324311087
AT1G06190.2	RHON1	RNA Binding	-1.79714697457	0.00121504421
ATCG00740.1	RPOA	transcription chloroplast	-1.58892443508	0.00035193653
ATCG00190.1	RPOB	transcription chloroplast	-2.30537869544	9.97589457520
ATCG00180.1	RPOC1	transcription chloroplast	-2.20070917071	3.26190694588
ATCG00170.1	RPOC2	transcription chloroplast	-1.54455038587	4.67062033097
AT5G15700.1	RPOT2	DNA Binding	0.833333333333	0.00127483930
AT5G20220.1	HP44	transcription ?	-0.36583125004	0.16779605782
AT3G46090.1	nd	nd	0.166666666666	0.39324311087
AT1G11490.1	nd	nd	-0.05555555555	0.39324311087
AT1G10480.1	ZP5 (ZFP5)	signaling gibberellic acid pathway	-0.38888888888	0.39324311087
AT5G17490.1	nd	nd	0	1
AT3G13840.1	SCL29	unknown	0,00	1,00
AT4G00730.1	ANL2	transcription	0.611111111111	0.03536276794
AT1G28420.1	nd	unknown	0,00	1,00
AT1G12800.1	OB-fold-like	RNA Binding ?	-0.16666666666	0.48959455631
AT3G05380.1	nd	nd	-0.05555555555	0.39324311087
AT5G10280.1	nd	nd	0.166666666666	0.39324311087
AT4G09450.1	HP23c	DNA Binding ?	0.333333333333	0.39324311087
AT3G11280.1	nd	nd	0.166666666666	0.39324311087
AT3G56390.1	nd	unknown	0.166666666666	0.39324311087

Accession	Protein name (this work)	Curated function (this work)	LogFC	Adj.pvalue
AT1G48410.2	nd	nd	0	1
AT1G48310.1	CHR18	RNA transcription ?	0.666666666666	0.01996908054
AT2G40770.1	nd	nd	0.166666666666	0.39324311087
AT5G09380.1	nd	nd	0.166666666666	0.39324311087
AT4G38070.1	BH131 (bHLH131)	transcription	0,00	1,00
AT2G14760.1	nd	nd	0.166666666666	0.39324311087
AT4G36540.1	nd	nd	0.166666666666	0.39324311087
AT5G08630.1	nd	nd	0.166666666666	0.39324311087
AT4G14920.1	RING-like	RNA Binding ?	0.5	0.08977044469
AT1G10200.1	nd	unknown	0,00	1,00
AT4G17950.1	nd	nd	0.166666666666	0.39324311087
AT1G13790.1	nd	nd	0.166666666666	0.39324311087
AT1G56110.1	NOP56-like	DNA Binding ?	0.333333333333	0.24291854354
AT1G14410.1	WHY1 (PTAC1)	DNA Binding	-1.90068582046	2.00463135112
AT3G07670.1	MLP3.12	protein modification PS RBCS	0,00	1,00
AT5G14260.1	nd	unknown	0,00	1,00
AT2G18850.1	nd	unknown	0,00	1,00
AT5G24330.1	nd	nd	0.166666666666	0.39324311087
AT5G07350.1	nd	nd	0.166666666666	0.39324311087
AT4G39260.1	RBG8	RNA Binding	0,00	1,00
AT1G64620.1	nd	nd	0.166666666666	0.39324311087
AT2G02740.2	WHY3 (PTAC11)	DNA Binding	-2.29313164264	1.47618801324
AT1G62150.1	HP52d	transcription ?	-0.05555555555	0.48959455631
AT3G54400.1	nd	DNA binding ?	0,00	1,00
AT5G07900.1	nd	nd	-0.19916458337	0.39324311087
AT2G37670.1	nd	nd	-0.19916458337	0.39324311087
AT5G54180.1	PTAC15	transcription ?	-0.05555555555	0.48959455631
AT3G63140.1	RAP41 (CSP41A)	RNA Binding	-0.96623800493	0.00995032650
AT3G08010.1	ATAB2	RNA binding ?	0.950892901338	0.02489050859
AT3G53460.4	CP29	RNA Binding	0,00	1,00
AT2G37220.1	CP29 (ROC1, CP29 B')	RNA Binding	0.333333333333	0.39904228713
AT4G39040.1	CRS1/YhbY-like	RNA Binding ?	-0.11111111111	0.48959455631
AT2G21660.1	GRP7	RNA Binding	0,00	1,00
AT1G01080.1	HP32d	RNA binding ?	-0.45876946842	0.12439838274
AT2G35410.1	HP33	RNA binding ?	0.170002050492	0.55320526630
AT4G09040.2	HP34	RNA binding ?	0.020389428220	1,00
AT3G10845.1	nd	RNA binding ?	0,00	1,00
AT4G01037.1	nd	nd	-0.11111111111	0.39324311087
AT4G16390.1	P67 (PPR-like)	RNA binding ?	-0.06509381610	1,00
AT5G08610.1	nd	RNA Binding ?	-0.05555555555	0.39324311087
AT5G26742.2	RH3 (EMB1138)	RNA Binding ?	-1.05538479312	0.00449580170
AT4G34830.1	MRL1 (PP349, PPR-like)	RNA binding RBCL transcript	-1.28699119154	0.00158085767
AT1G02150.1	nd	unknown	0,00	1,00
AT5G46580.1	P67.1-like (PPR-like)	RNA Binding ?	-1.53877506574	0.00014364733

Accession	Protein name (this work)	Curated function (this work)	LogFC	Adj.pvalue
AT2G37230.1	PP190 (TPR-like)	RNA Binding ?	0.5	0.08977044469
AT3G04760.1	PP213 (PPR-like)	RNA Binding ?	-1.03512951406	0.00214929779
AT3G29230.1	PP261 (PCMP-E27)	RNA Binding ?	-0.05555555555	0.48959455631
AT3G53700.1	PP281 (MEE40, PPR-like)	RNA Binding ?	-0.58805347226	0.04491796071
AT5G04810.1	PP365 (PPR4, PPR-like)	RNA Binding ?	-0.05555555555	0.48959455631
AT5G14080.1	PP380 (TPR-like)	RNA Binding ?	-0.39832916674	0.35407973350
AT5G42310.1	PPR-like	RNA Binding ?	-0.16666666666	0.39324311087
AT1G74850.1	PTAC2 (PPR-like)	RNA binding ?	-2.05837320476	2.08526784329
AT5G53490.3	TL17 (P17.4, PPR)	RNA Binding ?	1.567523660229	7.81016310089
AT1G12250.2	TL225 (PPR)	RNA Binding ?	-0.01192205869	1,00
AT2G44920.2	TPR-like	RNA Binding ?	0.423520572180	0.25940759006
AT5G04130.1	GYRB2 (GYRBM)	DNA Binding	-1.73016790541	2.36801513043
AT3G47490.1	nd	DNA binding ?	-0.16666666666	0.39324311087
AT5G67100.1	POLA	DNA Binding	1.767987837714	7.11783239129
AT1G60930.1	RQL4B (RECQL4B, RECQ4B)	DNA Binding	0.222222222222	0.53335688012
AT1G03750.1	SWI2 (SWITCH 2)	DNA Binding ?	-0.03249791670	1
AT5G27670.1	H2A5	DNA binding	0,00	1,00
AT5G59870.1	H2A7	DNA binding	0,00	1,00
AT1G08880.1	H2AXA	DNA binding	0,00	1,00
AT3G53650.1	H2B8	DNA binding	0,00	1,00
AT1G07820.2	H4	DNA synthesis/chromatin structure	-0.16666666666	0.48959455631
AT4G31210.1	nd	nd	-0.11111111111	0.39324311087
AT3G10690.1	GYRA (GYRBM)	DNA Binding	-2.80989787275	1.15294688230
AT1G63680.1	MURE	unknown	-2.12480955355	1.91916801528
AT3G16000.1	MFP1	DNA Binding	-0.56096295448	0.28951817356
AT3G48500.2	PTAC10 (PDE312)	DNA Binding ?	-0.96332500016	0.00139648861
AT2G34640.1	PTAC12 (HEMERA)	DNA Binding ?	-1.76799785583	1.22201564829
AT3G09210.1	PTAC13	DNA Binding ?	-0.50944027785	0.34311785110
AT4G20130.1	PTAC14	DNA Binding ?	-2.04893651468	2.53822389701
AT3G46780.1	PTAC16 (Ycf39-like, Tic62-like)	protein targeting Tic ?	-0.33845304215	0.00246974201
AT1G80480.1	PTAC17	DNA Binding ?	0.166666666666	0.48959455631
AT3G04260.1	PTAC3	DNA Binding ?	-3.07768784500	5.34800819389
AT1G21600.2	PTAC6	DNA Binding ?	-0.46240557635	0.23588258810
AT3G26580.1	TPR-like	RNA Binding ?	0.333333333333	0.39324311087
AT5G35970.1	HP105	DNA Binding ?	-1.11842361538	0.01208815499
AT1G06670.1	NIH	DNA Binding ?	-0.16666666666	0.48959455631
AT5G07710.1	RNAse-like	RNA Binding ?	0.166666666666	0.39324311087
AT2G06500.1	transposase-like	DNA Binding ?	0.5	0.33305884105
AT2G25840.2	OVA4	unknown	0,00	1,00
AT3G02660.1	nd	unknown	0,00	1,00
AT5G27470.1	SYS (SerRS)	protein modification	0.023057638848	1,00
AT3G48110.1	GlyRS2 (EDD1, SYGM2)	translation stroma	0.166666666666	0.48959455631
AT3G58140.1	nd	translation stroma	0,00	1,00
AT2G04842.1	nd	unknown	0,00	1,00

Accession	Protein name (this work)	Curated function (this work)	LogFC	Adj.pvalue
AT5G52520.1	OVA6	unknown	0,00	1,00
AT3G25660.1	GATA	unknown	0,00	1,00
AT5G22800.1	nd	translation stroma	0,00	1,00
AT4G25130.1	MSRA (PMSR4)	protein modification stress oxidative	0,00	1,00
AT3G52150.2	PSRP-2 (CP33-like)	translation stroma ?	0.647320271411	0.15204260692
ATCG00750.1	RPS11	translation stroma	0.918311426915	0.00053819944
ATCG01230.1	RPS12B	translation stroma	0.764160416786	0.02792654564
ATCG01120.1	RPS15	translation stroma	1.982751549551	5.51583985633
ATCG00650.1	RPS18	translation stroma	0.666666666666	0.00642703087
ATCG00820.1	RPS19	translation stroma	0.666666666666	0.01996908054
ATCG00160.1	RPS2	translation stroma	0.171153545497	0.90475525496
ATCG00800.1	RPS3	translation stroma	-0.01513879414	1,00
ATCG00380.1	RPS4	translation stroma	0.153631109406	0.61046662519
ATCG01240.1	RPS7.2	translation stroma	0.423754259018	0.30365919400
ATCG00770.1	RPS8	translation stroma	1.532893524957	6.95635720589
AT3G13120.1	RPS10	translation stroma	0.322937018401	0.39244655417
AT5G14320.1	RPS13 (EMB3137)	translation stroma	0.616146962708	0.14420877169
ATCG00330.1	RPS14	translation stroma	0.976084306772	0.01170416295
AT1G79850.1	RPS17 (PDE347)	translation stroma	0.205169014262	0.52379332293
AT3G15190.1	RPS20	translation stroma	0.256567406126	0.16425623197
AT2G38140.1	RPS31	translation stroma	0	1
AT2G33800.1	RPS5 (EMB3113)	translation stroma	-0.05142644910	1,00
AT5G24490.1	RPS30 (PSRP- 1, CS-S5, CS5, S22)	translation stroma	0.922572067764	0.00249966943
AT1G64510.1	RPS6 (RR6)	translation stroma	0.591372501016	0.16619329784
AT1G68590.1	PSRP-3-1 (PSRP-3A)	translation stroma	1.352788705355	9.01338868514
AT1G74970.1	RPS9 (TWN3)	translation stroma	0.769985039934	0.04572242107
ATCG00780.1	RPL14	translation stroma	1.021342102005	0.00507190215
ATCG00790.1	RPL16	translation stroma	1.204945416830	0.00472236468
ATCG00660.1	RPL20	translation stroma	1.646276459734	1.25950273487
ATCG00810.1	RPL22 50S	translation stroma	0.547765400784	0.29947070238
ATCG00840.1	RPL23.1	translation stroma ?	0.166666666666	0.48959455631
ATCG01020.1	RPL32	translation stroma	0.666666666666	0.11956915329
ATCG00640.1	RPL33	translation stroma	0.833333333333	0.01646410823
AT2G24090.1	RPL35	translation stroma	1.117559568005	0.00271659414
ATCG00760.1	RPL36	translation stroma	0.875271527897	0.00493670581
AT3G63490.1	RPL1 (EMB3126)	translation stroma	0.774833659172	0.05196714223
AT5G13510.1	RPL10 (EMB3136)	translation stroma	0.712983779563	0.04770310084
AT1G32990.1	PRPL11	translation stroma	0.671274519542	0.04765739980
AT3G27850.1	RPL12-C	translation stroma	0.442279230373	0.05482354165
AT1G78630.1	RPL13 (EMB1473)	translation stroma	0.842578917605	0.02779867153
AT3G25920.1	RPL15	translation stroma	0.985648012079	0.01996908054
AT3G54210.1	RPL17	translation stroma	1.405773595582	0.00127483930
AT1G48350.1	RPL18 (EMB3105)	translation stroma	-0.02882547423	1,00
AT4G17560.1	RPL19-1	translation stroma	1.285981743876	0.00170843462

Accession	Protein name (this work)	Curated function (this work)	LogFC	Adj.pvalue
AT5G47190.1	RPL19-2	translation stroma	1.228454169717	0.00171601321
AT1G35680.1	RPL21	translation stroma	0.728565662280	0.01053207561
AT5G54600.1	RPL24	translation stroma	0.085005427516	0.92115013925
AT5G40950.1	RPL27	translation stroma	0.690253570483	0.01439839128
AT2G33450.1	RPL28	translation stroma	0.755905401098	0.02704784438
ATCG00830.1	RPL2.1	translation stroma	1.093888874063	0.00397317383
AT5G65220.1	RPL29	translation stroma	0.161844764025	0.55320526630
AT2G43030.1	RPL3A	translation stroma	0.851043143198	0.10457623757
AT1G75350.1	RPL31 (EMB2184)	translation stroma	1.716863445592	1.91708518078
AT1G07320.1	RPL4	translation stroma	0.844824176916	0.17964593714
AT4G01310.1	RPL15	translation stroma	0.186350971098	0.64156088403
AT1G05190.1	RPL6 (EMB2394)	translation stroma	1.259134004616	0.00196111662
AT3G56910.1	PSRP5 (PsCL18)	translation stroma	1.251001060099	0.00208837830
AT3G44890.1	RPL9	translation stroma	0.859605791116	0.02367205192
AT5G30510.1	RPS1	translation stroma	-0.04602438453	1,00
AT1G71720.1	RPS1-like (PDE338)	translation stroma ?	-0.36583125004	0.24578680430
AT4G34620.1	RPS16 (SSR16)	translation stroma	0.800287715179	0.03203137445
AT3G27160.1	RPS21	translation stroma	0.770097578395	0.33814674370
AT2G36160.1	RPS14A	translation cytosol	0.444444444444	0.22515577914
AT2G31610.1	RPS3A	translation cytosol	0,00	1,00
AT1G72370.2	RSSA1 (p40, RPSaA)	translation cytosol	0.333333333333	0.39324311087
AT1G06380.1	RPL10a-like	translation stroma ?	1.260213873933	0.00028552941
AT3G53430.1	RPL12B (ABIP11, RL122)	translation cytosol	0.166666666666	0.48959455631
AT2G18020.1	RPL8A (RPL2, RL81)	translation cytosol	0.166666666666	0.39324311087
AT1G16790.1	RR8-like	translation stroma	0.333333333333	0.24291854354
AT1G17220.1	IF2	translation stroma	-0.63759571977	0.23588258810
AT2G24060.1	IF3	translation stroma	0,00	1,00
AT4G30690.1	IF3	translation stroma	-0.08805347226	1,00
AT1G26630.2	IF5A2	translation	0,00	1,00
AT2G18720.1	nd	translation	-0.16666666666	0.39324311087
AT3G13920.3	IF4A1	translation cytosol	0,00	1,00
AT1G07940.2	eEF-1A1 (EF-1-alpha 1)	translation cytosol	-0.57574628392	0.23588258810
AT4G20360.1	EFTU (EF-Tu-1, TUFA, RABE1b)	translation stroma / signalling / SNARE effector	0.207228053840	0.49872789307
AT1G62750.1	EF-Tu-G (EF-G, SCO1)	translation stroma	0.333333333333	0.24291854354
AT5G08650.1	GUFP (GUF1, EF-4)	translation stroma	-0.05555555555	0.48959455631
AT1G56070.1	nd	translation cytosol	0,00	1,00
AT3G08740.1	nd	translation stroma	0,00	1,00
AT4G29060.1	PSRP-7 (EF-Ts-like)	translation stroma	-0.86846284740	0.02332789672
AT5G13650.2	SVR3	translation stroma	0,00	1,00
AT5G36170.2	HCF109	unknown	0,00	1,00
AT3G62910.1	nd	unknown	0,00	1,00
AT5G66470.1	ERA-like	translation stroma ?	-0.16666666666	0.48959455631
AT3G12080.2	nd	unknown	0,00	1,00
AT2G19870.1	nd	unknown	-0.11111111111	0.39324311087

Accession	Protein name (this work)	Curated function (this work)	LogFC	Adj.pvalue
AT3G63190.1	RRFC (RRFHCP)	translation stroma	0,00	1,00
AT1G16720.1	HCF173	chaperone and protease or translation PSII ?	0.212407212477	0.31944346866
AT1G71480.1	NTF2-like	transporter ?	1.309902006375	1.03626170721
AT3G16480.1	MPPA2	chaperone and protease	0.5	0.33305884105
AT2G28800.1	ALB3	protein targeting	1.508253274326	0.00199349880
AT2G45770.1	cpFtsY	protein targeting	0.333333333333	0.24291854354
AT2G18710.1	cpSECY (SCY1)	protein targeting	2.362155274812	2.01803175592
AT5G03940.1	cpSRP54	protein targeting	1.707900718587	0.00127483930
AT5G52440.1	HCF106 (TatB)	protein targeting	0.861061270285	0.04814184174
AT5G12130.1	PDE149	unknown	0.833333333333	0.00127483930
AT4G01800.1	SECA1 (cpSecA, AGY1)	protein targeting	1.766787709618	0.00021203173
AT4G14870.1	SECE1	protein targeting thylakoid	0.764160416786	0.02792654564
AT2G01110.1	TATC	protein targeting Tic	0.422572067764	0.25940759006
AT2G20890.1	THF1 (TF1, PSB29)	vesicle formation	1.270607910817	0.01349850933
AT1G06950.1	TIC110 (HP112)	protein targeting Tic	1.883376760204	0.00036571939
AT2G47840.1	Tic20-II	protein targeting Tic ?	2.482734536985	1.51499853880
AT4G33350.1	Tic22 (HP27)	protein targeting Tic	0,00	1,00
AT5G16620.1	Tic40 (PDE120)	protein targeting Tic	2.816465029993	4.99080017229
AT2G24820.1	Tic55-II	protein targeting Tic	2.847419856444	5.11914647382
AT4G25650.1	Tic55-like (HP62, ACD1-Like)	protein targeting Tic ?	1.774017112947	2.87736032259
AT3G18890.1	Tic62 (UOS1-like)	protein targeting Tic	0.314658591433	0.22927504632
AT4G02510.1	Toc159 (OEP86)	protein targeting Toc	1.533529019870	0.00223620405
AT1G02280.2	Toc33 (HP32b)	protein targeting Toc	1.180090267548	0.05559886297
AT5G05000.1	Toc34 (OEP34)	protein targeting Toc	1.628324676707	0.00215703757
AT3G46740.1	Toc75-III (OEP75-3)	protein targeting Toc	1.120306939104	0.01175174866
AT5G19620.1	Toc75-V (OEP85, OEP80, IAP75)	protein targeting Toc	1.478885478885	0.01053396376
AT1G65260.1	Vipp1 (IM30, PspA, HCF155, PTAC	vesicle formation	-1.10577235591	0.00018332984
AT4G24840.1	nd	unknown	0,00	1,00
AT4G32640.2	SC24B	protein transport ?	0.166666666666	0.39324311087
AT5G14660.2	DEF1B	unknown	0,00	1,00
AT2G32850.2	Kinase-like	kinase	0.5	0.33305884105
AT2G34290.1	Kinase-like	kinase	0,00	1,00
AT4G29590.1	nd	unknown	0,00	1,00
AT5G46570.1	nd	nd	0	1
AT3G63340.1	nd	phosphatase	0,00	1,00
AT5G58140.3	PHOT2	signalling ?	0.166666666666	0.39324311087
AT5G20930.1	TOUSLED (TSL)	kinase	-0.42138680559	0.39324311087
AT3G54090.1	FLN1	Kinase	-2.52624503803	9.32386301805
AT1G69200.1	FLN2	kinase	-2.11492819055	8.77378699872
AT3G61080.1	nd	kinase	0,00	1,00
AT4G32250.2	nd	kinase	0.166666666666	0.39324311087
AT4G11890.2	Kinase-like	kinase	0.166666666666	0.39324311087
AT3G07070.1	PBS1-like	kinase	0.333333333333	0.24291854354
AT4G33500.1	PP2C62	phosphatase	0,00	1,00

Accession	Protein name (this work)	Curated function (this work)	LogFC	Adj.pvalue
AT1G14270.4	CAAX-like	chaperone and protease	0.333333333333	0.24291854354
AT4G30920.1	LAP3	chaperone and protease	0,00	1,00
AT3G02090.2	MPPB	chaperone and protease	0.666666666666	0.01996908054
AT1G06900.1	nd	protein degradation proteasome ?	0	1
AT1G73990.1	SPPA1	chaperone and protease	2.316020186074	0.00030873432
AT4G20850.1	nd	unknown	0,00	1,00
AT2G47110.2	nd	nd	0.166666666666	0.39324311087
AT2G12550.1	NUB1-like	protein degradation uniquitin	0	1
AT5G64760.2	nd	protein degradation proteasome ?	0	1
AT4G31300.1	PSB6 (PBA1)	protein degradation proteasome ?	0,00	1,00
AT1G22500.1	nd	protein degradation uniquitin E3	0.166666666666	0.39324311087
AT5G40140.1	PUB40	protein degradation uniquitin E3	0	1
AT5G60250.1	RING-like	protein degradation uniquitin E3	0.058173688410	1,00
AT1G78100.1	AUF1	protein degradation uniquitin E3	0.611111111111	0.03536276794
AT4G39590.1	F-Box-like	protein degradation uniquitin E3	0,00	1,00
AT5G57360.1	nd	nd	0.166666666666	0.39324311087
AT3G59250.1	nd	protein degradation uniquitin E3	-0.05555555555	0.39324311087
AT5G03100.1	nd	protein degradation uniquitin E3	0,00	1,00
AT2G24540.1	nd	protein degradation uniquitin E3	-0.16666666666	0.39324311087
AT5G05560.1	APC1 (EMB2771)	protein degradation uniquitin E3	-0.25472013892	0.39324311087
AT5G50920.1	ClpC1 (HSP93-V, Hsp100)	chaperone and protease	0.238014690199	0.38957216399
AT3G48870.1	ClpC2 (Hsp93-III)	chaperone and protease	0.893458948087	0.00475530950
AT5G51070.1	ClpD	chaperone and protease	0,00	1,00
ATCG00670.1	ClpP1	chaperone and protease	0.166666666666	0.48959455631
AT1G66670.1	ClpP3	chaperone and protease	0,00	1,00
AT5G45390.1	ClpP4 (nClpP4)	chaperone and protease	0.789836188490	0.03203137445
AT1G02560.1	ClpP5	chaperone and protease	0,00	1,00
AT1G11750.2	ClpP6	chaperone and protease	0,00	1,00
AT1G49970.1	ClpR1	chaperone and protease	0,00	1,00
AT1G12410.1	ClpR2	chaperone and protease	0,00	1,00
AT1G09130.2	ClpR3	chaperone and protease	0,00	1,00
AT4G17040.1	ClpR4	chaperone and protease	0,00	1,00
AT4G12060.1	ClpT2	chaperone and protease	0,00	1,00
AT3G27925.1	Deg1 (DegP1)	chaperone and protease	1.501753583656	1.80525526940
AT2G47940.1	DEGP2 (HhoA-like, DegQ)	chaperone and protease	0.166666666666	0.48959455631
AT1G65630.1	DEGP3	chaperone and protease	0.333333333333	0.39324311087
AT4G18370.1	DEGP5	chaperone and protease PS PSII	-0.05555555555	0.48959455631
AT5G39830.1	DEGP8	chaperone and protease PS PSII	0,00	1,00
AT2G18080.1	EDA2	chaperone and protease	0.166666666666	0.48959455631
AT2G32480.1	ARASP	chaperone and protease	1.991784583002	4.45934985694
AT5G35220.1	EGY1	chaperone and protease	2.433747456945	9.54387559416
AT5G05740.3	EGY2	chaperone and protease	2.439421797312	1.38007762855
AT3G16290.1	FtsH (EMB2083)	chaperone and protease	0.422572067764	0.25940759006
AT1G50250.1	FtsH1	chaperone and protease	1.406004118176	0.00381289320

Accession	Protein name (this work)	Curated function (this work)	LogFC	Adj.pvalue
AT5G53170.1	FtsH11	chaperone and protease	1.842882251591	5.80713239935
AT1G79560.1	FtsH12 (EMB1047)	chaperone and protease	1.021928170560	0.03518013219
AT2G30950.1	FtsH2 (VAR2)	chaperone and protease	1.670694891994	0.00030802815
AT5G42270.1	FtsH5 (FtsH2, VAR1)	chaperone and protease	1.053535898714	0.01208942379
AT1G06430.1	FtsH8	chaperone and protease	1.935577931956	0.00132175242
AT5G58870.1	FtsH9	chaperone and protease	0,00	1,00
AT4G23940.1	FtsHi1	chaperone and protease	1.677053791695	1.54071348907
AT5G64580.1	FtsH-like	chaperone and protease	0.809852590241	0.03588723627
AT1G13270.1	MAP1B	chaperone and protease ?	0,00	1,00
AT1G05140.1	PDZ-like	chaperone and protease ?	2.010690550585	2.16498577766
AT3G19170.1	PREP1	chaperone and protease	0,00	1,00
AT5G20720.3	CH10C (Cpn21, Cpn20, CH1C)	chaperone and protease	-0.05555555555	0.48959455631
AT5G15450.1	CLPB3 (APG6, CLPB-P)	chaperone and protease	0.277777777777	0.37277282012
AT3G62030.2	CP20C	chaperone and protease	0,00	1,00
AT4G24280.1	cpHsc70-1 (cpHSP70-1)	chaperone and protease	2.359733770847	2.89994524658
AT5G49910.1	cpHSP70-2	chaperone and protease	0,00	1,00
AT2G04030.1	CR88 (HTPG-like)	chaperone and protease	1.562181582026	1.68190065621
AT5G35100.1	CSA_PPIase-like	chaperone and protease	0.930827083453	0.00271659414
AT3G15520.1	CYP37 (PPIase CYP37, TLP38, p38)	chaperone and protease	2.733158430444	2.11201030643
AT1G74070.1	CYP-like	chaperone and protease	0.687680988967	0.10209399591
AT1G20810.1	FKBP18 (PPIase, Rotamase)	chaperone and protease	0.333333333333	0.24291854354
AT5G13410.1	FKBP19	chaperone and protease	0,00	1,00
AT2G43560.1	FKBP2 (PPIase, Rotamase)	chaperone and protease	0.923520572180	0.00251834260
AT3G60370.1	FKBP20-2	chaperone and protease	0,00	1,00
AT3G10060.1	FKBP-like	chaperone and protease	1.544521653086	0.00050375611
AT1G18170.1	FKBP-like	chaperone and protease	1.702797570367	0.00079816725
AT5G17710.1	nd	chaperone and protease	0,00	1,00
AT2G30695.2	nd	unknown	0,00	1,00
AT2G28000.1	RUBA (CPN60A, Cpn60-alpha-1)	chaperone and protease	3.060639107288	2.19972201178
AT1G55490.2	RUBB (CPN60B, Cpn60-beta-2)	chaperone and protease	1.775929043182	7.56443555312
AT3G13470.1	RUBB (Cpn60-beta-1)	chaperone and protease	0,00	1,00
AT5G55220.1	TF (HP65b)	chaperone and protease	0.589238734431	0.10457623757
AT3G01480.1	TLP40 (CYP38)	chaperone and protease	2.949837820521	1.25168910248
AT1G24490.1	ALB4	chloroplast biogenesis	0.5	0.33305884105
AT3G26710.1	CCB1	chaperone and protease PS b6f	1.043191043523	0.00019205194
AT5G36120.1	CCB3	chaperone and protease PS b6f	0.764160416786	0.14210339028
AT1G59840.2	CCB4	chaperone and protease PS b6f	1.829326365477	4.07890813122
AT5G54290.2	CCDA	PS b6f biogenesis	0.666666666666	0.01996908054
AT5G17170.1	ENH1	unknown	-0.43297926691	0.16779605782
AT5G45680.1	FKB13	chaperone and protease	0.333333333333	0.24291854354
AT3G24430.1	HCF101	chaperone and protease ?	0,00	1,00
AT4G37200.1	HCF164 (Trx-like)	redox ?	1.977632223960	9.19084275804
AT5G52110.2	HCF208	unknown	1.021014322300	0.00301776275
AT1G02910.1	LPA1 (TPR-like)	chaperone and protease PSII D1	2.177329933827	1.38007762855

Accession	Protein name (this work)	Curated function (this work)	LogFC	Adj.pvalue
AT4G39710.2	NDHL4 (FKBP16-2, PnsL4)	NDH	1.041972228558	0.00088847779
AT5G23120.1	P2SAF (HCF136)	chaperone and protease ?	3.573565774091	6.81662490401
AT4G19100.1	PAM68	PS PSII biogenesis	0.666666666666	0.11956915329
AT5G13120.2	PNSL5 (PPIase CYP20-2, TLP20)	NDH	1.349563487204	1.75592863108
AT1G22700.3	Pyg7 (YCF37-like, TPR-like)	chaperone and protease ?	1.086273408242	0.00083098408
AT1G54500.1	Rub-like	redox ?	2.830191336390	2.97767900849
AT5G44650.1	Y3IP1 (CEST)	chaperone and protease ?	2.534951948858	9.52726383427
ATCG01130.1	YCF1.2 (YCF1-B)	unknown	0.166666666666	0.63048204867
ATCG01280.1	YCF2	nd	0.166666666666	0.39324311087
ATCG00360.1	YCF3	chaperone and protease	1.330916328676	0.00132699996
ATCG00520.1	YCF4	chaperone and protease	0.704196533463	0.01534204434
AT3G24590.1	PLSP1	chaperone and protease	1.808592767303	7.30442160439
AT4G17740.1	S41	chaperone and protease PSII	0.166666666666	0.48959455631
AT5G46390.2	S41-like	chaperone and protease	0.590187238847	0.10465123788
AT1G56500.1	HP114	unknown	4.083690017582	2.83756531053
AT4G39970.1	nd	unknown	0,00	1,00
AT5G66530.2	APOC-like	metabolism carbon	0,00	1,00
AT2G27680.1	HP43d	redox ?	0.666666666666	0.01996908054
AT1G04420.1	nd	redox ?	0,00	1,00
AT5G53580.1	PLR1	metabolism vitamin and pigment vitamin b6 ?	0.322547898724	0.69602168020
AT5G13000.1	CALS3	unknown	0,00	1,00
AT2G13680.1	nd	nd	-0.16666666666	0.39324311087
AT3G07160.1	nd	nd	-0.19916458337	0.39324311087
AT1G16880.1	nd	metabolism carbon	0,00	1,00
AT2G13440.1	GIDA-like	translation stroma ?	-0.05555555555	0.48959455631
AT4G01900.1	GLNB	unknown	0,00	1,00
AT2G24710.1	GLR2.3	transporter ?	0	1
AT3G26740.1	CCL	signalling ?	0.5	0.08977044469
AT2G30520.2	nd	nd	-0.05555555555	0.39324311087
AT5G35840.1	nd	nd	-0.19916458337	0.39324311087
AT1G27190.1	LRR-RLK	kinase	-0.19916458337	0.48959455631
AT4G28490.1	nd	nd	0.166666666666	0.39324311087
AT1G08590.1	PXL1	kinase	-0.19916458337	0.48959455631
AT5G39020.1	nd	nd	-0.05555555555	0.39324311087
AT4G23310.1	CRK23	kinase signaling	0,00	1,00
AT3G45860.1	CRK4	kinase signaling	0,00	1,00
AT5G56890.1	nd	kinase	0	1
AT2G01210.1	nd	nd	0	1
AT1G53430.1	LRR-RLK-like	kinase	-0.36583125004	0.16779605782
AT3G05990.1	LRR-like	unknown	0,00	1,00
AT3G22910.1	ACA13	unknown	0,00	1,00
AT3G21180.1	ACA9	unknown	0,00	1,00
AT4G00820.1	nd	signaling ?	0.166666666666	0.39324311087
AT5G53010.1	nd	transporter ?	0,00	1,00

Accession	Protein name (this work)	Curated function (this work)	LogFC	Adj.pvalue
AT4G36080.1	nd	nd	0.166666666666	0.39324311087
AT1G56050.1	GTPB-like	signaling G-proteins	0.166666666666	0.48959455631
AT5G27540.1	nd	nd	-0.16666666666	0.39324311087
AT1G52280.1	nd	nd	0.166666666666	0.39324311087
AT4G18430.1	RAA1E (RABA1e)	signalling / SNARE effector	0.930827083453	0.02935288468
AT5G59840.1	RAB-8A (ara-3)	signaling	0.398329166746	0.40021853086
AT1G06400.1	RABA1A (ARA-2, RAB11E)	signalling / SNARE effector	1.118508072420	0.02935288468
AT4G17170.1	RABB1c (RAB2)	signalling / SNARE effector	0.666666666666	0.01996908054
AT4G17530.1	RABD2c (RAB1C)	signalling / SNARE effector	0.333333333333	0.39324311087
AT5G27510.1	Kinase-like	kinase	0.166666666666	0.48959455631
AT3G27000.1	ARP2 (WRM, WURM)	cell morphogenesis cytoskeleton actin	0.166666666666	0.48959455631
AT1G64330.1	HP64c	cell morphogenesis cytoskeleton myosin ?	0.333333333333	0.39324311087
AT1G72250.2	nd	plastid positioning ?	0,00	1,00
AT4G14390.1	nd	nd	0	1
AT1G43700.1	nd	nd	0.166666666666	0.39324311087
AT5G62700.1	TBB3	cell morphogenesis cytoskeleton actin	0,00	1,00
AT5G53080.1	TPR-like	RNA binding ?	-0.19916458337	0.39324311087
AT3G19720.3	ARC5	chloroplast division	0,00	1,00
AT5G42480.1	ARC6 (DNAJ, FTN2)	plastid division	0.422572067764	0.25940759006
AT5G55280.1	FtsZ1-1	plastid division	0.166666666666	0.48959455631
AT2G36250.2	FTSZ2-1	plastid division	0.5	0.08977044469
AT3G52750.1	FTSZ2-2	plastid division	-0.19916458337	0.48959455631
AT2G21280.1	GC1 (AtSulA)	plastid division	1.149996863064	0.00733511346
AT5G24020.1	MIND	plastid division	0,00	1,00
AT2G16070.2	PDV2	plastid division	0.456502855157	0.39324311087
AT1G53720.1	nd	nd	0	1
AT5G05010.2	nd	nd	0	1
AT3G50790.1	LEA-like	unknown	0.597493750120	0.34311785110
AT2G45330.1	EMB1067	RNA binding ?	0	1
AT1G49510.1	EMB1273	unknown	0.5	0.33305884105
AT5G49120.1	HP17z	unknown	0.166666666666	0.39324311087
AT2G37860.3	HP35b-like (LCD1)	unknown	1.633312854100	6.18646823097
AT1G10510.1	HP73 (EMB2004)	RNA metabolism?	1.971672087374	2.50320233107
AT1G45230.2	nd	nd	-0.11111111111	0.39324311087
AT2G21340.1	MATE4 (EDS5-like, Sid1)	transporter multidrug ?	0.422572067764	0.39324311087
AT1G78900.1	VATA (VHA-A)	transporter ATPase	1.553091393758	9.54749893889
AT1G12840.1	VATC	transporter ATPase	0,00	1,00
AT1G76030.1	VATB	transporter ATPase	0,00	1,00
AT4G37270.1	HMA1 (AHM1)	transporter ATPase Cu	0.166666666666	0.48959455631
AT3G19490.1	NHD1	transporter ?	0.930827083453	0.00271659414
AT5G21930.2	PAA2 (HMA8)	transporter ATPase Cu	2.059359001725	4.13456521090
AT2G15290.1	Tic21 (Cia5) or PIC1	protein targeting Tic ? Transporter Iron ?	0.5	0.11344341451
AT5G13490.2	AAC2	Mito transporter ATP/ADP	1.203153658526	0.00024779109
AT1G78560.1	IEP36-like	transporter Na/X ?	0.333333333333	0.39324311087

Accession	Protein name (this work)	Curated function (this work)	LogFC	Adj.pvalue
AT4G00630.2	KEA2 (HP64-like)	transporter K	1.112038688174	0.00108024089
AT4G04850.2	KEA3	transporter K ?	2.340616229805	3.17723657013
AT5G03910.1	ABC (ATH12)	transporter ABC	1.020065817885	0.00300669246
AT5G58270.1	ABCB25 (ATM3, STA1, STARIK 1)	transporter ABC	0.861654166907	0.02832359730
AT1G51500.1	ABCG12 (CER5 D3 WBC12)	transporter ABC	0.166666666666	0.39324311087
AT1G51460.1	ABCG13 (WBC13)	transporter ABC	0.333333333333	0.39324311087
AT2G01320.1	ABCG7 (WBC7)	transporter ABC ?	1.364059134551	3.28087701636
AT4G33460.1	NAP13 (EMB2751)	transporter ABC	0.166666666666	0.39324311087
AT5G14100.1	NAP14 (ABCI11)	transporter ABC Co ?	0.166666666666	0.39324311087
AT1G64550.1	nd	transporter ?	0.166666666666	0.39324311087
AT3G10350.2	P-loop-NTPase-like	transporter anion ?	0.166666666666	0.48959455631
AT3G16240.1	TIP21 (HP25c)	transporter aquaporin	0.740679673694	0.34311785110
AT2G38270.1	GRS16 (GrxS16, CAXIP1-like)	redox	0.833333333333	0.00127483930
AT1G69480.1	PHO1A	transporter Pi	-0.19916458337	0.39324311087
AT3G26570.2	PHt2-1 (IEP60)	transporter Pi	2.235911340345	1.47618801324
AT2G29650.2	PHt4-1 (P56-2, ANTR1)	transporter Pi ?	1.719961125546	2.77060572027
AT4G00370.1	PHt4-4 (P56-4, ANTR2)	transporter Pi ?	1,00	4.06321633668
AT1G54350.1	ABCD2	transporter ABC ?	2.930781426407	4.28069811833
AT2G26900.1	BASS2 (IEP36)	transporter Na/X ?	2.720648822868	1.20928546762
AT5G12860.2	DiT1 (IEP45, OMT)	transporter oxoglut/mal	2.192553730300	4.08592882623
AT5G64290.1	DiT2-1 (DCT1)	transporter oxoglut/mal	2.388084029491	2.48967708899
AT5G64280.1	DiT2-2	transporter glutamate/mal	0.166666666666	0.48959455631
AT5G23890.1	HP103	unknown	1.955869555581	0.00027238831
AT5G12470.1	HP35b-like (HP40, LCD1-like)	unknown	2.251382316049	1.04905098645
AT1G32080.1	HP45 LrgB-like	transporter ?	2.340378311909	2.35670617213
AT5G59250.1	HP59	transporter D-xylose-H+ ?	1.178306271463	0.00399112370
AT3G56160.1	IEP36-like	transporter Na/X ?	0.764160416786	0.14210339028
AT1G01790.1	KEA1 (HP64)	transporter K	2.483471538213	5.96069750110
AT2G35800.1	MCF (HP90)	unknown	1.461342945638	7.69583946539
AT5G01500.1	MCF (TAAC, HP45b)	transporter MCF ATP/ADP ?	1.089238734431	1.12657228926
AT4G32400.1	MCF Brittle-1	transporter MCF ATP/ADP ?	0.776919723398	0.08977044469
AT4G39460.2	MCF SAMC1/SAMT1 (HP35)	transporter MCF SAM	2.354142213057	5.58039513603
AT5G17520.1	MEX1 (RCP1)	transporter maltose	1.483965634352	7.14377663832
AT5G42130.1	Mfl1 (MCF)	transporter MCF Iron ?	2.144282311400	5.54876882428
AT5G22830.1	MGT10 (AtMRS2-11, GMN10)	transporter Mg	0.991352970397	0.01483372020
AT4G25450.3	NAP8 (HP77, ABCB28)	transporter ABC	2.889515735664	7.40011818962
AT2G28900.1	OEP16-1 (HP15)	aa channel / protein targeting ?	1.439234825842	0.00011882374
AT4G26670.1	OEP16-like	protein targeting / aa channel	0.430827083453	0.26133844539
AT3G49560.1	OEP16-like (HP30)	protein targeting / aa channel	1.269210446300	0.00249464993
AT5G24650.1	OEP16-like (HP30-2)	protein targeting / aa channel	1.963164246234	1.99706458082
AT1G76405.2	OEP21-1	transporter ion channel	0.288124014935	0.73582090453
AT5G42960.1	OEP24-II	transporter ion channel	1.265956671613	0.00015534871
AT2G43950.1	OEP37 (HP44)	transporter ion channel	1.065730799045	0.02012134496
AT5G16150.1	PGLCT (IEP62, GLT1)	transporter glucose ?	2.632114851233	5.01418412734

Accession	Protein name (this work)	Curated function (this work)	LogFC	Adj.pvalue
AT5G33320.1	PPT (IEP33, CUE1)	transporter Pi/PEP	2.027933080956	2.43984434099
AT1G80300.1	TLC1 (AATP1, NTT1)	transporter ATP/ADP	1.582000188962	1.62124248249
AT1G15500.1	TLC2 (AATP2, AtNTT2)	transporter ATP/ADP	0.747067182333	0.04900262693
AT5G46110.3	TPT (IEP30, APE2)	transporter Pi/TP	2.170491660335	4.32147334764
AT3G08580.1	AAC1	Mito transporter ATP/ADP	1.695497096471	0.00017366199
AT1G78180.1	BTL2 (MCF)	transporter ATP/ADP ?	0.166666666666	0.48959455631
AT5G19760.1	nd	transporter MCF	0.166666666666	0.39324311087
AT2G32040.1	FBT1	transporter folate/monoglutamate	0.333333333333	0.39324311087
AT2G38330.1	MATE2	transporter ?	0.166666666666	0.39324311087
AT2G29590.1	ACO-like	unknown	-0.19916458337	0.71280831938
AT2G34680.1	AIR9	unknown	0,00	1,00
AT1G55930.1	CorC-like	transporter Mg & Co ?	0.166666666666	0.39324311087
AT3G13070.1	CorC-like	transporter Mg & Co ?	0.666666666666	0.01996908054
AT1G29390.2	CRIM2 (COR413IM2, COR314TM2	stress cold	0.943586390065	0.14210339028
AT5G58770.1	DDPS2	protein modification	0.333333333333	0.24291854354
AT1G53280.1	DJ1B	unknown	0,00	1,00
AT5G22640.1	EMB1211	RNA binding ?	0.568799228437	0.25379656150
AT3G56010.1	HP21d	unknown	0.923520572180	0.00251834260
AT3G07430.1	HP24-like (YGGT-C, Ycf19-like)	cytochrome biogenesis ?	0.807811982038	0.19580758895
AT2G42770.1	HP25 (PMP22-like)	transporter ?	1.950058509092	9.71401459297
AT2G21530.1	HP25h	unknown	-0.11111111111	0.48959455631
AT5G19750.1	HP25-like (HP30c) PMP22-like	transporter ?	0.764160416786	0.02792654564
AT1G67700.2	HP26e	unknown	-0.89368722269	0.01022593891
AT3G08640.1	HP35b (LCD1-like)	unknown	1.074013007027	0.00447196839
AT2G37400.1	HP35c-like	unknown	0	1
AT2G41040.1	HP39	unknown	1.336729347616	0.00318321234
AT5G38520.2	HP40c	hydrolase ?	2.532700619590	4.47466582664
AT4G36530.1	HP41d	hydrolase ?	1.698040612868	1.45325194139
AT4G12830.1	HP43c	hydrolase ?	1.721454838370	0.00035446802
AT2G39670.1	HP47b	RNA Binding ?	-0.05555555555	0.48959455631
AT1G06690.1	HP52	redox ?	2.621199418096	4.66238767138
AT4G38650.1	HP63	unknown	0,00	1,00
AT5G46190.1	HP69	RNA Binding ?	-0.08805347226	1,00
AT5G43745.1	HP88-like	transporter ion channel ?	1.062347197765	0.00356058927
AT5G50780.1	HP91	unknown	-0.27777777777	0.39324311087
AT5G62720.1	IEP18	transporter ?	1.474131606649	0.00014988621
AT1G49750.1	LRR-like	unknown	0,00	1,00
AT1G53470.1	MSL4	unknown	0,00	1,00
AT5G19850.1	nd	hydrolase ?	0,00	1,00
AT1G03220.1	nd	unknown	0,00	1,00
AT3G48420.1	nd	unknown	0,00	1,00
AT5G06320.1	nd	unknown	0,00	1,00
AT4G34290.1	nd	unknown	0,00	1,00
AT2G25830.1	nd	unknown	0,00	1,00

Accession	Protein name (this work)	Curated function (this work)	LogFC	Adj.pvalue
AT5G44640.1	nd	nd	0,00	1,00
AT1G47271.1	nd	nd	0,00	1,00
AT1G79740.1	nd	nd	0	1
AT5G40290.1	nd	nd	0.166666666666	0.39324311087
AT3G08850.1	nd	nd	0.166666666666	0.39324311087
AT5G45510.1	nd	nd	0.166666666666	0.39324311087
AT3G13180.1	nd	nd	-0.11111111111	0.39324311087
AT1G32700.1	nd	nd	0	1
AT1G80630.1	nd	nd	0,00	1,00
AT3G59770.2	nd	nd	-0.16666666666	0.39324311087
AT3G01660.1	nd	nd	0,00	1,00
AT4G16045.1	nd	nd	0,00	1,00
AT5G50970.1	nd	nd	0.166666666666	0.39324311087
AT1G61000.1	nd	unknown	0.166666666666	0.39324311087
AT5G22140.2	nd	unknown	-0.05555555555	0.39324311087
AT3G27890.1	NQR	unknown	0,00	1,00
AT4G10750.1	PEPC-like	metabolism carbon ?	-0.60601460417	0.39324311087
AT2G45740.1	PEX11-like	unknown	-0.23166250008	0.65310387500
AT5G43140.1	PMP22-like	nd	-0.19916458337	0.39324311087
AT3G63540.1	PsbP-like (TL19, P19)	PS PSII OEE ?	1.229205256048	0.00741705618
AT5G38510.2	Rhomb-like	chaperone and protease ?	0.666666666666	0.01630157292
AT1G78140.1	SMT-like	protein modification	0.833333333333	0.00127483930
AT5G14440.1	SURF2	unknown	0.666666666666	0.01996908054
AT5G52970.1	TL15B	unknown	0,00	1,00
AT1G58270.1	TRAF-like	nd	-0.16666666666	0.39324311087
AT1G49320.1	USPL1	unknown	0,00	1,00
AT3G11945.2	VTE2-2 (HPT2, HST)	metabolism vitamin and pigment vitamin E	0.666666666666	0.11956915329
AT5G21920.1	YCF19-like	unknown	0.5	0.33305884105
AT2G34460.1	Ycf39-like (HP26c, Tic62-like)	protein targeting Tic ?	3.319539532302	7.79258261982
AT4G35250.1	Ycf39-like (Tic62-like)	protein targeting ?	2.209680937593	4.17948869378
AT4G27990.1	YLMG1-2 (HP24, YGGT-B, Ycf19-lik	cytochrome biogenesis ?	1.050501077759	0.09810268037
AT1G01920.2	nd	unknown	0.166666666666	0.39324311087
AT1G53120.1	nd	RNA Binding ?	0,00	1,00
AT3G23700.1	RPS1-like	translation stroma ?	-0.53249791670	0.10635533374
AT3G19830.1	CaLB-like	metabolism lipid ?	0,00	1,00
AT4G20080.1	nd	nd	0,00	1,00
AT3G25500.1	FH1 (AFH1)	cell morphogenesis cytoskeleton actin	0,00	1,00
AT3G43520.1	HP26b-like	unknown	1.427410226124	0.00062482741
AT3G25690.2	CHUP1	plastid positioning	0,00	1,00
AT1G14710.2	nd	unknown	0,00	1,00
AT5G07020.1	HP24c	unknown	1.941889014475	1.88234656075
AT2G18520.1	nd	unknown	0,00	1,00
AT3G22670.1	PP248	RNA Binding ?	0	1
AT3G28660.1	PP260 (PCMP-E80, TPR-like)	RNA Binding ?	-0.16666666666	0.58307524356

Accession	Protein name (this work)	Curated function (this work)	LogFC	Adj.pvalue
AT5G24830.1	PP396 (TPR-like)	RNA binding ?	0,00	1,00
AT5G55840.1	PP432 (PPR-like)	RNA Binding ?	0.166666666666	0.39324311087
AT4G13650.1	PPR-like	RNA Binding ?	0.166666666666	0.39324311087
AT2G38420.1	PPR-like	RNA Binding ?	0,00	1,00
AT1G43980.1	PPR-like	RNA Binding ?	0,00	1,00
AT5G24310.1	ABI-like	nd	-0.19916458337	0.39324311087
AT5G38660.1	APE1	unknown	2.688240864429	3.78508558091
AT4G09010.1	APX4 (TL29)	stress oxidative or redox	-1.09125818560	0.01127031774
AT2G31040.1	ATPI-like (ATPZ-like)	unknown	1.619839956855	5.43487982545
AT3G59780.1	CaS-like	unknown	2.774091842349	1.89728857818
AT3G55250.1	CHoR1 (PDE329)	signalling Calcium ?	1.962912791652	7.14377663832
AT3G17930.1	DAC	PS b6-F ?	1.612993823934	1.28157435895
AT4G31160.1	DCAF1	nd	-0.19916458337	0.39324311087
AT1G52590.1	DCC-like	redox	0.166666666666	0.39324311087
AT5G02160.1	DNAJ-like	chaperone and protease ?	0.945432093400	0.00131323039
AT5G53860.2	EMB2737	vesicular trafficking ?	0.900039829088	0.03215041761
AT5G58250.1	EMB3143 (Ycf54-like)	unknown	0.943586390065	0.02474331304
AT4G13590.1	GDT12 (HP28b)	translation stroma ?	0.597493750120	0.10635533374
AT5G45170.1	HAD-like	unknown	0.166666666666	0.48959455631
AT5G15802.1	HP10	unknown	0.5	0.33305884105
AT5G09840.1	HP102	RNA Binding ?	0,00	1,00
AT5G52410.2	HP103-like	unknown	1.117559568005	0.00271659414
AT3G25680.1	HP103-like	unknown	0.5	0.08977044469
AT4G13500.1	HP13	unknown	1.292481250360	6.18944511321
AT2G05310.1	HP13	unknown	1.012759306612	0.00285238715
AT4G20160.1	HP134z	unknown	-0.11111111111	0.39324311087
AT5G64816.1	HP14	unknown	1.115951201592	0.00144367524
AT1G33810.1	HP15b	unknown	1.558836695758	7.09005988688
AT3G53470.2	HP15c	unknown	2.026138004282	1.24968943810
AT3G50685.1	HP16	transporter ?	0.907916066870	0.06767953429
AT5G08050.1	HP16b	unknown	-0.06499583341	1,00
AT4G28025.2	HP16d	unknown	0.166666666666	0.48959455631
AT1G42960.1	HP17	unknown	1.562970920079	4.74125369451
AT5G42070.1	HP17b	unknown	0.166666666666	0.48959455631
AT3G02900.1	HP17-like	unknown	0.5	0.33305884105
AT5G16660.2	HP17-like	unknown	1.203223131014	0.00066149055
AT2G17972.1	HP18	unknown	1.169539952138	0.00357189622
AT4G02725.1	HP18b	unknown	0.930827083453	0.00271659414
AT2G36145.1	HP19	unknown	1.328303134528	0.00061530918
AT3G51510.1	HP19b	unknown	0.833333333333	0.00127483930
AT2G03420.1	HP19c	unknown	0.166666666666	0.39324311087
AT4G13220.1	HP19z	unknown	0.166666666666	0.39324311087
AT3G12345.1	HP20	unknown	1.204089822134	0.00567646078
AT1G74730.1	HP20	unknown	-0.23166250008	0.54184809401

Accession	Protein name (this work)	Curated function (this work)	LogFC	Adj.pvalue
AT2G42975.1	HP20b	unknown	1.701356433442	0.00023419449
AT4G13200.1	HP20c	unknown	1.415872781933	0.00021203173
AT1G14345.1	HP21	redox ?	0.562992843109	0.00436647810
AT2G27290.1	HP21b	unknown	1.856930506878	1.01351130489
AT4G38100.1	HP21c	unknown	1.240729089829	0.00218769464
AT5G28885.1	HP21e	unknown	0.166666666666	0.48959455631
AT1G22060.1	HP228	unknown	0.166666666666	0.48959455631
AT2G04039.2	HP22b	unknown	0.411946527737	0.29908781119
AT3G12685.1	HP22z	unknown	0.166666666666	0.39324311087
AT1G50020.1	HP23	unknown	0.423520572180	0.39324311087
AT2G17695.2	HP23b	unknown	1.097493750120	2.19972201178
AT3G04890.2	HP24b	unknown	0.789836188490	0.03203137445
AT5G41960.1	HP24d	unknown	0.495230020245	0.40406739462
AT5G42765.1	HP25e	unknown	1.688740026422	5.79092652333
AT1G18060.1	HP25f	unknown	2.793365315874	2.10025679100
AT2G26340.1	HP25g	unknown	2.301839101442	2.27573569866
AT4G27390.1	HP25i	unknown	0.333333333333	0.39324311087
AT3G57280.1	HP26b	unknown	1.713166549937	1.51214662139
AT2G38550.1	HP26b-like (HP36c)	unknown	2.647162692232	3.21973408585
AT3G32930.1	HP27b	unknown	0.666666666666	0.01996908054
AT1G44920.1	HP27c	unknown	2.244193278349	1.80404813558
AT4G01935.1	HP28	unknown	1,00	4.06321633668
AT3G51140.1	HP28 (AtCDF1-like)	signalling ?	1.452016135947	0.00087214586
AT5G09995.2	HP28c	unknown	0.666666666666	0.11956915329
AT1G08530.1	HP28c-like	unknown	0.590187238847	0.34311785110
AT3G15110.1	HP28d	unknown	0.940036116676	0.01897527599
AT1G64680.1	HP28e	unknown	1,00	4.06321633668
AT2G44870.1	HP28f	RNA transcription ?	0.166666666666	0.48959455631
AT5G23040.1	HP28-like (AtCDF1)	signalling ?	0.166666666666	0.48959455631
AT3G61870.1	HP29b	unknown	2.884855844640	1.25950273487
AT5G13720.1	HP29c	translation stroma ?	1.557877516841	2.24038334717
AT3G09050.1	HP29d	unknown	0.333333333333	0.24291854354
AT1G28140.1	HP30d	unknown	1.982655618504	2.11606719678
AT2G43630.1	HP30e	unknown	0.504667168402	0.25940759006
AT2G20920.1	HP30f	unknown	2.019338489967	9.52726383427
AT2G02730.1	HP30g	unknown	0,00	1,00
AT1G32220.1	HP31	unknown	2.108604455032	1.37234626020
AT1G65230.1	HP32e	unknown	2.446260313917	3.23177894678
AT4G24090.1	HP33b	unknown	1.678117935730	1.34276486971
AT5G37360.1	HP33c	unknown	2.631574286776	2.90197908341
AT5G65250.1	HP33d	unknown	0.444444444444	0.39324311087
AT2G34610.1	HP33e	unknown	-0.05555555555	0.39324311087
AT1G78620.2	HP34	unknown	-0.17610694452	0.83991494459
AT5G24690.1	HP35b-like (HP56b, LCD1-like)	unknown	1.121021677409	0.01284071325

Accession	Protein name (this work)	Curated function (this work)	LogFC	Adj.pvalue
AT5G48790.1	HP35d	unknown	1.845701677092	3.19055965874
AT2G21960.1	HP35e	unknown	3.094293308212	3.25618629079
AT4G31530.1	HP35f	unknown	0.5	0.08977044469
AT3G60590.2	HP36b	transporter aa ?	0.666666666666	0.11956915329
AT2G04360.1	HP36c	unknown	0.597493750120	0.34311785110
AT5G27290.1	HP37	unknown	1.922411313839	3.90387230745
AT5G63100.1	HP37b	protein modification ?	0	1
AT5G22340.1	HP38	unknown	0	1
AT3G25805.1	HP38	unknown	0,00	1,00
AT5G27560.1	HP38	unknown	0.686732484551	0.11858383047
AT1G29700.1	HP38b	unknown	0.5	0.08977044469
AT1G48460.1	HP38c	transporter ion channel ?	0.333333333333	0.24291854354
AT5G35066.1	HP4	unknown	0.5	0.08977044469
AT3G43540.1	HP40d	unknown	1.117014580087	0.00695390333
AT1G52315.1	HP40e	vesicular trafficking ?	0.333333333333	0.24291854354
AT1G52510.1	HP41c	hydrolase ?	2.255557920008	4.90972220025
AT1G74640.1	HP41e	unknown	0.5	0.08977044469
AT1G54520.1	HP42b	unknown	1.922438101470	0.00093334815
AT5G61200.3	HP45c	unknown	0.111111111111	0.62418415731
AT1G50450.1	HP46b	unknown	2.650931846675	2.22063681103
AT5G52540.1	HP47	transporter ?	1.692504192875	8.19772111178
AT3G01060.1	HP51	unknown	-0.74207320884	0.07758720926
AT5G19540.1	HP52c	unknown	0.666666666666	0.01996908054
AT5G08540.1	HP53	unknown	2.914421049879	7.10260315326
AT5G03900.2	HP59b	unknown	2.024942638273	3.54203598748
AT3G07210.1	HP59z	chaperone and protease ?	0.166666666666	0.39324311087
AT2G45840.1	HP61z	unknown	0	1
AT5G01590.1	HP65	unknown	0.696330414634	0.17456254128
AT3G22210.1	HP7	unknown	0.166666666666	0.39324311087
AT5G06930.1	HP80z	unknown	0	1
AT3G56140.1	HP82	unknown	1.053996605277	0.03449438174
AT4G08630.1	HP85z	unknown	-0.19916458337	0.39324311087
AT5G02940.1	HP88 (DMI1-like)	transporter ion channel ?	2.862002978514	1.04836331276
AT3G44380.1	LEA	stress desiccation	0.686732484551	0.10209399591
AT3G11560.4	LETM1-like	transporter K+/H+?	1.074013007027	0.00447196839
AT1G55280.1	Lipase-like	metabolism lipid ?	0.623169521824	0.35541784071
AT4G28740.1	LPA1-like	chaperone and protease ?	1.616824369354	0.00168997471
AT5G51545.1	LPA2	chaperone and protease	0.309002496908	0.51605968442
AT1G73060.1	LPA3	PS PSII ?	0.956502855157	0.00376629442
AT1G02475.1	LTP-like	transporter lipids ?	0.333333333333	0.24291854354
AT2G32640.1	Lycopene_cycl	metabolism vitamin and pigment ?	2.411262830079	1.26149808765
AT5G26230.1	MAKR1	kinase regulator ?	0	1
AT1G21440.1	nd	metabolism carbon ?	0,00	1,00
AT2G21385.1	nd	unknown	0,00	1,00

Accession	Protein name (this work)	Curated function (this work)	LogFC	Adj.pvalue
AT2G43945.1	nd	unknown	0,00	1,00
AT3G55760.3	nd	unknown	0,00	1,00
AT1G62780.1	nd	unknown	0,00	1,00
AT1G16080.1	nd	unknown	0,00	1,00
AT4G34090.3	nd	unknown	0,00	1,00
AT3G20680.1	nd	unknown	0,00	1,00
AT4G30720.1	nd	unknown	0,00	1,00
AT4G01883.1	nd	unknown	0,00	1,00
AT5G04440.1	nd	unknown	0,00	1,00
AT2G31890.1	nd	unknown	0,00	1,00
AT5G01730.1	nd	unknown	0,00	1,00
AT3G28220.1	nd	chaperone and protease ?	0	1
AT5G50930.1	nd	DNA binding	0,00	1,00
AT5G52800.1	nd	nd	0.166666666666	0.39324311087
AT5G04670.1	nd	nd	0.166666666666	0.39324311087
AT1G22882.1	nd	nd	0.166666666666	0.39324311087
AT4G32900.2	nd	nd	0	1
AT5G52780.1	nd	nd	0.166666666666	0.39324311087
AT1G33800.1	nd	nd	-0.05555555555	0.39324311087
AT1G47470.1	nd	nd	0	1
AT5G06970.1	nd	nd	-0.05555555555	0.39324311087
AT1G17820.1	nd	nd	0,00	1,00
AT4G30200.3	nd	nd	-0.11111111111	0.39324311087
AT4G17970.1	nd	transporter ?	0.166666666666	0.39324311087
AT4G28210.1	nd	transporter aa ?	0.166666666666	0.39324311087
AT5G06220.1	nd	transporter K+/H+?	0.166666666666	0.39324311087
AT5G63040.1	nd	unknown	0.166666666666	0.39324311087
AT3G09450.1	nd	unknown	0	1
AT3G26950.1	nd	unknown	0.166666666666	0.39324311087
AT4G24030.1	nd	unknown	0.166666666666	0.39324311087
AT3G28430.1	nd	unknown	0.166666666666	0.39324311087
AT2G36885.1	nd	unknown	0.166666666666	0.39324311087
AT5G65950.1	nd	unknown	0	1
AT1G67040.1	nd	unknown	0	1
AT1G36745.1	nd	unknown	-0.11111111111	0.39324311087
AT3G42786.1	nd	unknown	0.166666666666	0.39324311087
AT3G32180.1	nd	unknown	0.166666666666	0.39324311087
AT1G27300.1	nd	unknown	0,00	1,00
AT5G14990.1	nd	unknown	0,00	1,00
AT5G63540.1	nd	unknown	0,00	1,00
AT1G61097.1	nd	unknown	-0.05555555555	0.39324311087
AT1G71240.1	nd	unknown	-0.05555555555	0.39324311087
AT5G45540.1	nd	unknown	0.166666666666	0.39324311087
AT5G05840.1	nd	unknown	0,00	1,00

Accession	Protein name (this work)	Curated function (this work)	LogFC	Adj.pvalue
AT4G20095.1	nd	unknown	0.166666666666	0.39324311087
AT1G20816.1	OEP21-like	transporter ion channel	0.013519378296	1
AT3G52230.1	OEP24 (OMP24, E24)	transporter ion channel	2.046131785576	3.26190694588
AT3G63160.1	OEP6 (E10, E6)	unknown	0.216619837195	0.28127887502
AT3G05320.1	O-FucTrfase-like	protein modification ?	0.166666666666	0.39324311087
AT4G21210.2	PDRP1	unknown	0,00	1,00
AT5G17670.1	PGAP1-like	metabolism lipid / vesicular trafficking?	1.533303367529	3.89640559613
AT1G64355.1	PLCD-like	unknown	-0.03249791670	1,00
AT5G05480.1	PNGase-like	unknown	-0.19916458337	0.39324311087
AT1G64430.1	PPR-like	RNA Binding ?	0.764160416786	0.02792654564
AT4G01150.1	PSAP-like	PS PSI ?	3.048246721665	2.71716503329
AT5G27390.1	PSBP-like	PS PSII ?	1,00	4.06321633668
AT5G28500.1	RAF1	unknown	0,00	1,00
AT5G39410.1	SCPDH	metabolism aa Lys	1.667686236203	2.06503842104
AT1G22850.1	SNARE-like	unknown	0.564995833413	0.17854609485
AT4G24750.1	Str11	unknown	2.759652835307	2.71810937440
AT1G17850.1	STR8	unknown	0.166666666666	0.39324311087
AT2G37720.1	TBL15	unknown	1.292481250360	6.18944511321
AT2G44640.1	TGD4 (HP50, PDE320-like)	transporter lipids	1.810489061610	8.08046398819
AT5G55710.1	Tic20-V (Tic20-like, IEP16-like)	protein targeting Tic ?	0.645980302829	0.09008258544
AT5G62140.1	Tim50-like	protein targeting ?	1.707853280829	4.33124871481
AT4G02530.1	TL16.5	unknown	1.923289779869	1.77196578387
AT4G24930.1	TL1Y	unknown	1.233422578556	0.00218204114
AT1G54780.1	TLP18.3	unknown	-0.87076928849	0.00565763505
AT2G42400.1	VOZ2	transcription nucleus ?	-0.36583125004	0.16779605782
AT2G24020.1	YbaB-like	unknown	0.166666666666	0.48959455631
AT5G67370.1	YCF36-like (CGLD27)	unknown	0.833333333333	0.00127483930
AT2G23670.1	YCF37-like	unknown	-0.05555555555	0.48959455631
AT1G72640.1	Ycf39-like	protein targeting Tic ?	1.187680988967	5.86359413437
AT2G37660.1	Ycf39-like (Tic62-like)	protein targeting Tic ?	0,00	1,00
AT1G55480.1	ZKT (GAN)	RNA Binding ?	3.112301453637	7.54190201409
AT5G22620.3	nd	unknown	0,00	1,00
AT1G70820.1	nd	unknown	0,00	1,00
AT5G51820.1	PGMP	unknown	0,00	1,00
AT4G24620.1	PGI1	metabolism carbon	0,00	1,00
AT4G15530.2	PPDK1	unknown	0,00	1,00
AT5G03690.1	nd	metabolism carbon Calvin cycle	0,00	1,00
AT4G34240.1	ALDH3 (ALDH3I1)	metabolism carbon	2.533568843133	2.50523724984
AT5G09660.2	PMDH2	metabolism carbon	-0.90113739892	0.02167154212
AT5G35790.1	G6PD1	metabolism carbon	-1.37631009828	0.00124501976
AT1G64190.1	6PGD1	metabolism carbon	0,00	1,00
AT5G41670.1	6PGD2	metabolism carbon	0,00	1,00
AT1G17650.1	GLYR2	metabolism carbon	0,00	1,00
AT5G13420.1	nd	metabolism carbon	0,00	1,00

Accession	Protein name (this work)	Curated function (this work)	LogFC	Adj.pvalue
AT1G12230.2	ToTAL2	metabolism carbon	-1.27803688793	0.00323375691
AT5G58330.3	MDH	metabolism carbon	0,00	1,00
AT3G47520.1	MDHP (MDH)	metabolism carbon	1.869695831699	1.91916801528
AT3G01500.3	CA1 (CAHC)	metabolism carbon	3.391036832886	1.20928546762
AT3G01500.1	CA1 (CAHC)	metabolism carbon	1.535879381879	2.91133993285
AT5G14740.2	CA2 (CAH2)	metabolism carbon	1.580931253629	1.38007762855
AT2G27730.1	UMP2	resp NDH ?	0.166666666666	0.48959455631
AT5G47890.1	NDUA2	resp NDH ?	0.333333333333	0.39324311087
AT5G05370.1	nd	nd	0.166666666666	0.39324311087
AT1G49380.1	CCS1	chaperone and protease PS b6f	0.666666666666	0.01996908054
AT2G07698.1	ATPAM (ATPA, ATP1)	Mito ATPase	2.390597436912	2.22730266592
AT5G08690.1	ATPB2	Mito ATPase	3.145756581465	1.72445589110
AT2G33040.1	ATPC (ATPG3)	Mito ATPase	0.333333333333	0.24291854354
AT2G34660.2	ABCC2	transporter ABC	0,00	1,00
AT3G26085.3	CAAX-like	chaperone and protease	0.712408256255	0.10486701334
AT3G59210.2	nd	nd	0,00	1,00
AT2G07690.2	nd	nd	0.166666666666	0.39324311087
AT5G24314.2	PTAC7	chloroplast transcription ?	-0.11111111111	0.39324311087
AT2G45280.2	RAD51C	DNA binding ?	0.166666666666	0.39324311087

Chapter 3

Looking for new potential actors in state transitions

3.1 Introduction

In nature, photosynthetic organisms are constantly subjected to changes in environmental light, and they need to adjust their photosynthetic activity accordingly [280]. Because the antenna systems of PSII and PSI have a different composition and hence different light absorption properties, their excitation can be unbalanced under changing light conditions [281]. Two major mechanisms are known to assure efficient photosynthesis: *(i)* state transitions (ST), which act on a short-term timescale; and the *(ii)* long-term responses (LTR), which enable the plant to re-adjust photosystem stoichiometry in favour of the rate-limiting photosystem [124].

The molecular events triggering state transition process have been reviewed earlier in section 1.6.1.2 of this thesis (also see [282]). Briefly, state transitions occur in the minute-time scale and represent a mechanism to redistribute excitation energy between the photosystems by changing their relative antennae size [69]. This process is redox-controlled and it is promoted by the reversible phosphorylation of some light-harvesting proteins in the thylakoid membrane. Preferential excitation of PSII induces reduction of the plastoquinone pool, leading to a conformational change of the cytochrome b_6f which in turn activates a kinase. Activation of the kinase leads to the phosphorylation of a fraction of the LHCII (up to 15-20%[283]) and the migration of this latter away from the PSII-rich grana stacks, to accumulate in

the unstacked stroma-lamellae (state-2)[30]. Under condition in which PSI is more excited then PSII, the plastoquinone pool is oxidised and the kinase is inactivated [69]. This promotes the dephosphorylation of P-LHCII by means of a phosphatase (constitutively active) and the migration of LHCII back to the grana stacks (state-1)[30]. Recently, the kinase and phosphatase involved in state transitions have been identified and are referred to as STN7 [286] and PPH1 [119][126] respectively. Mutants of *Arabidopsis* devoid of STN7 and PPH1 cannot perform state transitions and are locked in state-1 and state-2 respectively. Studies on *stn7* mutant uncovered an interesting connection between state transitions and LTR (long term acclimation response)[287].

LTRs, compared to state transitions, occur in a longer-time scale (hours or days [287]), and involve the adjustment of the photosystem stoichiometry whenever the plant is subjected to long and stable light quality conditions [288]. LTRs, differently from state transitions, require changes in the expression of photosystem genes which lead, for example, into different accumulation of the photosystem core proteins [288]. LTRs, in plants are known to be modulated by a mechanism of phosphorylation cascade, which promotes the activation/ deactivation of proteins involved in post-transcriptional events, including RNA maturation, RNA editing and protein translation, which could modulate the abundance of nucleus-encoded photosynthesis-related proteins [289][290]. Both state transitions and long-term acclimation responses are controlled by the same redox signal. STN7 kinase, represents the common sensor and signal transducer [291] and plants devoid of STN7 lack also LTRs [124]. In the work presented here, we deliver a survey of the protein composition within the thylakoid sub-compartments in *stn7* and *pph1* mutants (locked in state-1 and state-2 respectively). We used a semi-quantitative proteomic approach to validate the differential distribution of thylakoid proteins between stroma-lamellae and BBY. Preliminary findings corroborate previous observations about the different distribution of Lhcb isoforms in state-1 and state-2. Besides, from the present results we could identify about 80 new candidate-proteins whose localisation might also be regulated in a redox-controlled manner by light in state transitions.

3.2 Results and discussions

3.2.1 Measure of state transitions in WT, *stn7* and *pph1*

Arabidopsis WT and *stn7*, *pph1* mutants were grown for 5 weeks and tested for their ability to perform state transitions *in vivo*. The measure was done by a fluorescence analysis taking advantage of the different composition in the antenna apparatus of PSII and PSI and hence of the different light absorption spectrum [50]. Leaf samples were switch either to state-1 or to state-2 using light sources that preferentially excite one of the two photosystems (see section 1.6.1.2 at page 41 for further details on state transitions). Concomitantly, fluorescence kinetics were collected. Red light was used to induce state-2, via its capacity to reduce the plastoquinone pool (referred to as state-2-actinic light) and far-red light was used to excite PSI (referred to as state-1-actinic light), since the latter complex has an intrinsic higher absorption capacity in this region of the spectrum. We started measuring minimum fluoresce in intact leaves in their dark-adapted state, F_0 (tab.3.1). In this condition all the PSII-reaction centers are fully oxidised (PSII centers open) and non-photochemical quenching is absent [292]. After F_0 was measured, a single and short (∼1s) light saturation pulse (∼ 3000 μmol m^{-2} s^{-1}) was applied causing a transient saturation of PSII reaction centers (PSII centers closed). This resulted in a very fast rise of the chlorophyll fluorescence to reach its maximum level denoted F_{max}. Once F_{max} was registered, the leaf was exposed for 10 minutes with 30 μmol m^{-2} s^{-1} state-2 actinic light. During these steady-state conditions, maximal fluorescence (F'_{max}) and steady-state fluorescence (F_{ss}) were regularly measured at intervals of 60 seconds (tab.3.1). After 10 minutes of illumination, 700 μmol m^{-2} s^{-1} of state-1 light was superimposed to the state-2 light for 10 minutes, F'_{max} and F_{ss} were measured at intervals of 60 seconds.

As shown in figure 3.1, *Arabidopsis* WT plants, when exposed to the solely state-2 light (time 0-10 min, figure 3.1), displayed a rapid increase in the F_0 to reach F_{ss} indicating that the primary electron acceptor from PSII, Q_A was reduced [293] (see section 1.3.1 at page 24). During illumination with state-2 light, both the F'_{max} and F_{ss} slowly decreased and reached a plateau after around minute 8. The relative amplitude of F'_{max} is proportional to the LHCII cross-section attached to PSII [150]; the larger is the size of the antenna, the larger is the amplitude of F'_{max}. We can interpret this progressive decrease of F'_{max} as the reduction of the antenna cross-section attached to

Parameters	Description
F_{max}	Maximal fluorescence of dark-adapted sample with all PS II centers closed
F'_{max}	Maximal fluorescence of illuminated sample with all PS II centers closed
F_0	Minimal fluorescence of dark-adapted sample with all PS II centers open
F_{ss}	Steady-state photosynthesis fluorescence

Table 3.1 – Description of the photosynthetic parameters measured during fluorescence kinetics of *Arabidopsis* WT, *stn7* and *pph1*

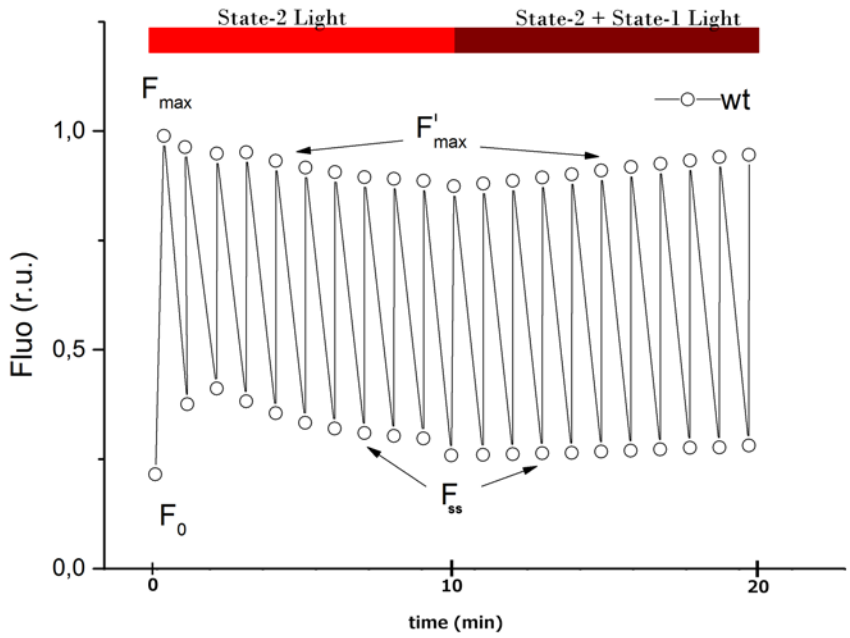

Figure 3.1 – *in vivo* measure of state transitions in WT. state-1 and state-2 are induced by 10 minutes illumination with 30μmol m^{-2} s^{-1} PSII-actinic (state-2) and with 30μmol m^{-2} s^{-1} PSII-actinic light + 700μmol m^{-2} s^{-1} PSI-actinic light (state-1)

PSII during the state1 - state2 transition following phosphorylation by the STN7 kinase. At the same time, the parallel decrease of F_{ss} indicate that oxidation of the plastoquinone pool has occurred. In fact progressive asso-

ciation of P-LHCII to the LHCI-PSI supercomplex (located in the stroma lamellae) promotes energy transfer to this photosystem which can accept electrons from plastocyanin (PC). When the leaf was illuminated with 700 μmol m^{-2} s^{-1} state-1-actinic light (time 10-20 min, figure 3.1) most of the reaction centers in PSI were also excited, together with PSII. We thus observe a quick drop in the F_{ss} indicating the instantaneous oxidation of the plastoquinone pool. In fact, under these conditions, electron-transfer from PSII to PSI proceeds at higher rate, and Q_A was reduced. This in turn inactivates the kinase and promotes dephosphorylation of the P-LHCII by the constitutive phosphatase. In parallel, gradual F'_{max} increase indicated the migrations of the LHCII from stroma-lamellae back to the stacked grana to increase the PSII antenna cross-section (state-1). We performed the same measure on the *Arabidopsis* state transition mutants *stn7* and *pph1* (figure 3.2A and B).

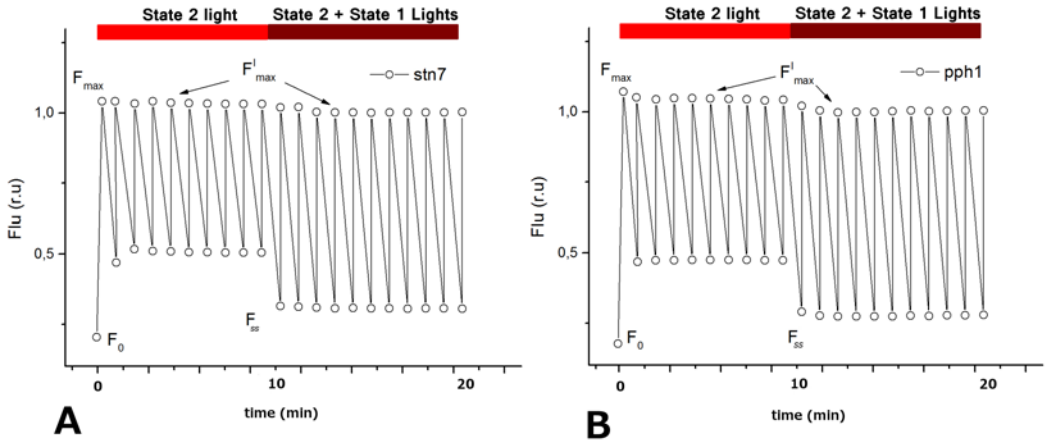

Figure 3.2 – *in vivo* measure of state transitions in (A) *stn7* and (B) *pph1*. state-1 and state-2 are induced by 10 minutes illumination with 30μE PSII-actinic (state2) and with 30μmol m^{-2} s^{-1} PSII-actinic light + 700μmol m^{-2} s^{-1} PSI-actinic light (state1)

After a first saturating pulse, continuous illumination with state-2-actinic light did not promote any variation in the F'_{max} in both *stn7* and *pph1* mutants. In *stn7* mutant, because of the lacking of the kinase, LHCII cannot be phosphorylated and migrations to the PSI-enriched lamellae was impaired. *pph1* mutant, on the other hand, possesses all its LHCII-phosphorylable pool already phosphorylated and state-2-actinic light could not promote further

antenna migration. Moreover F_{ss} evidenced reduced state of Q_A which could not be oxidised by PSI via Q_B and cytochrome b_6f (see section 1.3.1 at page 24). In both *stn7* and *pph1* mutants, addition of the state-1-actinic light while promoting rapid oxidation (figure 3.2A and B) of the photosynthetic chain, did not trigger variation of the PSII antenna size (F'_{max}). In *pph1* mutant, because of the lack of the phosphatase, P-LHCII cannot be dephosphorylated and it was stuck in stroma-lamellae. The *stn7* mutant, on the other hand, having all its antenna population already in a dephosphorylated state is unaffected by the action of the phosphatase.

LHCII phosphorylation state in *Arabidopsis stn7* and *pph1* mutants was further confirmed spectroscopically by measuring the fluorescence spectra of the different strains at 77K. As mentioned before, at room-temperature PSI is not fluorescent and reasons for this are given in section 2.2.3. To perform 77K measurements, samples of leaf from WT plants, *stn7* and *pph1* mutants were frozen in liquid nitrogen using a low temperature fluorometer (JBeam Bio, France, based on a detecting diode array AVS-USB 200, Ocean Optics, USA) and excited with blue light (470nm). When the relative fluorescence emission spectra is collected in the near infrared region three main peaks appear as shown in figure 3.3.

The two peaks between approximately 680 and 695 nm correspond to fluorescence emitted by chlorophyll molecules in PSII, while peak at 735 nm corresponds to the fluorescence emitted by chlorophyll molecules in PSI [294]. The ratio of the PSII/PSI-peaks is proportional to the cross-section of the antenna associated to PSII and PSI [150]. Leaves from state transition mutants (figure 3.3A red and green curves) displayed a significantly difference in the amplitude at the level of the PSII peaks. This is interpreted like a different PSII-antenna cross-section, consequence of a varying phosphorylation level of the LHCII-pool. Moreover leaves from WT (figure 3.3A black curve) were characterised by a PSII-peaks intensity which were intermediate between *stn7* and *pph1* mutants. We conclude that *Arabidopsis* WT plants, in our growing conditions, were in a phosphorylated state which is intermediate between that of *stn7* and *pph1* mutants but slightly closer to the one of *pph1* mutant (*i.e.* to the state-2 condition).

LHCII-phosphorylation levels of *Arabidopsis* WT, *stn7* and *pph1* mutant plants were also assessed biochemically and results are shown in figure 3.3B. In the western blot, thylakoid purified from WT, *stn7* and *pph1* are charged (0.5 μg Chl) and probed with antibodies raised against phosphorylated threonine-residues (LHCII *N*-termini). As evidenced, thylakoids from WT and *pph1* displayed a variable intensity of phosphorylation at the level of their LHCII (red-starred band); by contrast no P-LHCII was detected in the case of the *stn7* mutant.

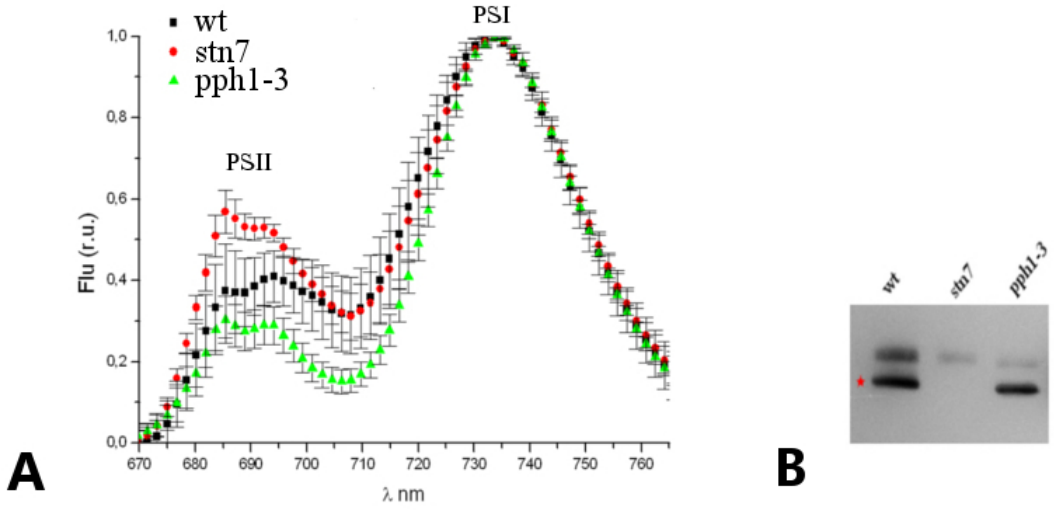

Figure 3.3 – (A) 77K chlorophyll fluorescence emission spectra of thylakoid membrane from *Arabidopsis* WT, *stn7* and *pph1* mutant plants. Thylakoid samples were loaded on to a metal cuvette, which was directly bathed into a liquid nitrogen solution. Fluorescence spectra were recorded upon excitation at 470 nm. Peaks were normalized for comparison purposes. (B) Western blot carried out on thylakoid samples from WT, *stn7* and *pph1* plants (0.5 μg Chl for each sample) using antibodies raised against phosphorylated threonine residues.

Eventually, fluorescence kinetics, spectroscopic and biochemical analysis confirmed that our thylakoid purified from *Arabidopsis pph1* and *stn7* mutants are indeed impaired in state transitions and could be used for the following proteomic-study.

3.3 Evaluation of the purity of the samples

Stroma-lamellae, BBY and margins fractions from *Arabidopsis stn7* and *pph1* mutants were purified according to the protocol reported in *Tomizioli et al., 2014* [139] (section 2.5.2 of this thesis). Evaluation of the purity of the fractions were firstly carried out on the basis of their polypeptide composition and compared with that of thylakoids. 6 μg proteins of each fraction (stroma-lamellae, BBY and thylakoids) were charged and separated on a 12% SDS-

polyacrylamide gel. fig.3.4 and 3.5 show the polypeptide profiles obtained after coomassie-blue staining for each fraction issued from *pph1* and *stn7* mutants respectively.

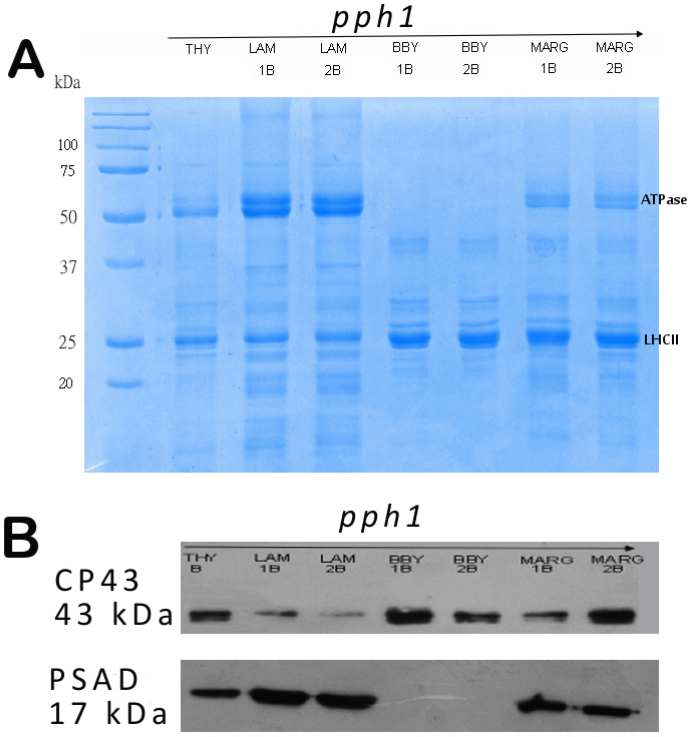

Figure 3.4 – A, characterisation of two technical replicates of *pph1* sub plastidial fractions by SDS-PAGE. THY thylakoids, LAM lamellae, BBY, MARG margins. B, characterisation of two technical replicates of *pph1* sub plastidial fractions by western blot. Western-blots were performed with using polyclonal antibodies raised against CP43 (PSII) and PSAD (PSI)

Each fraction displays a characteristic and unique composition. Light harvesting complex II, the major antenna complex associated to PSII is highly enriched in the grana-BBY fractions from both *stn7* and *pph1* mutants (figure 3.5A and 3.4A lanes BBY). By contrast, less and little accumulation of this complex was identified in stroma-lamellae fractions (figure 3.5A and 3.4A lanes LAM). α/β subunits of the ATPase are clearly enriched in the stroma-lamellae but not detected in the grana-BBY fraction. This is consistent with the fact that ATPase cannot be accumulated in the staked region of the thylakoid (grana-BBY) due to its size.

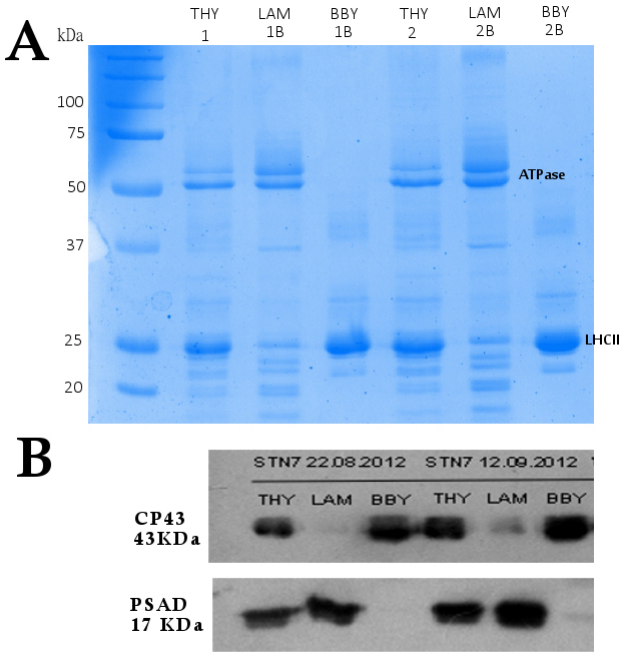

Figure 3.5 – A, characterisation of two biological replicates of *stn7* sub plastidial fractions by SDS-PAGE. THY thylakoids, LAM lamellae, BBY. B, characterisation of two biological replicates of *stn7* sub plastidial fractions by western blot. Western-blots were performed with using polyclonal antibodies raised against CP43 (PSII) and PSAD (PSI).

Enrichment in proteins associated to stroma-lamellae and grana-BBY was further confirmed by immunoblot analysis. In figures 3.5B and 3.4B, fractions are tested with antibodies raised against protein known to be localised within specific thylakoids sub-compartments. CP43 a chlorophyll protein associated to PSII is well accumulated in the grana-BBY but not detected in the stroma-lamellae, while the opposite is seen for the D subunit of the PSI. This was further confirmed by measuring the fluorescence spectra of the different fractions at cryogenic temperatures (principles of the technique explained above). In figures 3.6 and 3.7, the two PSII peaks were barely detectable in the purified stroma-lamellae fractions from *stn7* and *pph1*. PSI fluorescence peak alone turned out to be extremely reduced in the purified BBY fractions from *stn7* and *pph1* when compared to the thylakoids (figure 3.6).

Light envelope vesicles are known to represent a possible source of contamination and can co-purify with the stroma lamellae being the lighter frac-

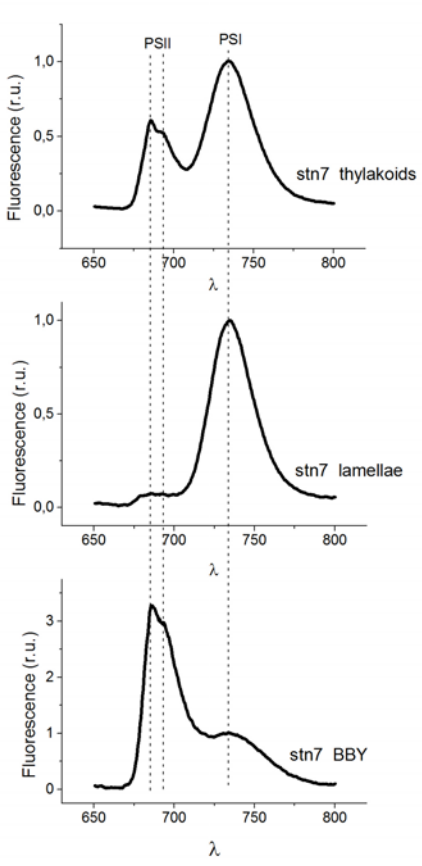

Figure 3.6 – 77K chlorophyll fluorescence emission spectra of thylakoid membrane and subfractions isolated from *Arabidopsis stn7* mutant. Thylakoid proteins (or thylakoid subfractions) samples were loaded on to a metal cuvette, which was directly bathed into a liquid nitrogen solution. Fluorescence spectra were recorded upon excitation at 470 nm. Top spectrum: isolated thylakoids. Medium spectrum: stroma lamellae. Bottom spectrum: BBY fraction

tion of the thylakoid membrane. We also quantified the cross-contamination of our stroma-lamellae preparations from *stn7* and *pph1* mutants with the chloroplast envelope fraction. At this purpose we used a specific antibodies raised against the envelope phosphate transporter PHT4;4 (ANTR1, At2g29650). In western blots reported in figure 3.8 different biological replicates of stroma lamellae are analysed. Samples tested are issued of different extractions (bio-

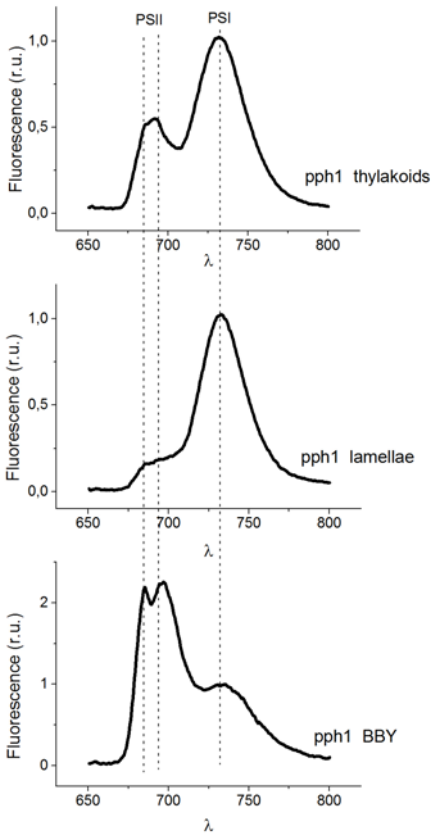

Figure 3.7 – 77K chlorophyll fluorescence emission spectra of thylakoid membrane and subfractions isolated from *Arabidopsis pph1* mutant. Thylakoid proteins (or thylakoid subfractions) samples were loaded on to a metal cuvette, which was directly bathed into a liquid nitrogen solution. Fluorescence spectra were recorded upon excitation at 470 nm. Top spectrum: isolated thylakoids. Medium spectrum: stroma lamellae. Bottom spectrum: BBY fraction

logical replicates) from *Arabidopsis* both WT and mutant plants (red-starred in figure 3.8). The level of cross-contamination was qualitatively evaluated by direct comparison of the intensities of the signals (Western-blots) arising from the fractions to be tested and those arising from a range of dilutions between 3 and 100 % of purified envelope fraction. In good agreement with the level of cross-contamination previously described in *Tomizioli et al., 2014* [139],

data reported in figure 3.8 indicate an average level of cross-contamination higher than 10 % and lower than 30 %. Moreover we evidence a certain level of variability between the biological replicates.

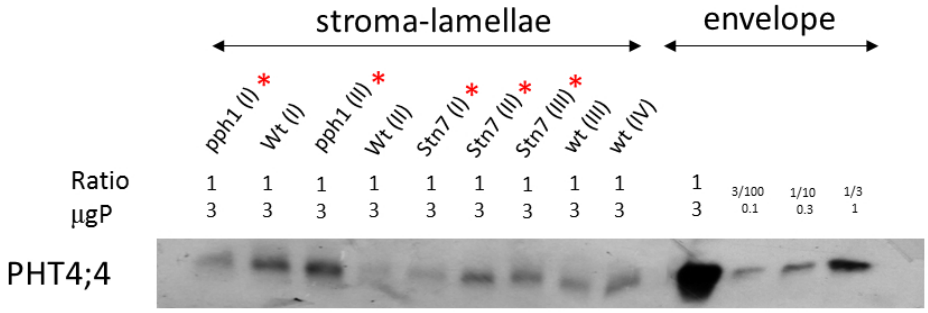

Figure 3.8 – Estimation of envelope cross-contamination in biological replicates of stroma-lamellae from *Arabidopsis* WT, *stn7* and *pph1* mutants (these two latter are red-starred). Western-blots were performed with using polyclonal antibodies raised PHT4;4 (At4g00370, envelope marker). Envelope fraction was purified from WT *Arabidopsis* chloroplasts.

3.3.1 Proteomic survey of the thylakoid subfractions from *stn7 and pph1* mutants

In order to perform LC-MS/MS analysis, proteins contained in the samples were concentrated on a SDS-PAGE between the stacking and the separating gels. LC-MS/MS analysis were performed as reported in *Tomizioli et al., 2014* [139] and spectral counting was used for relative quantification in order to determine the sub-thylakoid localisation of the identified proteins. According to conclusions drawn in *Tomizioli et al., 2014* [139], grana-margins, even if analysed in LC-MS/MS were not considered for the further statistical analysis (see section 2.5.2 at page 88 for further details).

Proteomic analysis was carried out in order to highlight proteins characterised by a different distribution between stroma-lamellae and BBY in the two *Arabidopsis stn7* and *pph1* mutants. To perform this we focused

on the values of protein logarithmic folding change (LogFC). As previously seen, value of LogFC can be associated to the enrichment of a given protein in either BBY or stroma-lamellae fractions. In particular, negative values of LogFC characterise protein enriched in the BBY, while positive values of LogFC characterise protein enriched in the stroma-lamellae. Moreover, for a given protein, the absolute value of the LogFC also allows to estimate in which extent the protein is shared between the two thylakoid subcompartments (*i.e* BBY and stroma-lamellae). For example, if the protein *A* is found in *stn7*(state-1) with a LogFC = -2 and the same protein *A* is found in the *pph1*(state-2) with a LogFc = -1.8, it means that this protein *A* is enriched in the BBY fraction in both the genotypes, but in the case of *pph1*(state-2) is more shared with stroma-lamellae and their difference in LogFC (ΔLogFC stn7-pph1) is 0.2. We exploited this information to put in evidence proteins characterised by a varied sub-thylakoid repartition between *stn7* and *pph1* mutants. Among the identified proteins, specific Lhcb isoforms are present and their identification is summarised in table 3.2.

LC-MS/MS analysis evidenced 10 different LHCII isoforms, namely Lhcb 1.4/1.5, Lhcb2, Lhcb 3.1, Lhcb 4.1/4.2 Lhcb 4.3, Lhcb 5 and Lhcb 6. Each antenna is characterised by a different enrichment in the stroma-lamellae and BBY sub compartments within the *stn7* and *pph1* mutants. Indeed these results reveal a clear trend in the antenna distribution, which is agreement with the traditional view of state transitions. In fact because of the lack of the specific kinase and phosphatase, Lhcb isoforms are more accumulated in stack membranes (*i.e.* BBY) in *stn7* than in *pph1*. However, when the statistical analysis is taken in consideration, only three antenna show a *p-value* lower than 0.05 (our confidence threshold). These three Lhcb isoforms are Lhcb 1.5, Lhcb 1.4 and Lhcb 2.2 (see tab.3.2).

In *Arabidopsis*, LHCII is a trimeric complex composed of a combination of three highly homologous Lhcb isoforms Lhcb1-3 encoded by a large multigene family [295]. LHCII trimers are normally distinguished in function of their (S)trong , (M)oderate or (L)oose association with the photosystem complex. In a recent work *Galka et al., 2012* [242] performed a detailed biochemical and mass-spectrometry analysis of the isoform composition of these three trimers and concluded that the trimers mainly involved in state transitions are the specific (L)oosely bound to PSII (also referred to as mobile). In our data (tab.3.2), isoforms Lhc1.5 and Lhc2.2 display a high differential accumulation between state-1 and state-2. This finding is in agreement with data reported in literature where it was demonstrated that Lhcb 1 and Lhcb 2 isoforms reach their higher content in the mobile subset of LHCII associated trimers (L) [242]. At the same time, Lhcb 1.5, Lhcb 1.4 (ΔLogFC 2.4) and Lhcb 2 (tab.3.2) are poorly represented in the fraction M which is thought

Isoform	Accession	ΔLogFC stn7-pph1	*p-value <0.05*
Lhcb4.1/CP29	At5g01530	1.8	no
Lhcb6	At1g15820	2.2	no
Lhcb4.2	At3g08940	2.2	no
Lhcb3.1	At5g54270	2.3	no
Lhcb1.4	At2g34430	2.4	yes
Lhcb5/CP26	At4g10340	2.5	no
Lhcb 4.3	At2g40100	2.7	no
Lhcb 1.5	At2g34420	3	yes
Lhcb 1.1	At1g29920	3.1	no
Lhcb 2.2	At2g05070	5.3	yes

Table 3.2 – List of the LhcII isoforms issued of the LC-MS/MS analysis. Antenna polypeptides are presented together with their accession number, absolute difference of their LogFc value between *Arabidopsis stn7/pph1* mutants and statistical significativity

to have a very limited role in state transitions [296]. One Lhcb isoform that we found with the highest ΔLogFC is Lhcb5 (also referred to as CP26). Studies in *Chlamydomonas* (where PSII is largely reorganized under state-2 conditions) have shown the participation of monomeric antennae CP26 and CP29 (ΔLogFC 2.2) in state transitions [297][298]; nevertheless involvement of their counterparts in plants has never been evidenced [242]. One interesting case is the Lhcb 3.1 controversy. According to our results, its differential accumulation between stroma-lamellae and BBY in state-1 and state-2 is not negligible (ΔLogFC 2.3, tab.3.2). *Bassi et al., 1988* analysed stroma-lamellae under state-2 conditions and concluded that the Lhcb 3 isoform was essentially absent from this thylakoid sub-compartment [296]. Indeed, Lhcb 3 is a highly enriched in trimer (M)oderate [39] which are not involved in state transitions [296], and lacks of the *N*-terminal phosphorylation site. However, more recent results suggested the contrary and that Lhcb 3 might play a key role in modulating the rate of state transitions. Moreover, *Galka et al., 2012* [242] purified PSI-LHCI-LHCII supercomplex in maize and performed an electrophoresis analysis. After staining with Sypro Ruby, they were capable to identify not-negligible quantity of Lhcb 3. This can be explained by the participation of a few M trimers in state transitions as was

proposed before [299] although the presence of some Lhcb 3 isoform in other trimers than M is still debated [242].

In addition to this we also compared antenna repartition in mutants with respect to WT (data not shown). We observed that, when compared, WT and *stn7* display an almost equivalent antenna distribution. Therefore, according to our proteomic analysis *Arabidopsis* WT seems to be in a state which is quite similar to that of *stn7*(*i.e.* state-1). This seems in contrast with data reported in figure 3.3 in which intact leaves of *Arabidopsis* WT were found in a state more close to state-2 (*i.e. pph1* mutant). Reasons for such a discrepancy can be due to the fact that we did not add any phosphatase inhibitor during the preparation and the conditions in which our fractions are purified essentially promote dephosphorylation of the LHCII and transition to state-1 in *Arabidopsis* WT plants.

In conclusion, our results about the distribution of the different Lhcb isoforms, partially support data previously reported and confirm that Lhcb1 and Lhcb2 are probably the two Lhcb isoforms mostly involved in state transitions. Nevertheless, as shown in table 3.2 p-values do not allow to draw definitive conclusions for most of the Lhcb isoforms.

3.4 Conclusion and perspectives

Other candidate proteins

To move a step forward, we proceeded to a preliminary data mining and we highlighted further interesting proteins. In order to analyse the data we arbitrarily chose not to consider proteins for which ΔLogFC stn7-pph1 was lower than that of Lhcb 4.1 (the antenna isoform with the lowest ΔLogFC stn7-pph1, see tab.3.2). Results of the differentially abundance analysis evidenced that *stn7* and *pph1* have 81 proteins for which the subthylakoids repartition was different between the two genotypes. Among them, 11 proteins are statistically significant and are summarised in figure 3.9 together with their curated function (*Tomizioli et al., 2014*) and thylakoid sub-compartment distribution (LogFc). Unfortunately, when we look to the description and to the function (lanes curated protein description and curated function) there is not a clear and common link between them. One interesting protein is subunit PsaH (At3g16140) of the PSI. As previously seen in section 1.6.1.2, PsaH represents the docking site of LHCII to PSI during state transitions. In the *stn7* mutant, this protein is found to be particularly enriched in stroma-lamellae with respect to *pph1* mutant. Given

that, at the moment of the dissertation, semiquantitative proteomic data is not yet available, we can only speculate that plants devoid of *stn7* might somehow accumulate more PsaH in the stroma-lamellae as direct/indirect response to the missing migration of LHCII from PSII. Moreover, among the 11 proteins in table 3.9, one other interesting candidate seems the PSII subunits PSBP1. However, the presence of a PSBP-Like protein in the list (At3g63540) might reflect a possible problem in distinguishing between true PSII subunits (PsbP) and PsbP-like subunits. These are proteins probably associated to the NDH complex (stroma-lamellae).

Prot.ID	Curated protein description (Tomizioli et al 2014)	Curated function (Tomizioli et al 2014)	LogFc pph1	LogFc stn7	ΔLogFC
AT1G32900.1	UDP-Glycosyltransferase superfamily protein	metabolism carbon	-2,4	-5,9	3,6
AT5G42310.1	PPR-like, Pentatricopeptide repeat superfamily protein;	RNA Binding ?	-2,8	-7,5	4,7
AT3G10690.1	GYRA (GYRBM) DNA gyrase subunit A	DNA Binding	-7,0	-9,2	2,2
AT1G06680.2	PSBP1 polypeptide of oxygen-evolving complex	PS PSII OEE	3,4	1,1	2,3
AT3G59400.1	GUN4 Tetrapyrrole-binding protein	vitamin , chlorophyl and signaling	8,0	5,8	2,2
AT5G42765.1	HP25e conserved plant protein	unknown	4,9	1,4	3,5
AT3G63540.1	PsbP-like (TL19, P19)	PS PSII OEE ?	3,7	-1,9	5,6
AT3G16470.3	Mannose-binding lectin superfamily protein;	lectin	-9,0	-4,9	4,1
AT2G24060.1	Translation initiation factor 3 protein;	translation stroma	-8,2	-3,8	4,4
AT3G16140.1	PSAH-1 Photosystem I reaction center subunit VI-1	PS PSI	1,7	4,9	3,2
AT1G11910.1	APA1 aspartic proteinase A1	chaperone and protease	5,3	8,4	3,0

Figure 3.9 – List of the 11 proteins found to have a statistically different distribution in thylakoid sub-compartments between *Arabidopsis stn7* and *pph1* mutants. Moreover these 11 proteins are characterised by a ΔLogFC stn7-pph1 greater than that of Lhcb1.4 (1.8). A negative value of LogFC indicates particular protein enrichment in the BBY fraction. A positive value of LogFC indicates particular protein enrichment in the stroma-lamellae fraction.

To conclude, as a whole, the data currently available indicate that around 80 chloroplast proteins are probably characterised by a trend in thylakoid repartition between stroma-lamellae and BBY during state transitions. However as mentioned above, statistical analysis does not corroborate this trend for most of them. Indeed, giving the limited extent of state transition in plant (max 15-20 %) together with the background noise of the measure, the number of biological/technical replicates that we performed might not be sufficient to extract fully reliable information. Hence, following steps of the study should firstly focus on increasing the number of biological/technical replicates. More replicates would allow to obtain an enlarged pool of statistically significant results. This will be also supported by the forthcoming generations of more-sensitive mass spectrometers.

Alternatively, a tempting hypothesis to explain the lack of clear differences in protein distribution between *stn7* and *pph1* would invoke the role of

grana-margins. As mentioned in section 1.6.1.2 of this thesis (page 41), it was recently proposed an alternative mechanism to account for state transitions [120]: instead of the sole LHCII being transferred between stroma-lamellae and BBY, there would be protein migrations in two directions: *(i)* movement of PSI-LHCI towards the grana by attractive electrostatic forces and/or by *van der Waals* forces and *(ii)* P-LHCII-PSII movement towards the stroma lamellae due to charge repulsion between adjacent P-LHCII proteins. The meeting point of these complexes would be the margin fraction. (see section 1.5.1 at page 38). According to this model, in fact, we would not be able to see any difference in protein composition of our fractions between BBY and stroma-lamellae in *stn7* with respect to *pph1*. This is explained by the fact that, the site where protein movement takes place during state transitions, is the margin fractions (and not the inner part of the grana disc *i.e.* BBY or the stroma-lamellae). At this purpose, we can hypothesize that analysis of our margin fractions would reveal a differential accumulation of LHCI-PSI/LHCII-PSII when purified from *stn7* and *pph1* mutants. However, we are conscious that this phenomena, even if occurring, might not be detectable in our margins fractions giving that their purity was found to be quite low. To successfully accomplish the analysis, it would be conceivable the development of an improved protocol to obtain highly purified grana-margin fractions. For this purpose successfully implementation of the yeda-press in *Spinacia oleracea* is already reported in literature [120] and would need to be adapted to our model organism *Arabidopsis*.

LTR: photosystem stoichiometry adjustment

Transcript levels of several protein subunits involved in photosynthesis are known to be regulated by photosynthetic redox signals (*i.e.* PQ). For example *Brautigam et al.*[151] demonstrated that, following a change to PSII light, a clear difference is observable in the expression of genes involved in photosynthesis or metabolism between WT and *stn7* plants. Up to 85% of the genes responding to the light shift do not longer respond in *stn7* mutant. This indicates that most of these genes are under STN7-mediated redox control. In this context, our semiquantitative approach based on the spectral counting, is expected to deliver significant insights into this phenomena. During the following steps of the research it will be interesting to compare the stoichiometry of the photosynthetic complexes between WT plants and plants devoid of STN7. It is expected that lack of the specific sensor of the redox-signal would translate into a varied composition of the photosynthetic chain. This varied composition can comprise not only changes at the level of

the whole complex stoichiometry but also at the level of the single subunit composition (*i.e.* LHC).

Seeking for the chloroplast-redox signal messenger toward the nucleus

STN7 kinase is of a key importance in LTR and acts as a sensor and signal transducer [291]. In particular, data on phosphorylation of chloroplast protein kinases (PKs) by other kinases have been obtained from phosphoproteomics studies [300], which support the existence of phosphorylation signalling cascades in the organelle. This would promote the activation/ deactivation of proteins involved in post-transcriptional events both in nucleus and chloroplast. At the moment the mechanisms by which redox signals are transduced to the nucleus are largely not understood. Nevertheless it is conceivable that an unknown protein that is phosphorylated in an STN7-dependent manner could relay the required signal for the LTR. Sensing of the redox signal by STN7, would promote the phosphorylation of this protein kinase *messenger* out of the chloroplast in order to reach the cellular cytosol and to phosphorylate another protein in a phosphorylation-cascade mediated mechanism (figure 3.10).

One approach to investigate this phenomena would take advantage of our semi-quantitative approach based on the spectral counting. In particular it would aim at identifying PKs characterised by a greater accumulation in the chloroplast stroma of *stn7*-plants with respect to *pph1*. These PKs would be in fact stacked inside the chloroplast of *stn7* mutants because STN7 (the sensor/signal transducer) is absent. Practically, the strategy should follow these steps:

- identify the PKs present in the stroma of *Arabidopsis stn7* and *pph1* mutants
- evaluate their relative abundance on a spectral counting-based approach
- evidence interesting differences between the two strains in terms of PKs abundance

However, this phenomenon should be observed in the chloroplast stroma and our purified fractions (stroma-lamellae and BBY) would probably not be the suitable samples for this study. At this purpose, proteomic analysis performed on either intact chloroplasts or stroma, purified from both *Arabidopsisstn7* and *pph1* mutants would be definitely informative. This would be undoubtedly interesting and some possible candidates have already been reported in literature [281]. For example TSP9, a 9 kDa thylakoid

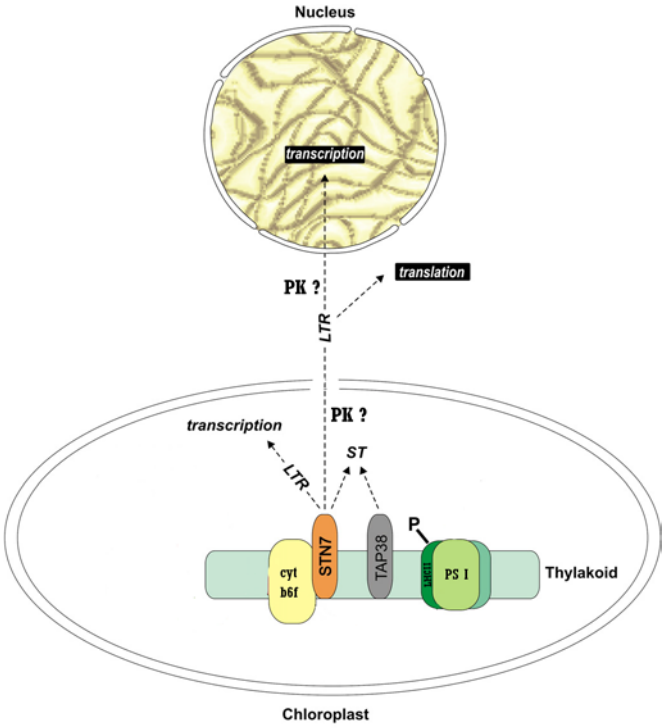

Figure 3.10 – Hypothetical scheme of the stn7-mediated LTR signaling. Adapted from *Pesaresi et al* [281]

soluble phosphoprotein, has been suggested to be a component of the redox-dependent signaling cascade due to its mobile nature [301].

To conclude, plastids are essential organelles because they contribute to primary and secondary metabolism and plant signaling networks. A high-quality inventory of the plastid proteome is therefore a critical tool in plant research. Despite significant efforts by many laboratories, the coverage of the plastid proteome is far from complete. In our current study, we targeted specific plastid structures (chloroplasts) and associated sub-structure (thylakoid sub-compartments) to successfully improve coverage. Moreover we paved the way for direct comparison of the proteomes of different knock-out mutants in order to understand protein functions and dynamics.

Semiquantitative proteomic analysis of *Arabidopsis* WT and state transition mutants delivered in this thesis project produced a huge quantity of data. Because of its nature, MS-MS data, needed to be carefully mined, and semi-automated mathematical approaches (as protein clustering) seems a promising way to dramatically reduce the complexity of the information

and at the same time to obtain statistically-significant results. According to our experience, even if these mathematical approaches proved to be of an inestimable help in our research they can never prescind from a deep and solid knowledge of the biology discipline; wrong interpretations or biological non-senses are always behind the corner. At the moment we are just at the front-door of data exploitation and the most exciting results are expected to come in the near future.

3.5 Materials and methods

Plant growth conditions. *Arabidopsis thaliana* (ecotype Columbia, Col-0) WT, *stn7* and *pph1* mutants were grown in culture chambers at 22°C with a light intensity of 100 μmol m^{-2} s^{-1} (10-h light cycle) for 5 weeks before harvesting.

Purification of intact chloroplasts and thylakoid sub-compartments. Purification of intact chloroplasts and thylakoid sub-compartments were performed according to *Tomizioli et al., 2014* [139].

SDS-PAGE and Western blot analysis. Proteins were separated by SDS-PAGE as described by Chua [260]. For Western-blot analyses, proteins were transferred to a nitrocellulose membrane (BA85, Schleicher and Schuell, Whatman) which was blocked with 5% (w/v) dried-milk in Tris-buffered saline (TBS) containing 0.5% (v/v) Triton X-100. To assess the purity of the samples, antibodies raised against proteins associated to specific chloroplast sub-compartments were used: PsaD (stroma-lamellae marker, Agrisera) at a 1:3000 dilution, CP43 (BBY marker) at a 1:10,000 dilution, PHT4;4 (chloroplast envelope marker) at a 1:1,000 dilution. To perform phosphorylation test, antibody raised against phosphorylated threonine residues (agrisera) at a 1:40,000 dilution was used.

Fluorescence kinetics. Fluorescence kinetics were measured in intact leaves using a JTS-10 spectrophotometer used as fluorimeter. The experiments presented in figures 3.1 and 3.2 were performed using plants incubated for 30 min in the dark. Illumination was supplied with red light (625 nm) to preferentially excite PSII or with a combination of red and far-red lights to excite both PSII and PSI. The detection beam was provided by a white LED source.

77K fluorescence emission 77K fluorescence emission spectra were recorded as in *Tomizioli et al., 2014* [139].

Proteomic analysis Protein digestion, nano-LC-MS/MS analyses, database searching, data processing, data normalisation and statistical analysis of differential abundance were carried out according to *Tomizioli et al., 2014* [139].

Chapter 4

A thylakoid-located two-pore potassium channel regulates photosensitivity in higher plants

4.1 Preface

The article presented in this chapter (*Carraretto et al., 2013*) represents a secon study issue during my Ph.D project. The work is part of a collaboration instaurated between our laboratory and the research team directed by doc. Ildikó Szabó at the University of Padua (Italy).

The project is focused on the characterisation of TPK3, a putative channel selective for potassium (K^+) wich was predicted to localise in the chloroplast of higher plants, from biochemical, physiological and electrophysiological point of view. TPK3 belongs to the TPK channel family (from Tandem-Pore K^+ channel) and according to homology with another K^+ channel from cyanobacteria (SynK,[265]), it was hypothesized to be involved in the regulation of photosynthetic processes in higher plants. In order to study the physiological role of TPK3, *knock out* mutants were produced by RNA interference. The resulting *tpk*3-silenced plants were studied under different

growth conditions to determine changes in physiology of the plants including their photosynthetic parameters. My contribution in the project concerned the sub-thylakoid localisation of TPK3 and its biophysical characterisation (ECS measures).

The chapter is organised in two sections. In the first section (section 4.2) I will give a short introduction about potassium channels and some preliminary concepts for those who might not be familiar with the subject (*i.e.* proton motive force, $\Delta\Psi$, ΔpH). Moreover, I will deliver major details about the ECS techniques which were employed in *Carraretto et al., 2013* in order to estimate the proton motive force composition. In the second section (section 4.3), the article *Carraretto et al., 2013* is presented; supplemental figure are also available on line at `http://www.sciencemag.org/content/342/6154/114/suppl/DC1`. Finally, in the third section (section 4.4) I will introduce some further aspects that were developed after the publication of the paper. They mostly concern the regulation of the STN7-dependent LHCII phosphorylation in *tpk3* mutants.

4.2 Introduction

4.2.1 The proton motive force : ΔpH and ΔΨ

Photosynthetic electron transport triggers the translocation of protons into the thylakoid lumen which generates a pH gradient (ΔpH). This pH gradient is accompanied by the development of an electric field between the stroma and the thylakoid lumen of the chloroplast (ΔΨ). The ΔΨ is mainly due to the electron transport across the thylakoids (catalyzed by charge separation in PSI and PSII, and by electron flow in the *low potential* chain of the cytochrome b_6f complex during the Q cycle) promotes the development of an electric field. Both ΔpH and the ΔΨ contribute to the electrochemical proton gradient (or proton motive force, pmf) gradient, which is consumed for ATP synthesis from ADP by the CF_0-CF_1 synthase. This *pmf* used to synthesize ATP is the sum of the ΔΨ and ΔpH given by equation 4.1 where where $\Delta\Psi_{i-o}$ and ΔpH_{o-i} represent the electric field and the difference in pH, respectively, calculated as outside (stroma) minus inside (lumen), R is the universal gas constant, T is the temperature and F is Faraday's constant.

$$pmf = \Delta\Psi_{i-o} + \frac{2,3RT}{F}\Delta pH_{o-i} \tag{4.1}$$

In mitochondria, the *pmf* is stored mainly as ΔΨ, due to the low permeability of the mitochondrial inner membrane to ions, with a pH contribution of ∼0.5 pH units [302]. By contrast, in chloroplasts, *pmf* is thought to be stored mainly as ΔpH rather than ΔΨ. However, these conclusion are derived from *in vitro* experiments, and have not yet been fully confirmed *in vivo* (for details see [303]). The experimental approach used for this PhD project to monitor the size and composition of the *pmf* is the electrochromic shift (or ECS). This consists in a shift of the spectrum of the photosynthetic pigments, which is linearly related to the generation of the ΔΨ [304]. This feature is extremely interesting because a linear ECS signal is an intrinsic membrane voltmeter, which rapidly responds to changes in the membrane potential, ultimately revealing the features of electron and proton flow in the thylakoids. For example, upon exposure of photosynthetic samples (membranes, cells or leaves) to repetitive single turnover flash spectroscopy [305], several phases can be seen in the ECS signal (see figure 4.1), when measured at appropriate wavelengths. A first phase, faster than 100 μs, is reflecting photochemistry performed by the photosystems. Cytochrome b_6f activity appears as the second phase, which is slower, and occurs in the range of the milli-seconds [306], because electron transfer catalyzed by this complex is much slower that primary photochemistry. After completion of this phase, a decay phase

is seen [306], which represents *pmf* dissipation by H^+ flux through the ATP synthase complex. Under continuous illumination, this decay phase can be exploited to evaluate (at least qualitatively) the two components of the *pmf*.

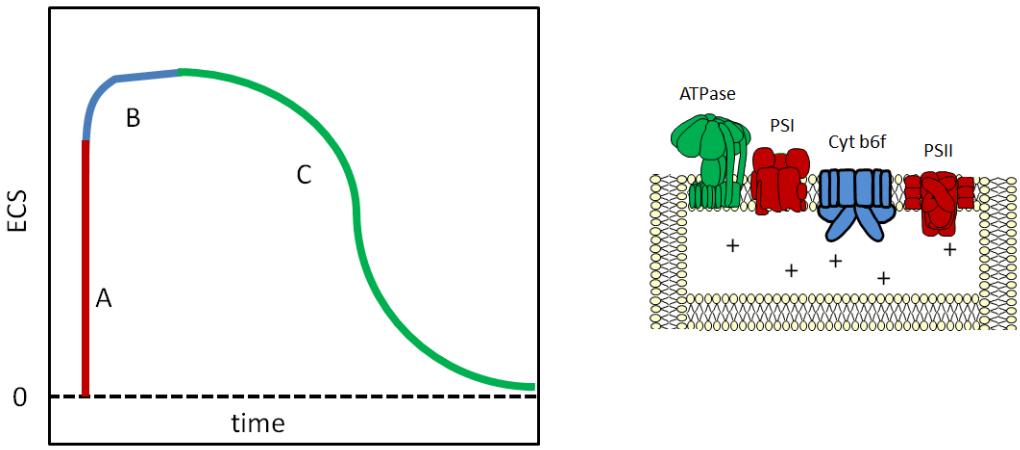

Figure 4.1 – Kinetics of the ECS upon excitation with a saturating laser pulse. The A fast rise phase corresponds to PSI and PSII charge separations, B phase corresponds to electron flow in the cytochrome b chain of the cytochrome b_6f. The ECS decay C phase is due to charge leakage through the membrane, mainly H^+ via the ATP-synthase. Adapted from *Bailleul et al* [304]

In particular, after the initial decay, related to H^+ flux, a slower rise component is seen, which leads to an inversion of the ECS signal (see figure 4.2). This inversion has been interpreted in terms of a different relaxation rate of the two components, the ΔpH relaxing much slower than the $\Delta\Psi$ due to the high buffering capacity of the lumen and the slow rate of charge redistribution along the membranes [307][308][309]. This would lead to a transient inversion of the membrane potential, to compensate for the presence of a buffered ΔpH, during the first phase (positive). During the second phase (negative), the slow relaxation of the ΔpH would lead to a readjustment of the $\Delta\Psi$, accounting for the slow negative phase of the ECS signal until a dark equilibrium state is reached (see [303] for further discussion). According to this hypothesis, the relative amplitude of the positive and negative phase of the ECS signal would be proportional to the relative size of the $\Delta\Psi$ and ΔpH, respectively (figure 4.2).

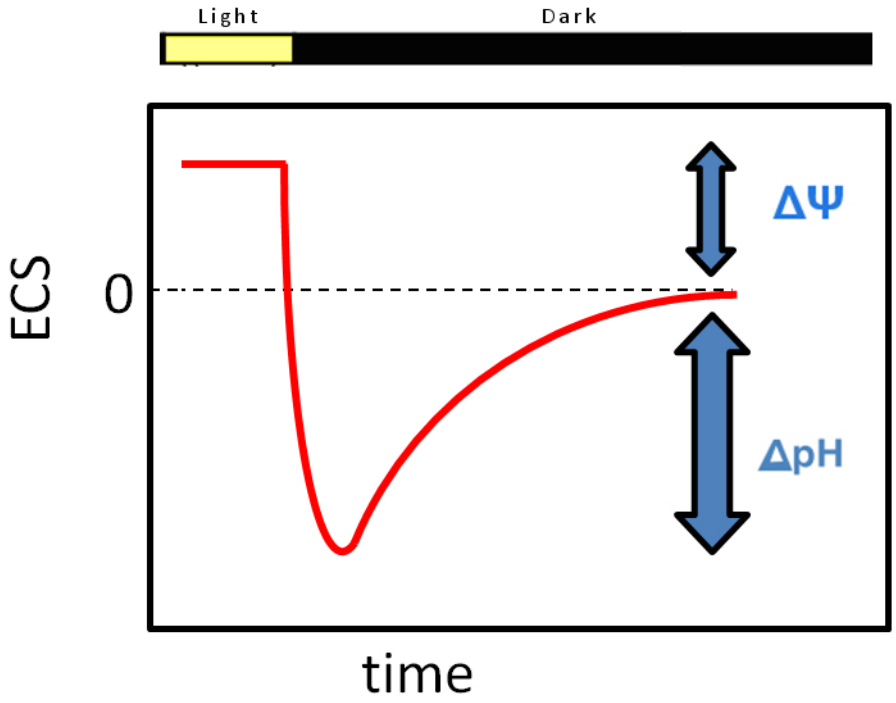

Figure 4.2 – ECS kinetics. After switching the light off, a fast decay followed by a slower rise phase are seen, which have been interpreted in terms of the different rates of relaxation of the two components of the *pmf* ($\Delta\Psi$ and ΔpH, blue arrows) and lead to an inversion of the ECS signal. Black and yellow bars represent dark and light phases, respectively. Image adapted from *Bailleul et al* [304]

4.2.2 Ion channels are involved in *pmf* control

Proton pumping into the thylakoid lumen during light-phase of the photosynthesis is associated to the release of Mg^{2+} from the thylakoid membrane into the stroma. This increase in Mg^{2+} concentration not only promotes the activity of several enzymes but also improves ATP and NADPH synthesis by controlling thylakoid stacking [50]. Despite the key role of Mg^{2+} in the control of photosynthesis, the transporters involved in its translocation across the thylakoid membrane are at the moment poorly characterized. Beside Mg^{2+}, an other major ion playing a key role in photosynthesis is potassium. Potassium (K^{+}) is the most abundant ion present in the cytosol of the cells.

Unlike other cations, concentrations of K^+ does not interfere with the structures and reactions of macromolecules such as DNA, RNA and proteins in aqueous solutions. The consequence of this abundance of K^+ (and its counterions glutamate, organic phosphates) is that it serves as the main osmolar component inside the cell. Biological membrane can regulate the difference in K^+ concentration between its two sides essentially with three types of proteins: *(i)* pumps, which hydrolyse ATP to move ions against gradient, *(ii)*, exchangers, which use gradient of other ions and *(iii)* ion channels, which are pores through which ions can diffuse following their electrochemical gradient. The electrochemical gradient of K^+ through the membrane is expressed in equation 4.2

$$\Delta\mu K^+ = F\Delta\Psi + RT \ln \frac{[K^+]_{in}}{[K^+]_{out}} \tag{4.2}$$

where $\Delta\Psi$ is the membrane potential (for example, the electric potential of the lumen respect to the stroma), F is the Faraday constant, R is the gas constant and T is the temperature. Ion channels allow the flow of more than a million ions per second from one side to the other of a biological membrane. K^+ channels are tetramers, generally consisting of identical subunits called α subunits which constitute the channel. α subunits are associated to other auxiliary subunits (β,γ, etc..) which serve to regulate the main α subunits. In *Arabidopsis*, 15 putative K^+ channels were identified so far and they can be classified into three different groups: Shaker, Kir and TPK. Shaker channels have six transmembrane segments and, in *Arabidopsis*, 9 proteins belonging to the Shaker family were characterised and divided into three subfamilies depending on their rectification properties: inward, outward and weakly inward rectifier [315]. The available information suggests that these channels are involved in nutrition and regulating the osmotic state of the cell. Kir channels are characterised by a hydrophobic core consisting of only two segments and a transmembrane P domain [316] and were observed in root plasma membrane. Plant TPK channels have a hydrophobic core consisting of four transmembrane segments containing two P domains. At the moment, 5 TPK channels have been identified in *Arabidopsis*, AtTPK1/5. Channels of the TPK family are characterised by a duplicated structure with four transmembrane domains and two-pore domains. TPK channels were proposed to form dimers consisting of two identical subunits [317]. There is still a huge gap in knowledge about the physiological roles of TPK channels in plants. Nevertheless some information can be obtained from the homologous channels in mammalians where they act in concert with other membrane transporters and play key roles in fine-tuning of the resting membrane potential and cell excitability. By analogy, it might therefore be speculated that

plant TPKs are also targets of external and internal *stimuli* to fine-tune the electrical properties of the membrane (mostly the tonoplast) for specialized transport tasks. Among the five AtTPKs, activity and physiological roles are only available for AtTPK1 and AtTPK4 [318][319][322]. So far, no information is available about the properties of AtTPK3, nor about its physiological roles and its possible involvement in photosynthesis. In the article presented in the next section, the biochemical and electrophysiological characterisation of AtTPK3 channel and its possible involvement in the regulation of photosynthesis in higher plants is presented for the first time.

4.3 A Thylakoid-Located Two-Pore K^+ Channel Controls Photosynthetic Light Utilization in Plants

Luca Carraretto[1], Elide Formentin[1], Enrico Teardo[1], Vanessa Checchetto[1,2,3,4,5], Martino Tomizioli[2,3,4,5], Tomas Morosinotto[1], Giorgio Mario Giacometti[1], Giovanni Finazzi[2,3,4,5]‡, Ildiko Szabo[1]‡

1-Department of Biology, University of Padua
2-Laboratoire Physiologie Cellulaire et Végétale
3-iRTSV, CEA Grenoble
4-Université Grenoble Alpes
5-Institut National Recherche Agronomique
‡ To whom correspondence should be addressed: E-mail: `ildiko.szabo@unipd.it` and `giovanni.finazzi@cea.fr`

Abstract

The size of the light-induced proton motive force (*pmf*) across the thylakoid membrane of chloroplasts is regulated in response to environmental *stimuli*. Here, we describe a component of the thylakoid membrane, the two-pore potassium (K^+) channel TPK3, which modulates the composition of the *pmf* through ion counterbalancing. Recombinant TPK3 exhibited potassium-selective channel activity sensitive to Ca^{2+} and H^+. In *Arabidopsis* plants, the channel is found in the thylakoid stroma-lamellae. *Arabidopsis* plants silenced for the TPK3 gene display reduced growth and altered thylakoid membrane organization. This phenotype reflects an impaired capacity to generate a normal *pmf*, which results in reduced CO_2 assimilation and deficient non-photochemical dissipation of excess absorbed light. Thus, the TPK3 channel manages the *pmf* necessary to convert photochemical energy into physiological functions.

In plants, photosynthesis converts light energy into organic carbon through the transient production of highly reactive intermediate species. Nevertheless, damage to the plant cell engine is limited because the production of reducing equivalents via the electron flow (NADPH) is commensurate with energy production (ATP) for CO_2 assimilation [323]. The key element bridging the two processes is the transmembrane electrochemical proton gradient or proton motive force (*pmf*) [305], which is produced by electron transfer. The *pmf* supports ATP synthesis [305], controls the rate of electron flow [photosynthetic control [324]] and enhances the thermal dissipation of excess absorbed light (non-photochemical quenching, NPQ [325]). While both components of the *pmf* (the proton gradient, ΔpH, and the electric field, $\Delta\Psi$) are equally necessary for ATP synthesis [305], the ΔpH specifically regulates photosynthetic control and NPQ by modulating both the protonation state of key regulatory proteins (PsbS) [326] and the rate of electron flow in the cytochrome b_6f complex [324]. It is therefore assumed that the size of the ΔpH must be regulated in response to environmental *stimuli* through a still elusive mechanism [327]. The present work identifies a new component of thylakoid membranes, the two-pore potassium channel TPK3, which regulates the transmembrane proton gradient through ion counterbalancing in the thylakoid membrane and, thus, controls the nature of the *pmf*.

The plant TPK channel (Tandem-Pore K^+ Channel) family represents the counterpart of the animal leak TWIK/TREK channels [333]. Among the 5 members of this family, AtTPK1 of *Arabidopsis* was the first to be identified through in silico searches. Vacuolar TPK1 affects germination, seedling growth and stomatal movement [319] by mediating intracellular K^+ homeostasis [320][321]. AtTKP4, which is targeted to the plasma membrane, is a voltage-independent, open rectifier, calcium and proton-sensitive K^+ channel [322]. The biophysical properties and physiological role of AtTPK2/3/5 [317][328][329] remain unknown. However, pore domain-swapping experiments have highlighted a similar selectivity and instantaneous activity of chimeric channels (between AtTPK2/3/5 and AtTPK4) compared to TPK4 [330]. AtTPK1/2/5 restored growth of K^+ uptake deficient *E. coli* mutant [331].

Activity of AtTPK3 was evaluated in planar lipid bilayer experiments using recombinant purified AtTPK3, given that patch clamping of the *Arabidopsis* thylakoid membrane was not feasible. The apparent molecular weight (51 kDa) of AtTPK3 expressed in *E. coli* as a fusion protein with an N-terminal His6-TAG is in good agreement with the predicted weight (54 kDa) (fig.4.3A). The eluted protein was recognized by both an anti-TPK3 monoclonal antibody [332] and a more general antibody raised against the highly conserved selectivity filter region of K^+ channels (fig. 4.3B), indicating suc-

cessful purification of AtTPK3. Channel activity was recorded in symmetric potassium gluconate solution (250 mM), in the presence of calcium, using gluconate as an impermeant anion (fig.4.4A).

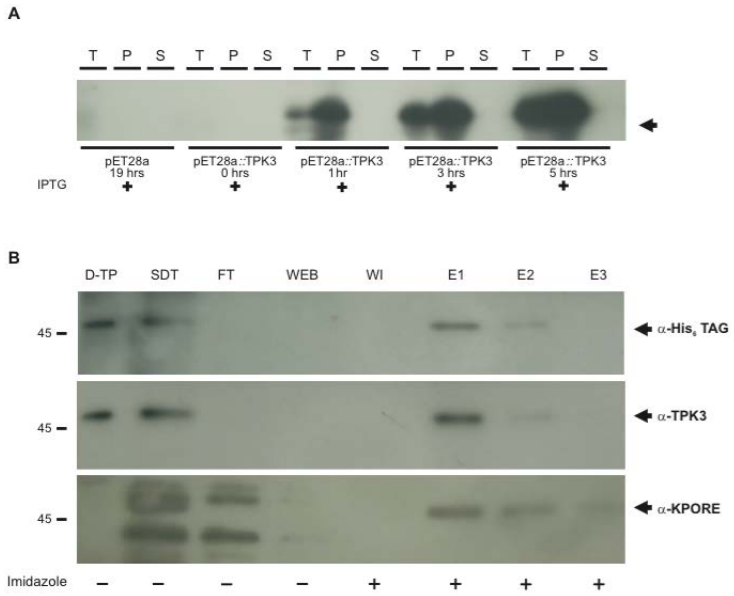

Figure 4.3 – **Expression and purification of the AtTPK3 protein from *E. coli*** A) Expression of AtTPK3 in *E. coli* C41(DE3) cells, Western blotting and immunodetection with anti-His6 TAG antibody (T: entire bacteria; P: pellet after sonication; S: supernatant after sonication). The first set represents bacteria transformed with the empty pET28a vector and induced for 19 hours as a negative control. The other 4 sets represent bacteria transformed with the pET28a::TPK3 vector and induced for 0, 1, 3 and 5 hours. For induction, IPTG was added (final concentration, 700 μM) to the cell culture at OD_{600} = 0,800. B) Purification of recombinant AtTPK3 expressed in *E. coli*, followed by Western blotting and immunodetection with anti-His6 TAG antibody, monoclonal anti-TPK3 serum and anti-KPORE antibody (D-T P: detergent-treated pellet following sonication; SDT: supernatant from the detergent treatment; FT: column flow-through; WEB: column washing with equilibration buffer; WI: column washing with 5 mM imidazole; E1, E2, E3: fractions eluted in 250 mM imidazole). AtTPK3 (51 kDa) is indicated with arrows.

The current-voltage relationship (i-V curve) yielded a conductance of 35 pS (fig.4.5A). Measurements performed in asymmetric ionic conditions (500/100 mM KCl, fig. 1B) led to the generation of an i-V curve (fig.4.5B) yielding a reversal potential (Erev) of -28 mV (the theoretical Erev for a perfectly selective K^+ channel is -36 mV), confirming a preference for potassium versus chloride. In accordance with the presence of an EF hand in the

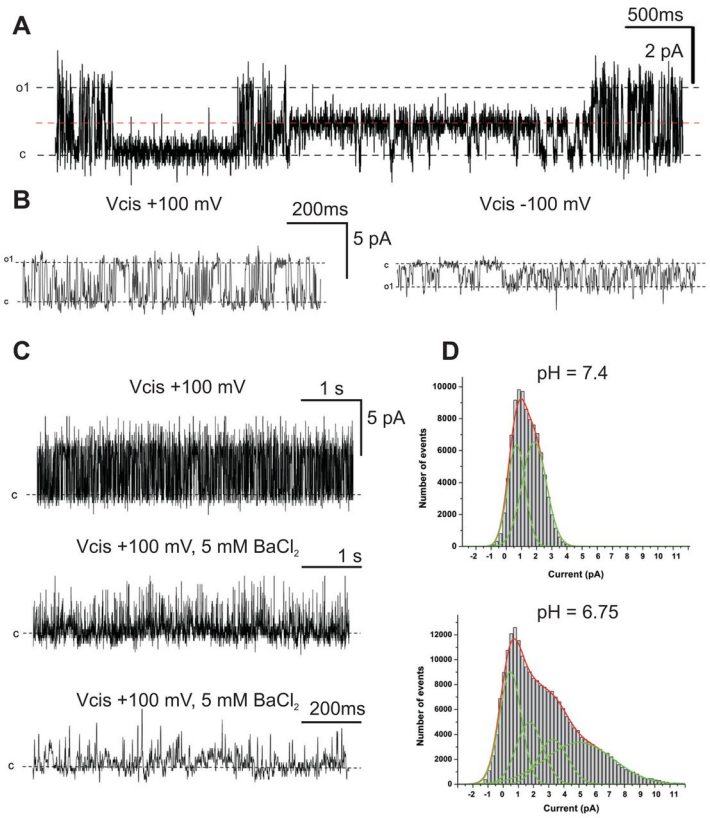

Figure 4.4 – Recombinant TPK3 induces barium-sensitive channel activity in planar lipid bilayers. (A) Representative current trace showing the transition to a half-conductance substate (red line) recorded at 100 mV in 250 mM K gluconate. (B) Current traces recorded in an asymmetric KCl solution at the indicated voltages (cis: 500 mM KCl; trans: 100 mM KCl). The open probability was 0.65 at -100 mV and 0.57 at + 100 mV (from 120-s trace). (C) Ionic conditions are as in B). The addition of 5 mM Barium to the cis side resulted in a fast block of the activity (middle trace). The lower trace indicates the activity on an extended time scale. Closed state is indicated by dashed line. (D) Decreasing the pH from 7.4 to 6.75 increased activity, as observed from the amplitude histograms, obtained from current traces recorded in symmetrical K gluconate at +50 mV. Fitting was done using the Origin software. Peak values yield conductance values in the range of 29-35 pS. All of the presented data are representative of at least 4 experiments

protein, calcium was required for channel activity (fig.4.5C). Studies with classical potassium channel inhibitors confirmed the nature of AtTPK3. Barium added to the cis side resulted in a fast block at a 5 mM concentration (fig.4.4C), while 50 mM tetraethylammonium (TEA+) did not affect channel activity (fig.4.5D). AtTPK1 can be activated by protons [319]. Activity

of AtTPK3 also increased upon acidification of the cis compartment, as indicated by an increased current level in the resultant amplitude histogram (fig.4.4D). Overall, the main biophysical properties of the AtTPK3 activity are in accordance with those of two-pore potassium channels [319][333].

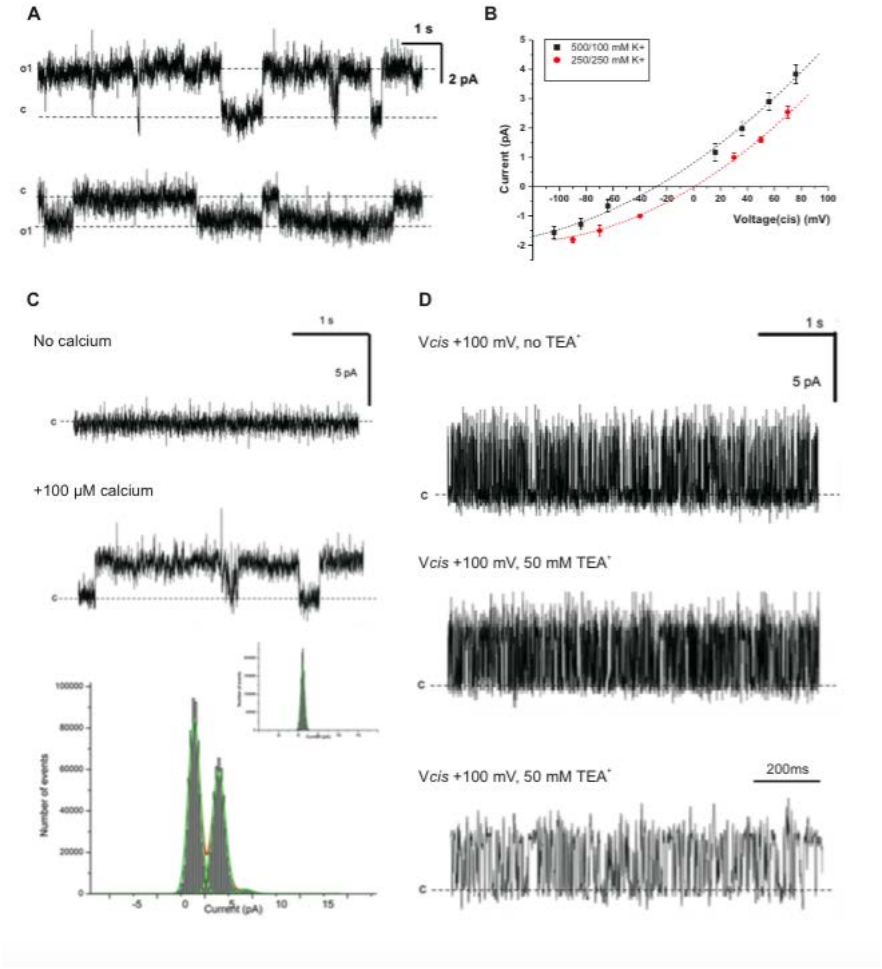

Figure 4.5 – **Selectivity of TPK3 and sensitivity to calcium and TEA+**. A) Representative activity at + and - 80 mV (upper and lower traces, respectively) recorded in 250 mM K gluconate in the presence of 100 μM calcium. B) Single-channel i-V curves obtained from different experiments under symmetric (red) and asymmetric (black) ionic conditions (mean value ± S.D., n greater equal 50 from 3 different experiments). Mean currents ± S.D. are shown. Fitting revealed a chord conductance of 36.4 pS. C) Current recordings before (upper trace) and after (lower trace) the addition of 100 μM calcium to the cis side. Vcis = 80 mV. Lower panel: the associated amplitude histograms (inset: without calcium). Similar results were obtained in 7 other experiments. D) Channel activity in the absence (upper trace) and presence (lower two traces) of 50 mM TEA+. A lack of inhibition was confirmed in 3 other experiments.

Using an AtTPK3::DsRed2 fusion protein, we localise AtTPK3 in the chloroplast of *Arabidopsis* leaves (fig. 4.6A) and sub-chloroplast localisation in wild type (WT) plants by immunoblotting with anti-TPK3 antibody revealed that this protein is located in the stroma lamellae (fig. 4.9A and **??**B), the same compartment where the chloroplast H^+ carrier (the ATP synthase CF_0F_1) is found. To investigate the physiological role of AtTPK3, *Arabidopsis* knock-down (KD) lines were generated because knock-out t-DNA insertion lines could not be found in existing mutant banks [332].

Three genetically independent lines were obtained where silencing of the gene was confirmed by transcript analysis (fig. 4.7A) and Western blot of thylakoids (fig. 4.7B). WT and silenced seedlings grown on agar plates did not show any differences in germination (fig.4.8).

Silenced plants grown in soil under a light regime consisting of a light-dark 12:12 photoperiod at a light intensity of 40 μmol photons m^{-2} s^{-1} showed no difference with respect to WT (fig.4.9B), ruling out any detrimental effect of the silencing construct and of the applied procedure. However, when the light intensity was increased to 90 μmol photons m^{-2} s^{-1}, the silenced plants exhibited a decreased rosette size (fig.4.9 and fig.4.10, A and B) and an enhanced accumulation of anthocyans (fig.4.10C) but comparable contents of other photosynthetic pigments (table S1) compared to WT.

No significant differences were found between WT plants and plants that were subjected to the same transformation protocol but were not completely silenced (figs.4.7A and 4.11A).

In silenced AtTPK3 plants, no change in the thylakoid structure was observed at 40 μmol photons $m^{-2}s^{-1}$, while the organization of the photosynthetic membranes was compromised in all three silenced lines under a light intensity of 90 μmol photons $m^{-2}s^{-1}$ (fig.4.9C and fig. S7B). This thylakoid disorganisation could reflect an altered composition of the photosynthetic chain. However, we found no differences at the level of the main components of the photosynthetic apparatus, including Photosystem (PS) I, PSII, the ATP synthase and the cytochrome b_6f complexes (fig.4.12A). Non-denaturing Deriphat PAGE [335] analysis of thylakoids solubilized with 0.6% α-dodecyl-maltoside confirmed the intactness and the similar relative abundance of the photosynthetic complexes and supercomplexes in the different genotypes (fig.4.12B). We note, however, that the phosphorylation pattern of photosynthetic membranes in the light was different in WT and silenced plants lines at 90 μmol photons $m^{-2}s^{-1}$ (fig.4.12C).

The observed mutant phenotype should stem from changes in the photosynthetic activity rather than from differences in the thylakoid protein composition. Because of the central role of the *pmf* in regulating light utilization in oxygenic photosynthesis and its potential sensitivity to changes in

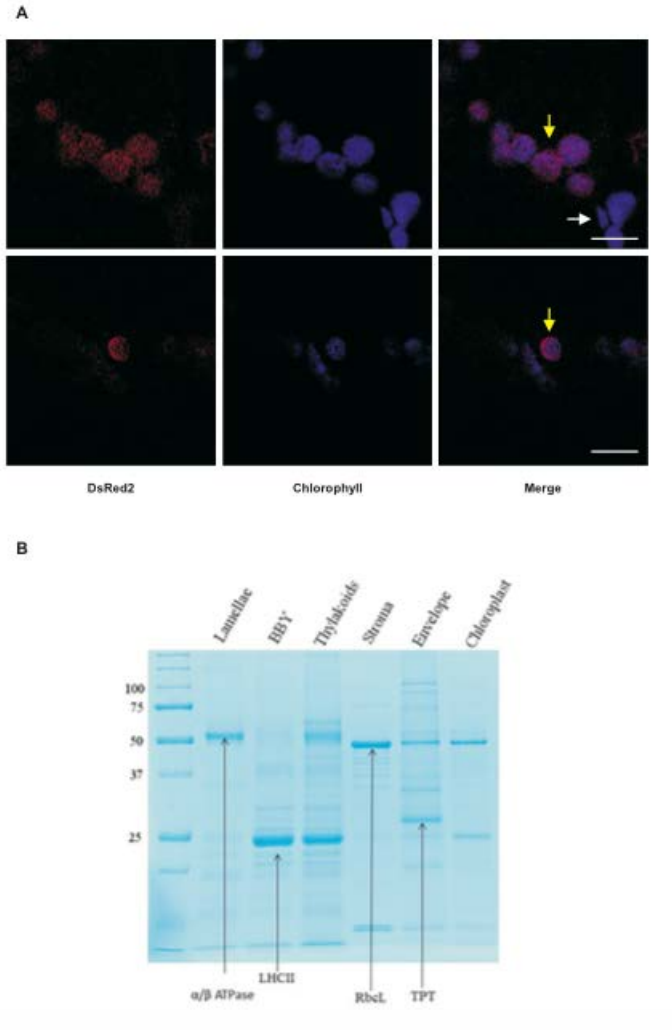

Figure 4.6 – **TPK3 is located in the chloroplast of *Arabidopsis* cells.** A) Localisation of AtTPK3 in chloroplasts. Co-localisation with chloroplasts was confirmed by merging the images of DsRed2 fluorescence and chlorophyll autofluorescence obtained from intact agro-infiltrated *Arabidopsis* leaves. Left panel: DsRed2 signal; middle panel: chlorophyll signal; right panel: merged image. Yellow arrows indicate the AtTPK3::DsRed2 fluorophore in chloroplasts, and the white arrow indicates non-transformed chloroplasts. Bars: 7.5 (upper) and 10 (lower) μm. Images of the upper and lower row were obtained from two different agro-infiltrated leaves. B). Coomassie blue staining of fractions isolated from intact chloroplast of *Arabidopsis thaliana*. The position of the major bands in the lamellar, BBY (inner grana fraction), thylakoid, stroma, envelope and intact chloroplasts fractions is indicated. α/β ATPase: ATP synthase CF_0F_1; LHCII: Light Harvesting Complexes II; RbcL: large subunit of RuBisCo; TPT: Triose Phosphate Transporter

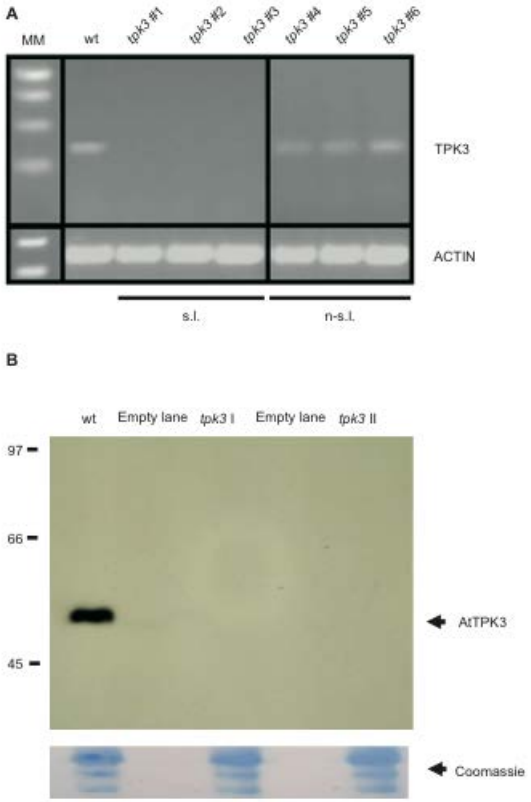

Figure 4.7 – **Stable silencing of the TPK3 gene results in a lack of TPK3 protein in thylakoid membranes.** A) PCR amplification of cDNA retro-transcribed from total RNA extracted from wt and 6 putative silenced lines for the TPK3 messenger. The band corresponding to the TPK3 messenger is visible in wt plants and in tpk3 ln 4, ln 5 and ln 6 (non-completely silenced lines, n-s.l.). In contrast, this mRNA band is absent in *Arabidopsis* lines tpk3 ln 1, ln 2 and ln 3 (silenced lines, s.l.). Amplification of actin as a control is also shown (1^{st} lane: molecular markers). B) Western blotting and immunodetection of thylakoid fractions from wt and TPK3-silenced lines using monoclonal anti-TPK3 serum. The amount of total protein per lane is 200 μg. To show comparable loading, the membrane was coloured with Coomassie (GelMate Blue, Euroclone). Experiments were repeated 3 times.

ion fluxes, we addressed possible differences in the *pmf* arising as a consequence of the mutation. We compared WT and mutant lines grown at a light intensity of either 40 or 90 μmol photons $m^{-2}s^{-1}$, taking advantage of the relationship between the $\Delta\mu H^+$ and the electrochromic shift (ECS). This signal stems from a shift in the absorption spectrum of specific pigments embedded in the thylakoid membranes upon exposure to the electric field

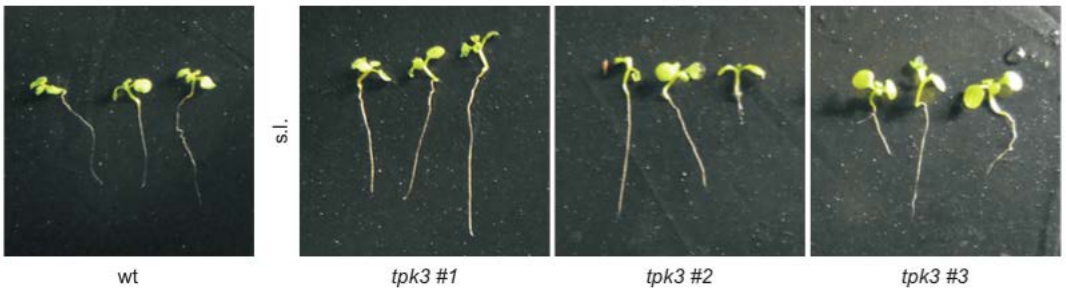

Figure 4.8 – **Agar plate-germinated 2-week-old seedlings of the wt and silenced (s.l.) lines for the TPK3 messenger.** No differences in germination were observed in any of the genotypes. Representative photos are shown.

component ($\Delta\Psi$) of the *pmf* due to the Stark effect [305]. Under continuous illumination, the extent of the ECS signal (fig.4.13A) reflects the amplitude of the proton motive force (19).

Moreover, the rapid decay in the signal reflects H^+ leakage through ATP synthase ($g_H{}^+$), which can be evaluated by fitting the kinetics with a first-order decay (fig.4.13A and B, red lines). On a longer time scale, an inversion of the ECS is seen, which has been interpreted as a transient inversion of the membrane potential to compensate for the slower relaxation of the ΔpH [309]. Thus, the amplitude of this inverted signal can be taken as an indicator of the size of the light-stimulated proton gradient. Again, no differences were found between the two genotypes under low light. However, under a higher light intensity, the putative amplitude of the ΔpH and the proton conductivity of the membranes ($g_H{}^+$) were reduced in the silenced plants (fig.4.13B) while the overall size of the *pmf* was only slightly diminished. The consequences of the mutation were similar to those induced by the H^+/K^+ exchanger nigericin (wine-colored circles in fig.4.13A), which was used here as a control to fully suppress the ΔpH without affecting the $\Delta\Psi$. The moderate effect on the $g_H{}^+$ in the silenced lines corroborates the notion that both the ΔpH and the $\Delta\Psi$ are able to fuel the H^+ flux through the ATP synthase [305]. Indeed, while the relative amplitude of ΔpH and the $\Delta\Psi$ is very different between WT and the silenced the lines, their sum is weakly decreased in the silenced plants. This likely explains the moderate effect of the lack of the channel on $g_H{}^+$.

We conclude that *tpk*3-silenced plants exhibit a reduced (although not abolished) capacity to generate a proton gradient, while maintaining a higher electric potential in light than in the WT. This result suggests that the

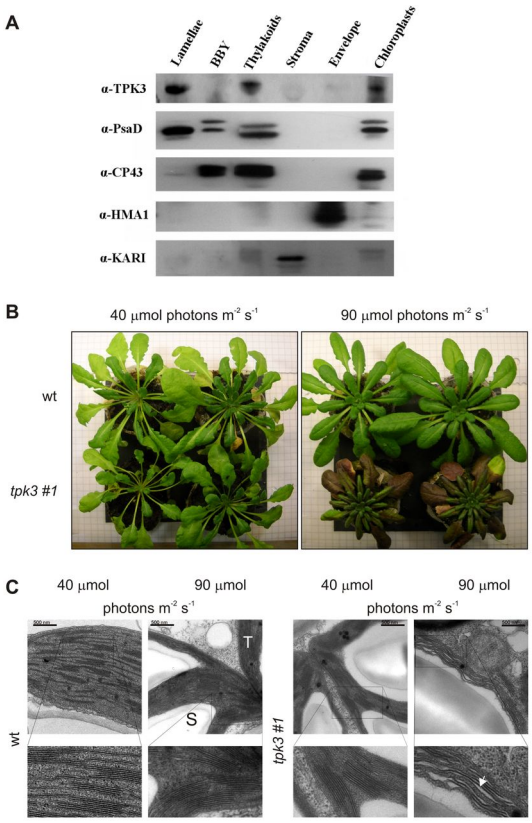

Figure 4.9 – TPK3 is located in the stromal lamellae of thylakoid membranes, and modulates growth and thylakoid ultrastructure. (A) Subchloroplast localisation of TPK3. The lamellar, BBY (inner grana fraction), thylakoid, stroma, envelope fractions (3 μg of total protein/lane was loaded) were purified form intact chloroplast isolated from WT *Arabidopsis* leaves and probed using a specific monoclonal antibody raised against TPK3. The purity of these fractions was tested using antibodies against proteins known to be mostly localised in the inner part of the grana (BBY, PSII CP43), in the stromal lamellae (PSI PsaD) [334], in the chloroplast envelope (HMA1) or in the stroma (KARI) (see supplementary mat). (B) Representative features of WT and *tpk3*-silenced plants, grown under a light intensity of 40 or 90 μmol photons m^{-2} s^{-1}. Rosette size was significantly different between WT and silenced plants at the higher light intensity (see also fig. S6B). (C) The microscopic phenotype of WT and *tpk3*-silenced lines. Electron microscopy images of 6-week-old plants grown at the indicated light intensities. *tpk3*-silenced plants showed abnormal thylakoid structures (arrow) only when grown at the higher light intensity. T: thylakoid membrane; S: starch. Bars: 500 nm.

TPK3-mediated K^+ efflux from the lumen is required for the regulation of the transmembrane electrical potential, the enhancement of the pH gradient for ATP synthesis, the regulation of electron flow, and pH-mediated photo-

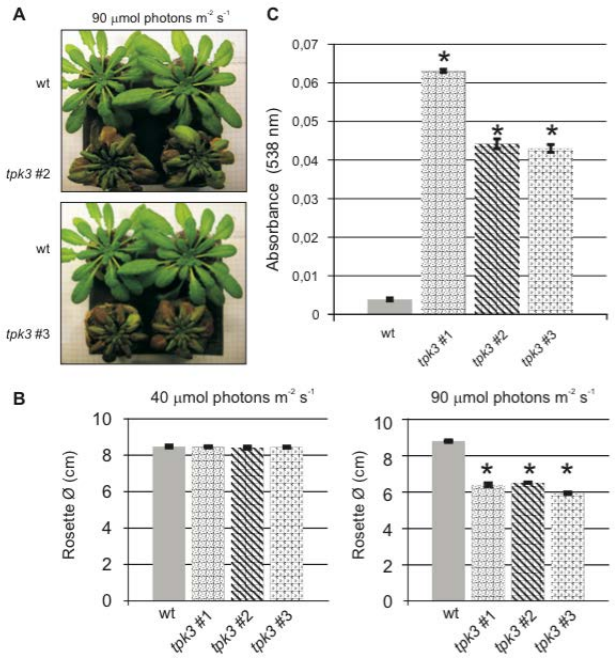

Figure 4.10 – **Plants in which TPK3 is silenced grown at a light intensity of 90 μmol photons m^{-2} s^{-1} show a reduced growth rate and increased anthocyanin content.** A) Representative photographs of the wt and two TPK3-silenced lines. B) Comparison of the rosette dimensions of wt and TPK3-silenced plants. At 40 μmol photons m^{-2} s^{-1}, there are no significant differences in rosette diameter observed, whereas at 90 μmol photons m^{-2} s^{-1}, rosette dimensions are reduced (n = 5 plants per genotype). Asterisks show statistically significant differences (p lower than 0.05) between wt and silenced plants. C) Anthocyanin absorbance value / 10 μg of isolated thylakoids. Anthocyanin content in the aqueous phase was determined spectrophotometrically at 538 nm as described in Stettler et al. (42) (n=3). Asterisk show statistically significant differences (p lower than 0.05) between wt and silenced plants

protective responses [280]. To investigate this possibility, we measured the capacity of the silenced plants to thermally dissipate excess light through non-photochemical quenching (NPQ) in the antenna complexes using a fluorescence setup to image whole plants. We detected significantly reduced NPQ in mutant plants shifted from low to higher light compared to WT plants (fig.4.13C), confirming that the partitioning between the ΔpH and the $\Delta\Psi$ is a critical parameter for light acclimation in plants ([338][339]). Interestingly, putrescine, a diamine, which increases the $\Delta\Psi/\Delta$pH ratio reduces NPQ and induces a modification of the thylakoid structure [340] in

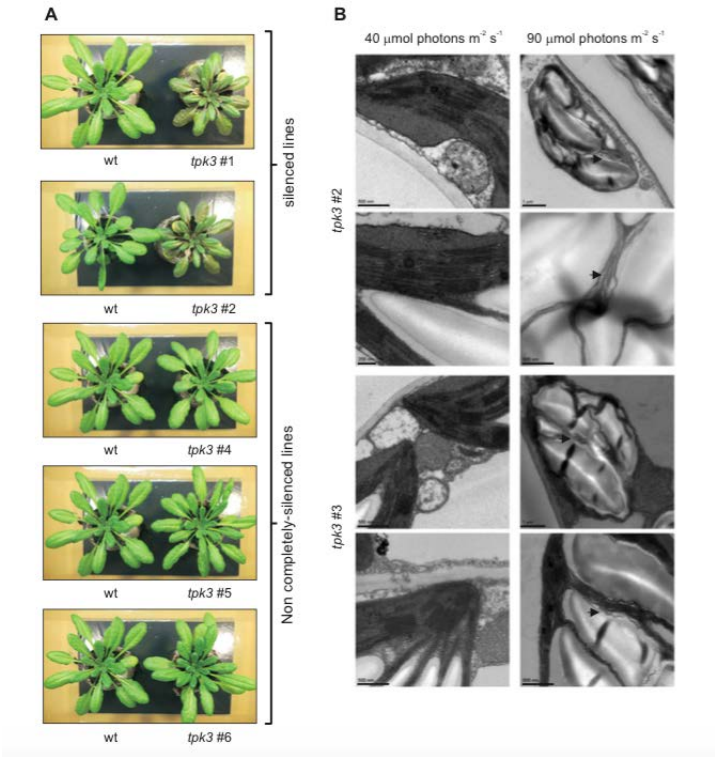

Figure 4.11 – **Plants silenced for TPK3 show abnormal thylakoid structures when grown at a light intensity of 90 μmol photons m^{-2} s^{-1}.** A) Silenced and non-completely silenced plants (as demonstrated by PCR analysis; see fig.4.7) were seeded together and grown under the same conditions. Only the silenced plants (shown are tpk3 ln 1 ln 2) showed an altered phenotype. B) A lack of TPK3 results in altered thylakoid membrane organisation in plants cultured under 90 μmol photons m^{-2} s^{-1}. The TPK3-silenced plants subjected to high light conditions showed abnormal thylakoid structures (see arrows)

WT plants, similarly to what we observed here. Decreased NPQ often paves the way to light sensitivity, as observed in *tpk*3-silenced plants during experiments where photoinhibition was measured in intact plants (fig.4.13D). The difference between the two genotypes disappeared progressively when the plants were shifted from 40 to 300 and 1000 μmol photons m^{-2} s^{-1} (fig.4.14), *i.e.*, at light intensities where photoinhibition was also visible in the WT. This confirms the higher photosensitivity of the mutant. The observed over-reduction of the electron flow chain in silenced plants (fig.4.14) could also explain the observed decreased phosphorylation of light harvesting complexes at 90 μmol photons m^{-2} s^{-1} in these plants (fig.4.12C), due to

enhanced redox inhibition of membrane bound kinases [341] by the reduced electron carriers.

In photosynthetic membranes, photophosphorylation is driven by the electrochemical proton gradient. It is acknowledged that the light-induced proton influx must be electrically balanced by ion fluxes in the opposite direction. Previous works have demonstrated Cl^- channel [342] and potassium channel [343] activities in the thylakoid membrane and hypothesized a role for these channels in such counterbalance. Our findings show that AtTPK3 (the sole TPK channel in the thylakoids) modulates the partitioning of the *pmf* between the $\Delta\Psi$ and ΔpH in chloroplasts *in vivo* at physiological light intensities. By controlling the size and composition of the *pmf*, AtTPK3 directly affects light utilization and dissipation, thereby influencing chloroplast ultrastructure and plant fitness. TPK3 is therefore the missing element responsible for the electroneutrality of proton pumping in this organelle, as originally conceived under the chemiosmotic theory.

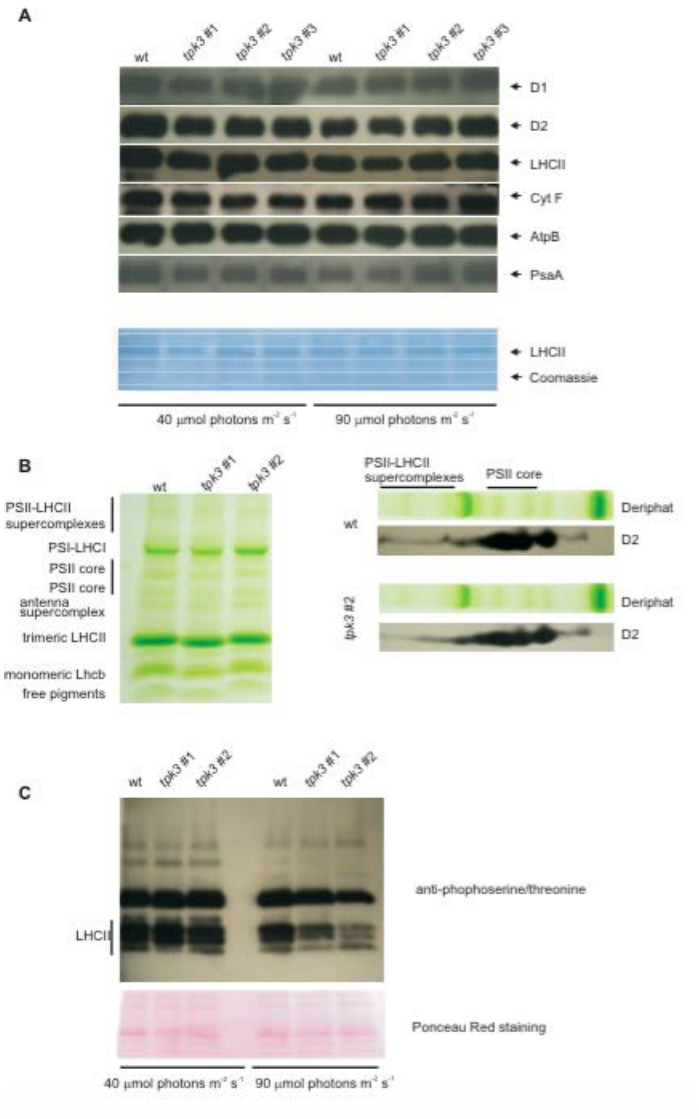

Figure 4.12 – **The main components of the photosynthesis system are not altered in silenced plants but protein phosphorylation in the light is diminished** A) Western blotting and immunodetection with antibodies specific for proteins of the photosynthetic apparatus. Thylakoid membranes (loaded on the basis of chlorophyll contents, at 0.1 to 5 μg of chlorophyll) were analysed with the indicated antibodies. Results are representative of three experiments. The lower part of the figure shows loading control, obtained by colouring the same membrane (with 5 μg of chlorophyll/lane loaded) with GelMate Blue solution (Euroclone). B) Deriphat-PAGE analysis of thylakoids isolated from wt and TPK3-silenced plants grown at 90 μmol photons $m^{-2}s^{-1}$, solubilized with 0.6% ?-dodecyl-maltoside to visualise the entire photosynthetic complexes (according to 18). No differences could be detected between samples (25 μg of chlorophyll loaded per lane). Strips (wt and tpk ln 1) from the Deriphat-PAGE of B) were cut, solubilized in sample buffer before analysis in a second dimension through SDS-PAGE. After transblotting, membranes were decorated with anti-D2 antibody. The result show the presence of the PSII core protein D2 also in the positions corresponding to the PSII-LHCII supercomplexes on the Deriphat-PAGE, further confirming the nature of these higher bands in B). C) Western blot of thylakoid proteins separated from wt and TPK3-silenced plants after illumination with 40 or 90 μmol photons $m^{-2}s^{-1}$ decorated with anti-phosphoserine/threonine antibody (Biolab). 5 μg of chlorophyll was loaded (the lower part of the figure shows loading control, obtained by colouring the same membrane of the upper part with Ponceau Red solution. The blot is representative of two experiments giving similar results. The position of the phosphorylated LHCII bands is indicated.

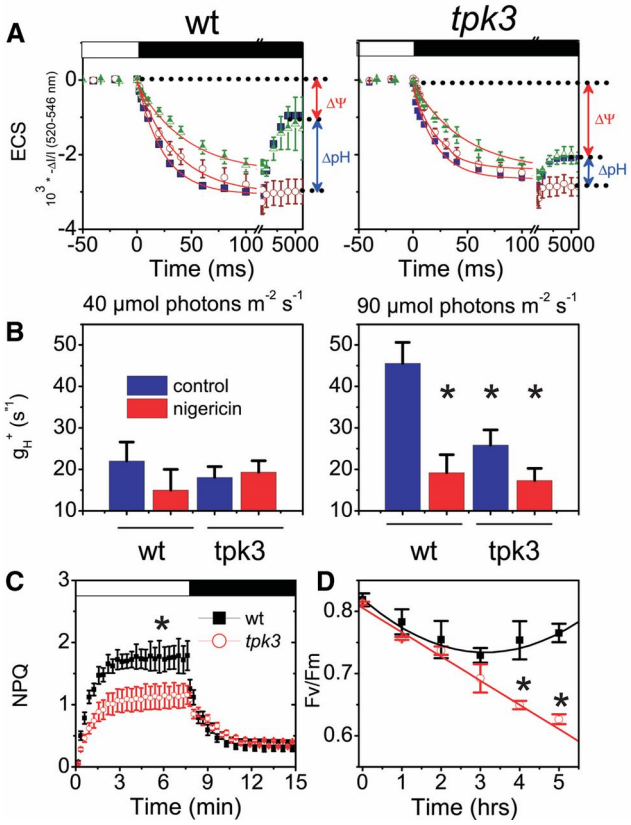

Figure 4.13 – Functional characterisation of WT and *tpk*3 plants grown at a light intensity of 40 or 90 μmol photons $m^{-2}s^{-1}$. (A) Dark relaxation of the ECS signal following illumination (white box) with 1100 μmol photons m^{-2} s^{-1}. Triangles: 40 μmol photons $m^{-2}s^{-1}$; squares: 90 μmol photons m^{-2} s^{-1}; circles: nigericin (10 μM). While the relative amplitude of ΔpH and the $\Delta\Psi$ is very different between the lines, their sum is only slightly decreased in the silenced plants (< 20%). (B) H^+ conductivity through ATP synthase ($g_H{}^+$) in the presence and absence of the H^+/K^+ exchanger nigericin. Differences are statistically significant (p<0.05) between WT and *tpk*3 plants grown at 90 μmol photons $m^{-2}s^{-1}$. Proton permeability was evaluated as $g_H{}^+ = 1/\tau$ after fitting the decay kinetics with a single exponential (panel A, red lines). Fitting the traces with two exponentials did not improve the quality of the fit; mean ± SEM (n = 4-10). (C) NPQ capacity; NPQ was estimated according to the formula Fm-Fm'/Fm' [337]; mean ± SEM (n = 20-25). (D) Fv/Fm values for WT and *tpk*3-silenced lines following photoinhibitory treatment. Plants, grown at a light intensity of 40 μmol photons m^{-2} s^{-1}, were exposed to 1500 μmol photons m^{-2} s^{-1} for the indicated times. Mean Fv/Fm values ± SEM were collected after 20 min of dark adaptation (n = 75 (25 plants per genotype)). All experiments of this figure refer to data from all three silenced lines

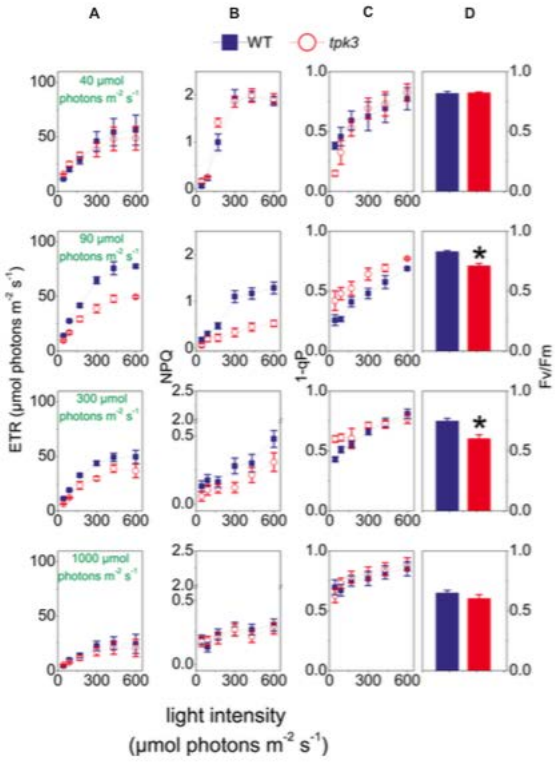

Figure 4.14 – **Photosynthetic parameters in wt and TPK3-silenced plants grown at a light intensity of 40 μmol photons m^{-2} s^{-1} and then transferred to 90, 300 or 1000 μmol photons m^{-2} s^{-1} for 48 hours.** Electron transfer rate (ETR) (column A), non-photochemical quenching (NPQ) (column B), 1-qP (column C) and Fv/Fm (column D) values, obtained with plants left at 40 μmol photons m^{-2} s^{-1} (first row), or transferred to 90 (second row), 300 (third row) or 1000 (fourth row) μmol photons m^{-2} s^{-1} are shown (n greater and equal to 3). qP was calculated as 1- (Fm- Fm′/(Fm′-Fo′)) where Fo′ is the minimum fluorescence measured upon exposure to light. The mean values ± S.E. of measurements performed in different silenced lines are reported. For Fv/Fm, asterisks show statistically significant differences (p lower than 0.05) between wt and silenced plants. For ETR, NPQ and 1- qP measurements there are statistically significant differences (p lower than 0.05) for all points of the graphs only at 90 μmol photons m^{-2} s^{-1}

4.4 Conclusions and further perspectives

4.4.1 STN7 kinase is regulated in an altered way at low light intensity in the *tpk*3 mutant

In the paper *Carraretto et al., 2013* we showed that TPK3 actively modulates the composition of the chloroplast *pmf* through ion counterbalancing. In plants, TPK3 is found in the thylakoid stromal-lamellae and *Arabidopsis* plants silenced for the *TPK*3 gene display reduced growth and altered thylakoid membrane organisation. This phenotype reflects an impaired capacity to generate a normal *pmf*, resulting in reduced CO_2 assimilation and deficient non-photochemical dissipation of excess absorbed light.

An interesting finding of the research was the fact that when *Arabidopsis* *tpk*3 mutants were grown at 90 μE $m^{-2}s^{-1}$, they displayed a significantly reduced level of phosphorylation of their phosphorylable LHCII polypeptides (figure 4.15A). This was accompanied by a reduced redox state of the chloroplast, as indicated by the 1-qP parameter (proportion of the closed, and thus reduced, PSII reaction centres figure 4.15B). As already mentioned (see section 1.6.1.2 at page 41), in *Arabidopsis*, the light harvesting complex of the PSII is phoshorylable (up to 15-20%) by the thylakoid-bound protein kinase STN7. To explain this reduced phosphorylation we first hypothesized a reduced activity of STN7 kinase in *Arabidopsis* *tpk*3 mutants. STN7 is activated by the reduced state of the plastoquinone pool in low light and this phenomena triggers migration of some LHCII from PSII to PSI as previously seen in state transitions (section 1.6.1.2). In order to shed some light on STN7 activity in the *tpk*3 mutant, we investigated the ability of *tpk*3 mutants to perform state transitions following changes in the redox state of the chloroplast at low light.

At this purpose, we proceeded with an experimental set-up as that described in section 3.2.1 (page 151). Briefly, leaf samples from WT and silenced *tpk*3 plants (lines 1-2) were switched either to state-1 or to state-2 using light sources that preferentially excite one of the two photosystems. Red light was used to induce state-2, via its capacity to reduce the plastoquinone pool (referred to as state-2-actinic light) and far-red light was used to excite PSI (referred to as state-1-actinic light), since the latter complex has an intrinsic higher absorption capacity in this region of the spectrum. Concomitantly, fluorescence kinetics were collected.

As demonstrated by fluorescence kinetics reported in figure 4.16, *tpk*3 silenced plants, when compared to WT plants (figure 4.16A), display a comparable

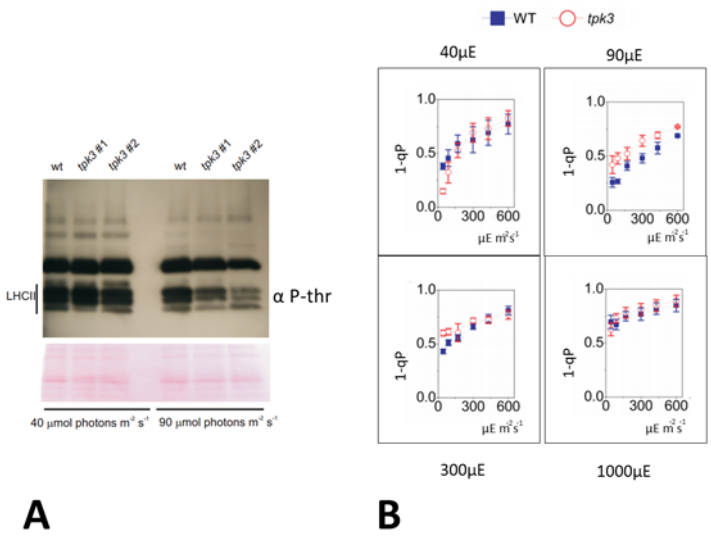

Figure 4.15 – (A) Western blot of thylakoid proteins from WT and *tpk*3 mutants after illumination with 40 or 90 μE $m^{-2}s^{-1}$ carried out with antibodies raised against threonine phosphorylated residues. The position of the phosphorylated LHCII bands is indicated. (B) 1-qP parameter in WT and *tpk*3 mutants grown at a light intensity of 40 μE $m^{-2}s^{-1}$ (top left) and then transferred to 90 (top right), 300 (bottom left) or 1000 (bottom right) μE $m^{-2}s^{-1}$ for 48 hours

capacity to perform state transitions *in vivo*(figure 4.16B,C). Moreover, difference between F'_{max} in state-1 and state-2 allowed to conclude that around 10% of the LHCII pool is translocated from PSII to PSI during state transitions for all the genotypes (4.16D).

This was further confirmed biochemically using antibodies raised against phosphorylated threonine residues. Intact leaves from WT and silenced *tpk3* plants (lines 1-2) grown at 90 μE $m^{-2}s^{-1}$ were switch either to state-1 or to state-2 by illumination for 10 minutes with light sources that preferentially excite one of the two photosystems. Immediately after, leaves were frozen in liquid nitrogen in dark and lysate was resuspended in a buffer containing 10 mM NaF as phosphatase inhibitor. Results from western blots reported in figure 4.17 indicate no difference in the level of phosphorylation of the LHCII in state-1 or state-2 between *Arabidopsis* WT and *tpk*3-silenced lines. Spectroscopic and biochemical analyses indicated that the redox state of the plastoquinone pool can regulate the activity of STN7 in *tpk*3-silenced mutants

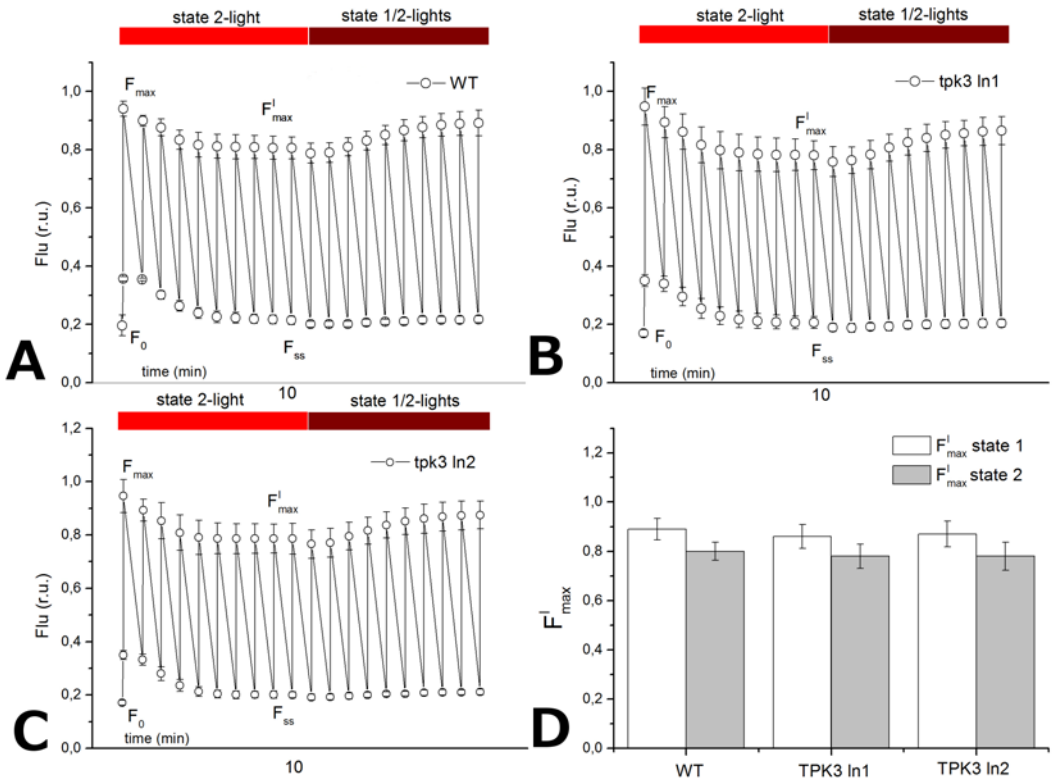

Figure 4.16 – *in vivo* measure of state transitions in (A) WT ,(B) *tpk*3 line 1 and (C) *tpk*33 line 2. state-1 and state-2 are induced by 10 minutes illumination with 30μE PSII-actinic (state2) and with 30μmol m^{-2} s^{-1} PSII-actinic light + 700μmol m^{-2} s^{-1} PSI-actinic light (state1). (D) F'_{max} in state-1 and state-2 are compared for each genotype.

to the same extent as in WT at low light. In other words, in the *tpk*3 mutant, the reduced level of LHCII phosphorylation is not due to an impairment of STN7 activation by the redox state of the PQ pool.

A second hypothesis to explain the reduced level of phosphorylation of the *tpk*3 mutants (figure 4.15A) is based on the fact that other mechanisms for STN7 regulation are possible. This is demonstrated by the observation that LHCII phosphorylation is down-regulated at high irradiance although the PQ pool is reduced [124]. In fact it exists a second regulatory step in which the stromal ferredoxin/thioredoxin system inactivates the kinase under

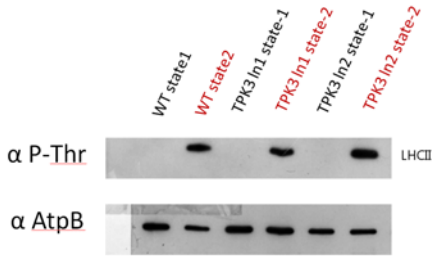

Figure 4.17 – Western blot of cellular lysate proteins from WT and *tpk*3 mutants switched either to state-1 or state-2 by 10 minutes illumination with light sources that preferentially excite one of the two photosystems. ATPase was used as marker of protein loading.

reducing conditions (*i.e.* under high light) [341]. In this view, the two cysteines residues (of STN7) exposed to the thylakoid lumen seem to be involved in this oxidation/reduction regulation and they have been experimentally demonstrated to be essential for the STN7 kinase activity [282]. In *Arabidopsis* WT plants, in our growing conditions, this ferredoxin/thioredoxin pathway for STN7-downregulation is probably not active because of the low light intensity (90 μE $m^{-2}s^{-1}$). On the other hand, when the same light intensity is delivered to *tpk*3 mutant, this latter shows a series of responses which are typically those observable during high-light conditions (*e.g.* high photosensitivity, enhanced anthocyanin accumulation). In our hypothesis, *tpk*3 mutants grown at 90 μE $m^{-2}s^{-1}$ could behave somehow as they were grown at higher light intensity. Therefore, this could explain the decreased level of LHCII-phosphorylation in *tpk*3 thanks to the inactivation of the STN7 kinase through the ferredoxin/ thioredoxin pathway. Moreover this hypothesis is also consistent with the observation of the over-reduced state of the chloroplast (1-qP parameters figure 4.15). To verify this hypothesis more experiments are needed. For example, one possible strategy would be to artificially block the ferredoxin/ thioredoxin regulatory pathway. This could be performed by infiltrating intact leaves of *Arabidopsis* WT and *tpk*3 mutants with a solution of Methyl Viologen and subsequently comparing their level of LHCII phosphorylation by western-blot.

4.4.2 K^+ channels are involved in plant responses to high-light

As previously mentioned, with up to 10 % of the dry weight, K^+ is the most abundant cation found in plants and it fulfills numerous essential roles. Two possible mechanisms have been proposed for K^+ transport across the chloroplast membranes: K^+ channels [344] and K^+/H^+ antiporters [345]. As described above, TPK3-mediated K^+ efflux indeed plays an important role in the ΔpH component of the *pmf*. The existence of this K^+ channel calls for a K^+ loading mechanism into the thylakoid lumen to avoid osmotic swelling. Recently, the K^+/H^+ antiporter - KEA3 was proposed to play this role [346]. When compared to WT, *Arabidopsis* mutants lacking the KEA3 antiporter display slightly increased ΔpH and a compensatory decreased $\Delta\Psi$ across the thylakoid membrane [346]. Together with an increased NPQ ($\sim$ 20%), these are opposite effects to those described for mutants lacking TPK3 activity [347], suggesting that both K^+ channels TPK3 and KEA3 modulate the partitioning of *pmf* through K^+ ion counter-exchange across the thylakoid membrane.

In order to get a better understanding about the physiological connections between these two transporters and the high-light responses in plants, we performed some preliminary measures on *Arabidopsis tpk3kea3* double mutants (mutants obtained in collaboration with the research team directed by doc. Ildiko Szabo at the University of Padua, Italy) in a work that will continue after this PhD thesis. *Arabidopsis* WT and three independent lines of the *tpk3kea3* double mutant were tested and compared for their ability to cope with high light conditions. In particular some interesting results were obtained during the assessment of the high-energy quenching component (*qE*) of NPQ. *Arabidopsis* WT and *tpk3kea3* lines 3/10/11 (referred to as ln3, ln10 and ln11) grown at 90μE $m^{-2}s^{-1}$ were kept in the dark for 30 minutes before the measure. Samples were then illuminated for 4 minutes at 600 μE $m^{-2}s^{-1}$. NPQ, calculated as (F_{max}-F'_{max}/F'_{max}) was continuously monitored. As evidenced by data reported in figure 4.18, all *tpk3kea3* lines display a reduced level of NPQ ($\sim$ 25%) when compared to WT. This reduction in the amplitude of the NPQ is roughly intermediate between the two opposite effects observed in *kea3* and *tpk3* single mutants (+ 20% and -50% respectively) which could be reasonable in the case of the synergic actions of the two mutations. During the first minutes of illumination (minutes 1-4), we observe that high-light, rapidly induces *qE* which promotes activation of the enzymes involved in the interconversion of violaxanthin to zeaxanthin and instauration of NPQ. In WT plants this effect is rapid and it is evident

from the graph (figure 4.18) after around 30 seconds. Interestingly, NPQ kinetics of *tpk*3*kea*3 double mutants is evidently modified (figure 4.18). In fact, when compared to WT plants, lines 3/10/11 display a retarded NPQ induction which is characterised by a lag phase at around minute 1 (figure 4.18). Later, a dark period of 20 minutes is applied before a second cycle of 4 minutes illumination at 600 μE $m^{-2}s^{-1}$.

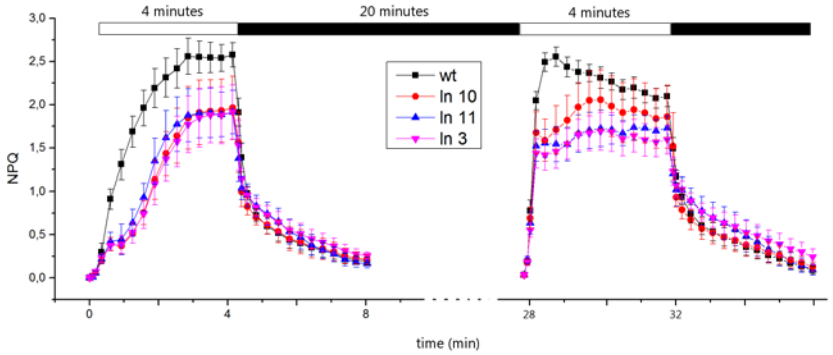

Figure 4.18 – Non-photochemical quenching (NPQ) of WT and *tpk*3*kea*3 silenced plants. Plants are grown at 90 μE $m^{-2}s^{-1}$ and incubated 20 minutes before NPQ induction at 600 μE. After the measure, the same samples are again dark-incubated for 20 minutes to relax the NPQ components. A second NPQ induction is performed at 600 μE.

During this second period of illumination, light rapidly induces NPQ in all the genotypes (figure 4.18) and, even if *tpk*3*kea*3 double mutants still display a reduced level of NPQ, no more difference is observable in the initial kinetics (minutes 28-29). The effect here described, closely remind that observed in mutants lacking both CP26 and CP24 (the two most effective Lhc proteins in Violaxanthin/Zeaxanthin exchange) [234]. We hypothesize that the initial retard (minutes 1-2 figure 4.18) in the NPQ induction in *tpk*3*kea*3 double mutants could be due to a slowed activation of the enzyme involved in the xanthophyll cycle. In principle, at this stage zeaxanthin is not yet synthesized neither in WT nor in *tpk*3*kea*3 double mutants. Later, during the second period of illumination (minutes 28-29), *tpk*3*kea*3 double mutants can rapidly induce NPQ because zeaxanthin is already synthesized, and 20 minutes of dark relaxation were not sufficient for the interconversion of zeaxanthin back to violaxanthin. To verify this hypothesis more experiments are needed. For example, one possible strategy would rely on the use of the liquid-chromatography. Measure should compare pigments evolution in WT

and mutants during the first 2-3 minutes of NPQ-induction. This measure is relatively quick and facilities for its accomplishment are already present in our laboratory.

In order to deeply investigate the physiological role of TPK3 and KEA3 in high-light responses of *Arabidopsis*, one other approach would be to challenge our mutants (*tpk*3*, kea*3 single mutants and *tpk*3*kea*3 double mutants) with artificially fluctuating light conditions. Repeating fluctuations between low and high illumination phases expose the leaves to opposite, rapid, and mixed signals and thus are expected to challenge the light acclimation capacity of the photosynthetic machinery. At this purpose it is conceivable an experimental set-up as that described in *Tikkanen et al., 2010* [348] where plants are exposed to 90μE $m^{-2}s^{-1}$ light intensity for 5 min, followed by a high light illumination pulse for 1 min, after which the cycle is repeated for the entire photoperiod (16h light). In literature, growth analyses under fluctuating light conditions of several *Arabidopsis* mutants defective in the regulatory proteins, like STN7 and PGR5, have revealed a retarded growth phenotype for the *Arabidopsis stn7* mutant (impaired in the qT component of photoprotection, see section 1.6.1.2 at page 41) and a complete lethality of the *pgr5* mutant [348]. It was demonstrated that the primary target of photodamage caused by fluctuating light conditions is PSI and, WT plants exposed to such conditions, respond with increasing amount of PSI centers in the thylakoid membrane together with a diminished linear electron flow (LEF)[348]. Moreover, it was recently shown that the formation of ΔpH via regulation of the cytochrome b_6f (in which PGR5 has an essential role) is indispensable for photoprotection of PSI [349]. In our *tpk*3 mutants, the capacity to build a normal ΔpH was demonstrated to be largely affected. Therefore, what we could expect is an enhanced PSI photosensitivity when plant are grown during fluctuating light conditions. Moreover giving that electrical flow from PSII is essential for PSI photoinhibition [106],this effect could also be worsened by the impaired ability to perform NPQ and by the over-reduced state of the photosynthetic chain (figure 4.15). Such an enhanced PSI-photodamage could also be observable in our *tpk*3*kea*3 double mutants even though the diminished ΔpH promoted by the TPK3 mutations may, at least in part, be compensated by the slightly enhanced ΔpH observed in *kea*3 single mutant [346]. Experiments are in course and results are expected to give some preliminary hints.

Chapter 5

Concluding remarks

Plant science is central to addressing many of the most important questions that humanity is facing. Our century is experiencing one of the most intense climate changes since the appearance of the humanity and understanding how plants interact with their immediate environment and respond to stress is one of the major challenges. In this context, study of the chloroplast is strategic. Findings included in this thesis, are of a great scientific impact and pave the way for a multitude of future developments.

This thesis explored the way plant respond to different light *stimuli* with a particular regard to unbalanced light conditions and protection from high-light stress. In detail, we aimed at giving new insights about two components of the NPQ: state transitions (qT) and the high energy state quenching (qE). The main question that we posed when investigating qT, concerned the effects of state transitions on the protein segregation within the photosynthetic membrane. In particular, we were interested in identifying new candidate proteins that, together with LHCII, take part to the rebalancing of the light-energy excitation between the two photosystems. To answer to the question, we chose a strategy based on a multi-step approach. We firstly performed a complete survey of the protein composition of the thylakoid sub-compartments of *Arabidopsis* WT. At this purpose we developed different protocols to, starting from Percoll-purified chloroplasts, obtain highly purified fractions of *(i)* the BBY region of the thylakoids and *(ii)* the stroma-lamellae region of the thylakoids. Intact chloroplasts were used as a starting material, to avoid contamination by nucleus/mitochondria proteins. In fact, while contamination (usually around 10% in the case of isolated thylakoids) might not be a problem in the case of classical biochemical approaches (*e.g.* western blot), it can severely affect data analysis in the case of proteomics.

Therefore, we adapted already-existing protocols for other species (*i.e. Zea mays*), to our model plant *Arabidopsis*. A first evaluation of the quality of the preparations was carried out biochemically and biophysically. In particular, thanks to the non-homogeneous distribution of the photosynthetic complexes among the thylakoids sub-compartments, it was possible to show, by western-blot analysis, how BBY and stroma lamellae fractions were largely enriched in PSII and PSI-related complexes respectively. Moreover, cross contamination with other chloroplastic compartments (envelope, stroma etc.) was estimated by means of specific markers. Good level of purification was also assessed by relative fluorescence emissions measurements of the two photosystems in the different preparations. In particular, emission of PSII and PSI in thylakoids, BBY and stroma lamellae were used to determine the enrichment of PSII in BBY and of PSI in stroma lamellae, taking advantage of the fact that their emission spectra at 77°K are different.

We next combined mass-spectrometry analysis and statistical data treatment of our fractions to assess protein repartition between the two sub compartments of the thylakoid membrane. 1295 proteins were identified from all the analyses performed and, among them, 294 thylakoid proteins were found to be differentially distributed between stroma-lamellae and BBY (27 and 267 more abundant in BBY and in stroma-lamellae fractions, respectively). Proteomic data allowed to corroborate the biochemical data concerning the differential localisation of some maxi complexes embedded in the thylakoid membrane. Moreover, it allowed also to point out possible differences in every complex between thylakoid fractions analysed here. The overall picture emerging from this proteomic study is a way more dynamic than previously hypothesized. With the only exception of ATPase, all the other photosynthetic complexes display a localisation which is, in a different extent, more or less shared between the two sub-compartments of the thylakoid membrane. PSI is more accumulated in the unstacked stroma-lamellae (together with the NDH complex), while PSII is mostly found in the grana stacks. The cytochrome b_6f complex is more ubiquitous, although slightly more concentrated in the stroma-lamellae. In all complexes most of the subunits followed the same patterns, with some specific differences between the grana and stroma-lamellae. This, in general, concerned small subunits probably having regulatory roles. However, a closer look at these data evidenced that most of the complexes possess a subunit composition which varies if the complex localises in the BBY or in the stroma-lamellae. It is clear that the information provided by this study links differences in the stoichiometric composition of the photosynthetic complexes to actual functional differences performed by a given complex when it is localised either in stroma-lamellae or BBY.

Later, we used the informations provided from this proteomic analysis

to investigate differences in the protein segregation during state transitions. At this purpose, different sub thylakoid fractions were obtained from two *Arabidopsis* mutants unable to perform state-transitions. *stn7* is deficient in the STN7 kinase responsible for LHCII phosphorylation, and *pph1* is deficient in the PPH1 phosphatase of the LHCII complex. These two mutants are respectively locked in state-1 and state-2 and they cannot perform state transitions. As for WT, fractions obtained from *stn7* and *pph1* mutants were evaluated for their level of contamination biochemically and biophysically.

Thanks to the proteomic analysis of the *Arabidopsis stn7* and *pph1* state transition mutants, we could firstly corroborate previous observations indicating Lhcb1 and Lhcb2 as the major LHCII isoforms involved in state transitions. Secondly, we could suggest new potential-actors participating to the membrane reorganization during state transitions. Unfortunately, due to time limitation, this second objective (which in principle was the main aim of the thesis) was only partially accomplished, and results were delivered in their preliminary-form. This, even if it represents a little fail in the PhD project, allowed to collects a large amount of data and experimental evidences. This data is in its ready-to-use form and can be easily exploited in a large variety of further investigations.

In the second part of this thesis, we investigated the high-energy quenching component (qE) of the NPQ. The main question that we posed concerned the mechanisms that can regulate ΔpH (and thus NPQ) in plants. To answer to the question we focused on a new and recently identified two-pore potassium channel, TPK3. Firstly, taking advantage of the purification protocol of the thylakoid subfractions developed in *Tomizioli et al., 2014* [139] we demonstrated that TPK3 is localised in the stroma-lamellae. Secondly, we focused on the physiological role of TPK3. At this purpose three independent lines of *Arabidopsis* were produced, in which TPK3 expression was stably silenced via RNA interference. *Tpk*3 mutants displayed enhanced anthocyanin accumulation, reduced growth and altered thylakoid membrane organization, already at moderate growth light intensity (90μE m^{-2}.s^{-1}). For instance, biochemical analysis did not evidence any differences at the level of the main components of the photosynthetic apparatus (including PSI, PSII, ATPase, and cytochrome b_6f) even though we evidenced a varied phosphorylation pattern in LHCII. On the other hand, such an altered thylakoid structure is expected to arise from changes in the photosynthetic activity. To test this hypothesis we challenged our *tpk*3 mutants for their ability to build a normal *pmf in vivo*. This was based on the rationale that *pmf* is essential in regulating light utilization in photosynthesis, and changes in ion fluxes (*i.e* K^+) are likely to affect its two components, the ΔpH and the $\Delta\Psi$ (see section 4.2 at page 173). In order to experimentally evaluate the *pmf*

composition we took advantage of the relationship existing between the $\Delta\Psi$ and the electrochromic shift (ECS) (see section.4.2.1 at page 173). Results on the *tpk*3 mutants indicated that, even if the *pmf* was roughly unaltered, the ΔpH component was considerably reduced as well as the proton conductivity of the membranes. Consistent with this conclusion, NPQ measures evidenced that *tpk*3 mutants possessed reduced ability to dissipate excessive energy as heat. In conclusion, our findings indicated that TPK3 actively control photosynthesis *in vivo* by modulating the partitioning of the *pmf* between the ΔpH and $\Delta\Psi$ at physiological light intensities. This translates into an impaired ability to dissipate excess energy as heat and to an altered chloroplast structure.

Later, we investigated possible reasons for the different phosphorylation pattern of PSII antenna in *tpk*3 mutants and WT plants grown at 90μE $m^{-2}.s^{-1}$ with a particular regard to state transitions. Preliminary results indicated that *tpk*3 can correctly perform state transitions and causes for reduced phosphorilation could be addressed to an aberrant down-regulation of the STN7 kinase by the ferredoxin/ thioredoxin regulatory pathway even at low light intensities. Further investigation is however needed to confirm this hypothesis.

To conclude, during these three years, I had a great opportunity to enlarge my knowledge about plant biology, with a particular regard to the photosynthesis process. I acquired solid theoretical and technical skills in the field of the biochemistry and biophysics. Moreover thanks to the close cooperation with the EdyP laboratory I had the possibility to integrate my education/training with some aspects of the MS/MS analysis. All these competences will be undoubtedly helpful and exploitable during the following steps of my professional career.

Bibliography

[1] Douzery EJP, Snell EA, Bapteste E, Delsuc Fdr, Philippe H (2004) The timing of eukaryotic evolution: does a relaxed molecular clock reconcile proteins and fossils? PNAS 101: 15386-15391

[2] Yoon HS, Hackett JD, Ciniglia C, Pinto G, Bhattacharya D (2004) A molecular timeline for the origin of photosynthetic eukaryotes. Mol Biol Evol 21: 809-818

[3] Bock, R. and Timmis, J.N. (2008) Reconstructing evolution: gene transfer from plastids to the nucleus. Bioessays 30, 556-566

[4] Martin, W. (2003) Gene transfer from organelles to the nucleus: frequent and in big chunks. Proc. Natl. Acad. Sci. U.S.A. 100, 8612-8614

[5] Stegemann, S. et al. (2003) High-frequency gene transfer from the chloroplast genome to the nucleus. Proc. Natl. Acad. Sci. U.S.A. 100, 8828-8833

[6] Timmis, J.N. et al. (2004) Endosymbiotic gene transfer: organelle genomes forge eukaryotic chromosomes. Nat. Rev. Genet. 5, 123- 135

[7] Jarvis, P. (2008). Targeting of nucleus-encoded proteins to chloroplasts in plants. New Phytologist, 179(2), 257-285

[8] Jarvis, P., and Lopez-Juez, E. (2013). Biogenesis and homeostasis of chloroplasts and other plastids. Nature reviews. Molecular cell biology, 14(12), 787-802

[9] Sharma, M.R. et al. (2007) Cryo-EM study of the spinach chloroplast ribosome reveals the structural and functional roles of plastid-specific ribosomal proteins. Proc. Natl. Acad. Sci. U.S.A. 104, 19315-19320

[10] Soll, J. and Schleiff, E. (2004) Protein import into chloroplasts. Nat. Rev. Mol. Cell Biol. 5, 198-208

[11] Block, M. a, Douce, R., Joyard, J., and Rolland, N. (2007). Chloroplast envelope membranes: a dynamic interface between plastids and the cytosol. Photosynthesis research, 92(2), 225-44

[12] Benson AA (1964) Plant membrane lipids. Annu Rev Plant Physiol 15:1-16

[13] Joyard, J., Teyssier, E., Miege, C., Berny-Seigneurin, D., Marechal, E., Block, M. A., Dorne, A. J., Rolland, N., Ajlani, G., and Douce, R. (1998) The biochemical machinery of plastid envelope membranes. Plant Physiol. 118, 715-723

[14] F. Kessler, D.J. Schnell, The function and diversity of plastid protein import pathways: a multilane GTPase highway into plastids, Traffic 7 (2006) 248-257.

[15] P. Jarvis, Targeting of nucleus-encoded proteins to chloroplasts in plants (Tansley review), New Phytol. 179 (2008) 257-285.

[16] H.M. Li, C.C. Chiu, Protein transport into chloroplasts, Annu. Rev. Plant Biol. 61 (2010) 157-180.

[17] Kleffmann T, et al. (2004) The protochlorophyllArabidopsis thaliana chloroplast proteome reveals pathway abundance and novel protein functions. Curr Biol 14(5):354-362.

[18] ada A, Soll J (2004) Inner envelope protein 32 is imported into chloroplasts by a novel pathway. J Cell Sci 117(Pt 17):3975-3982.

[19] Miras S, Salvi D, Ferro M, Grunwald D, Garin J, Joyard J, Rolland N. (2002) Non-canonical transit peptide for import into the chloroplast. J Biol Chem. 2002 Dec 6;277(49)

[20] Miras S, et al. (2007) Toc159- and Toc75-independent import of a transit sequence-less precursor into the inner envelope of chloroplasts. J Biol Chem 282(40)

[21] Campbell, Neil A.; Brad Williamson; Robin J. Heyden (2006). Biology: Exploring Life. Boston, Massachusetts: Pearson Prentice Hall. ISBN 978-0-13-250882-7

[22] Cooper, Geoffrey M. (2000). The Chloroplast Genome. The Cell: A Molecular Approach (2nd ed.). Washington, D.C: ASM Press. ISBN 0-87893-106-6

[23] Shimoni E, Rav-Hon O, Ohad I, Brumfeld V, Reich Z. 2005. Three-dimensional organization of higher-plant chloroplast thylakoid membranes revealed by electron tomography. The Plant Cell 17, 2580-2586.

[24] Murphy DJ. 1986. The molecular organisation of the photosynthetic membranes of higher plants. Biochimica et Biophysica Acta 864, 33-94.

[25] Rosinski J, Rosen WG. 1972. Chloroplast development: fine structure and chlorophyll synthesis. Quarterly Review of Biology 47, 160-191.

[26] Solymosi K, Schoefs B. 2010. Etioplast and etio-chloroplast formation under natural conditions: the dark side of chlorophyll biosynthesis in angiosperms. Photosynthesis Research 105, 143-166.

[27] Kirchhoff H, Mukherjee U, Galla HJ. 2002. Molecular architecture of the thylakoid membrane: lipid diffusion space for plastoquinone. Biochemistry 41, 4872-4882.

[28] Goss R, Wilhelm C. 2010. Lipids in algae, lichens and mosses. In: Wada H, Murata N, eds. Lipids in photosynthesis: essential and regulatory functions, Vol. 30. Dordrecht, The Netherlands: Springer, 117-137.

[29] Ben-Shem, A., Frolow, F. and Nelson, N. (2003) Crystal structure of plant photosystem I. Nature, 426, 630-635

[30] Nevo R, Charuvi D, Tsabari O, Reich Z. 2012. Composition, architecture and dynamics of the photosynthetic apparatus in higher plants. The Plant Journal 70, 157-176.

[31] Amunts A, Drory O, Nelson N. The structure of a plant photosystem I supercomplex at 3.4 Å resolution. Nature. 2007 May 3;447(7140):58-63

[32] Y. Takahashi, M. Goldschmidtclermont, S.Y. Soen, L.G. Franzen, J.D. Rochaix, EMBO J. 10 (1991) 2033-2040

[33] Choquet, Y., and Vallon, O. (2000). Synthesis, assembly and degradation of thylakoid membrane proteins. Biochimie, 82(6-7), 615-34

[34] B. Andersen, B. Koch, H.V. Scheller, Physiol. Plant. 84 (1992) 154-161

[35] P. Jordan, P. Fromme, H.T. Witt, O. Kuklas, W. Saenger, N. Krauss, Three-dimensional structure of cyanobacterial photosystem I at 2.5 A, Nature 411 (2001) 909-917.

[36] Varotto C, Pesaresi P, Meurer J, Oelmuller R, Steiner-Lange S, Salamini F, Leister D. Disruption of the Arabidopsis photosystem I gene psaE1 affects photosynthesis and impairs growth. Plant J. 2000 Apr;22(2):115-24.

[37] A. Mant, C.A.Woolhead, M. Moore, R. Henry, C. Robinson, Insertion of PsaK into the thylakoid membrane in a horseshoe conformation occurs in the absence of Signal Recognition Particle, nucleoside triphosphates, or functional Albino3, J. Biol. Chem. 276 (2001) 36200-36206

[38] L. Rosgaard, A. Zygadlo, H.V. Scheller, A. Mant, P.E. Jensen, Insertion of the plant photosystem I subunit G into the thylakoid membrane: in vitro and in vivo studies of wild-type and tagged versions of the protein, FEBS J. 272 (2005) 4002-4010

[39] Boekema, E.J., van Roon, H. and Dekker, J.P. (1998) Specific association of photosystem II and light-harvesting complex II in partially solubilized photosystem II membranes. FEBS Lett. 424, 95-99

[40] P.E. Jensen, M. Gilpin, J. Knoetzel, H.V. Scheller, The PSI-K subunit of photosystem I is involved in the interaction between light-harvesting complex I and the photosystem I reaction center core, J. Biol. Chem. 275 (2000) 24701-24708

[41] P.E. Jensen, L. Rosgaard, J. Knoetzel, H.V. Scheller, Photosystem I activity is increased in the absence of the PSI-G subunit, J. Biol. Chem. 277 (2002) 2798-2803.

[42] C. Varotto, P. Pesaresi, P. Jahns, A. Lebnick, M. Tizzano, F. Schiavon, F. Salamini, D. Leister, Single and double knockouts of the genes for photosystem I subunits G, K, and H of Arabidopsis, effects on photosystem I composition, photosynthetic electron flow, and state transitions, Plant Physiol. 129 (2002) 616-624.

[43] Bengis C., Nelson N. Subunit structure of chloroplast photosystem I reaction center (1977) Journal of Biological Chemistry, 252 (13) , pp. 4564-4569.

[44] A. Haldrup, D.J. Simpson, H.V. Scheller, J. Biol. Chem. 275 (2000) 31211-31218.

[45] Naver H, Haldrup A, Scheller HV. Cosuppression of photosystem I subunit PSI-H in Arabidopsis thaliana. Efficient electron transfer and stability of photosystem I is dependent upon the PSI-H subunit. J Biol Chem. 1999 Apr 16;274(16):10784-9.

[46] Lunde C, Jensen PE, Haldrup A, Knoetzel J, Scheller HV. The PSI-H subunit of photosystem I is essential for state transitions in plant photosynthesis. Nature. 2000 Nov 30;408(6812):613-615.

[47] J. Knoetzel, A. Mant, A. Haldrup, P.E. Jensen, H.V. Scheller, PSI-O, a new 10-kDa subunit of eukaryotic photosystem I, FEBS Lett. 510 (2002) 145-148.

[48] A. Hansson, K. Amann, A. Zygadlo, J. Meurer, H. Vibe Scheller, P.E. Jensen, Knock-out of the chloroplast encoded PSI-J Subunit of Photosystem I in Nicotiana tabacum: PSI-J is required for efficient electron transfer and stable accumulation of photosystem I, FEBS J. 274 (2007) 1734-1746

[49] Vandenbogaert M, Li-Thiao-Te S, Kaltenbach H, Zhang R, Aittokallio T, Schwikowski B. 2008.Alignment ofLC-MS images, with applications to biomarker discovery and protein identification. Proteomics 8:650?672

[50] Dekker JP, Boekema EJ. 2005. Supramolecular organization of thylakoid membrane proteins in green plants. Biochimica et Biophysica Acta 1706, 12-39.

[51] M. Miyao, N. Murata, Role of the 33 kDa polypeptide in preserving Mn in photosynthetic oxygen-evolution, FEBS Lett. 170 (1984) 350-354.

[52] R.L. Burnap, L.A. Sherman, Deletion mutagenesis in Synechocystis sp. PCC 6803 indicates that the Mn-stabilizing protein of Photosystem II is not essential for oxygen evolution, Biochemistry 30 (1991) 440-446.

[53] T.M. Bricker, Oxygen evolution in the absence of the 33 kDa manganese stabilizing protein, Biochemistry 31 (1992) 4623-4628. (1984) 350-354.

[54] Ono T, Inoue Y (1984) Ca2-dependant restoration of O2-evolving activity in CaCl2-washed Photosystem II particles depleted of 33, 24, and 16 kDa polypeptides. FEBS Lett 168:281-286

[55] T.-A. Ono, Y. Inoue, Mn-preserving extraction of 33-, 24- and 16-kDa proteins from O2-evolving PS II particles by divalent salt-washing, FEBS Lett. 164 (1983)255-260.

[56] R. Murakami, K. Ifuku, A. Takabayashi, T. Shikanai, T. Endo, F. Sato, characterisation of an Arabidopsis thaliana mutant with impaired psbO, one of two genes encoding extrinsic 33-kDa proteins in Photosystem II, FEBS Lett. 523 (2002) 138-142.

[57] B. Lundin, M. Hansson, B. Schoefs, A.V. Vener, C. Spetea, The Arabidopsis PsbO2 protein regulates dephosphorylation and turnover of the Photosystem II reaction center D1 protein, Plant J. 49 (2007) 528-539.

[58] T. Jansen, C. Rother, J. Steppuhn, H. Reinke, K. Beyreuther, C. Jansson, B. Andersson, R.G. Herrmann, Nucleotide sequence of cDNA clones encoding the complete 23 kDa and 16 kDa precursor proteins associated with the oxygen- evolving complex from spinach, FEBS Lett. 216 (1987) 234-240.

[59] K. Ido, K. Ifuku, Y. Yamamoto, S. Ishihara, A. Murakami, M. Kusano, C. Miyake, F. Sato, Knockdown of the PsbP protein does not prevent assembly of the dimeric PSII core complex but impairs accumulation of photosystem II supercomplexes in tobacco, Biochim. Biophys. Acta 1787 (2009) 873-881.

[60] K. Ifuku, S. Ishihara, R. Shimamoto, K. Ido, F. Sato, Structure, function, and evolution of the PsbP protein family in higher plants, Photosynth. Res. 98 (2008) 427-437

[61] K. Ifuku, S. Ishihara, F. Sato, Molecular functions of oxygen-evolving complex family proteins in photosynthetic electron flow, J. Integr. Plant Biol. 52 (2010) 723-734.

[62] Bassi R, Sandona D, Croce R (1997) Novel aspects of chlorophyll a/b-binding proteins. Physiol Plant 100: 769-779

[63] Jansson, S. (1994) The light-harvesting chlorophyll a/b-binding proteins. Biochim. Biophys. Acta, 1184, 1-19

[64] Liu, Z., Yan, H., Wang, K., Kuang, T., Zhang, J., Gui, L., An, X. and Chang, W. (2004) Crystal structure of spinach major light-harvesting complex at 2.72 a resolution. Nature, 428, 287-292

[65] Stroebel, D., Choquet, Y., Popot, J.-L., and Picot, D. (2003). An atypical haem in the cytochrome b(6)f complex. Nature, 426(6965), 413-8

[66] Kurisu, G., Zhang, H., Smith, J. L., and Cramer, W. a. (2003). Structure of the cytochrome b6f complex of oxygenic photosynthesis: tuning the cavity. Science (New York, N.Y.), 302(5647), 1009-14

[67] Lemaire , C. , Girard-Bascou , J. , Wollman , F.-A. , and Bennoun , P. (1986). Studies on the cytochrome b6 f complex. I. characterisation of the complex subunits in Chlamydomonas reinhardtii . Biochim. Biophys. Acta 851, 229-238.

[68] Wollman , F.A. and Lemaire , C. (1988). Studies on kinase-controlled state transitions in Photosystem II and b 6 f mutants from Chlamydomonas reinhardtii which lack quinone-binding proteins . Biochim. Biophys. Acta 933, 85-94.

[69] Wollman , F.A. (2001). State transitions reveal the dynamics and flexibility of the photosynthetic apparatus . EMBO J. 20 , 3623 - 3630 .

[70] Lane N, Allen JF, Martin W. 2010. How did LUCA make a living? Chemiosmosis in the origin of life. BioEssays 32:271-80

[71] Seelert , H. , Dencher , N.A. , and Muller , D.J. (2003). Fourteen protomers compose the oligomer III of the proton-rotor in spinach chloroplast ATP synthase . J. Mol.Biol. 333 , 337 - 344 .

[72] Johnson GN. Physiology of PSI cyclic electron transport in higher plants. Biochim Biophys Acta. 2011 Mar;1807(3):384-9

[73] Shikanai, T. (2007) Cyclic electron transport around photosystem I: genetic approaches. Annu. Rev. Plant Biol. 58, 199-217.

[74] Matsubayashi, T., Wakasugi, T., Shinozaki, K. et al. (1987) Six chloroplast genes (ndhA-F) homologous to human mitochondrial genes encoding components of the respiratory chain NADH dehydrogenase are actively expressed: determination of the splice sites in ndhA and ndhB premRNAs. Mol. Gen. Genet. 210, 385-393.

[75] Baradaran, R., Berrisford, J.M., Minhas, G.S. and Sazanov, L.A. (2013) Crystal structure of the entire respiratory complex I. Nature, 494,443-448.

[76] Arteni, A.A., Zhang, P., Battchikova, N., Ogawa, T., Aro, E.M. and Boekema, E.J. (2006) Structural characterisation of NDH-1 complexes of Thermosynechococcus elongatus by single particle electron microscopy. Biochim.Biophys. Acta, 1757, 1469-1475.

[77] Peng, L., Fukao, Y., Fujiwara, M., Takami, T. and Shikanai, T. (2009) Efficient operation of NAD(P)H dehydrogenase requires supercomplex formation with photosystem I via minor LHCI in Arabidopsis. Plant Cell, 21, 3623-3640.

[78] S. Ishihara, A. Takabayashi, T. Endo, K. Ifuku, F. Sato, Distinct functions for the two PsbP-like proteins PPL1 and PPL2 in the chloroplast thylakoid lumen of Arabidopsis, Plant Physiol. 145 (2007) 668-679.

[79] M. Suorsa, S. Sirpi, V. Paakkarinen, N. Kumari, M. Holmstrm, E.M. Aro, Two proteins homologous to PsbQ are novel subunits of the chloroplast NAD(P)H dehydrogenase, Plant Cell Physiol. 51 (2010) 877883

[80] S. Yabuta, K. Ifuku, A. Takabayashi, S. Ishihara, K. Ido, N. Ishikawa, T. Endo, F. Sato, Three PsbQ-like proteins are required for the function of the chloroplast NAD(P)H dehydrogenase complex in Arabidopsis, Plant Cell Physiol. 51 (2010) 866-876.

[81] Kirchhoff H. 2013a. Architectural switches in plant thylakoid membranes. Photosynthesis Research 116, 481-487.

[82] Andersson B, Anderson JM. 1980. Lateral heterogeneity in the distribution of chlorophyll-protein complexes of the thylakoid membranes of spinach chloroplasts. Biochimica et Biophysica Acta 593, 427-440.

[83] Albertsson P. 2001. A quantitative model of the domain structure of the photosynthetic membrane. Trends in Plant Science 6, 349-358.

[84] Barros T, Royant A, Standfuss J, Dreuw A, Kuhlbrandt W (2009) Crystal structure of plant light-harvesting complex shows the active, energy-transmitting state. EMBO J 28:298-306

[85] Daum B, Kuhlbrandt W. 2011. Electron tomography of plant thylakoid membranes. Journal of Experimental Botany 62, 2393-2402.

[86] Amunts A, Nelson N (2008) Functional organization of plant Photosystem I: evolution of a highly efficient photochemical machine. Plant Physiol Biochem 46:228-237

[87] Junge W, Sielaff H, Engelbrecht S (2009) Torque generation and elastic power transmission in the rotary FoF1-ATPase. Nature 459:364-370

[88] Kirchhoff H, Hall C, Wood M, Herbstova M, Tsabari O, Nevo R, Charuvi D, Shimoni E, Reich Z. 2011. Dynamic control of protein dif-

fusion within the granal thylakoid lumen. Proceedings of the National Academy of Sciences, USA 108, 20248-20253.

[89] Trissl HW, Wilhelm C. 1993. Why do thylakoid membranes from higher plants form grana stacks? Trends in Biochemical Sciences 18, 415-419.

[90] Horton P. 1999. Are grana necessary for regulation of light harvesting? Australian Journal of Plant Physiology 26, 659-669.

[91] Mustardy L, Garab G. 2003. Granum revisited. A three-dimensional model where things fall into place. Trends in Plant Science 8, 117-122.

[92] Mullineaux CW. 2005. Function and evolution of grana. Trends in Plant Science 10, 521-525.

[93] Anderson JM, Chow WS, De Las Rivas J. 2008. Dynamic flexibility in the structure and function of photosystem II in higher plant thylakoid membranes: the grana enigma. Photosynthesis Research 98, 575-587.

[94] Paolillo DJ Jr. 1970. The three-dimensional arrangement of intergranal lamellae in chloroplasts. Journal of Cell Science 6, 243-255

[95] Mustardy L, Buttle K, Steinbach G, Garab G. 2008. The three-dimensional network of the thylakoid membranes in plants: quasi-helical model of the granum-stroma assembly. The Plant Cell 20, 2552-2557.

[96] Arvidsson PO, Sundby C. 1999. A model for the topology of the chloroplast thylakoid membrane. Australian Journal of Plant Physiology 26, 687-694.

[97] Austin JR 2nd, Staehelin LA. 2011. Three-dimensional architecture of grana and stroma thylakoids of higher plants as determined by electron tomography. Plant Physiology 155, 1601-1611

[98] Anderson JM. 1986. Photoregulation of the composition, function and structure of thylakoid membranes. Annual Review of Plant Physiology 37, 93-136.

[99] Fristedt R, Willig A, Granath P, Crevecoeur M, Rochaix JD,Vener AV. 2009. Phosphorylation of photosystem II controls functional macroscopic folding of photosynthetic membranes in Arabidopsis. The Plant Cell 21, 3950-3964.

[100] Khatoon M, Inagawa K, Pospisil P, Yamashita A, Yoshioka M, Lundin B, Horie J, Morita N, Jajoo A, Yamamoto Y. 2009. Quality control of photosystem II: thylakoid unstacking is necessary to avoid further damage to the D1 protein and to facilitate D1 degradation under light stress in spinach thylakoids. Journal of Biological Chemistry 284, 25343-25352.

[101] Herbstova M, Tietz S, Kinzel C, Turkina MV, Kirchhoff H. 2012. Architectural switch in plant photosynthetic membranes induced by light stress. Proceedings of the National Academy of Sciences, USA 109, 20130-20135.

[102] Kirchhoff H. 2013b. Structural constraints for protein repair in plant photosynthetic membranes. Plant Signaling and Behavior 8, e23634.

[103] Pribil, M., Labs, M., and Leister, D. (2014). Structure and dynamics of thylakoids in land plants. Journal of experimental botany, 65(8), 1955-72

[104] Armbruster U, Labs M, Pribil M, et al. 2013. Arabidopsis CURVATURE THYLAKOID1 proteins modify thylakoid architecture by inducing membrane curvature. The Plant Cell 25, 2661-2678.

[105] Aro, E. M., Virgin, I. and Andersson, B. 1993 Photoinhibition of Photosystem II. Inactivation, protein damage and turnover. Biochim. Biophys. Acta 1143, 113-134

[106] Sonoike, K. 2010 Photoinhibition of photosystem I. Physiol. Plant 142, 56-64.

[107] Horton P, Ruban AV, Walters RG (1994) Regulation of light harvesting in green plants: indication by non- photochemical quenching of chlorophyll fluorescence. Plant Physiol 106: 415-420

[108] Horton P, Hague A (1988) Studies on the induction of chlorophyll fluorescence in isolated barley protoplasts: IV. Resolution of non-photochemical quenching. Biochim Biophys Acta 932: 107-115

[109] Yamamoto HY (1979) Biochemistry of the violaxanthin cycle in higher plants. Pure Appl Chem 51:639-648

[110] Gilmore AM (1997) Mechanistic aspects of xanthophyll cycle-dependent photoprotection in higher plant chloro- plasts and leaves. Physiol Plant 99: 197-209

[111] Li XP, Bjorkman O, Shih C, Grossman AR, Rosenquist M, Jansson S, Niyogi KK (2000) A pigment-binding protein essential for regulation of photosynthetic light harvesting. Nature 403: 391-395

[112] Peterson RB, Havir EA (2000) A non-photochemical- quenching-deficient mutant of Arabidopsis thaliana possessing normal pigment composition and xanthophyll- cycle activity. Planta 210: 205-214

[113] Funk C, Schroder WP, Napiwotzki A, Tjus SE, Renger G, Andersson B (1995) The PSII-S protein of higher plants: a new type of pigment-binding protein. Biochemistry 34: 11133-11141

[114] Bonente G, Howes BD, Caffarri S, Smulevich G, Bassi R: Interactions between the photosystem II subunit PsbS and xanthophylls studied in vivo and in vitro. J Biol Chem 2008, 283:8434-8445.

[115] Li X-P, Gilmore AM, Caffarri S, Bassi R, Golan T, Kramer D, Niyogi KK: Regulation of photosynthetic light harvesting involves intrathylakoid lumen pH sensing by the PsbS protein. J Biol Chem 2004, 279:22866-22874.

[116] Betterle N, Ballottari M, Zorzan S, de Bianchi S, Cazzaniga S, Dall Osto L, Morosinotto T, Bassi R: Light induced dissociation of an antenna hetero-oligomer is needed for non- photochemical quenching induction. J Biol Chem 2009, 284:15255-15266

[117] Goral TK, Johnson MP, Duffy CDP, Brain APR, Ruban AV, Mullineaux CW: Light-harvesting antenna composition controls the macrostructure and dynamics of thylakoid membranes in Arabidopsis. Plant J 2012, 69: 289-301.

[118] Niyogi KK (1999) Photoprotection revisited: genetic and molecular approaches. Annu Rev Plant Physiol Plant Mol Biol 50: 333-359

[119] Shapiguzov, A., Ingelsson, B., Samol, I., Andres, C., Kessler, F., Rochaix, J.D., Vener, A.V. and Goldschmidt-Clermont, M. (2010) The PPH1 phophatase is specifically involved in LHCII dephosphorylation and state transitions in Arabidopsis. Proc. Natl. Acad. Sci. USA 107, 4782-4787.

[120] Tikkanen, M., Nurmi, M., Suorsa, M., Danielsson, R., Mamedov, F., Styring, S., and Aro, E.-M. (2008). Phosphorylation-dependent regulation of excitation energy distribution between the two photosystems in higher plants. Biochimica et biophysica acta, 1777(5), 425-432

[121] Tikkanen, M., Nurmi, M., Kangasjarvi, S. and Aro, E.-M. (2008) Core protein phosphorylation facilitates the repair of photodamaged photosystem II at high light. Biochim. Biophys. Acta 1777, 1432-1437.

[122] Harrison, M.A. and Allen, J.F. (1991) Light-dependent phosphorylation of photosystem II polypeptides maintains electron transport at high light intensity: separation from effects of phosphorylation of LHC-II. Biochim. Biophys. Acta 1058, 289-296.

[123] Aro, E.-M., Kettunen, R. and Tyystjarvi, E. (1992) ATP and light regulate D1 protein modification and degradation. Role of D1 in photoinhibition. FEBS Lett. 297, 29-33.

[124] Bonarddi, V., Pesaresi, P., Becker, T., Schleiff, E., Wagner, R., Pfannschmidt, T.,Jahns, P. and Leister, D. (2005) Photosystem II core

phosphorylation and photosynthetic acclimation require two different protein kinases. Nature 43,1179-1182.

[125] Vainonen, J.P., Hansson, M. and Alexander, A.V. (2005) STN8 protein kinase in Arabidopsis thaliana is specific in phosphorylation of photosystem II core proteins. J. Biol. Chem. 280, 33679-33686.

[126] Pribil, M., Pesaresi, P., Hertle, A., Barbato, R. and Leister, D. (2010) Role of plastid protein phosphatase TAP38 in LHCII dephosphorylation and thylakoid electron flow. PLoS Biol. 8, 1-12.

[127] Samol, I., Shapiguzov, A., Ingelsson, B., Fucile, G., Crevecoeur, M., Vener, A.V.,Rochaix, J.D. and Clermont, G.-M. (2012) Identification of a Photosystem II Phosphatase Involved in Light Acclimation in Arabidopsis. Plant Cell 24,2596-2609.

[128] Bailey, S., Thompson, E., Nixon, P.J., Horton, P., Mullineaux, C.W., Robinson, C. and Mann, N.H. (2002) Critical roles for the Var2 FtsH homologue of Arabidopsis thaliana in the photosystem II repair cycle in vivo. J. Biol. Chem. 277, 2006-2011.

[129] Sun, X.W., Peng, L.W., Guo, J.K., Chi, W., Ma, J.F., Lu, C.M. and Zhang, L.X.(2007) Formation of DEG5 and DEG8 complexes and their involvement in the degradation of photodamaged photosystem II reaction center D1 protein in Arabidopsis thaliana. Plant Cell 19, 1347-1361.

[130] Sun, X.W., Wang, L.Y. and Zhang, L.X. (2007) Involvement of DEG5 and DEG8 proteases in the turnover of the photosystem II reaction center D1 protein under heat stress in Arabidopsis thaliana. Chin. Sci. Bull. 52, 1742-1745.

[131] Yamamoto, Y., Aminaka, R., Yoshioka, M., Khatoon, M., Komayama, K.,Takenaka, D., Yamashita, A., Nijo, N., Inagawa, K., Morita, N., Sasaki, T. and Yamamoto, Y. (2008) Quality control of photosystem II: impact of light and heat stresses. Photosynth. Res. 98, 589-609.

[132] Wagner, R., Aigner, H. and Funk, C. (2012). FtsH proteases located in the plant chloroplast. Physiol Plant 145, 203-214

[133] Huesgen, P.F., Schuhmann, H. and Adamska, I. (2005) The family of Deg proteases in cyanobacteria and chloroplasts of higher plants. Physiol. Plant.123, 413-420.

[134] Neidhardt J, Benemann JR, Zhang LP, Melis A (1998) Photosystem II repair and chloroplast recovery from irradiance stress: relationship between chronic photoinhibition, light-harvesting antenna size and photosynthetic productivity in Dunaliella salina (green algae). Photosynth Res 56: 175-184

[135] Sundby C, McCaffery S, Anderson JM (1993) Turnover of the photosystem II D1 protein in higher plants under photoinhibitory and non-photoinhibitory irradiance. J Biol Chem 268: 25476-25482

[136] Kudoh H, Sonoike K (2002a) Irreversible damage to photosystem I by chilling in the light: cause of the degradation of chlorophyll after returning to normal growth temperature. Planta 215: 541-548

[137] Sonoike K, Terashima I, Iwaki M, Itoh S (1995b) Destruction of photosystem I iron-sulfur centers in leaves of Cucumis sativus L. by weak illumination at chilling temperatures. FEBS Lett 362: 235-238

[138] Sonoike K (1996b) Degradation of psaB gene product, the reaction center subunit of photosystem I, is caused during hotoinhibition of photosystem I: possible involvement of active oxygen species. Plant Sci 115:157-164

[139] Tomizioli, M., Lazar, C., Brugiere, S., Burger, T., Salvi, D., Gatto, L., Moyet, L., et al. (2014). Deciphering thylakoid sub-compartments using a mass spectrometry-based approach. Molecular and cellular proteomics : MCP, (1), 2147-2167

[140] Ferro, M., Brugiere, S., Salvi, D., Seigneurin-Berny, D., Court, M., Moyet, L., Ramus, C., et al. (2010). AT_CHLORO, a comprehensive chloroplast proteome database with subplastidial localisation and curated information on envelope proteins. Molecular and cellular proteomics : MCP, 9(6), 1063-84

[141] Salvi, D., Rolland, N., Joyard, J., and Ferro, M. (2008). Purification and proteomic analysis of chloroplasts and their sub-organellar compartments. Methods Mol. Biol. 432, 19-36.

[142] D.Walker, The Use of the Oxygen Electrode and Fluorescence Probes in Simple Measurements of Photosynthesis, Oxygraphics Ltd., University of Sheffield, South Yorkshire, UK, 1990

[143] Leech, R. M. (1965). Comparative biochemistry and comparative morphology of chloroplasts isolated by different methods. In: Biochemistry of Chloroplasts. L Ed. by T. W. Goodwin, pp. 65-74. Academic Press, London

[144] Lilley R.McC., M.P. Fitzgerald, K.G. Rienits, D.A. Walker, Criteria of intactness and the photosynthetic activity of spinach chloroplasts preparations, New Phytol. 75 (1975) 1-10

[145] Bassi R, Giacometti G, Simpson D. Changes in the organization of stroma membranes induced by in vivo state 1-state 2 transition. Biochimica et Biophysica Acta (BBA) - Bioenergetics 01/1988

[146] Deborah A, Berthold Gerald T, Babcock Charles F. Yocum. Volume 134, Issue 2, 16 November 1981,231-234

[147] Morosinotto T, Segalla A, Giacometti GM, Bassi R. Purification of structurally intact grana from plants thylakoids membranes. J Bioenerg Biomembr. 2010 Feb;42(1):37-45

[148] Nelson, N. and Yocum, C.F. (2006). Structure and function of photosystems I and II. Annu Rev Plant Biol 57, 521-565

[149] W. L. Butler Chlorophyll Fluorescence: A Probe for Electron Transfer and Energy Transfer Photosynthesis I Encyclopedia of Plant Physiology Volume 5, 1977, pp 149-167

[150] Mullineaux CW (1992) Excitation energy transfer from phycobilisomes to photosystem I in a cyanobacterium. Biochim Biophys Acta 1100:285-292

[151] Brautigam K, Dietzel L, Kleine T, Stroher E, Wormuth D, Dietz KJ, Radke D, Wirtz M, Hell R, Dormann P, Nunes-Nesi A, Schauer N, Fernie AR, Oliver SN, Geigenberger P, Leister D, Pfannschmidt T (2009) Dynamic plastid redox signals integrate gene expression and metabolism to induce distinct metabolic states in photosynthetic acclimation in Arabidopsis. Plant Cell 21:2715?2732

[152] Microclimate for Cultural Heritage : Conservation, Restoration, and Maintenance of Indoor and Outdoor Monuments, Edition 2 D. Camuffo - 4 ottobre 2013 Elsevier - Editore

[153] Allen CF, Good P, Trosper T, Park RB (1972) Chlorophyll, glycerolipid and protein ratios in spinach chloroplast grana and stroma lamellae. Biochem Biophys Res Commun 48: 907-913

[154] Papers, M. C. P. (2014). MCP Papers in Press. Published on May 28, 2014 as Manuscript M114.040923, 33(0), 1-65

[155] Jung HS, Chory J. Signaling between Chloroplasts and the Nucleus: Can a Systems Biology Approach Bring Clarity to a Complex and Highly Regulated Pathway - Plant Physiol 2010;152:453-9

[156] Sutherland BW, Toews J, Kast J. 2008. Utility of formaldehyde cross-linking and mass spectrometry in the study of protein-protein interactions. J Mass Spectrom 43:699-715

[157] Agrawal, G. K., Bourguignon, J., Rolland, N., Ferro, M., Jaquinod, M., Alexiou, K. G., Chardot, T., et al. (2011). Plant organelle proteomics : collaborating for optimal cell function , Mass Spectrometry Reviews 772-853

[158] Walther TC, Mann M (2010) Mass spectrometry-based proteomics in cell biology. J Cell Biol 190: 491-500

[159] Baginsky S (2009) Plant proteomics: concepts, applications, and novel strategies for data interpretation. Mass Spectrom Rev 28: 93-120

[160] Salvi, D., Rolland, N., Joyard, J., and Ferro, M. (2008). Purification and proteomic analysis of chloroplasts and their sub-organellar compartments. Methods in molecular biology (Clifton, N.J.), 432, 19-36

[161] Haynes PA, Roberts TH. 2007. Subcellular shotgun proteomics in plants: Looking beyond the usual suspects. Proteomics 7:2963-2975

[162] Nesvizhskii AI, Vitek O, Aebersold R. 2007. Analysis and validation of proteomic data generated by tandem mass spectrometry. Nat Methods 4:787-797

[163] Taylor JA, Johnson RS. 1997. Sequence database searches via de novo peptide sequencing by tandem mass spectrometry. Rapid Commun Mass Spectrom 11:1067-1075

[164] Chen T, Kao MY, Tepel M, Rush J, Church GM. 2001. A dynamic programming approach to de novo peptide sequencing via tandem mass spectrometry. J Comput Biol 8: 325-337

[165] Grossmann J, Roos FF, Cieliebak M, Liptak Z, Mathis LK, Muller M, Gruissem W, Baginsky S. 2005. AUDENS: A tool for automated peptide de novo sequencing. J Proteome Res 4: 1768-1774

[166] Grossmann J, Fischer B, Baerenfaller K, Owiti J, Buhmann JM, Gruissem W, Baginsky S. 2007. A workflow to increase the detection rate of proteins from unsequenced organisms in high-throughput proteomics experiments. Proteomics 7: 4245-4254

[167] Shevchenko A, Sunyaev S, Loboda A, Shevchenko A, Bork P, Ens W, Standing KG. 2001. Charting the proteomes of organisms with unsequenced genomes by MALDI-quadrupole time-of-flight mass spectrometry and blast homology searching. Anal Chem 73:1917- 1926

[168] Mackey AJ, Haystead TAJ, Pearson WR. 2002. Getting more from less: Algorithms for rapid protein identification with multiple short peptide sequences. Mol Cell Proteomics 1:139-147

[169] Chalkley RJ, Baker PR, Huang L, Hansen KC, Allen NP, Rexach M, Burlingame AL. 2005a. Comprehensive analysis of a multidimensional liquid chromatography mass spectrometry dataset acquired on a quadrupole selecting, quadrupole collision cell, time-of-flight mass spectrometer: II. New developments in protein prospector allow for reliable and comprehensive automatic analysis of large datasets. Mol Cell Proteomics 4:1194-1204

[170] Chalkley RJ, Baker PR, Hansen KC, Medzihradszky KF, Allen NP, Rexach M, Burlingame AL. 2005b. Comprehensive analysis of a multidimensional liquid chromatography mass spectrometry dataset acquired on a quadrupole selecting, quadrupole collision cell, time of-flight mass spectrometer: I. How much of the data is theoretically interpretable by search engines? Mol Cell Proteomics 4:1189-1193

[171] Keller A, Nesvizhskii AI, Kolker E, Aebersold R. 2002. Empirical statistical model to estimate the accuracy of peptide identifications made by MS/MS and database search. Anal Chem 74:5383-5392

[172] Liu H, Sadygov RG, Yates JR III. 2004. A model for random sampling and estimation of relative protein abundance in shotgun proteomics. Anal Chem 76:4193-4201.

[173] Karp NA, Lilley KS. 2007. Design and analysis issues in quantitative proteomics studies. Proteomics 7:42-50

[174] Aggarwal K, Choe LH, Lee KH. 2006. Shotgun proteomics using the iTRAQ isobaric tags. Brief Funct Genomic Proteomic 5:112-120

[175] Ong S, Mann M. 2006.Apractical recipe for stable isotope labeling by amino acids in cell culture (silac). Nat Protoc 1:2650-2660

[176] Nelson CJ, Hegeman AD, Harms AC, Sussman MR. 2006. A quantitative analysis of arabidopsis plasma membrane using trypsin-catalyzed (18)O labeling. Mol Cell Proteomics 5:1382-1395

[177] Bantscheff M, Schirle M, Sweetman G, Rick J, Kuster B. 2007. Quantitative mass spectrometry in proteomics: A critical review. Anal Bioanal Chem 389:1017-1031

[178] Gerber SA, Rush J, Stemman O, Kirschner MW, Gygi SP. 2003. Absolute quantification of proteins and phosphoproteins from cell lysates by tandem MS. Proc Natl Acad Sci USA 100:6940-6945

[179] Zybailov B, Rutschow H, Friso G, Rudella A, Emanuelsson O, Sun Q, van Wijk KJ. 2008. Sorting signals, N-terminal modifications and abundance of the chloroplast proteome. PLoS ONE 3(4):1994

[180] Joyard J, Ferro M, Masselon C, Seigneurin-Berny D, Salvi D, Garin J, Rolland N. 2009. Chloroplast proteomics and the compartmentation of plastidial isoprenoid biosynthetic pathways. Mol Plant 2:1154- 1180.

[181] Seigneurin-Berny D, Rolland N, Garin J, Joyard J. 1999. Technical advance: Differential extraction of hydrophobic proteins from chloroplast envelope membranes: A subcellular-specific proteomic approach to identify rare intrinsic membrane proteins. Plant J 19:217-228

[182] Jones AME, Bennett MH, Mansfield JW, Grant M. 2006. Analysis of the defence phosphoproteome of Arabidopsis thaliana using differential mass tagging. Proteomics 6:4155?4165

[183] Ferro M, Salvi D, Riviere-Rolland H, Vermat T, Seigneurin-Berny D, Grunwald D, Garin J, Joyard J, Rolland N. 2002. Integral membrane proteins of the chloroplast envelope: Identification and subcellular localisation of new transporters. Proc Natl Acad Sci USA 99:11487- 11492

[184] Ferro M, Salvi D, Brugiere S, Miras S, Kowalski S, Louwagie M, Garin J, Joyard J, Rolland N. 2003. Proteomics of the chloroplast envelope membranes from Arabidopsis thaliana. Mol Cell Proteomics 2:325- 345

[185] Froehlich JE, Wilkerson CG, Ray WK, McAndrew RS, Osteryoung KW, Gage DA, Phinney BS. 2003. Proteomic study of the Arabidopsis thaliana chloroplastic envelope membrane utilizing alternatives to traditional two-dimensional electrophoresis. J Proteome Res 2:413- 425

[186] van Wijk KJ. 2004. Plastid proteomics. Plant Physiol Biochem 42:963-977

[187] Baginsky S, Gruissen W. 2004. Chloroplast proteomics: Potentials and challenges. J Exp Bot 55:1213-1220

[188] Peltier JB, Cai Y, Sun Q, Zabrouskov V, Giacomelli L, Rudella A, Ytterberg AJ, Rutschow H, van Wijk KJ. 2006. The oligomeric stromal proteome of Arabidopsis thaliana chloroplasts. Mol Cell Proteomics 5:114-133

[189] Goulas E, Schubert M, Kieselbach T, Kleczkowski LA, Gardestrom P, Schroder W, Hurry V. 2006. The chloroplast lumen and stromal proteomes of Arabidopsis thaliana show differential sensitivity to short- and long-term exposure to low temperature. Plant J 47:720-734

[190] Kieselbach T, Hagman A, Andersson B, Schroder WP. 1998. The thylakoid lumen of chloroplasts. Isolation and characterisation. J Biol Chem 273:6710-6716

[191] Kieselbach T, Bystedt M, Hynds P, Robinson C, Schroder WP. 2000. A peroxidase homologue and novel plastocyanin located by proteomics to the Arabidopsis chloroplast thylakoid lumen. FEBS Lett 480:271-276

[192] Schubert M, Petersson UA, Haas BJ, Funk C, Schroder WP, Kieselbach T. 2002. Proteome map of the chloroplast lumen of Arabidopsis thaliana.J Biol Chem 277:8354-8365

[193] Peltier JB, Emanuelsson O, Kalume DE, Ytterberg J, Friso G, Rudella A, Liberles DA, Soderberg L, Roepstorff P, von Heijne G, van Wijk KJ. 2002. Central functions of the lumenal and peripheral thylakoid

proteome of Arabidopsis determined by experimentation and genome-wide prediction. Plant Cell 14:211-236

[194] Rolland, N., Curien, G., Finazzi, G., Kuntz, M., Marechal, E., Matringe, M., Ravanel, S. and Seigneurin-Berny, D. (2012). The biosynthetic capacities of the plastids and integration between cytoplasmic and chloroplast processes. Annu Rev Genet 46, 233-264

[195] Joyard, J., Ferro, M., Masselon, C., Seigneurin-Berny, D., Salvi, D., Garin, J. and Rolland, N. (2010). Chloroplast proteomics highlights the subcellular compartmentation of lipid metabolism. Prog Lipid Res 49, 128-158

[196] Block, M.A., Douce, R., Joyard, J. and Rolland, N. (2007). Chloroplast envelope membranes: a dynamic interface between plastids and the cytosol. Photosynth Res 92, 225-244

[197] Weber, A.P.M., Schwacke, R. and Flugge, U. (2005). Solute transporters of the plastid envelope membrane. Annu Rev Plant Biol 56, 133-164

[198] Tonkin, C.J., Kalanon, M. and McFadden, G.I. (2008). Protein targeting to the malaria parasite plastid. Traffic 9, 166-175

[199] Obornik, M., Janouskovec, J., Chrudimsky, T. and Lukes, J. (2009). Evolution of the apicoplast and its hosts: from heterotrophy to autotrophy and back again. Int J Parasitol 39,1-12

[200] Rochaix, J. (2013). Redox regulation of thylakoid protein kinases and photosynthetic gene expression. Antioxid Redox Signal 18, 2184-2201

[201] Agarwal, R., Matros, A., Melzer, M., Mock, H. and Sainis, J.K. (2010). Heterogeneity in thylakoid membrane proteome of Synechocystis 6803. J Proteomics 73, 976-991

[202] Lilley, K.S. and Dupree, P. (2007). Plant organelle proteomics. Curr Opin Plant Biol 10, 594-599

[203] Dunkley, T. P., Hester, S., Shadforth, I. P., Runions, J., Weimar, T.,Hanton, S. L., Griffin, J. L., Bessant, C., Brandizzi, F., Hawes, C.,Watson, R. B., Dupree, P., and Lilley, K. S. (2006) Mapping the Arabidopsis organelle proteome. Proc. Natl. Acad. Sci. U.S.A. 103,6518-6523

[204] Kleffmann, T., Hirsch-Hoffmann, M., Gruissem, W. and Baginsky, S. (2006). plprot: a comprehensive proteome database for different plastid types. Plant Cell Physiol 47, 432-436

[205] Peltier, J.B., Friso, G., Kalume, D.E., Roepstorff, P., Nilsson, F., Adamska, I. and van Wijk, K.J. (2000). Proteomics of the chloroplast:

systematic identification and targeting analysis of lumenal and peripheral thylakoid proteins. Plant Cell 12, 319-341

[206] Whitelegge JP, Gundersen CB, Faull KF. 1998. Electrospray-ionization mass spectrometry of intact intrinsic membrane proteins. Protein Sci 7:1423- 1430

[207] Vener AV, Harms A, Sussman MR, Vierstra RD. 2001. Mass spectrometric resolution of reversible protein phosphorylation in photosynthetic membranes of Arabidopsis thaliana. J Biol Chem 276:6959-6966

[208] Zolla L, Rinalducci S, Timperio AM, Huber CG. 2002. Proteomics of light- harvesting proteins in different plant species. Analysis and comparison by liquid chromatography-electrospray ionization mass spectrometry. Photosystem I. Plant Physiol 130:1938-1950

[209] Gomez, S.M., Nishio, J.N., Faull, K.F. and Whitelegge, J.P. (2002). The chloroplast grana proteome defined by intact mass measurements from liquid chromatography mass spectrometry. Mol Cell Proteomics 1, 46-59

[210] Gomez, S.M., Bill, K.Y., Aguilera, R., Nishio, J.N., Faull, K.F. and Whitelegge, J.P. (2003). Transit peptide cleavage sites of integral thylakoid membrane proteins. Mol Cell Proteomics 2, 1068-1085

[211] Friso G, Giacomelli L, Ytterberg AJ, Peltier JB, Rudella A, Sun Q, Wijk KJ. 2004. In-depth analysis of the thylakoid membrane proteome of Arabidopsis thaliana chloroplasts: New proteins, new functions, and a plastid proteome database. Plant Cell 16:478-499

[212] Peltier, J., Ripoll, D.R., Friso, G., Rudella, A., Cai, Y., Ytterberg, J., Giacomelli, L., Pillardy, J. and van Wijk, K.J. (2004). Clp protease complexes from photosynthetic and nonphotosynthetic plastids and mitochondria of plants, their predicted three-dimensional structures, and functional implications. J Biol Chem 279, 4768-4781

[213] Turkina, M.V., Kargul, J., Blanco-Rivero, A., Villarejo, A., Barber, J. and Vener, A.V. (2006). Environmentally modulated phosphoproteome of photosynthetic membranes in the green alga Chlamydomonas reinhardtii. Mol Cell Proteomics 5, 1412-1425

[214] Zolla L, Rinalducci S, Timperio AM. 2007. Proteomic analysis of photosystem I components from different plant species. Proteomics 7:1866-1876

[215] Zhang, Y., Wen, Z., Washburn, M.P. and Florens, L. (2010). Refinements to label free proteome quantitation: how to deal with peptides shared by multiple proteins. Anal Chem 82, 2272-2281

[216] Fermin, D., Basrur, V., Yocum, A.K. and Nesvizhskii, A.I. (2011). Abacus: a computational tool for extracting and pre-processing spectral count data for label-free quantitative proteomic analysis. Proteomics 11, 1340-1345

[217] Thimm, O., Blasing, O., Gibon, Y., Nagel, A., Meyer, S., Kruger, P., Selbig, J., Muller, L.A., Rhee, S.Y. and Stitt, M. (2004). MAPMAN: a user-driven tool to display genomics data sets onto diagrams of metabolic pathways and other biological processes. Plant J 37, 914-939

[218] BrunV, Dupuis A, Adrait A, Marcellin M, Thomas D, Court M,Vandenesch F, Garin J. 2007. Isotope-labeled protein standards: Toward absolute quantitative proteomics. Mol Cell Proteomics 6:2139?2149

[219] Glynn, J.M., Froehlich, J.E. and Osteryoung, K.W. (2008). Arabidopsis ARC6 coordinates the division machineries of the inner and outer chloroplast membranes through interaction with PDV2 in the intermembrane space. Plant Cell 20, 2460-2470

[220] Lazar, C., Taminau, J., Meganck, S., Steenhoff, D., Coletta, A., Molter, C., de Schaetzen, V., Duque, R., Bersini, H. and Now, A. (2012). A survey on filter techniques for feature selection in gene expression microarray analysis. IEEE/ACM Transactions on Computational Biology and Bioinformatics , 1106-1119

[221] Smyth, G.K. (2005).Limma: linear models for microarray data. Edition (Springer)

[222] Benjamini, Y. and Hochberg, Y. (1995). Controlling the false discovery rate: A practical and powerful approach to multiple testing. Journal of the Royal Statistical Society 57, 289-300

[223] Mamedov, F., Stefansson, H., Albertsson, P.A. and Styring, S. (2000). Photosystem II in different parts of the thylakoid membrane: a functional comparison between different domains. Biochemistry 39, 10478-10486

[224] Sato, N., Rolland, N., Block, M.A. and Joyard, J. (1999). Do plastid envelope membranes play a role in the expression of the plastid genome?. Biochimie 81, 619-629

[225] Sato, N., Albrieux, C., Joyard, J., Douce, R. and Kuroiwa, T. (1993). Detection and characterisation of a plastid envelope DNA-binding protein which may anchor plastid nucleoids. EMBO J 12, 555-561

[226] Liu, J.W. and Rose, R.J. (1992). The spinach chloroplast chromosome is bound to the thylakoid membrane in the region of the inverted repeat. Biochem Biophys Res Commun 184, 993-1000

[227] Small I, Peeters N, Legeai F, Lurin C. 2004. Predotar: A tool for rapidly screening proteomes for N-terminal targeting sequences. Proteomics 4:1581-1590

[228] Takahashi, Y., Goldschmidt-Clermont, M., Soen, S.Y., Franzen, L.G. and Rochaix, J.D. (1991). Directed chloroplast transformation in Chlamydomonas reinhardtii: insertional inactivation of the psaC gene encoding the iron sulfur protein destabilizes photosystem I. EMBO J 10, 2033-2040

[229] Mannan, R.M., Whitmarsh, J., Nyman, P. and Pakrasi, H.B. (1991). Directed mutagenesis of an iron-sulfur protein of the photosystem I complex in the filamentous cyanobacterium Anabaena variabilis ATCC 29413. Proc Natl Acad Sci U S A 88, 10168- 10172

[230] Rochaix, J., Lemeille, S., Shapiguzov, A., Samol, I., Fucile, G., Willig, A. and Goldschmidt-Clermont, M. (2012). Protein kinases and phosphatases involved in the acclimation of the photosynthetic apparatus to a changing light environment. Philos Trans R Soc Lond B Biol Sci 367, 3466-3474

[231] Leister, D. and Shikanai, T. (2013). Complexities and protein complexes in the antimycin A-sensitive pathway of cyclic electron flow in plants. Front Plant Sci 4, 161

[232] Vallon, O., Bulte, L., Dainese, P., Olive, J., Bassi, R. and Wollman, F.A. (1991). Lateral redistribution of cytochrome b6f complexes along thylakoid membranes upon state transitions. Proc Natl Acad Sci U S A 88, 8262-8266

[233] Allred, D.R. and Staehelin, L.A. (1985). Lateral Distribution of the Cytochrome b6f and Coupling Factor ATP Synthetase Complexes of Chloroplast Thylakoid Membranes. Plant Physiol 78, 199-202

[234] De Bianchi, S., Dall Osto, L., Tognon, G., Morosinotto, T., and Bassi, R. (2008). Minor antenna proteins CP24 and CP26 affect the interactions between photosystem II subunits and the electron transport rate in grana membranes of Arabidopsis. The Plant cell, 20(4), 1012?28. doi:10.1105/tpc.107.055749

[235] Anderson, J.M. and Andersson, B. (1982). The architecture of thylakoid membranes: lateral and transverse organization. Trends Biochem. Sci 7, 288-292

[236] Kuras, R. and Wollman, F.A. (1994). The assembly of cytochrome b6/f complexes: an approach using genetic transformation of the green alga Chlamydomonas reinhardtii. EMBO J 13, 1019-1027

[237] D. Stroebel, Y. Choquet, J.L. Popot, D. Picot, An atypical haem in the cytochrome b6f complex, Nature 426 (2003) 413-418

[238] Zhang, L. and Aro, E.M. (2002). Synthesis, membrane insertion and assembly of the chloroplast-encoded D1 protein into photosystem II. FEBS Lett 512, 13-18

[239] Kiss, A.Z., Ruban, A.V. and Horton, P. (2008). The PsbS protein controls the organization of the photosystem II antenna in higher plant thylakoid membranes. J Biol Chem 283, 3972-3978

[240] Allorent, G., Tokutsu, R., Roach, T., Peers, G., Cardol, P., Girard-Bascou, J., Seigneurin-Berny, D., Petroutsos, D., Kuntz, M., Breyton, C., Franck, F., Wollman, F., Niyogi, K.K., Krieger-Liszkay, A., Minagawa, J. and Finazzi, G. (2013). A dual strategy to cope with high light in Chlamydomonas reinhardtii. Plant Cell 25, 545-557

[241] Boekema, E.J., van Roon, H., Calkoen, F., Bassi, R. and Dekker, J.P. (1999). Multiple types of association of photosystem II and its light-harvesting antenna in partially solubilized photosystem II membranes. Biochemistry 38, 2233-2239

[242] Galka, P., Santabarbara, S., Khuong, T.T.H., Degand, H., Morsomme, P., Jennings, R.C., Boekema, E.J. and Caffarri, S. (2012). Functional analyses of the plant photosystem I light- harvesting complex II supercomplex reveal that light-harvesting complex II loosely bound to photosystem II is a very efficient antenna for photosystem I in state II. Plant Cell 24, 2963-2978

[243] Zhang, H., Whitelegge, J.P. and Cramer, W.A. (2001). Ferredoxin:NADP+ oxidoreductase is a subunit of the chloroplast cytochrome b6f complex. J Biol Chem 276, 38159-38165

[244] Schuhmann, H. and Adamska, I. (2012). Deg proteases and their role in protein quality control and processing in different subcellular compartments of the plant cell. Physiol Plant 145, 224-234

[245] Kato, Y. and Sakamoto, W. (2009). Protein quality control in chloroplasts: a current model of D1 protein degradation in the photosystem II repair cycle. J Biochem 146, 463-469

[246] Lucinski, R., Misztal, L., Samardakiewicz, S. and Jackowski, G. (2011). The thylakoid protease Deg2 is involved in stress-related degradation of the photosystem II light-harvesting protein Lhcb6 in Arabidopsis thaliana. New Phytol 192, 74-86

[247] Ferro, M., Seigneurin-Berny, D., Rolland, N., Chapel, A., Salvi, D., Garin, J. and Joyard, J. (2000). Organic solvent extraction as a versatile procedure to identify hydrophobic chloroplast membrane proteins. Electrophoresis 21, 3517-3526

[248] Abdel-Ghany, S.E., Muller-Moule, P., Niyogi, K.K., Pilon, M. and Shikanai, T. (2005). Two P-type ATPases are required for copper delivery in Arabidopsis thaliana chloroplasts. Plant Cell 17, 1233-1251

[249] Mitra, S.K., Walters, B.T., Clouse, S.D. and Goshe, M.B. (2009). An efficient organic solvent based extraction method for the proteomic analysis of Arabidopsis plasma membranes. J Proteome Res 8, 2752-2767

[250] Furumoto, T., Yamaguchi, T., Ohshima-Ichie, Y., Nakamura, M., Tsuchida-Iwata, Y., Shimamura, M., Ohnishi, J., Hata, S., Gowik, U., Westhoff, P., Brautigam, A., Weber, A.P.M. and Izui, K. (2011). A plastidial sodium-dependent pyruvate transporter. Nature 476, 472-475

[251] Muller, M., Kunz, H., Schroeder, J.I., Kemp, G., Young, H.S. and Neuhaus, H.E. (2014). Decreased capacity of sodium export out of Arabidopsis chloroplasts impairs salt tolerance, photosynthesis and plant performance. Plant J , in press

[252] Pavon, L.R., Lundh, F., Lundin, B., Mishra, A., Persson, B.L. and Spetea, C. (2008). Arabidopsis ANTR1 is a thylakoid Na+-dependent phosphate transporter: functional characterisation in Escherichia coli. J Biol Chem 283, 13520-13527

[253] Thuswaldner, S., Lagerstedt, J.O., Rojas-Stutz, M., Bouhidel, K., Der, C., Leborgne- Castel, N., Mishra, A., Marty, F., Schoefs, B., Adamska, I., Persson, B.L. and Spetea, C. (2007). Identification, expression, and functional analyses of a thylakoid ATP/ADP carrier

[254] Gigolashvili, T., Geier, M., Ashykhmina, N., Frerigmann, H., Wulfert, S., Krueger, S., Mugford, S.G., Kopriva, S., Haferkamp, I. and Flugge, U. (2012). The Arabidopsis thylakoid ADP/ATP carrier TAAC has an additional role in supplying plastidic phosphoadenosine 5- phosphosulfate to the cytosol. Plant Cell 24, 4187-4204.

[255] Ling, Q., Huang, W., Baldwin, A. and Jarvis, P. (2012). Chloroplast biogenesis is regulated by direct action of the ubiquitin-proteasome system. Science 338, 655-659

[256] Livingston, A. K., Cruz, J. A., Kohzuma, K., Dhingra, A., and Kramer, D. M. (2010) An Arabidopsis mutant with high cyclic electron flow around photosystem I (hcef) involving the NADPH dehydrogenase complex. Plant Cell 22, 221?233

[257] Page, M. L., Hamel, P. P., Gabilly, S. T., Zegzouti, H., Perea, J. V., Alonso, J. M., Ecker, J. R., Theg, S. M., Christensen, S.K., and Merchant, S. (2004) A homolog of prokaryotic thiol disulfide transporter CcdA is required for the assembly of the cytochrome b6f complex in Arabidopsis chloroplasts. J. Biol. Chem. 279, 32474?32482

[258] Porra, R.J., Thomson, W.A. and Kriedemann, P.E. (1989). Determination of accurate extinction coefficients and simultaneous equations for assaying chlorophylls a and b extracted with four different solvents: verification of the concentration of chlorophyll standards by atomic absorption spectroscopy. Biochimica et Biophysica Acta 975, 384-394

[259] Berthold, D. A., Babcock, G. T., and Yocum, C. F. (1981). A highly resolved, oxygen-evolving photosystem ii preparation from spinach thylakoid membranes, FEBS letter 134(2), 0-3

[260] Wilkins MR, Sanchez JC, Gooley AA, Appel RD, Humphery-Smith I, Hochstrasser DF,Williams KL. 1995. Progress with proteome projects: Why all proteins expressed by a genome should be identified and how to do it. Biotechnol Genet Eng Rev 13:19-50

[261] Dupierris, V., Masselon, C., Court, M., Kieffer-Jaquinod, S. and Bruley, C. (2009). A toolbox for validation of mass spectrometry peptides identification and generation of database: IRMa. BIOINFORMATICS 25, 1980-1981

[262] R Development Core Team (2008). R: A Language and Environment for Statistical Computing

[263] Gatto, L. and Lilley, K.S. (2012). MSnbase-an R/Bioconductor package for isobaric tagged mass spectrometry data visualization, processing and quantitation. Bioinformatics 28, 288-289.

[264] Gatto, L., Breckels, L.M., Wieczorek, S., Burger, T. and Lilley, K.S. (2014). Massspectrometry-based spatial proteomics data analysis using pRoloc and pRolocdata. Bioinformatics 30, 1322-1324

[265] Zanetti, M., Teardo, E., La Rocca, N., Zulkifli, L., Checchetto, V., Shijuku, T., Sato, Y., et al. (2010). A novel potassium channel in photosynthetic cyanobacteria. PloS one, 5(4), e10118

[266] Karpievitch, Y.V., Dabney, A.R. and Smith, R.D. (2012). Normalization and missing value imputation for label-free LC-MS analysis. BMC Bioinformatics 13 Suppl 16, S5

[267] Little, R.J.A. and Rubin, D.B. (2002).Statistical analysis with missing data Edition (Wiley-Interscience)

[268] Luo, R., Colangelo, C.M., Sessa, W.C. and Zhao, H. (2009). Bayesian Analysis of iTRAQ Data with Nonrandom Missingness: Identification of Differentially Expressed Proteins. Statistics in Biosciences 1, 228-245

[269] Karpievitch, Y., Stanley, J., Taverner, T., Huang, J., Adkins, J.N., Ansong, C., Heffron, F., Metz, T.O., Qian, W., Yoon, H., Smith, R.D. and Dabney, A.R. (2009). A statistical framework for protein quantitation in bottom-up MS-based proteomics. Bioinformatics 25, 2028-2034.

[270] Troyanskaya, O., Cantor, M., Sherlock, G., Brown, P., Hastie, T., Tibshirani, R., Botstein, D. and Altman, R.B. (2001). Missing value estimation methods for DNA microarrays. Bioinformatics 17, 520-525.

[271] Bolstad, B.M., Irizarry, R.A., Astrand, M. and Speed, T.P. (2003). A comparison of normalization methods for high density oligonucleotide array data based on variance and bias. Bioinformatics 19, 185-193

[272] Kooperberg, C., Aragaki, A., Strand, A.D. and Olson, J.M. (2005). Significance testing for small microarray experiments. Stat Med 24, 2281-2298

[273] Park, H. and Jun, C. (2009). A simple and fast algorithm for k-medoids clustering. Expert Systems with Applications 36, 3336-3341

[274] Dhillon, I.S., Guan, Y. and Kulis, B. (2004). Kernel k-means: spectral clustering and normalized cuts. Proceedings of the tenth ACM SIGKDD international conference on Knowledge discovery and data mining , 551-556

[275] Karatzoglou, A., Smola, A., Hornik, K. and Zeileis, A. (2004). kernlaban S4 package for kernel methods in R. Report

[276] Courty, N., Burger, T. and Marteau, P. (2012). Geodesic analysis on the gaussian RKHS hypersphere. Machine Learning and Knowledge Discovery in Databases, 299-313

[277] Sun, Q., Zybailov, B., Majeran, W., Friso, G., Olinares, P.D.B. and van Wijk, K.J. (2009). PPDB, the Plant Proteomics Database at Cornell. Nucleic Acids Res 37, D969-74

[278] Tanz, S.K., Castleden, I., Hooper, C.M., Vacher, M., Small, I. and Millar, H.A. (2013). SUBA3: a database for integrating experimentation and prediction to define the SUBcellular location of proteins in Arabidopsis. Nucleic Acids Res 41, D1185-91

[279] Klie, S. and Nikoloski, Z. (2012). The Choice between MapMan and Gene Ontology for Automated Gene Function Prediction in Plant Science. Front Genet 3, 115

[280] S. Eberhard, G. Finazzi, F. A. Wollman, The dynamics of photosynthesis. Annu. Rev. Genet. 42, 463-515 (2008)

[281] Pesaresi, P., Pribil, M., Wunder, T., and Leister, D. (2011). Dynamics of reversible protein phosphorylation in thylakoids of flowering plants: the roles of STN7, STN8 and TAP38. Biochimica et biophysica acta, 1807(8), 887-96

[282] J.D. Rochaix, Role of thylakoid protein kinases in photosynthetic acclimation, FEBS Lett. 581 (2007) 2768-2775

[283] K. Islam, The rate and extent of phosphorylation of the two light-harvesting chlorophyll a/b binding protein complex (LHC-II) polypeptides in isolated thylakoids, Biochim. Biophys. Acta 893 (1987) 333-341

[284] Muhlhaus, T., Weiss, J., Hemme, D., Sommer, F., and Schroda, M. (2011). Quantitative shotgun proteomics using a uniform 15N-labeled standard to monitor proteome dynamics in time course experiments reveals new insights into the heat stress response of Chlamydomonas reinhardtii. Molecular and cellular proteomics : MCP, 10(9)

[285] Hebeler R, Oeljeklaus S, Reidegeld KA, Eisenacher M, Stephan C, Sitek B, Stuhler K, Meyer HE, Sturre MJ, Dijkwel PP,Warscheid B. 2008. Study of early leaf senescence in Arabidopsis thaliana by quantitative proteomics using reciprocal 14N/15N labeling and difference gel electrophoresis. Mol Cell Proteomics 7:108?120

[286] Bellafiore, S., Barneche, F., Peltier, G., and Rochaix, J.-D. (2005). State transitions and light adaptation require chloroplast thylakoid protein kinase STN7. Nature, 433(7028), 892-895

[287] Anderson JM, Chow WS and Park Y-I (1995) The grand design of photosynthesis: acclimation of the photosynthetic apparatus to environmental cues. Photosynthesis Res 46, 129-139

[288] Fey V, Wagner R, Brautigam K, Wirtz M, Hell R, Dietzmann A, Leister D, Oelmuller R and Pfannschmidt T (2005) Retrograde plastid redox signals in the expression of nuclear genes for chloroplast proteins of Arabidopsis thaliana. J Biol Chem 280, 5318-5328

[289] M. Tikkanen, M. Piippo, M. Suorsa, S. Sirpio, P. Mulo, J. Vainonen, A.V. Vener, Y. Allahverdiyeva, E.M. Aro, State transitions revisited-a buffering system for dynamic low light acclimation of Arabidopsis, Plant Mol. Biol. 62 (2006) 779-793

[290] P. Pesaresi, A. Hertle, M. Pribil, T. Kleine, R. Wagner, H. Strissel, A. Ihnatowicz, V. Bonardi, M. Scharfenberg, A. Schneider, T. Pfannschmidt, D. Leister, Arabidopsis STN7 kinase provides a link

between short- and long-term photosynthetic acclimation, Plant Cell 21 (2009) 2402-2423

[291] Allen JF and Pfannschmidt T (2000) Balancing the two photosystems: photosynthetic electron transfer governs transcription of reaction centre genes in chloroplasts. Philos Trans R Soc Lond B Biol Sci 355, 1351-1359

[292] Horton, P, and Hague, A 1988, Biochim. Biophys. Acta, 932, 107

[293] Investigation of the plastoquinone pool size and fluorescence quenching in thylakoid membranes and Photosystem II (PS II) membrane fragments Photosynthesis Research 02-2000, Volume 63, Issue 2, pp 171-182

[294] Murata N, Nishimura M and Takamiya A (1966) Fluorescence of chlorophyll in photosynthetic systems. III. Emission and action spectra of fluorescence - three emission bands of chlorophyll a and the energy transfer between two pigment systems. Biochim Biophys Acta 126: 234-243

[295] Jansson, S. (1999). A guide to the Lhc genes and their relatives in Arabidopsis. Trends Plant Sci. 4: 236-240.

[296] Bassi,R.,Rigoni,F.,Barbato,R.,andGiacometti,G.M. (1988). Light-harvesting chlorophyll a/b proteins (LHCII) populations in phosphorylated membranes. Biochim. Biophys. Acta 936: 29-38

[297] H. Takahashi, M. Iwai, Y. Takahashi, J. Minagawa, Identification of the mobile light harvesting complex II polypeptides for state transitions in Chlamydomonas reinhardtii, Proc. Natl Acad. Sci. USA 103 (2006) 477-482

[298] Iwai, M., Takahashi, Y., and Minagawa, J. (2008). Molecular re- modeling of photosystem II during state transitions in Chlamydo- monas reinhardtii.Plant Cell 20: 2177-2189

[299] Kouril,R., Zygadlo,A.,Arteni, A.A.,de Wit,C.D.,Dekker,J.P., Jensen, P.E., Scheller, H.V., and Boekema, E.J. (2005). Structural characterisation of a complex of photosystem I and light-harvesting complex II of Arabidopsis thaliana. Biochemistry 44: 10935-10940

[300] S. Reiland, G. Messerli, K. Baerenfaller, B. Gerrits, A. Endler, J. Grossmann, W. Gruissem, S. Baginsky, Large-scale Arabidopsis phosphoproteome profiling reveals novel chloroplast kinase substrates and phosphorylation networks, Plant Physiol. 150 (2009) 889-903

[301] Carlberg, I., Hansson, M., Kieselbach, T., Schroder, W.P., Andersson, B., and Vener, A.V. (2003). A novel plant protein undergoing light-induced phosphorylation and release from the photosynthetic thylakoid membranes. Proc. Natl. Acad. Sci. USA 100: 757-762

[302] Mitchell P (1966) Chemiosmotic coupling in oxidative and photosynthetic phosphorylation. Biol Rev 41:445-502

[303] Kramer, D.M., Avenson, T.J. and Edwards, G.E. (2004) Dynamics flexibility in the light reactions of photosynthesis governed by both electron and proton transfer reactions. Trends Plant Sci. 9, 349-357.

[304] Bailleul, B., Cardol, P., Breyton, C., and Finazzi, G. (2010). Electrochromism: a useful probe to study algal photosynthesis. Photosynthesis research, 106(1-2), 179-89

[305] Witt HT (1979) Energy conversion in the functional membrane of photosynthesis. Analysis by light pulse and electric pulse methods. The central role of the electric field. Biochim Biophys Acta 505:355-427

[306] Joliot P, Delosme R (1974) Flash induced 529 nm absorption change in green algae. Biochim Biophys Acta 357:267-284

[307] Vredemberg WJ (1976) Electrostatic interactions and gradients between chloroplast compartments and cytoplasm. In: Barber J (ed) The intact chloroplast. Elsevier/North Holland Biomedical Press, Amsterdam, The Netherlands, pp 53-87

[308] Junge W, McLaughlin S (1987) The role of fixed and mobile buffers in the kinetics of proton movement. Biochim Biophys Acta 890:1-5

[309] Cruz JA, Sacksteder CA, Kanazawa A, Kramer DM (2001) Contribution of electric field to steady-state transthylakoid proton motive force (pmf) in vitro and in vivo. Control of pmf parsing into DW and DpH by ionic strength. Biochemistry 40:1226-1237

[310] D.I. Arnon, F.R. Whatley, M.B. Allen, Vitamin K as a cofactor of photosynthetic phosphorylation, Biochim. Biophys. Acta 16 (1955) 607-608

[311] U. Heber, D. Walker, Concerning a dual function of coupled cyclic electron- transport in leaves, Plant Physiol. 100 (1992) 1621-1626.

[312] Joliot, P., and Joliot, A. (2006). Cyclic electron flow in C3 plants. Biochimica et biophysica acta, 1757(5-6), 362-8

[313] Yamamoto, H., Peng, L., Fukao, Y. and Shikanai, T. (2011) An Src homology 3 domain-like fold protein forms a ferredoxin binding site for the chloroplast NADH dehydrogenase-lie complex in Arabidopsis. Plant Cell, 23,1480-1493.

[314] Munekage, Y., Hojo, M., Meurer, J., Endo, T., Tasaka, M., and Shikanai, T. (2002). PGR5 is involved in cyclic electron flow around photosystem I and is essential for photoprotection in Arabidopsis. Cell, 110(3), 361-71

[315] Schachtman D.P. (2000) - Molecular insights into the structure and function of plant K^+ transport mechanisms. Biochimica et Biophysica Acta vol. 1465, 127-139

[316] Very A.A., Sentenac H. (2002) - Cation channels in the Arabidopsis plasma membrane. Trends Plant Sci. 7, 168-175

[317] Voelker C., Schmidt D., Mueller-Roeber B., Czempinski K. (2006) - Members of the Arabidopsis AtTPK/KCO family form homomeric vacuolar channels in planta. The Plant Journal vol. 48, 296-306

[318] MacRobbie E.A.C. (1998) - Philos. Trans. R. Soc. Lond. B. 353, 1475-1488

[319] Gobert A., Isayenkov S., Voelker C., Czempinski K., Maathuis F.J.M. (2007) - The twopore channel TPK1 gene encodes the vacuolar K+ conductance and plays a role in K+ homeostasis. PNAS vol. 104(25), 10726-1073

[320] G. Schonknecht, P. Spoormaker, R. Steinmeyer, L. Bruggeman, P. Ache, R. Dutta, B. Reintanz, M. Godde, R. Hedrich, K. Palme, KCO1 is a component of the slow-vacuolar (SV) ion channel. FEBS Lett. 511, 28-32 (2002)

[321] H. Bihler, C. Eing, S. Hebeisen, A. Roller, K. Czempinski, A. Bertl, TPK1 is a vacuolar ion channel different from the slow-vacuolar cation channel. Plant Physiol. 139, 417-424 (2005)

[322] Becker D., Geiger D., Dunkel M., Roller A., Bertl A., Latz A., Carpaneto A., Dietrich P., Roelfsema M.R.G., Voelker C., Schmidt D., Mueller-Roeber B., Czempinski K., Hedrich R. (2004) - AtTPK4, an Arabidopsis tandem-pore K+ channel, poised to control the pollen membrane voltage in a pH- and Ca2+-dependent manner. PNAS vol. 101, No. 44, 15621-15626

[323] J. F. Allen, Photosynthesis of ATP-electrons, proton pumps, rotors, and poise. Cell 110, 273-276 (2002)

[324] D. S. Bendall, Photosynthetic cytochromes of oxygenic organisms. Biochim. Biophys. Acta 683, 119-151 (1982)

[325] C. A. Wraight, A. R. Crofts, Energy-dependent quenching of chlorophyll alpha fluorescence in isolated chloroplasts. Eur. J. Biochem. 17, 319-327 (1970)

[326] Z. Li, S. Wakao, B. B. Fischer, K. K. Niyogi, Sensing and responding to excess light. Annu. Rev. Plant Biol. 60, 239-260 (2009)

[327] D. M. Kramer, J. A. Cruz, A. Kanazawa, Balancing the central roles of the thylakoid proton gradient. Trends Plant Sci. 8, 27-32 (2003)

[328] M. Dunkel, A. Latz, K. Schumacher, T. Muller, D. Becker, R. Hedrich, Targeting of vacuolar membrane localised members of the TPK channel family. Mol. Plant 1, 938-949 (2008)

[329] C. Voelker, J. L. Gomez-Porras, D. Becker, S. Hamamoto, N. Uozumi, F. Gambale, B. Mueller-Roeber, K. Czempinski, I. Dreyer, Roles of tandem-pore K+ channels in plants - a puzzle still to be solved. Plant Biol. (Stuttg.) 12, (Suppl 1), 56-63 (2010)

[330] D. Marcel, T. Muller, R. Hedrich, D. Geiger, K+ transport characteristics of the plasma membrane tandem-pore channel TPK4 and pore chimeras with its vacuolar homologs. FEBS Lett. 584, 2433-2439 (2010)

[331] S. Isayenkov, F. J. Maathuis, Arabidopsis thaliana vacuolar TPK channels form functional K (+) uptake pathways in Escherichia coli. Plant Signal. Behav. 8, e24665 (2013)

[332] M. Zanetti, E. Teardo, N. La Rocca, L. Zulkifli, V. Checchetto, T. Shijuku, Y. Sato, G. M. Giacometti, N. Uozumi, E. Bergantino, I. Szabo, A novel potassium channel in photosynthetic cyanobacteria. PLoS ONE 5, e10118 (2010)

[333] P. Enyedi, G. Czirjak, Molecular background of leak K+ currents: two-pore domain potassium channels. Physiol. Rev. 90, 559-605 (2010)

[334] V. Checchetto, E. Formentin, L. Carraretto, A. Segalla, G. M. Giacometti, I. Szabo, E. Bergantino, Functional characterisation and determination of the physiological role of a calcium-dependent potassium channel from cyanobacteria. Plant Physiol. 162, 953-964 (2013)

[335] S. de Bianchi, N. Betterle, R. Kouril, S. Cazzaniga, E. Boekema, R. Bassi, L. Dall Osto, Arabidopsis mutants deleted in the light-harvesting protein Lhcb4 have a disrupted photosystem II macrostructure and are defective in photoprotection. Plant Cell 23, 2659-2679 (2011)

[336] Shikanai, T. Central role of cyclic electron transport around photosystem I in the regulation of photosynthesis. Current Opinion in Biotechnology, (2014) 26 25-30

[337] K. Maxwell, G. N. Johnson, Chlorophyll fluorescence a practical guide. J. Exp. Bot. 51, 659-668 (2000)

[338] N. E. Ioannidis, J. A. Cruz, K. Kotzabasis, D. M. Kramer, Evidence that putrescine modulates the higher plant photosynthetic proton circuit. PLoS ONE 7, e29864 (2012)

[339] T. J. Avenson, J. A. Cruz, D. M. Kramer, Modulation of energy-dependent quenching of excitons in antennae of higher plants. Proc. Natl. Acad. Sci. U.S.A. 101, 5530-5535 (2004)

[340] N. V. Paramonova, N. I. Shevyakova, V. V. Kuznetsov, Ultrastructure of chloroplasts and their storage inclusions in the primary leaves of Mesembryanthemum crystallinum affected by putrescine and NaCl. Russ. J. Plant Physiol. 51, 86-96 (2004)

[341] E. Rintamaki, P. Martinsuo, S. Pursiheimo, E. M. Aro, Cooperative regulation of light-harvesting complex II phosphorylation via the plastoquinol and ferredoxin-thioredoxin system in chloroplasts. Proc. Natl. Acad. Sci. U.S.A. 97, 11644-11649 (2000)

[342] G. Schonknecht, R. Hedrich, W. Junge, K. Raschke, A voltage-dependent chloride channel in the photosynthetic membrane of a higher plant. Nature 336, 589-592 (1988)

[343] M. Tester, M. R. Blatt, Direct measurement of K+ channels in thylakoid membranes by incorporation of vesicles into planar lipid bilayers. Plant Physiol. 91, 249-252 (1989)

[344] Heiber T, et al. (1995) Ion channels in the chloroplast envelope membrane. Biochemistry 34(49):15906-15917

[345] Bernardi P (1999) Mitochondrial transport of cations: Channels, exchangers, and permeability transition. Physiol Rev 79(4):1127-1155

[346] Kunz, H.-H., Gierth, M., Herdean, A., Satoh-Cruz, M., Kramer, D. M., Spetea, C., and Schroeder, J. I. (2014). Plastidial transporters KEA1, -2, and -3 are essential for chloroplast osmoregulation, integrity, and pH regulation in Arabidopsis. PNAS, 111(20), 7480-5

[347] Carraretto, L., Formentin, E., Teardo, E., Checchetto, V., Tomizioli, M., Morosinotto, T., Giacometti, G. M., et al. (2013). A thylakoid-located two-pore K+ channel controls photosynthetic light utilization in plants. Science (New York, N.Y.), 342(6154), 114-8

[348] Tikkanen, M., Grieco, M., Kangasjarvi, S., and Aro, E.-M. (2010). Thylakoid protein phosphorylation in higher plant chloroplasts optimizes electron transfer under fluctuating light. Plant physiology, 152(2)

[349] Joliot P., Johnson G.N. (2011). Regulation of cyclic and linear electron flow in higher plants. Proc. Natl. Acad. Sci. USA 108: 13317-13322

[350] B.B.Buchanan (1980). Role of light in the regulation of chloroplast enzymes. Annual review of plant physiology. 31: 341-374